

**UNIVERSITY OF RIJEKA
FACULTY OF ENGINEERING**

**COUPLED NONLINEAR PARAMETRIC RESONANCE MODEL
FOR CONTAINER SHIPS**

Doctoral dissertation

Anton Turk

Rijeka, 2012.

**SVEUČILIŠTE U RIJECI
TEHNIČKI FAKULTET**

**SPREGNUTI NELINEARNI MODEL PARAMETARSKE
REZONANCIJE KOD KONTEJNERSKIH BRODOVA**

Doktorska disertacija

Anton Turk

**Mentor: Prof. Jasna Prpić-Oršić, Ph. D.
Mentor: Prof. Carlos Guedes Soares, Ph. D.**

Rijeka, 2012.

**UNIVERSITY OF RIJEKA
FACULTY OF ENGINEERING**

**COUPLED NONLINEAR PARAMETRIC RESONANCE MODEL
FOR CONTAINER SHIPS**

Doctoral dissertation

Anton Turk

**Supervisor: Prof. Jasna Prpić-Oršić, Ph. D.
Supervisor: Prof. Carlos Guedes Soares, Ph. D.**

Rijeka, 2012.

SUMMARY

The objective of the present work is to develop and validate a computational tool for the calculation of large amplitude parametric rolling motions that can be used in conceptual design in a computationally efficient and robust manner. The contribution of this work to the general body of knowledge is in the development of a theory that captures hull interaction effects for a given range of ship speeds, sea states and loading conditions, where interaction effects are likely to materialize in certain non-linear phenomena of dynamic instability known as parametric resonance, while retaining the numerical efficiency of strip theory. The numerical code is based on an hybrid model which transfers frequency domain data to time domain and includes the so called Froude-Krylov nonlinear part of the loading in time domain. The use of a simplified 2½D method showed slight improvement over the classical 2D method with the disadvantage of being more computationally intense than standard strip theory. Furthermore, the implementation of strip theory, with respect to functionality, has been shown to require a more advanced method for including roll damping. The viscous contribution proved far superior in terms of the effect it has on the proneness towards parametric rolling. The problem of viscous roll damping is separated in two models, first when the experimental results are not known with the blending method and second when the roll decrement test are at hand. An extensive experimental program of the Parametric Rolling on a C11 Class Containership was utilized to investigate and explain two consisting inseparable treatments of the damping and seakeeping simulations, respectively. The validation has shown good agreement with the experimental results for roll, both in the experiments where parametric roll resonance occurred and in the experiments where it did not occur. The simulated results, including polychromatic and irregular wave excitation, and the subsequent analysis, provided insight and improved the understanding of the parametric roll resonance mechanism, as well provided the basis for setting a probabilistic methodology proposition.

SAŽETAK

Cilj ovog rada bio je razviti i validirati računalni alat za određivanje velikih amplituda odziva uslijed parametarskog ljuljanja koji se može koristiti u konceptualnom dizajnu na računalno učinkovit i robustan način. Doprinos ovog rada je u razvoju teorije koja hvata dominantne čimbenike interakcije broskog trupa i okoline za određeni raspon brzina brodova, stanja mora i stanja krcanja. Efekti interakcije manifestiraju se nelinearnim fenomenom dinamičke nestabilnosti, parametarskim ljuljanjem, dok se pritom, zadržava numerička učinkovitost vrpčaste teorije. Numerički kod temelji se na hibridnom modelu s prijenosom hidrodinamičkih podataka iz frekventne domene u vremensku domenu uključujući tzv. Froude-Krylovljevu nelinearnu silu u vremenskoj domeni. Korištenje pojednostavljene 2½D metode rezultirao je blagim napredakom u odnosu na klasičnu 2D metodu nauštrb vremenski intenzivniji simulacije. Nadalje, provedba vrpčaste teorije zahtijeva napredniju metodu, kod definiranje prigušenja ljuljanja. Doprinos viskoznih efekata pokazao se kao daleko superiorniji u odnosu na ostale nelinearne učinke koje rezultiraju parametarskim ljuljanjem. Problem viskoznih prigušenja ljuljanja je odvojen u dva modela, prvo kada eksperimentalni rezultati nisu poznati korištenjem tzv. "blending" metode i drugi kada su poznati testovi zamiranja ljuljanja. Opsežni eksperimentalni program koristiti za istraživanje i objašnjenje dva nerazdvojiva aspekta simulacija prigušnja i pomorstvenosti. Eksperimenti su provedeni u okviru projekta pod nazivom "Experimental Assessment of the Parametric Rolling on a C11 Class Containership". Općenito, validacija svih računalnih simulacija je pokazala vrlo dobro slaganje s odrađenim eksperimentalnim mjerenjima. Simulirani rezultati uključujući polihromatsku i nepravilnu valnu uzbudu kao i naknadne analize pružaju uvid i bolje razumijevanje mehanizma parametarske rezonancije, kao temelj prijedloga postavljene vjerojatnosne metodologije.

ACKNOWLEDGEMENTS

I would like to give a special thanks to Prof. Jasna Prpić-Oršić for being my thesis adviser and if I may say so a great friend. I have been indebted in the preparation of this thesis and for making it possible, and whose patience and kindness, as well as her academic experience, has been invaluable to me. It was her professional resume that opened the door for me to work and collaborate with some of the leading experts in the field.

Also special thanks to my other adviser Prof. Carlos Guedes Soares for his vast insight, attention to detail, and guidance during my research. This thesis is submitted by virtue of his invitation to the European Community's Sixth Framework Programme HYDRALAB III, with Project title: Experimental Assessment of the Parametric Rolling on a C11 Class Containership. This work has been supported through the grant and this experimental work is considered of paramount importance to support and validate the two PhD studies of the participants involved.

I feel fortunate to have been a member of that group that also included Prof. Sergio Ribeiro e Silva and Emre Uzunoglu, with whom I had many productive scientific discussions and gained a true friendship. Validation of the work has been made during my stay at El Pardo Ship Model Basin in Madrid where I received the friendly cooperation and extensive feedback with the staff, especially Cesar Gutierrez, Mariu Prieto and Adolfo Maron.

During my stay at the University degli Studi di Trieste as a part of the Erasmus postgraduate scholarship I collaborated with Gabriele Bulian whom I would also thank for providing an excellent environment for learning and helping with problems I stumbled upon along the way.

A very special thanks to my committee members, Prof. Bruno Čalić, Prof. Roko Dejhalla, and Prof. Većeslav Čorić for their individual contributions to my education and helpful discussions about research. I feel obligated to head of department Prof. Roko Dejhalla for his informal support and encouragement and for acting as my observational co-advisor, without ever really having been asked and I mean it in a good way.

I would especially like to thank my colleague and office-mate, Dunja Matulja, for countless meaningful conversations, whether they'd be about work or not.

Lastly but not least, I would like to thank my loving family, especially my mother for the continuous support, encouragement, and understanding throughout my entire academic career.

Table of Contents

1	Introduction.....	3
1.1	Relevance of the problem	3
1.2	Prior investigations	4
1.3	Classification society guidelines regarding parametric rolling.....	8
1.4	Motivation.....	10
1.5	Objectives.....	11
1.6	Outline.....	13
2	Theoretical background	15
2.1	Introduction.....	15
2.1.1	Physics of parametric roll resonance.....	15
2.1.2	Influence of Roll Damping.....	17
2.1.3	Amplitude of Parametric Roll	18
2.1.4	Influence of hull forms	19
2.1.5	Influence of ahead speed and wave direction.....	19
2.2	Prediction of occurrence of parametric rolling in regular waves (susceptibility criteria).....	20
2.2.1	Linearization procedure of the righting arm variation.....	20
2.2.2	Stability charts.....	23
2.3	Prediction of amplitude of parametric rolling (severity criteria)	30
3	Formulation of the seakeeping problem	33
3.1	Potential flow theory	33
3.2	Strip theory – frequency domain solution.....	36
3.2.1	Radiation Forces.....	37
3.2.2	Excitation Forces.....	40
3.2.3	Restoring Forces.....	42
3.2.4	Equations of Motion.....	43
3.2.5	Frequency domain results.....	45
3.3	Time domain strip theory	50
3.3.1	Introduction to modeling and simulation of the instabilities in time domain.....	50
3.3.2	Hydrodynamic coefficients and forces in regular waves.....	52
3.3.3	Equations of motion and time domain responses	60
3.3.4	Time domain strip theory in irregular waves	61
3.3.5	Effects of forward speed on hydrostatic and Froude-Krylov forces.....	66
4	Roll damping contribution.....	67
4.1	Introduction.....	67
4.2	Numerical damping model.....	68
4.2.1	Frictional Component.....	70
4.2.2	Wave Making Component.....	72
4.2.3	Eddy Making Component by Naked Hull.....	73
4.2.4	Lift component by naked hull	79
4.2.5	Bilge Keel Component	82
4.3	Roll damping calculation	84
5	Numerical implementation of seakeeping model for parametric rolling assessment	91
5.1	Introduction.....	91
5.2	Implementation of time domain strip theory and numerical computing schemes.....	91
5.3	Preliminary results in time domain simulations.....	97
5.3.1	Mathematical model implementation for head waves.....	97
5.3.2	Mathematical model implementation for following waves.....	100
5.4	Implementation of the damping blending method with comparison to original methodology.....	102
5.5	Graphical visualizations of the parametric rolling simulations.....	110
6	Experimental setup and program	117
6.1	Introduction.....	117

6.2	Roll decay experiments in both calm water and waves	119
6.2.1	First group of decay tests.....	120
6.2.2	Second group of decay tests with different loading condition	125
6.2.3	Third group of decay tests in waves	126
6.3	Free parametric rolling tests in both regular and irregular waves	128
6.3.1	Parametric rolling experiments in regular waves	128
6.3.2	Parametric rolling experiments in polychromatic waves	131
6.3.3	Parametric rolling experiments in irregular waves.....	134
7	Analysis of roll damping experiments	135
7.1	Theoretical background of the fitting procedure used for the analysis of roll decrement tests	135
7.2	Decay tests processing for the first group of tests.....	141
7.2.1	Alternative exponential fitting technique	146
7.2.2	Summary of the results: Discussion and doubts.....	148
7.3	Decay tests processing for the second group of decay tests with different loading condition	151
7.4	Decay tests processing for the third group of decay tests with different loading condition	154
7.5	Comparison between numerical model and experiments.....	155
8	Analysis of parametric rolling experiments.....	161
8.1	Parametric rolling in regular waves with experimental validation.....	161
8.2	Direct damping calculation and decay test implementation on parametric rolling simulations	164
8.3	Final observations on regular waves parametric rolling	171
8.4	Parametric rolling in polychromatic waves with experimental validation	173
8.5	Parametric rolling in irregular waves with experimental validation	180
8.6	Proposition of probabilistic methodology for irregular waves parametric rolling survey	187
8.7	Proposition of blending methodology for irregular waves parametric rolling survey contained within the regular waves analysis	190
9	Conclusion	194
9.1	Physical insights.....	194
9.2	Overview.....	195
9.3	Further work.....	197
	REFERENCES	199
	NOMENCLATURE	205
	LIST OF FIGURES	208
	LIST OF TABLES	212

1 Introduction

1.1 Relevance of the problem

Large amplitude rolling has become a significant problem with relevance to new ship designs, such as large container vessels or Ro-Ro ships. Incidents as the “APL China”, which involved litigation on the order of \$100 million, have proven that parametric roll exists beyond theory and carries substantial financial risk and grave potential for loss of life. Although its theoretical existence has been known of for decades, parametric roll has only recently garnered attention from a regulatory and prevention standpoint. Large amplitude rolling may occur due to parametric excitation and pure loss of stability on the crest or sometimes in a beam sea resonance condition. Today, parametric roll represents potentially as great a stability issue as the beam sea condition in the past. Parametric excitation has its source in the change of righting lever between crest and trough in longitudinal seas. It depends on the relationship between the frequency of these changes, i.e. the wave encounter frequency, and the roll natural frequency. The phenomenon typically occurs when the natural roll period is almost twice as large as the wave encounter period.

The prediction of the parametric roll phenomenon and its impact on ship’s intact stability and safety has attracted in the last decade great scientific interest, as documented in a series of scientific publications and presentations at relevant international conferences and workshops. The subject has gained, also, significant practical importance and the interest of national and international regulatory authorities (IMO, class societies), because of the risk for the inception of large ship roll motions, shift or loss of cargo and eventually ship capsizing.

In real-life, these ships have sustained one of the largest casualties in history with hundreds of containers damaged or lost overboard as shown in the figure 1-1.



Figure 1-1. Casualties due to the parametric rolling on APL China.

A first attempt to prevent the occurrence of such devastating phenomena was issued by ABS with the main purpose of supplementing the Rules and the other design and analysis criteria for the classification of container carriers in relation to parametric roll resonance. The Guide also contains a description of criteria used to determine if a particular vessel is vulnerable to parametric roll (susceptibility criteria) and how large these roll motions might be (severity criteria). Within the recent framework for the development of IMO New Generation Intact Stability Criteria, a significant role is played for the development of a "vulnerability assessment methodology" to be applied in the early design stage with the aim of identifying ships prone to the inception of parametrically excited rolling motion. The term susceptibility is omitted on purpose and the new term vulnerability is introduced to distinguish the basic difference since it accounts for the case of irregular waves based on a "regular wave environment" by considering the following "practical equivalence". However, the overall proposition from both organizations is still either inaccurate or complex and thus very far away from real application. Often, these steps are not enough to ensure safety and it is important to carry out

extensive studies of dynamic instabilities. Therefore it is evident that a new approach must be implemented aiming to present a trustworthy and validated methodology to provide the shipmaster with a decision support tool to prevent large amplitude motions in different encounter conditions. The most convenient way seems to be a database output filled by a numerical model that can be easily read and interpreted to help navigation in rough weather conditions as oppose to onboard realtime numerical simulation program which is difficult even with the latest developments in computer technologies.

1.2 Prior investigations

In its service life, a ship will involuntarily experience many occasions of stormy weather and rough seas, during which a number of dynamic problems can be attributed to ship behaviour. For example, parametric rolling as an unstable phenomenon, which can quickly generate large roll angles that are coupled with significant pitch motions. Parametrically excited rolling motion can occur due to variations of restoring in waves when certain conditions are met. This could mean that the small perturbations in roll motion can grow, leading to excessive roll motion and possible capsizing.

One of the early investigations of coupling between heave and roll is that by Froude (1863) who observed that ships have undesirable roll characteristics if the natural frequencies in heave and roll are in the ratio of 2:1, and if the roll axis does not lie in the plane of the water surface, i.e. when the frequency of a small, free oscillation in pitch is twice the frequency of a small, free oscillation in roll.

A brief history of parametric roll starts with mention of some work conducted principally in Germany in the late 1930s (Kempf, 1938). The simplest possible scenario is when the forward velocity is nearly constant and the ship can be assumed in quasi-static equilibrium in the vertical direction. This work was initiated in an effort to explain the capsizing of some small ships such as coasters and fishing vessels in severe following seas. The work included experiments with models in open water as well as numerical and theoretical computations. During the 50s, Grim (1952) and Kerwin (1955) have examined the stability of rolling motion of ships in longitudinal waves. In their work the restoring moment in roll is a periodic function of time because of the periodicity of wave encounter and, in consequence, the (single) equation of motion in roll is a Mathieu equation, even when only linear terms are included in the forces.

However, the parametric excitation was originally introduced into the analysis of ship motions by Paulling and Rosenberg, (1959) and Paulling, (1961). They investigated nonlinear equations of motion of a ship having the three degrees of freedom of heave, pitch, and roll. They showed that unstable motion may occur in any one of the degrees of freedom through excitation by one of the other two, which was confirmed by the experiments carried out for the roll-heave systems, assuming that the variation of roll restoring moment of a ship is a result of forced heave motion of the ship in still water. The wave effect is primarily geometric arising from a consecutive loss or gain of waterline, combined with vertical shifts of the centre of buoyancy.

These studies enabled to discuss parametric roll resonance with the Mathieu equation, which then characterizes the rolling motion of a ship in longitudinal waves. Depending on the values of the coefficients, this equation yields a stable or unstable solution. It is well-known that the directly excited pitch can create growth of roll, which will influence back pitch and so forth. A critical consequence can be saturation of the pitch response and transfer of all the energy that enters the pitch mode into roll, for example (Nayfeh, 1973).

The phenomenon was thought to be of concern principally in following seas and for small, low freeboard ships. In the 1980s, however, there were reports of containerships and even some cruise ships experiencing heavy rolling in head seas. These were ships having a hull form characterized by great flare forward and wide flaring stern sections, features that are known to lead to significant stability variations in waves. Although naval architects have been aware of the problem

mathematically for decades, the development of the so-called parametric resonance became an area that was starting to receive wider attention (Blocki, 1980; Skomedal, 1982). Blocki presented a method that enabled calculations of the probability of capsizing caused by parametric roll in a particular loading condition for a certain state of wind waving, for both heave-roll and pitch-roll couplings. Skomedal considered the parametric resonance in head seas is due to energy transfer from the vertical motions to the roll motions. The randomness of the wave environment has also been under consideration, with the parametric forcing seen as a stochastic random process that ‘enters’ into the roll equation. Vinje (1976), Haddara (1980), Muhuri (1980), Roberts (1982) and Dunwoody (1989) have sought random-wave stability criteria for parametric rolling. Haddara analyzed the problem by using a combination of the method of slowly varying parameters and the stochastic averaging technique. Roberts studied the same problem, by formulating some simple expression for the stationary response distribution. Helas (1982), on the other hand, applied the effective-regular-wave concept of Grim.

It can be observed that in some circumstances an oscillatory rolling motion may build up very rapidly, reaching very large amplitudes, conducive to a ship capsizing (Umeda et al., 1999; Hamamoto and Panjaitan, 1996; Munif and Umeda, 2000). In order to investigate capsizing, nonlinearity of restoring moment in still water needed to be taken into account. At this stage, nonlinear dynamical system approach including geometrical and analytical studies is required to identify all potential dangers among co-existing states. Such examples can be found in Sanchez and Nayfeh (1990), Soliman and Thompson (1992), and Oh et al. (2000) for pitch-roll model. These theoretical studies focused on understanding fundamental mechanism of the phenomena with rather simplified mathematical modelling. For example, the amplitude of restoring arm is often provided a priori without any relationship with wave steepness or exciting moment. Umeda’s and Hamamoto’s work led to a proposal for criteria taking into account pure loss of stability, broaching to, surf-riding and parametric resonance in astern seas, which was accepted and published by IMO.

Initially, as it was thought to be a phenomenon mainly limited to the following seas condition and of significance for smaller, high-speed displacement vessels such as some fishing boats and seagoing tugs a number of research was conducted by Neves and Valerio (1994), Perez and Sanguinetti (1995) and Neves et al. (1999). Neves et al. (1999) conducted model experiments and numerical investigations on the parametric resonance of two fishing vessels even in head seas. They considered the change of GM in waves in their mathematical model, with the effects of heave and pitch motions as well as that of wave passage. Spyrou (2000) established the boundary separating parametric instability from pure-loss stability. Instability regions were identified in terms of transient motions, rather than in terms of the customary asymptotic stability chart associated with Mathieu’s equation.

It is well accepted that wave effect on roll restoring moment can be qualitatively estimated with the Froude-Krylov assumption. However, some of the authors (Umeda et al., 2001) reported that the Froude-Krylov prediction could overestimate for a fishing vessel known as the ITTC Ship A-2 as a result of captive model experiments.

A 3-DOF nonlinear fully coupled model was then developed by Neves (2002). A first attempt was done by using Taylor series expansion up to 2nd-order to describe the coupled restoring forces and moments in heave, pitch and roll. This model, although it provided a quite thorough description of the nonlinear interactions among the different modes, tended to overestimate the roll oscillation above the stability threshold. Neves and Rodríguez (2005) proposed a 3rd-order analytical model where the couplings among the three modes are expressed as a 3rd-order Taylor series expansion. In this new model the nonlinear coefficients are mathematically derived as a function of the characteristics of the hull shape.

Furthermore, roll motion of a RO-RO ship in resonance with the wave excitation, and as such the GM -variation of a ship in waves is an important evaluation factor in that problem for both the following and heading waves (Hua, 1992). The non-linear characteristics of the GM -variation in an

irregular wave can be analyzed by means of available nonlinear probability theories or Monte-Carlo simulation technique (Hua et al., 1999).

The “APL China” casualty in October 1998 focused attention on parametric rolling in head seas. The topic has come to the forefront of research in academic, insurer (Roenbeck, 2003), and regulatory settings (ABS, 2004; Sweden, 2004; ITTC, 2005). Several different types of vessel have reported to experience parametric roll in head seas, e.g. destroyers (Francescutto, 2001), ro-paxes (Francescutto and Bulian, 2002) and PCTC (Palmquist and Nygren, 2004). Spyrou (2004) showed that if the ship experienced parametric rolling, the amplitude of roll was small to moderate, and with certain limits on the detailed shape of the restoring lever where a third-order polynomial could represent reasonably the exact shape of the initial part of the lever. His work along with Francescutto’s, (2001) was a foundation for the ITTC guidelines that describes how to predict the occurrence and magnitude of parametric rolling while also pointing out the uncertainties and limitations of these prediction methods.

The investigation of this casualty included theoretical computations of GZ variations, model experiments and numerical simulations as well as meteorological studies of the wind and sea conditions prevailing at the time. Results of the investigation received wide dissemination in the technical press. Since the “APL China” casualty and other similar incidents, much theoretical and experimental work has been focused on head seas parametric roll. IMO and many of the class societies now have recommendations to designers and masters for avoiding head seas parametric rolling situations. Ribeiro e Silva and Guedes Soares (2000) demonstrated that both linearised and nonlinear theories could be used to predict parametric rolling in regular head waves.

Evidence of parametric rolling in head seas on a post-Panamax C11 class container ship, as stated above received wide and renewed attention and this incident was analysed by means of numerical simulations and model tests (France et al., 2001; Kreuzer and Sicherman, 2004; Carmel, 2006). France used the FREDYN (DeKat and Paulling, 1989) and LAMP (Lin and Yue, 1990) codes, which include nonlinear effects, in their numerical analyses and showed that such tools are suitable for simulating these phenomena. In regular waves the authors confirmed a set of conditions for the occurrence of parametric roll, namely: wave encounter frequency nearly twice the roll natural frequency, ship length of the same order as wave length, roll damping (which is speed dependent) below a certain threshold and wave height above a certain threshold. However, most time domain ship motion programs are potential methods and hence cannot account for viscous effects without recourse to empirical data derived from model tests or more recently from CFD calculations.

Levadou and Gaillarde (2003) followed with numerical simulations for the C11 containership, using FREDYN, by investigating a range of speeds, headings (head and bow quartering seas), significant wave heights and load conditions. Their investigations showed that high sustained speeds reduce the risk of parametric roll. Following seas were not investigated, but the authors noted the possibility of parametric roll occurrence for such cases at low or zero speed. Continuing the work, Levadou and Van Walree (2004) compared numerical model tests with numerical predictions of the C11 class containership. Shin et al. (2004) applied several codes (i.e. FREDYN and 3D LAMP) to a range of large container vessels to evaluate criteria for parametric roll, showing both codes capable of predicting the relevant phenomena in head seas with sufficient accuracy. The results confirmed that the vessel suffered from a severe case of parametric roll during the storm. This paper discusses the technical background of the American Bureau of Shipping (ABS).

From full scale observations at high values of metacentric height, parametric rolling problems are typically associated with head sea scenarios (Löfstadt and Bloch Helmers, 2004). However, systematic model tests have demonstrated clearly that the problem also occurs in stern quartering seas and low values of initial stability, especially when the vessel has sufficient time to stay on the crest (Krüger et al., 2004). Due to the alteration of the initial metacentric height between crest and trough, as well as due to the acceleration/deceleration of the vessel, critical resonances may differ significantly from linear estimations of resonance scenarios and cover typically a range of courses, speeds and wave lengths. In this respect, the behaviour of the vessel in regular and irregular

waves differs significantly. Krüger (2006) analysed the cargo loss of a Panamax container vessel in stern quartering seas applying Cramer and Krüger's (2001) nonlinear strip theory. Krüger (2006) concluded that the vessel suffered from large amplitude motions caused by 1:1 resonance parametric roll problem in irregular stern quartering seas when encounter frequency is close to the natural frequency of the vessel, mainly associated with the so called dead ship condition.

Ribeiro e Silva et al. (2005) applied a partly-nonlinear time domain model with five degrees of freedom (all rigid body motions except surge) to analyse parametric roll in head seas paying attention to the validity of the numerical results and the consequence of the validity. The nonlinearities included correspondence to the evaluation of restoring coefficients using the instantaneous wetted surface. Other hydrodynamic effects were obtained from a strip theory, although viscous effects were included in roll damping by comparison with decay tests. Comparisons were made with experiments in regular waves on a containership and the authors conclude that the method is capable of predicting parametric roll in regular and irregular head seas.

Levadou and van't Veer (2006) presented results of a study on the effect of main dimension variations, hull form variations and different appendages configuration on the occurrence of parametric roll of post-Panamax containership. The original hull form and variations at the bow and aft of the hull form were investigated while keeping the draft, GM and natural roll period the same. McCue et al. (2007) also presented a numerical study of the influence of topside shape on parametric roll in longitudinal seas.

A systematic investigation on the prediction of parametric rolling exhibited by a post-panamax containership is by Spyrou et al. (2008), on the basis of the analytical formulae that appear in current industrial guidelines which are evaluated in a step-by-step process against various numerical predictions. The method of continuation of nonlinear dynamics is introduced in order to expedite the identification of the instability boundary and the prediction of steady amplitudes of roll oscillation is utilized by a numerical time-domain panel code SWAN2 for the analysis of the steady and unsteady free surface flows past ships.

Since the parametric roll phenomenon is caused by time variation of transverse stability, the numerical simulation method must be able to adequately model the changes of geometry of the immersed part of the hull due to large waves and ship motions. Belenky et al. (2003) described a background for assessing the risk of parametric roll in head seas. If the waves can be described as quasi-stationary (which is practicable for short periods of time) then, with the assumption of linearity, the motions themselves would be quasi-stationary also. They described an ergodic process as applicable to a stationary stochastic process in which the statistical moments can be estimated from one sufficiently long realization. In this paper it was also stated that the same behaviour was seen for encountered waves, heave displacement, heave and pitch velocity. Bulian et al. (2004) presented some preliminary results regarding the problem of no-ergodicity of parametric rolling. This is addressing the issue of obtaining reliable information from ensemble averages. The main conclusion of the paper was that temporal averages for parametric rolling responses can lead to very large coefficients of variation. McCue and Bulian (2007) studied the practicality of using finite-time Lyapunov exponents (FTLEs) to detect the inception of parametric resonance for vessels operating in irregular longitudinal seas.

The alternative approach to using a 6 DOF roll equation to determine the magnitude of parametric rolling is a 1 DOF development to avoid the use of complex fully coupled ship motion programs. Unlike a 6 DOF roll equation where the restoring function is implicit in the determination of the position of the metacenter for the instantaneous underwater hull form, the form of the restoring and damping terms need to be known a priori. Bulian and Francescutto (2003) proposed a 1.5-DOF model where the dynamic interaction between the vertical motions and the roll oscillation was relaxed by the assumption of quasi-static heave and pitch. Moreover, that assumption allowed an analytical description of the GZ curve (extended degrees of freedom) that was approximated as a surface varying with roll angle and wave crest position. This model is considered valid for moderate

ship speed in head seas, and it showed that the principal factor determining the extent of the instability region is the non-linearities of a cubic function of restoring moment.

Umeda et al. (2004), used a model, in which the roll-damping coefficients were estimated from roll decay tests, and the change of the roll-restoring moment (5th order restoring function) was obtained from the Froude–Krylov assumption or captive model tests. The continuation of their work (Munif and Umeda, 2006) was a parametric resonance observed in head seas for a model of an Icelandic trawler that has no distinct wave-induced change in its metacentric height, which is hydrostatically calculated. Two mathematical models, a 1 DOF model with balanced heave and pitch motions and a 6 DOF model were used to explain the parametric roll resonance of the ship in head waves. Only the 6 DOF model, however, successfully reproduced the occurrence of parametric rolling of the ship.

Matusiak (2003) compared numerical prediction of parametric rolling with model tests conducted on a free running fast Ro-Pax vessel. Tests were conducted in head and following seas. The numerical approach is described as a two-stage approach whereby the linear approximations and non-linear portions in the ship dynamics model are decomposed. A full numerical procedure that was conducted for the post-Panamax container vessel for predicting the onset of parametric rolling based on the Duffing method with excitation taken from the difference in restoring force from trough to crest condition when the ship is encountering head seas proved it can push the ship into a parametric mode of rolling (Surendrana et al., 2007). A containership (Taylan, 2007) is taken as an example to analyze its stability in longitudinal waves based on the method worked out by American Bureau of Shipping (ABS). Chang (2008) examined a Ro-Ro passenger vessel and showed a numerical motion simulation method which can be employed to study on parametric rolling of ships in a seaway. The method takes account of the main nonlinear terms in the rolling equation which stabilize parametric rolling, including the nonlinear shape of the righting arm curve, nonlinear damping and cross coupling among all 6 DOF. Nielsen and Jensen (2009) elaborated further on an existing (simplified) model for the rolling of a ship. The model can be integrated with a probabilistic tool which enables evaluations of numerical simulations by the first order reliability method (FORM) and by Monte Carlo simulation (MCS).

Despite the progress in the understanding of the phenomenon, a few issues remain open, such as the development of effective criteria for the prevention of parametric rolling by design, the assessment of the effects of coupling with other motions, and the derivation of optimal experimental/numerical procedures for safety assessment in a realistic sea. And although despite the theoretical, numerical and experimental evidence of the potential danger associated to this phenomenon, the real encountering evidenced at sea is up to now, according to ship operators, quite limited in comparison to what scientific literature would lead to imagine.

1.3 Classification society guidelines regarding parametric rolling

The problem of parametric roll returned to prominence quite recently as a result of significant cargo loss and damage sustained by post-Panamax container carriers which led classification societies to take interest in such phenomenon. Authoritative organizations of the maritime industry responded promptly by publishing prediction guidelines (ABS, 2004, ITTC, 2006). For the non-specialist, the ABS and ITTC guidelines represent very accessible means that one could trust for predicting whether, in the urge for extra deck area and higher speed, a containership has inherited a tendency for parametric rolling.

The American Bureau of Shipping (ABS, 2004) is the leading classification society concerning the documentation on parametric roll, as they issued the first guide for the assessment of parametric roll resonance in the design of container carriers in September 2004, with the main purpose to supplement the Rules and the other design and analysis criteria that ABS issues for the classification of container carriers. The Guide contains a brief description of the physical

phenomenon of parametric roll resonance, which may cause an excessive roll of a containership in longitudinal (head and following) waves. The Guide also contains a description of the criteria used to determine if a particular vessel is vulnerable to parametric roll (susceptibility criteria) and how large these roll motions might be (severity criteria). The procedure based on work conducted by Shin et al. (2004) which is the basis of the technical background of ABS guide is explained and cited in detail in the following chapters.

In March 2008 ABS has awarded the first class notation specific to parametric roll to three ships in the Hyundai Merchant Marine fleet (Maritime Reporter Magazine, 2008). The optional class notation was issued against criteria contained in the ABS Guide for the Assessment of Parametric Roll Resonance in the Design of Container Carriers, which provides design and analysis measures to determine if a particular vessel is vulnerable to parametric roll and the potential magnitude of the roll motions. The “PARR C1” notation has been granted to the 4,700 TEU “Hyundai Forward”, and 8,600 TEU vessels “Hyundai Faith” and “Hyundai Force”.

Lloyd’s Register of Shipping (2003) supports initiatives made to introduce guidance on avoidance of parametric roll. At present the IMO sub-committee on stability and load lines and on fishing vessel safety (IMO SLF) is tasked with addressing this issue. In response to concerns voiced in the industry, Lloyd’s Register has investigated its container securing requirements. LR suggests simplified Susceptibility Assessment Method which considers the roll motions of the vessel, treating them as a simple mass-spring damper system with a single degree of freedom. Any seakeeping software can be used to determine the ship motions in chosen wave conditions, for a range of speeds and headings. From the resulting data, the variation in vessel stability through the waves and the relationships between the wave encounter frequency and the roll natural frequency and using the results gained to help avoiding the possibility of parametric rolling.

Bureau Veritas (2005) is recommending appropriate solutions of the simplest mathematical model of parametric roll considering the one degree of freedom roll motion equation, in which, the restoring coefficient has been made time dependent. Calculated hydrostatic variations are approximated by the sinusoidal function which leads to the Mathieu type equation for roll, from which the regions where the roll instability takes place can be identified. In preliminary stages BV suggest simplified analytical models, as presented above, which allows for quick identification of the dangerous zones, however in the final phase of parametric roll evaluation, it is preferred to use the nonlinear numerical models which are able to include all sort of nonlinearities in a natural way. To summarize, BV approach defines a two step procedure,

- preliminary checks using the simplified semi-analytical model
 - fully non-linear simulations for critical cases,
- after which it is possible to produce the polar plots which represents the maximum expected roll motion for a given sea state with respect to ship speed and heading.

Det Norske Veritas issued a containership update, in addition to traditional class services during the design, construction and operational phases. They provide owners and operators with increasingly ‘popular’ services, such as Active Operator Guidance, advice on extreme roll motions (parametric rolling) and how to avoid these for a sea state in which the vessel’s hull, given the wave length and height as well as the distance between waves, may be subject to extreme roll motions.

The way to deal with that problem could be more stringent lashing requirements or thorough redesign. But DNV believes a very effective measure would be the deployment of support systems, such as the aforementioned Active Operator Guidance system being jointly developed by DNV based on the Wasim program to bring forward a guidance system to be put on the bridge of large containerships. The idea is to use wave radar technology, provided by Miros, designed to report sea state in real time – wave height, direction and so on - with motion recorders coupled with ship specific acceptance criteria produced by advanced hydrodynamic calculation tools to yield guidance concerning how fast containerships, or similar vessel types, may be operated safely in rough weather. The information obtained will be used to ensure that limits of hull loading, impact pressure, water on deck, motions and accelerations are not being exceeded. Recent full-scale observations (DNV 2005)

have shown that especially container vessels are very often operated in bow or stern quartering seas which lead to large rolling motions. Consequently, a necessity to update wave induced hull pressures based on the consideration of large rolling is necessary. The cargo loss for container vessels has been the subject of several investigations. Modules for the Active Operator Guidance system are planned to include decision support for route planning, trend analysis and advice on the actual situations for the vessel and will ultimately be integrated into the bridge system.

At IMO, whilst no direct technical measure against the occurrence of this phenomenon is found among the revised intact stability requirements, submissions referring to parametric rolling seem, in the first instance, to have paved the way towards the adoption of an improved “Guidance to the Master” (IMO, 2006, 2007). IMO has published revised guidance to the master for avoiding dangerous situations in adverse weather and sea conditions where the physical phenomena of parametric roll motions are explained. Operational guidance on how to avoid dangerous conditions with risk of successive high wave attack in following and head seas is given for an encounter period is close to one half of the ship roll period. At the same time, more attention was given to the possibility of inception of parametric roll in head waves, not necessarily so dangerous in terms of possible capsizing, but potentially onerous for safe cargo handling, due to the potentially significant accelerations involved. Therefore, apart from special checks on hull forms and the need to fit roll suppression devices a revision of the “Guidance to the Master for Avoiding Dangerous Situations in Following and Quartering Seas” is seen as appropriate. More specifically, as statistically demonstrated, a special attention to the referred bow seas scenario should be given, where the best first course of action should be rather to increase speed than reduce the ship’s speed, as mentioned in the document (IMO, 2005).

However, these unresolved scenarios have been recently addressed with the well known revision of Intact Stability Code which has been completed at IMO with the adoption of the “International Code on Intact Stability, 2008 (2008 IS Code)” (IMO, 2008b). The activity of the Working Group for the Revision of Intact Stability Code is however continuing, finalized to the development of the “New Generation Intact Stability Criteria” suitable to address phenomena, not or insufficiently covered by present criteria. Among these phenomena, an important role is being played by the parametric rolling in longitudinal/quartering waves.

In addition, the various classification society criteria may not predict equivalent lifetime roll responses and accelerations. Accordingly, current classification society criteria do not provide uniform design standards for container ships experiencing head-sea parametric rolling.

1.4 Motivation

Numerical simulation methods of varying complexity are nowadays routinely employed for the prediction of ship motions in waves and they are often also applied to the prediction of parametric roll phenomena. As the employed methods are of varying complexity and capabilities, their accuracy in predicting parametric rolling is accordingly of mixed quality.

The direction of this work is very analytical one, aiming at providing simulation tools that could e.g. be used in studies of active stabilization and control. The model parameters are identified based upon the ship line drawings and the loading conditions. A new implementation of the above model is then presented. In the early design phase, when usually not much more than the hull form, the design speed and a range of roughly possible loading conditions are available to the designer, it could be useful to have at hand a methodology for checking the relative level of vulnerability of a ship (or different design alternatives) to the risk of inception of parametric roll. In order for the methodology to be viable in the early design process:

- It should have a clear physical background;
- It should be sufficiently easy to apply;
- It should require a limited number of parameters for its application;

- It should be based on relatively standard computational tools, generally available to the majority of designers.

Another important feature of a good methodology should be its robustness with respect to possible differences in the practical implementation (usually as a computer code). Starting from such ideas a method is presented where the takes into account (although under a series of simplifications/approximations):

- Ship geometry;
- Realistic environmental conditions;
- Loading conditions;
- Operational speed range.

The foundation of the methodology is the determination of the range of potentially dangerous speeds for a series of reference regular waves. Regular waves are defined starting from the analysis of standard wave scatter diagrams, using a "practical equivalence" that only serves the scope of having a standardized (empirical) correspondence between regular waves and irregular sea for the application of the present methodology. Although generally less severe, the parametric roll phenomenon is also present in irregular waves. The reliability of the implemented model in simulating parametric resonance behaviour is validated against experimental data. The validation has shown good agreement with the experimental results for roll both in the experiments where parametric roll resonance occurred and in the experiments where it did not occur.

The main goal of this work is to provide a benchmark for simulating parametric roll of a container ship over a large range of ship speeds and sea states. In case of irregular waves, however, the theory seems to be not yet ready to give reliable values for threshold and amplitude. This benchmark has been designed to be a fully integrated part of parametric rolling code for onboard application as well. The availability of such a powerful tool opens up a great wealth of opportunities, notably the design and testing of novel model-based roll motion stabilizers. A correct definition of the most dangerous phenomena for every ship is thus of utmost importance: the designer should indeed provide information to the master of the vessel regarding the best way to respond to harsh weather conditions.

1.5 Objectives

Following the work on the development of a mathematical and numerical model for the calculation of the movements of vessels in either regular and irregular waves by Ribeiro e Silva and Guedes Soares, a method for predicting large amplitude roll motions in a computationally efficient and robust manner has been enhanced and demonstrated. The criteria to develop a computational design tool for the calculation of parametric rolling that can be used in conceptual design are:

- Robustness of the method;
- Reasonable computational time on state-of-the-art PC;
- Accuracy within engineering practice;
- Linear as well as nonlinear predictions should be available.

The contribution of this work to the general body of knowledge is in the development of a theory that captures hull interaction effects for a given range of ship speeds, sea states and loading conditions, where interaction effects are likely to materialize in certain non-linear phenomena of dynamic instability known as parametric resonance, while retaining the numerical efficiency of strip theory. The present theory utilizes frequency domain hydrodynamic coefficients that include hull interactions in the radiation problem and a body-exact solution of the time-varying hydrostatic and Froude-Krylov forces in the time-domain.

The conditions that are found to be most prone to parametric rolling were identified beforehand by means of numerical simulations with original program even though the procedure to obtain the results was extremely cumbersome, given that original programs work separately and

independently. For that reason transfer functions were introduced enabling the frequency-domain and a time domain part of the codes to be used in conjunction for numerical calculations. The transfer functions can also provide the degree of complexity used in the mathematical model associated with the nonlinearities introduced in the model.

With this aim, a series of experiments were carried out to assess the instantaneous hydrodynamic coefficients and the parametric rolling characteristics of a C11 class container vessel model. The experimental programme consisted of captive model tests at various heel angles, forced oscillation tests, free-decay tests and parametric rolling tests. The model experiments have been conducted at Canal de Experiencias Hidrodinámicas de El Pardo (CEHIPAR), Madrid. Preliminary results with original methodology at hand compared to the experimental outings were underperforming for a certain aspects of the overall contributions to parametric resonance.

Given that any ship motion routine requires validation of its results to demonstrate reliability in future conditions, the experimental research was focused on the 2 latter groups of tests with the aim to upgrade the model taking into account overwhelming contribution of the incident Froude-Krylov forcing and roll damping towards parametric rolling effectuation. The theory and computational tool have been developed with a stated objective of supporting design optimization to foresee the susceptibility of a vessel to dynamic instabilities in a seaway, particularly to occurrence and realisation of parametric rolling, which requires extremely fast and stable computations that can accurately assess the seakeeping measure of merit in a relative sense. Therefore, an upgraded assessment of the nonlinear Froude-Krylov forcing summed within $2\frac{1}{2}D$ method is introduced. The results showed improvement especially in terms of physical roll response but the increased computational effort is not quite in line with the designated numerical efficiency.

The implementation of strip theory has with respect to functionality been shown to require a more advanced method for including roll damping. The viscous contribution proved far superior in terms of the effect it has on the proneness towards parametric rolling. The problem of viscous roll damping is separated in two models, first when the experimental results are not known and second when the roll decrement test are at hand.

A completely new module for the damping assessment based on the modified Ikeda's method is introduced. Following this very comprehensive approach an upgrade of the existing commonly used platform for the damping assessment was designed while the reliability of the implemented model in simulating damping behaviour was validated against experimental data. The proposed methodology very much enables scrutinizing the damping components that contribute to it. An iterative process based on the convergence method is introduced in which equivalent damping becomes continuously updated starting from pre-calculated values for the roll amplitudes acting as nonlinear variables, in order to achieve an acceptable system characterization of predefined margins for the converging solutions. The direct calculation is also introduced to calculate the hydrodynamic damping coefficient at each time step, however this again lead to the complication of the program and an increase of the calculation time.

Special attention was given in analysing viscous roll damping contribution from the roll decay tests that resulted in the proposition of the novel model for the parametric fitting of the amplitude dependent equivalent linear damping, performed assuming that the oscillation frequency is, with good accuracy, almost independent from the rolling amplitude. This method enables aggregating the data coming from different roll decays performed on the same model in the same conditions with possibly changing initial heel angle. The aggregation of data could be an important aspect to the selection of the roll decrement approach for the determination of the nonlinear damping due to the fact that perfect repeatability of initial conditions for different decays is not possible.

Following the unorthodox data acquisition from the roll decrement readings a dual nonlinear damping fitting model is introduced into the motions program dealing with highly nonlinear attitude in the moderate range of roll amplitudes, while covering good extrapolation capabilities observed for higher roll angles due to its linear asymptotic behavior.

Comparisons of the present theory to model test data and 6 DOF computations have shown very good agreement for container ship designs while capturing correct trends, especially dealing with polychromatic waves assumed necessary towards the understanding and identification of the specific conditions of parametric rolling in irregular head waves. The experiments on irregular waves were focused on characteristic wave groupiness necessary to invoke parametric excitation.

For that reason a methodology is proposed tackling the non-ergodicity of inception towards parametric rolling with respect to the nonlinear irregular wave's response. A generalized weighted formula is applied where data points contribute with their weighted coefficients, in this case roll angles, determining the relative importance of each quantity on the average. The intention was to stress out the link in between the deterministic and stochastic excitation for the parametric rolling becoming obvious with the ability to minimize the inherent uncertainties related to the simulation in irregular waves.

In order for the simulations to be more plausible and visually more enhancing the 3D "Matlab simulink" program was created. The program constitutes of two subroutines, the first utilises the data gathering while the second enables 2D and 3D polar representation.

Since the real-time calculation onboard the vessel might not be practically applicable, a methodology as such using pre-calculated data could be obtained and presented for vessels in form of such polar diagrams for each sea state and loading condition governing decision support systems. Given the fact there is no direct technical measure against the occurrence of this phenomenon found among the revised intact stability requirements it is believed that this work could lead to the proposition of the effective generalized criteria to avoid parametric rolling. Finally, a completely non-linear solution would be nearly impossible to achieve with the current computational resources. Higher fidelity tools can be used subsequent to a converged design to obtain a more accurate assessment of seakeeping performance.

1.6 Outline

The work starts with the introductory chapter. Motivations are also presented. In order to carry out any further work in any field, it is a necessity to be aware of the latest advancements. Therefore chapter 1 provides a review of the state of the art and classification societies stands toward parametric rolling phenomena. The methods that are currently in use are presented along with their applications and limitations.

Chapter 2 gives an outline and a brief description of the basic concepts of dynamic instabilities that contribute towards inception to parametric rolling along with the concepts of susceptibility and severity criteria.

Chapter 3 presents the theoretical background and the classical formulation of the hydrodynamic problem and its proposed solution. Linear seakeeping theory in regular and irregular waves is also discussed. The chapter concludes with a discussion of the proposed non-linear time domain seakeeping theory particularly the Froude-Krylov force contribution.

The viscous contribution summed within chapters 4 and 7 is divided in the presentation of the numerical roll damping method and the nonlinear model based on the decay data acquisition. Both of the approaches are cross-referenced and validated.

Chapter 5 introduces numerical implementation of seakeeping model for parametric rolling assessment based on software implemented. The structure and the user interface along with functions and the usage are also outlined. The blending method for roll damping contribution is emphasized. Polar plots are delivered to present results for all of the possible ranges of headings, sea states and speeds that the vessel may encounter and are attributed to parametric rolling.

Chapter 6 presents, in detail, the tests that have been carried out in the El Pardo towing tank, Madrid. The structure of the experiments is presented, along with the methodology used.

Chapter 7 is the chapter that deals with the analysis of roll damping results and with comparisons to numerical obtained using modified Ikeda's method.

Chapter 8 gives the analysis of parametric rolling experiments with comparisons to regular waves. Polychromatic waves parametric rolling is also compared the experimental data. The presentation of results for irregular waves and comparison with the experimental data is also presented. The novel probabilistic methodology is introduced as well.

The work is concluded with chapter 9, presenting the general conclusion and recommendations for future works.

2 Theoretical background

2.1 Introduction

2.1.1 Physics of parametric roll resonance

Excitation of roll motion caused by a wave slope is well known and comparatively easily explained, especially when the ship is under way or drifting in beam seas, which can lead to considerably greater roll angles in case of resonance, i.e. when the wave period is approximately equal to the ship's period of roll. When the period of encounter is approximately equal to the period of roll, additional momentum is gained only once during each complete roll, i.e. during every other half roll. Roll cycles are asymmetric. The half roll contributing to excitation is of longer duration with greater roll angles, whereas the other half roll is determined by maximum stability and therefore is shorter with moderate roll angles.

Nevertheless, under certain conditions of encounter period, roll motion can be excited in longitudinal seas, via a different phenomenon, where the wave slope is of negligible influence, it is parametric excitation of roll. For the latest container ships and passenger vessels, with their typical hull shape, a physically different cause of roll motion is becoming more and more relevant to ship operation. There are certain environmental and physical conditions that should simultaneously overlap in order parametric resonance to occur. These conditions may be summarized as: the ship must be sailing in head, quartering or following seas, the wave length should be approximately around the range of the ship length, the encountering frequency may be twice the natural frequency of roll. Although these processes always occur simultaneously, they will be explained individually in order to get a clear idea of the different effects.

Looking at a static case of ship in calm water any disturbance in transversal (as from a wind gust) will lead to roll motions mainly dominated by the so called “natural roll period” as a period of such roll oscillations. The forward and aft parts of the ship contribute considerably to the development of righting levers owing to the flare of the sections and superstructures (e.g. the forecabin). If the waves crest passes the midships part of the hull (Fig. 2-1), both ends emerge in troughs. Righting levers are smaller, with a minimum when the crest is approximately amidships, since the waterplane at the immersed portions of the bow and stern are narrower than in calm water. Consequently, the GM is correspondingly decreased in comparison to calm water.

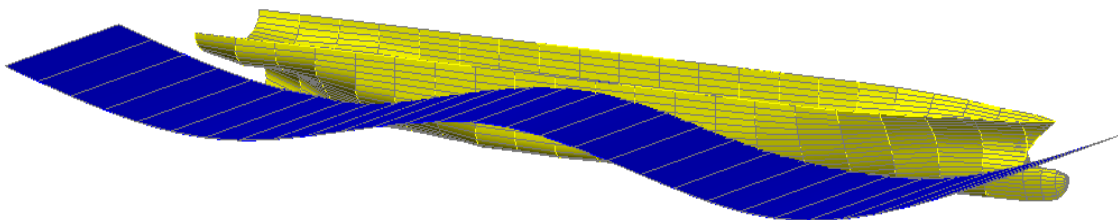


Figure 2-1. Profile of waterline in wave crest.

In contrast to the above, if a ship is located in a wave trough (Fig. 2-2), the flared parts of the bow and stern are more deeply immersed than in calm water and the wall-sided midship is less deep, making the instantaneous waterplane wider than in calm water and as a result the metacentric height (GM) is increased over the calm water value, subsequently leading to the condition of improving or increasing stability. Righting levers are greater, with a maximum when a trough is approximately amidships, as both ends immerse deeper than in still water.

In both cases, as mentioned above it is assumed that wave crest or wave trough is located near amidship. This in turn affects instantaneous restoring energy in rolling motion and eventually total stability qualities. One can no longer treat metacentric height of the ship as constant. Metacentric height becomes the function of wave crest position along ship length that is, function of

time. This complicates the evaluation of ship stability. Standard ship stability curve (GZ) is dependent on wave crest position along the ship length and must be determined instantaneously.

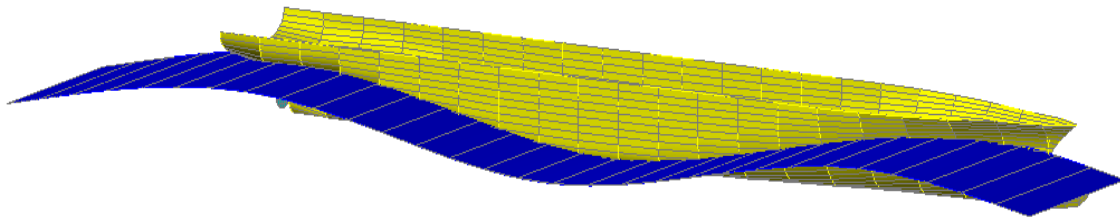


Figure 2-2. Profile of waterline in wave trough.

In pure longitudinal seas condition, the first order roll wave excitation is zero, meaning, if a ship sailed on a course exactly perpendicular to the crests of head or following seas, there would be no wave induced heeling moment. However, the ship may experience a very small roll disturbance from some external or internal cause (in reality, roll disturbances can always exist, e.g., wind). Nevertheless, if the period of wave encounter is approximately one-half the natural period of roll, a rolling motion can exist even in the absence of a direct roll exciting moment, but from the periodic variation of ship's righting arms with the ship's longitudinal position relative to wave profile. This phenomenon is referred to as auto parametrically excited motion which is usually shortened to parametric motion or parametric roll. The term describes a state of motion that results not from direct excitation by a time-varying external force or moment but from the periodic variation of certain parameters of the oscillating system.

This can be illustrated by a simple case of pendulum with its momentum, speed and distance interactions. The problem of the swing is undoubtedly one of the classical problems in mechanics. It is well known that, to swing a swing one must crouch in the middle vertical position and straighten up in the extreme positions, i.e. perform oscillations with a frequency which is approximately double the frequency of natural oscillations of the swing. While swinging, to maintain the oscillations one can crouch half as often.

For ships, forces that induce roll are always present at sea. They are resisted by a righting moment, a balancing force inherent to its shape that makes the vessel behave like a pendulum in its give-and-take with the sea. Should a force cause the ship to roll, stability provides the counter force that tries to return it to the neutral position (Fig. 2-3).

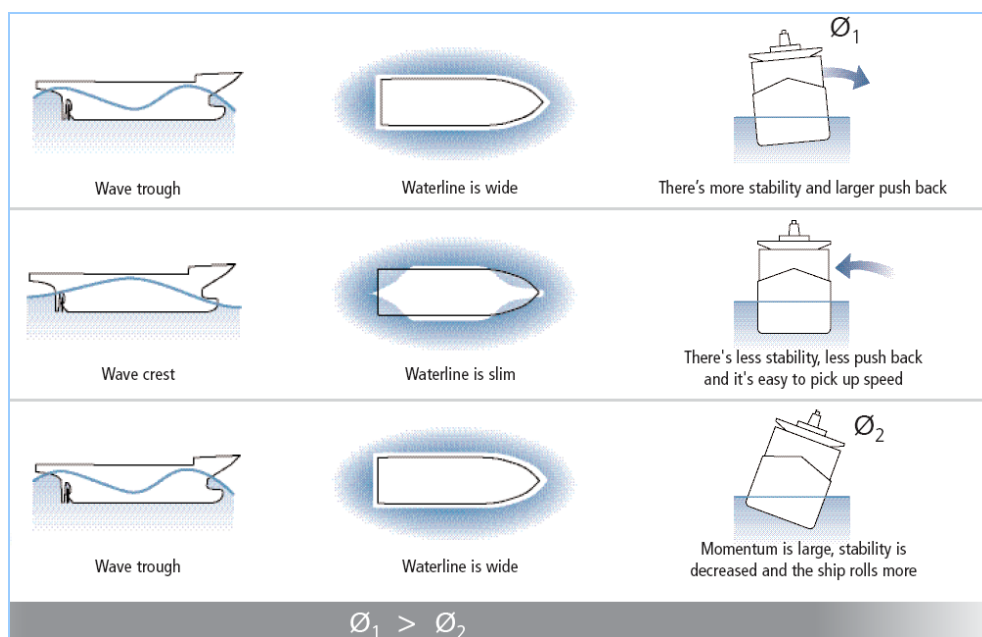


Figure 2-3. Schematic representation of a hull contact with the sea, with respect to beam changes as a cause of parametric roll resonance.

The momentum of the return movement pushes the ship a little beyond the neutral position, a process that continues in ever smaller swings until momentum is exhausted and the rolling stops. If the ship length is close to the wavelength, it will experience a series of situations in which the midship is sitting either deep into a peak or shallow in a trough, while, at the same moment, the bow and stern are each either shallow in a trough or deep in a peak respectively. In terms of the hull's contact with the sea, the ship effectively changes its beam on a regular basis, from slim (when the midship is on a peak) to wide (when the bow and stern are on peaks). Because stability varies with beam, as the vessel drives through the series of wave fronts, its stability – the source of its resistance to roll – changes dramatically as the midship moves from crest (maximum) to trough (minimum). This variation is the underlying condition that drives parametric roll.

Thus in parametric resonance, one can observe that the roll motion and periodic variations of stability coincide in a certain distinctive way. This combination of restoring (with a larger-than-calm-water) and resisting the roll (with less-than-calm-water), can cause the roll angle to progressively increase to a large and possibly dangerous level. During a number of consecutive rolls, the momentum inherent in the rolling ship at the end of each righting is greater than it had been at the beginning of the preceding inclining, due to the surplus of effective stability gathered during righting. The fact that inclining at reduced stability alternates with righting at increased stability can only lead to excitation of roll if this alternation is repeated regularly and sufficiently often.

To be precise, the ship gains additional momentum during each righting and thus twice during a complete roll motion, while stability changes at twice the rate relative to the roll motion. This causes stability to shift closer to its maximum prior to and during righting. The difference between effective stability during inclining on one hand and during righting on the other is intensified, which increases the additional momentum gained during each half roll.

2.1.2 Influence of Roll Damping

Roll damping is another important parameter in parametric rolling realisation. As it is known, in calm water, roll damping decreases roll amplitudes owing to the ship generated waves, eddies and viscous drag. Meaning, the roll amplitudes of a disturbed ship decrease successively due to roll damping. Normally, the damping coefficients can be obtained from free decay experiments, in which the model is released for a free roll from a given inclination. In this work, the roll damping coefficient for C11 post-Panamax containership is investigated experimentally.

Usage of such an empirical roll damping assessment, established from the free decay model tests led to a few applicable analytical methods (Miller 1974, Ikeda et al. 1978). Ikeda (1978) divided the roll damping into a number of components and he also proposed different empirical formulae for the various components comprising the roll damping.

The prediction of roll motion is directly affected by roll damping coefficients. The methodology to obtain the non-linear roll damping from decay tests is very old. It has been proposed by Froude in the 19th century and used from then on. Behind it, there is a quadratic or cubic model for the damping and a subsequent equivalent linearization. The solution is obtained by means of the averaging technique. The obtained expression is used in a fitting procedure in order to evaluate the parameters of the analytical model. Probably all model basins in the world follow this approach to assess the damping from a decay test. This is very general in the sense that in principle, it could be applied to any kind of hull. Accurate estimation of the roll-damping coefficient is of central interest in roll motion analysis because the roll motion is sensitive to the roll damping near resonance.

There is a term associated with the before mentioned effect of roll damping called roll damping threshold for parametric roll resonance. The parametric roll resonance can take place if the roll damping moment is below the threshold, meaning that the energy “gain” per cycle caused by the changing stability in longitudinal seas is more than the energy “loss” due to damping. This fact can simply be explained by the energy balance between damping and change of stability, basically the

condition that has to be met is that the energy loss due to roll damping is not large enough to completely consume the increase of energy caused by parametric roll resonance (Taylan 2007). Linear damping increases with speed due to lift effect, while nonlinear damping due to hull vortex shedding tends to reduce. Nonlinear damping due to bilge keels tends to be quite unaffected by speed. However, since parametric roll inception is associated to linear damping, the increase of speed increases also the threshold for the inception of parametric rolling. Thus, the damping will increase, some time or later, up to a certain extent. At that time, the dissipated energy from damping is more than the extra input energy from parametric resonance. As a result, nonlinearity of damping has a function to stabilize the parametric rolling motion of ships.

2.1.3 Amplitude of Parametric Roll

When considering the amplitude of parametric rolling one of the most important factors that determine it is the shape of the GZ curve. Apart from the above condition of frequencies to build-up a parametric rolling, meaning that the ship gains additional momentum during each righting and thus twice during a complete roll motion, a threshold wave height must be determined as well.

While the GZ curve usually is practically linear in the first 10-12 degrees of heel angle (at least for sufficiently large GM), the GM does not change, so both natural roll period and frequency remain constant for small values of roll angle. If the righting lever curve rises considerably above its slope at zero inclination (tangent at its origin) it shows a pronounced non-linearity. The reason for this is mainly high freeboard. With a righting lever curve (GZ curve) of the typical character, once the roll angle increases beyond the linear portion of the GZ curve, the instantaneous GM value changes as the GZ curve bends.

As already stated this affects instantaneous restoring energy in rolling motion and eventually total stability qualities. One can no longer treat metacentric height of the ship as constant. This complicates the evaluation of ship stability. Standard ship stability curve (GZ) is dependent on wave crest position along the ship length and must be determined instantaneously (Fig. 2-4). It can be said that periods of encounter which are half the period of roll at dangerous roll amplitudes are in a way a function of GM as well, since the periods of roll as a function of GM vary much less at large angles with a change of GM than the period at small angles.

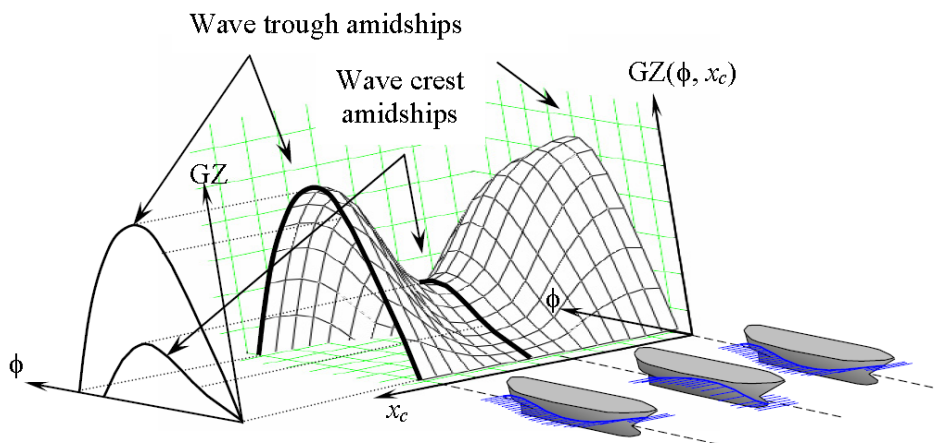


Figure 2-4. Schematics of the restoring moment as a function of wave position and heel angle, ABS (2004)

Because of the pronounced tendency of the roll period being adapted to the encounter period, parametric resonance will exist for a range of periods of encounter. Since the wave encounter frequency remains the same, the roll natural frequency may no longer be close to twice the encounter frequency. As a result, parametric resonance conditions no longer exist and roll motions no longer receive additional energy at each cycle. Therefore, after certain angles of roll, conditions for parametric resonance cannot be established and the growth stops.

2.1.4 Influence of hull forms

Hull forms with pronounced bow flare, flat transom stern and nonvertical ship sides near the waterline are most vulnerable to the parametric roll. Such ships have wide deck beam to store large number of containers and at the same time, the underwater hull is streamlined to minimize the resistance. Certain ship typologies, typically characterised by former attributes, can be susceptible to the inception of parametrically excited rolling motions, while others, typically full and mainly with practically vertical sides, are relatively free from the risk associated to this phenomenon. With respect to the inception of parametric roll, the former can be considered as potentially "vulnerable", while the latter can be considered as likely "not vulnerable". Ironically, part of the problem is a consequence of good design. Above the waterline, it is designed to maximize on-deck stowage capacity by extending a wide main deck as far forward as possible, inducing significant bow flare, and as far aft as possible with a large stern overhang. It is extremely important to note that parametric roll, for certain ship typologies, cannot be completely avoided by design, at least if the design is to be kept cost effective. For this reason part of the countermeasures to reduce the inception of parametrically excited rolling motion can be taken in terms of design parameter, while part of the safety against parametric roll could be guaranteed by means of ship-specific operational guidance.

In the forebody the breadth is sharply reduced whereas in the afterbody there is pronounced flare and the hull's full breadth extends up to the transom. It must be mentioned that although the bow flare does not directly influence the occurrence of parametric roll it can indirectly influence it. A more pronounced bow flare will result in more slamming events which in turn will make a vessel master decide to reduce the speed earlier than a vessel with a less pronounced bow flare. Because the roll damping at low speed is smaller it is generally more vulnerable to parametric roll than at high speed. So, indirectly the bow flare can have influence on the occurrence of parametric roll. Such hull features contribute to the variation of the ship's stability characteristics due to the constant change of the underwater hull geometry as waves travel along the ship (Fig. 2-1).

2.1.5 Influence of ahead speed and wave direction

Longitudinal waves (head and following) cause the largest change in ship's intact stability and, therefore, create maximum parametric excitation. As the vessel passes through the waves, it encounters a series of wave peaks and troughs. The speed at which this happens is called the encounter frequency.

A ship moving through the waves encounters them with a different frequency than a ship that is not moving. Encounter frequency which may be defined as the frequency that ship passes through wave troughs and crests with or frequency of change of ship stability, is another important factor for a ship moving in waves. It is smaller for following seas (ship speed is subtracted from wave celerity) and larger for head seas (wave celerity is added to ship ahead speed). In terms of parametric resonance, the relative direction of ship's heading with respect to waves is very critical (Shin et al., 2004). As stated, following and head seas are the most critical directions in this respect. A chain of events between the suitable combination of ship speed, direction, metacentric height and wave characteristics leads to parametric roll resonance. Because frequency of encounter depends on the wave frequency it is also related to the wavelength.

To conclude, all these parameters that are encountered with the aim of identifying ships prone to the inception of parametrically excited rolling motion, while trying to be clarified and understood, have to be considered critical since they are associated as a precondition for sudden severe roll motions. Important parameters that are effective in roll resonance were pointed out. An unfavourable combination of those parameters possesses a great danger especially for container ships sailing in following or head seas and can lead to momentous roll motion.

2.2 Prediction of occurrence of parametric rolling in regular waves (susceptibility criteria)

Some essential elements of roll motion are reviewed first. At a fundamental level, the equation of linear rolling motion is that of an excited ($M_x(t)$) or non excited oscillator. Oscillatory motion is periodic motion where the displacement from equilibrium varies from a maximum in one direction to a maximum in the opposite or negative direction.

Whilst considering a single degree of freedom equation for roll motion in longitudinal seas, and taking into account the changing GM due to wave encounter (Shin et al. 2004) it follows,

$$\ddot{\eta}_4 + 2\mu\dot{\eta}_4 + \frac{M \cdot GM(t)}{I_{44} + A_{44}}\eta_4 = 0 \quad (2-1)$$

Here, η_4 represents the rolling amplitude, μ is the linearised damping coefficient, M is the displacement of a ship, I_{44} is the transverse moment of inertia, and A_{44} is the added mass moment of inertia in roll.

Parametric rolling typically occurs in various combinations of ship speed and wave frequency, provided that the resulting frequency of encounter is near to $(2/n)$ times the natural frequency, where n is any integer. Theoretically it can occur at approximately $2:n$ ratios between these two frequencies, where the integer $n = 1, 2, 3, \dots$. In practice the cases for $n = 1$, when the wave encounter frequency is approximately twice the roll natural frequency, and $n = 2$, when the wave encounter and roll natural frequencies are nearly equal, are of importance. Typically the former case ($n \approx 1$) occurs in head and bow quartering seas (e.g. France et al. 2003, Belenky et al. 2003, Kreuzer et al. 2004), but it can also occur in following seas (Umeda et al. 2004). The latter case ($n \approx 2$) is typically associated with following and stern quartering seas (Krüger et al. 2004).

The single degree of freedom rolling motion of a ship in head or following seas may then be described by an equation of motion similar to that for still water. However, the restoring moment is not only a function of angle of heel but it also varies sinusoidally with time, so we may use the small amplitude moment expression with a time varying metacentric height which may result in parametric resonance (ABS, 2004),

$$\begin{aligned} GM(t) &= GM_m + GM_a \cos(\omega t) \\ GM_m &= 0.5(GM_{\max} + GM_{\min}) \\ GM_a &= 0.5(GM_{\max} - GM_{\min}) \end{aligned} \quad (2-2)$$

Here, GM_m is the mean value of the GM and GM_a is the amplitude of the GM changes in waves. Mean rolling frequency and its variation amplitude are as follows:

$$\omega_m = \sqrt{\frac{M \cdot GM_m}{I_{44} + A_{44}}}; \quad \omega_a = \sqrt{\frac{M \cdot GM_a}{I_{44} + A_{44}}} \quad (2-3)$$

and can be included in (2-1), with the following equation derived:

$$\ddot{\eta}_4 + 2\mu\dot{\eta}_4 + (\omega_m^2 + \omega_a^2 \cos(\omega t))\eta_4 = 0 \quad (2-4)$$

2.2.1 Linearization procedure of the righting arm variation

Considering the righting arm variation with respect to the relative position of ship in waves GZ (wave) on longitudinal waves, the GZ (wave) decreases with the wave crest amidships and increases with the wave trough amidships, in comparison with the still water righting arm GZ (still).

Additionally, Figure 2-5 shows the righting arm curves of the C11 post-Panamax container ship referring to the ship on the wave crest GZ (crest), wave trough GZ (trough), and in still water GZ (still). The results shown in figure 2-5, were calculated in Matlab for a regular sine wave with a length about the same length of the ship (262.00 m).

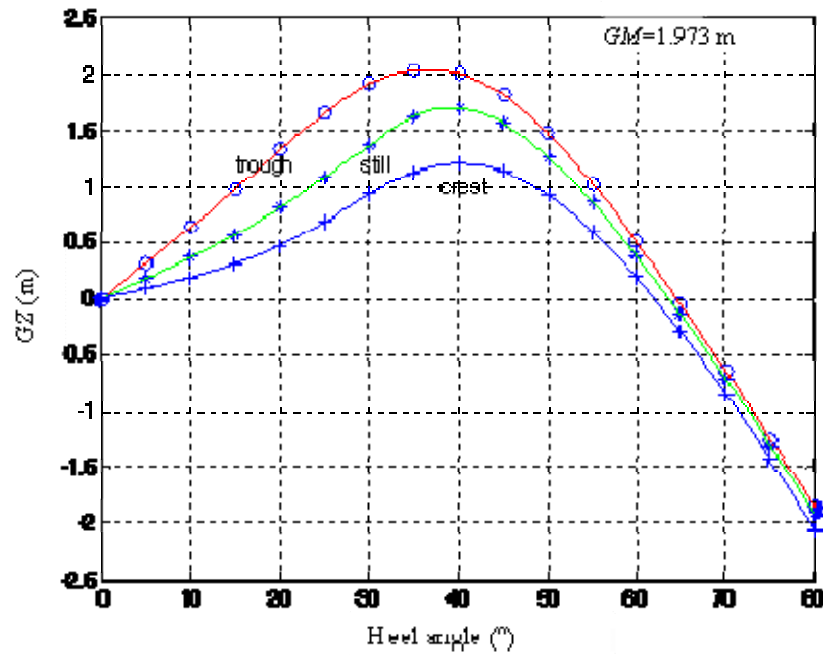


Figure 2-5. The righting arm (GZ) curves

According to Hamamoto et. al (1996), when the ship is rolling in head seas at large inclination angles, the equivalent metacentric height can be determined on the basis of the linearised righting arm up to an appropriate roll angle as follows on figure 2-6.

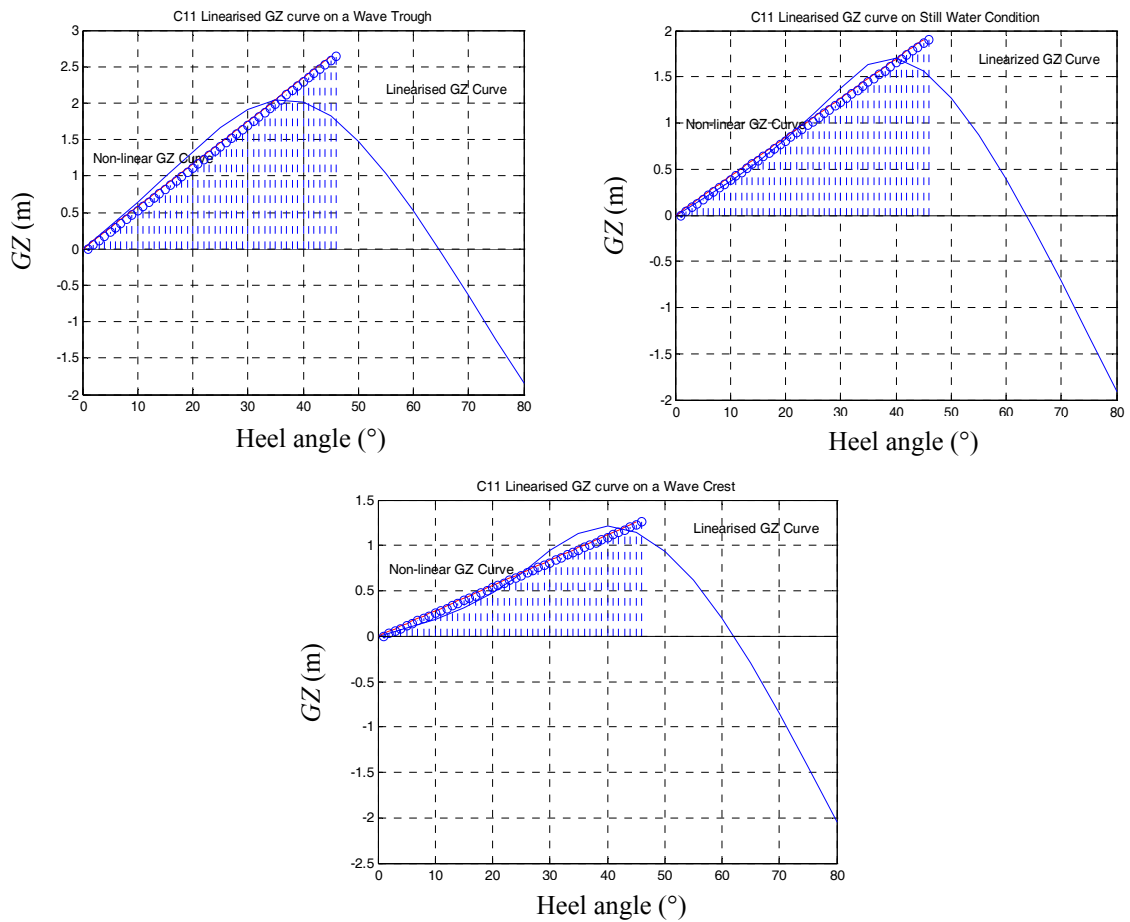


Figure 2-6. Equivalent righting arm curves up to 45° on a wave trough GZ (trough), in still water GZ (still) conditions, and on a wave crest GZ (crest) condition.

Figure 2-6 shows the linearisation procedure of the metacentric heights, is graphically represented (equivalent area under the righting arm curves) for a specific condition and mathematically given by,

$$GM_{(cond)} = \frac{2}{\eta_4} \int_0^{\eta_4} GZ_{(cond)} d\eta_4 \tag{2-5}$$

Stability in waves is to be computed for a number of positions of wave crest along the hull, then maximal and minimal GM values are to be evaluated. The difference between maximum and minimum values defines the amplitude of parametric excitation. In order for the susceptibility criteria to be used, the parametric excitation is presented in the form of a value oscillating as cosine function about the mean value (Kerwin, 1955), assumption of the variation of the metacentric height relative to the position of the wave along the ship hull), which is obtained by averaging the GM from the above-mentioned calculations and numerically given by ,

$$GM_{(wave)} = GM_{(still)} \left[1 + \overbrace{\left(\frac{GM_m}{GM_{(still)}} - 1 \right)}^{a_0} + \overbrace{\frac{GM_a}{GM_{(still)}} \cos \omega_e t}^{a_1} \right] \tag{2-6}$$

Maximal GM value is expected when the wave trough is close to amidships and the minimum GM value is expected when the wave crest is close to (but not necessarily exactly at) amidships. Further considerations are required to specify this variation on the basis of a reasonable method leading to an equivalent solution. Therefore, the equivalent linearised righting arm curve is,

$$GZ(\eta_4, t) = GM_{(wave)} \cdot d\eta_4 \tag{2-7}$$

Fig. 2-7 depicts a form for the GM variation and hence can be approximated into Mathieu’s equation. The comparison between the Mathieu fit and actual GM is also shown in Fig. 2-7. As shown by (Spyrou et al., 2008) a case of cosine fit of GM with a phase shift has a better fit. The phase shift used there is $\pi/8$.

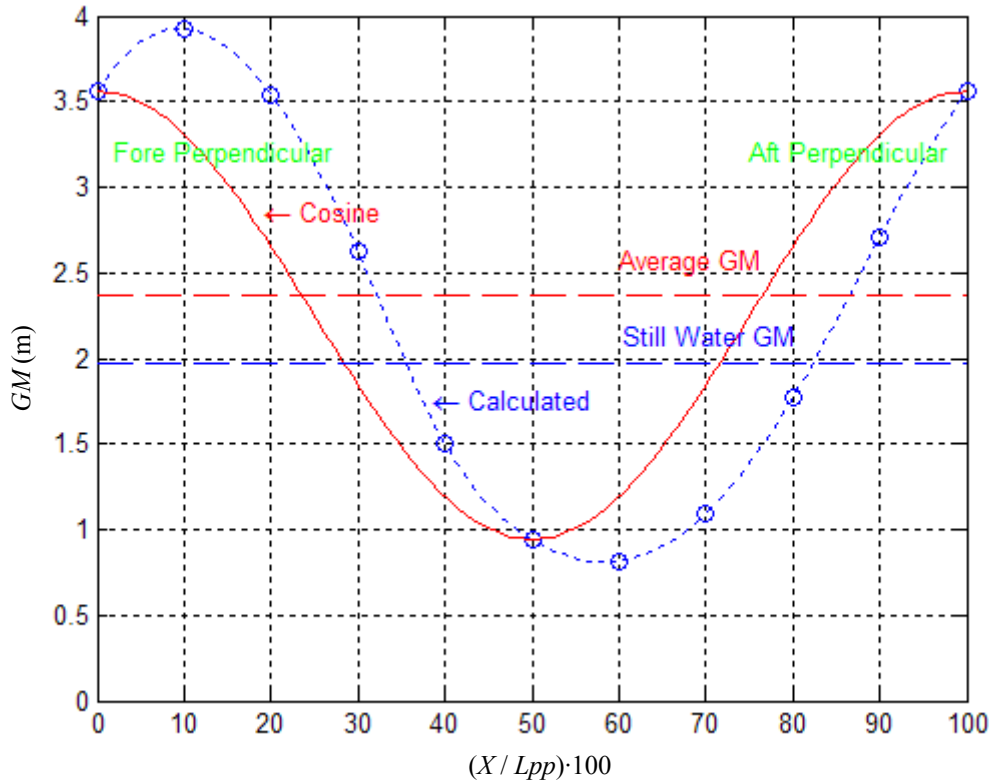


Figure 2-7. Wave-induced variation of the metacentric height $GM_{(wave)}$.

The poor fit of the Mathieu approximation (even with phase shifted) to the actual GM variation is clearly evident. Hence, there is a need to use a method with which approximates the GM variation more accurately. To check if parametric resonance is possible, the roll equation (2-4) must be transformed to the Mathieu type varying restoring coefficient of the form,

$$\frac{d^2 \eta_4}{d\tau^2} + (p + q \cos \tau) \eta_4 = 0 \quad (2-8)$$

where p is a function of the ratio of forcing and natural frequency, q the parameter that dictates the amplitude of parametric excitation, and τ represents non-dimensional time. It must be noted that individual calculation of the GM values for successive instantaneous wave positions along the ship gives a more realistic picture, instead of the sinusoidal expression.

2.2.2 Stability charts

If the ship rolling is of Mathieu-type then there is a possibility of parametric resonance. It will be manifested by an oscillatory build-up of roll, despite the absence of direct excitation. The physical phenomenon is based on successive alterations of the restoring rolling moment lever between crests and troughs, exhibited by many ships in steep longitudinal waves with a clear analogy with a simple oscillator governed by the Mathieu equation with damping.

To obtain the standard form of the Mathieu equation (2-8) it is necessary to transform equation (2-4) by introducing a dimensionless time $\tau = \omega t \Rightarrow t = \tau / \omega$. That gives the following expression,

$$\frac{d^2 \eta_4}{d\tau^2} + 2\mu \frac{d\eta_4}{d\tau} + (\bar{\omega}_m^2 + \bar{\omega}_a^2 \cos(\tau)) \eta_4 = 0 \quad (2-9)$$

By doing that and dividing both terms by the square of the wave frequency ω^2 , the dimensionless quantities:

$$\bar{\mu} = \frac{\mu}{\omega}; \quad \bar{\omega}_m = \frac{\omega_m}{\omega}; \quad \bar{\omega}_a = \frac{\omega_a}{\omega} \quad (2-10)$$

are obtained, where ω_a is the rolling variation frequency and ω_m is the mean value of rolling frequency. The damping part is excluded by:

$$\eta_4(\tau) = x(\tau) e^{(-\mu\tau)} \quad (2-11)$$

This finally expresses roll in the form of a Mathieu equation (2-11) with coefficients,

$$p = (\bar{\omega}_m^2 - \bar{\mu}^2); \quad q = \bar{\omega}_a^2. \quad (2-12)$$

Another proposition to tackle the prediction of parametric rolling due to principal resonance is made by following simple rule based on consideration of the asymptotic stability of the up-right state of a ship in longitudinal waves, by ITTC guidelines.

If GM varies on the wave between GM_{\min} and GM_{\max} , and the scaled amplitude of variation of metacentric height, defined as follows:

$$h = \frac{GM_{\max} - GM_{\min}}{2 \cdot GM_m} \quad (2-13)$$

exceeds 4 times roll damping ratio (2-14) which is a well known result. Then, the occurrence of parametric rolling is possible. It is associated with so called threshold values for the excitation of parametric rolling in different instability zones, corresponding to the frequency ratios $\omega_e = (2/n)\omega_0$,

$$\frac{\delta GM_m}{GM_m} = \frac{GM_a}{GM_m} = \frac{4\mu}{\omega_0} \quad (2-14)$$

The threshold of the parametric rolling phenomena as far as the first instability zone is concerned is given by the Francescutto deterministic method (2001) by following inequalities:

$$2 - \frac{\omega_e^2}{2\omega_0^2} < \frac{GM_a}{GM_m} < \frac{\omega_e^2}{2\omega_0^2} - 2 \quad (2-15)$$

By introducing ω_e as the encounter frequency and ε as an appropriate phase difference, this variation of GM can be reflected in the equation of roll motion as follows:

$$\ddot{\eta}_4 + 2\mu\omega_0\dot{\eta}_4 + \omega_0^2\{1 - h\cos(\omega_e t - \varepsilon)\}\eta_4 = 0 \quad (2-16)$$

The ITTC procedures for parametric roll implicitly address the presence of multiple steady states when providing the analytical solution of the steady rolling amplitude for a nonlinear 1-DOF model. The variation of the roll natural frequency,

$$\omega_0 = \sqrt{m \cdot g \cdot GM_m / (I_X + A_{44})} \quad (2-17)$$

ITTC's boundary of instability (h threshold) refers to infinitesimal perturbations of the upright state; therefore, nonlinear restoring terms do not participate. The proposed expression for the first region or in the vicinity of exact principal resonance may be used for the threshold level of the scaled GM fluctuation:

$$h = \sqrt{\left(2 - \frac{\omega_e^2}{2\omega_0^2}\right)^2 + 4\mu^2 \frac{\omega_e^2}{\omega_0^2}} \quad (2-18)$$

where,

$$\omega_e^2 p = \omega_m^2 - \omega_0^2 \mu^2 = \frac{M(GM_{\max} + GM_{\min})}{2(I_{44} + A_{44})} - \omega_0^2 \mu^2 \quad (2-19)$$

$$\omega_e^2 p = \omega_a^2 = \frac{M(GM_{\max} - GM_{\min})}{2(I_{44} + A_{44})} - \omega_0^2 \mu^2$$

Moving upwards, from the above boundary curve, in terms of h , the build-up of parametric rolling becomes quicker. It is actually the 1st-order approximation of the Mathieu functions that truly define the boundary. At this point a first analogy between two proposed guidelines can be established, with respect to the consideration for establishing susceptibility criteria. Both guidelines contain analytical ‘‘closed-form’’ expressions for assessing, to first approximation, a ship's susceptibility to parametric instability and the steady amplitude of the incurred oscillatory response.

An expression from Hayashi (1953) is the basis of a higher-order approximation targeted by ABS. The ship is said to be susceptible to parametric resonance if the following inequality holds,

$$0.25 - 0.5 \cdot q - 0.125 \cdot q^2 + 0.03125 \cdot q^3 - \frac{q^4}{384} \leq p \leq 0.25 + 0.5 \cdot q \quad (2-20)$$

The full ABS procedure can be presented upon request to the author as a spreadsheet calculation technique for wave influence on GM . If the inequality (2-20) is not satisfied, the ship may not be susceptible to parametric roll.

ABS have calibrated eq. (2-20) with reference to numerical data and then converted it to an expression of damping threshold. In the case when the inequality (2-20) is met, the damping criterion of susceptibility is to be checked:

$$\mu \frac{\omega_0}{\omega_e} < q \cdot k_1 \cdot k_2 \cdot \sqrt{1 - k_3^2} \quad (2-21)$$

Coefficients k_1 , k_2 and k_3 can be calculated as follows:

$$k_1 = 1 - 0.1875 \cdot q^2$$

$$k_2 = 1.002 \cdot p + 0.16 \cdot q + 0.759 \quad (2-22)$$

$$k_3 = \frac{q^2 - 16 + \sqrt{q^4 + 352 \cdot q^2 + 1024 \cdot p}}{16 \cdot q}$$

If $k_3 > 1$, damping criterion is considered as not satisfied. If $k_3 < 1$ and inequality (2-21) is not satisfied, the ship's susceptibility to parametric roll is unlikely. If both inequalities (2-20) and (2-21) are satisfied, the severity criterion is to be checked. As already stated, if the inequality (2-20) does not hold, then the vessel may not be susceptible to parametric resonance.

However, whilst plotting the stability charts an anomaly is traced. As seen from figure 2-8, the equation (2-20) used to develop Mathieu charts, within the range of validity of these charts is very limited, opposite as expected. The graph obtained using ABS procedure is inconsistent with the theory and a separation of stability regions is evident.

The basis of equation (2-20) is a higher-order approximation targeted assuming small perturbations, enabling to adopt a perturbation method given by the appropriate series expansion. The whole procedure and expression for the desired solution in terms of a formal power series in some "small" parameter that quantifies the deviation from the exactly solvable problem is given in Ribeiro e Silva et al., 2008. The equation represents the change in oscillation frequency resulting from the temporal variation of restoring term and associating the terms of the same order in q . It follows system of linear equations, to be solved sequentially. However, the expansion is not represented with the same higher-order on both sides that may be found iteratively by some systematic procedure. The right side of equation is an approximate "perturbation solution" obtained by truncating the series, by keeping only the first two terms, leading to the initial solution and the "first order" perturbation correction. In essence this is wrong. For that reason as reported in Turk et al. (2008), a number of suspect ships evaluated were prone to parametric rolling which questions the procedure implemented and the guidelines as well. The correct approach would be to expand the desired deviation in the solution, due to the deviation from the initial problem up to the same order (4th order).

Solution of the Mathieu equation may be found in many references and depends strictly on the values of p and q . The parameter q reflects the level of GM change in waves, therefore plays the role of amplitude of parametric excitation. Thus, the solution may be periodic (since the damping was excluded by the substitution (2-11)), increasing or decreasing in nature. Figure 2-9 is the stability diagram for this equation. The shaded regions are stable corresponding to (p,q) pairs where motion cannot exist and the unshaded regions which are unstable, i.e., motion can exist. If (p,q) lie in an unstable region, an arbitrarily small initial disturbance will trigger an oscillatory motion that tends to increase indefinitely with time. In a stable region, the initial disturbance will cease to exist with time (Turk et al. 2008).

The Ince–Strutt diagram in Fig. 2-9 shows zones where combinations of parameters p and q in Mathieu equation result in unstable solutions (Zone 1 and Zone 2, in fig. 2-9). There are several zones of instability: the first zone starts exactly from $p = 0.25$ and corresponds to a natural period exactly twice the period of parametric excitation, (or ratio of natural frequency to frequency of GM variation of 0.5) commonly referred to as the principal parametric resonance. The predominant value of this ratio (0.5) means that this instability phenomenon is an example of a dynamic motion "bifurcation", that is, a situation in which either of two states of motion, zero or the growing oscillation, can exist depending on the absence or presence of an initial disturbance.

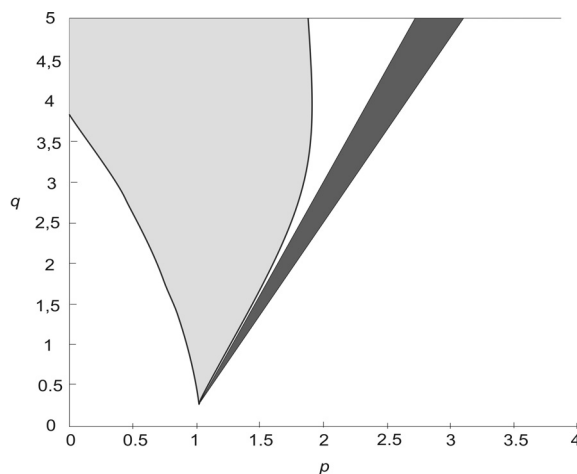


Figure 2-8. Stability charts using ABS procedure

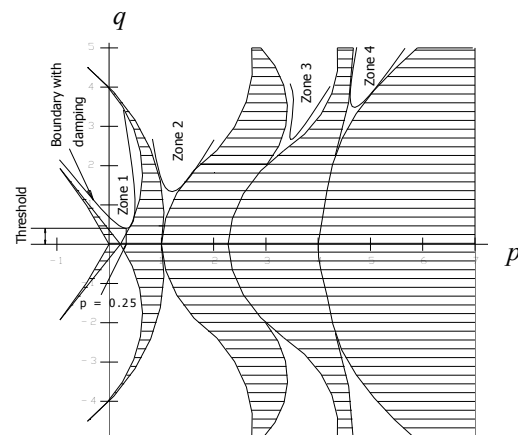


Figure 2-9. Stability diagram for the Mathieu equation

Each zone touches the p -axis and, with an increase of q , becomes wider. Furthermore, the zones with the smaller values of p -intercept grow in width even faster. For instance, the second zone referred to as the fundamental parametric resonance, starts at $p = 1$, which corresponds to excitation frequency that is equal to the natural roll frequency.

To summarize, if the damping function is ignored ($\mu = 0$), the unstable zones: Zone 1, Zone 2, Zone 3, touch the p -axis at $p = 0.25, 1, 2.25, \dots$ respectively. The unstable zones correspond to the period ratios shown by eq. (2-20):

$$\frac{T_e}{T_0} = \frac{1}{2}, 1, 1\frac{1}{2}, 2, 2\frac{1}{2} \dots \tag{2-23}$$

where T_0 is the natural frequency of ship rolling, and T_e denotes the variation period of GM values, namely the encounter frequency ω_e .

Grim (1952) has shown a result that the parametric roll angles will rapidly decrease with increasing p values (reduction of ω_e). Thus only the preceding two unstable zones (Zone 1 and Zone 2) could bring about a danger of ship capsizing. France (2003) however, identified only the principal parametric regimes during analysis of extreme ship motion of the C11 post-Panamax container. Since the first zone is wider, and thus frequency range as well only the principal parametric resonance will be considered (Fig. 2-23).

The transformation into the Mathieu type equation was a prerequisite in order to use the Ince-Strutt diagram to examine the properties of the solutions. Linear approximations for the boundaries of the first instability zone of the Ince-Strutt diagram are given by (Stoker, 1950):

$$p_{b1} = 0,25 - 0,5 \cdot q \quad p_{b2} = 0,25 + 0,5 \cdot q \tag{2-24}$$

while higher order approximations, as mentioned previously, are available from (Hayashi, 1953), transformed for the Mathieu equation (2-8):

$$p_{b1} = 0,25 - 0,5 \cdot q - 0,125 \cdot q^2 + 0,03125 \cdot q^3 - \frac{q^4}{384}$$

$$p_{b2} = 0,25 + 0,5 \cdot q - 0,125 \cdot q^2 - 0,03125 \cdot q^3 - \frac{q^4}{384} \tag{2-25}$$

Just as an illustration, both approximations for the first instability zone are shown in Figure 2-10. An example for C11 post-Panamax is given. Depending on where the (p, q) pair falls in the chart, it becomes trivial to predict parametric instability. As shown in Figure 2-10, the operational conditions fall into a Mathieu type zone of instability. The ship may be susceptible to parametric rolling and the severity criterion has to be checked.

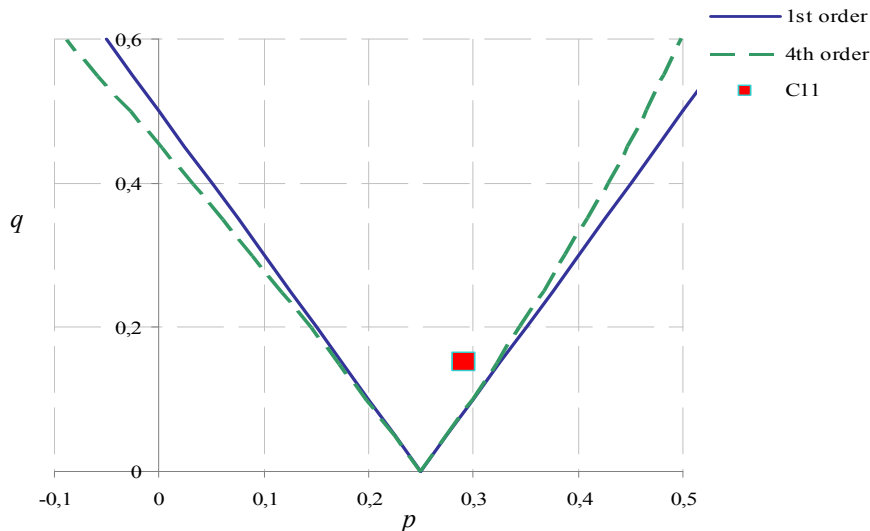


Figure 2-10. Linear (solid) and high-order (dashed) approximations for the boundary of the first instability zone (Turk et al. 2009).

Since the $\lambda/Lpp = 262.00$ m, for deep water the wave frequency is given by $\omega^2 = g \frac{2\pi}{\lambda} = 0.485$ rad/s, and the ship's natural frequency of roll is given by $\omega_0 = \frac{2\pi}{T_0} = 0.25$ rad/s,

while the damping ratio is $\mu = \frac{B_{44}(\omega_0)}{2(I_{44} + A(\omega_0))\omega_0} \approx 0.003$. Hence, the parameter $p = \left(\frac{\omega_0}{\omega}\right)^2 = 0.275$,

since $\omega_D \approx \omega_0$. Looking at the Mathieu Chart (Fig.2-10) this value is very close to principal parametric resonance zone ($p = 0.25$).

A major drawback of the method is that the Ince-Strutt diagram for Mathieu's equation is generic and does not depend on the ship characteristics. A stability chart which depends on the ship parameters would be a more accurate approach. A linear damping to Mathieu equation does not limit the amplitude of a solution. The effect of linear damping is only raising the boundary of unstable zones, i.e. creating a threshold for the amplitude of GM variation in waves (q value). The unstable rolling motions will still happen if the p value is larger than the threshold value. This is why it is possible to use Mathieu equation for modelling the occurrence amplified motions caused by parametric excitation, but not for evaluating how large the parametric oscillations might develop. To do so, nonlinear damping and/or stiffness terms must be added to "stabilize" the rising oscillations. In particular for evaluating the actual value of parametric rolling, the factors, which have to be taken into account, include at least the nonlinear shape of righting arm curve, nonlinear damping and cross coupling among 6 DOF.

Furthermore, it also means that there is a threshold value for roll damping for each pair of Mathieu parameters p and q . To calculate this threshold, it is necessary to find a way to express the increment of the unbounded solution of the Mathieu equation (e.g. ABS).

$$\mu_T = \frac{1}{2}q \left(1 - \frac{3}{16}q\right) \sqrt{1 - \left(\frac{q^2 - 16 - \sqrt{q^4 + 352q^2 + 1024p}}{16q}\right)^2} \quad (2-26)$$

Damping is initially set equal to the threshold according to equation (2-26) and then increased until the solution becomes bounded. The correction coefficient with different combinations of the dimensionless frequencies is searched in the form:

$$f(\bar{\omega}_a, \bar{\omega}_m) = a_1 \bar{\omega}_a + a_2 \bar{\omega}_m + a_3 \quad (2-27)$$

while the corresponding coefficients are found by a linear regression based on numerical integration of the roll equation (2-1) as a part of a calibration procedure that yields,

$$k = 1.022\bar{\omega}_a + 0.16a_2\bar{\omega}_m - 0.744 \quad (2-28)$$

It represents a correction of the error, intended to obtain the final form of the damping threshold coefficient given by (2-21).

Depending on the critical values of roll damping, parametric resonance may or may not take place. This fact can simply be explained by the energy balance between damping and change of stability. The nonlinearity in restoring and/or in damping was considered by a number of researchers, including Blocki (1980), Sanchez and Nayfeh (1990). It has been shown that if restoring and/or damping are nonlinear, then stable oscillations may exist. The nonlinearity may in fact be beneficial, impeding capsizing by 'arresting' the growing oscillation incurred at an instability point. Remarkably, this can happen although the nonlinear system may possess less restoring at similar angles because the change in restoring causes de-tuning from resonance, in other words the exponential term $e^{(-\mu r)}$ might undo the effect of boundlessness by damping the solution back to a decaying form.

The Mathieu instability criterion is the most common method used to determine the onset of parametric roll. Most of the studies have been done with stability charts that do not indicate the effects of damping. Since parametric excitation can lead to large amplitude roll motion, the effects of nonlinear damping cannot be neglected. Damping dramatically affects the boundaries between the stable and unstable region. Among container ships the post-panamax container ship (C11 class) is the

most studied vessel as a result of the cargo damage it suffered in 1998. Nonlinear roll damping may lead to bounded motion. Hence incorporating the effects of non-linear damping into stability charts would give a more realistic prospect of predicting roll behaviour. The standard Mathieu Equation with damping is given by,

$$\frac{d^2\eta_4}{d\tau^2} + 2\mu\frac{d\eta_4}{d\tau} + (p + q \cos \tau) \eta_4 = 0 \quad (2-29)$$

Using the method called the Hill's infinite determinant method (Moideen and Falzarano, 2010.) the solution (2π & 4π) of the equation is expressed as Fourier series,

$$\eta_{4(2\pi)}(t) = a_0 + \sum_{n=1}^{\infty} (a_n \cos(n\pi) + b_n \sin(n\pi)) \quad (2-30)$$

$$\eta_{4(4\pi)}(t) = a_0 + \sum_{n=1}^{\infty} \left(a_n \cos\left(\frac{n\pi}{2}\right) + b_n \sin\left(\frac{n\pi}{2}\right) \right) \quad (2-31)$$

Substituting Eq. (2-30) & Eq. (2-31) into Eq. (2-29) and setting the second terms to zero, we get two matrices for each solution as given below,

$$\begin{bmatrix} p & \frac{q}{2} & 0 & 0 & 0 & \dots & 0 \\ q & p-1 & \mu & \frac{q}{2} & 0 & \dots & 0 \\ 0 & -\mu & p-1 & 0 & \frac{q}{2} & \dots & 0 \\ 0 & \frac{q}{2} & 0 & p-4 & 2\mu & \frac{q}{2} & 0 \\ \dots & & & & & & \end{bmatrix} \cdot \begin{bmatrix} a_0 \\ b_0 \\ a_1 \\ b_1 \\ a_2 \\ b_2 \\ \dots \\ \dots \end{bmatrix} = 0 \quad (2-32)$$

$$\begin{bmatrix} p - \frac{1}{4} + \frac{q}{2} & \frac{\mu}{2} & \frac{q}{2} & 0 & 0 & \dots & 0 \\ -\frac{\mu}{2} & p - \frac{1}{4} - \frac{q}{2} & 0 & \frac{q}{2} & 0 & \dots & 0 \\ \frac{q}{2} & 0 & p - \frac{9}{4} & \frac{3\mu}{2} & \frac{q}{2} & \dots & 0 \\ 0 & \frac{q}{2} & -\frac{3\mu}{2} & p - \frac{9}{4} & 0 & \dots & \frac{q}{2} \\ \dots & & & & & & \end{bmatrix} \cdot \begin{bmatrix} a_0 \\ b_0 \\ a_1 \\ b_1 \\ a_2 \\ b_2 \\ \dots \\ \dots \end{bmatrix} = 0 \quad (2-33)$$

Neglecting the trivial case of $a_0 = a_1 = b_1 \dots = 0$, the determinant of the parametric matrix (matrix containing p and q) should be zero. This gives the relationship between the parameters p and q . Equation (2-9) can be reduced to its standard form using the exponential transformation resulting in (2-34). The instability boundaries for various damping ratios are shown in figure 2-11.

$$\frac{d^2\eta_4}{d\tau^2} + \left(p - \frac{\mu^2}{4} + q \cos \tau \right) \eta_4 = 0 \quad (2-34)$$

The shaded regions indicate the unstable zone. As seen from equation (2-29) the effect of damping is to elevate the curves from the p axis, thereby reducing the unstable region. In terms of energy one can imagine damping tending to drain the energy from the excitation until the threshold energy is reached to instigate parametric resonance.

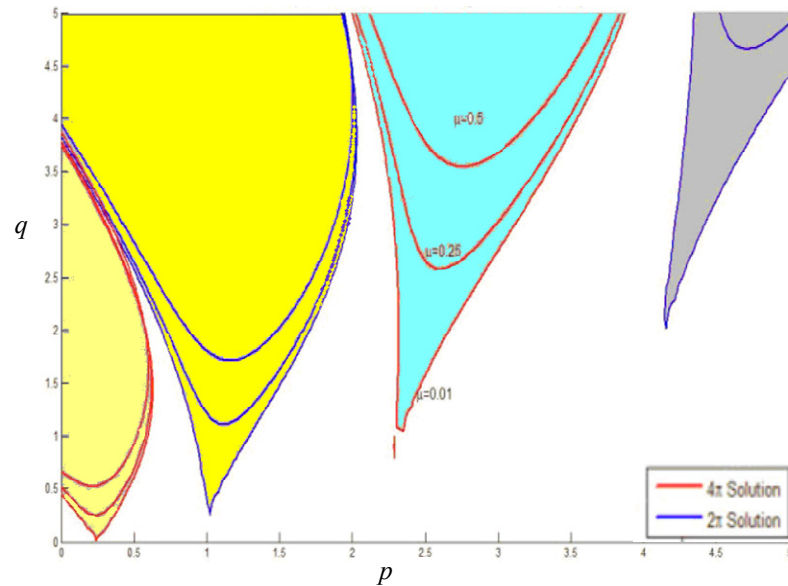


Figure 2-11. Ince-Strutt diagram for Mathieu's equation with constant damping.

To summarize, the most comprehensive mathematical method to assess susceptibility to parametric rolling is the solution of the Mathieu equation in order to see if parametric rolling occurs in numerical simulations. Technically speaking, it would be better to use a linearised (with respect to roll) 3-DOF system coupling pitch heave and roll. This is what Neves et al. (2006) has been doing and Nabergoj et al. (1994) as well. The "pure Mathieu" approach is reasonable when the amplitude of the parametric oscillation (and also the remaining parameters) takes heave and pitch into account. To conclude, from theory and as validated by model tests (Dallinga et al., 1998; and France et al., 2003), parametric roll occurs when the following requirements are satisfied:

1. natural period of roll is equal to approximately twice the wave encounter period, which in terms of the Mathieu parameters p and q should belong to an instability zone on the Ince-Strutt diagram,
 2. wave length is on the order of the ship length (between 0.8 and 2 times L_{pp}) which affects stability changes for the given ship geometry,
 3. wave height exceeds a critical level,
- which is summarized as the *frequency condition*, making the encounter frequency, ω_e major factor in the development of parametric roll;
4. roll damping should be below the damping threshold.
- which is summarized as the *damping condition*.

However, within the recent framework for the development of IMO New Generation Intact Stability Criteria mentioned in the previous chapter, a significant role is played for the development of a "vulnerability assessment methodology" to be applied in the early design stage with the aim of identifying ships prone to the inception of parametrically excited rolling motion. The term susceptibility is omitted on purpose and the new term vulnerability is introduced to distinguish the basic difference since it accounts for the case of irregular waves based on a "regular wave environment" by considering the following "practical equivalence":

- wave length is equal to the wave length associated to the modal spectral frequency,
- wave height is equal to the significant wave height.

2.3 Prediction of amplitude of parametric rolling (severity criteria)

Susceptibility criterion as already stated, is utilized to check whether the situation indicates any vulnerability. Finally, if any susceptibility is detected, the severity of parametric roll can be calculated following a couple of the proposed numerical procedures (ABS, 2004; ITTC, 2005). Any solution based on the Mathieu equation can only indicate the conditions when parametric rolling can occur, but it's unable to predict the rolling amplitude i.e. the unstable motion will grow without bound. Therefore, one can say that applicability of Mathieu equation is limited because it's linear, and as such not enough for engineering practice. Whilst the onset of instability is a "linear" phenomenon, the finite roll amplitude that accrues from the loss of stability is critically influenced by nonlinearities. The effect of linear damping is merely to raise the threshold value for the amplitude of GM variation in waves at a given frequency of variation, ω .

However, if conditions do satisfy the susceptibility criteria the solution must determine how large the parametric rolling might develop. Parametric rolling is limited to finite steady state amplitude, even though the motion angles develop rapidly and up to large amplitudes. Real circumstances, therefore present much more complex situation. To evaluate the actual amplitude of parametric rolling, the factors, that have to be weighted in, include at least the nonlinear shape of righting arm curve, nonlinear damping and cross coupling among 6 DOF, among others. Direct, as well as parametric excitation of roll and other motions from wave components oblique to the ship affect the motion response.

The chain of events between the suitable combination of ship speed, direction, metacentric height and wave characteristics leads to parametric roll resonance. The two major nonlinear terms in the one-degree-of-freedom rolling equation that stabilize parametric rolling refer to the shape of righting arm curve and rolling damping. Both of the factors can limit parametric roll, but the physics of their actions are different. The restoring term associated with nonlinearity of righting arm curve at larger heeling angles leads to a variations of natural rolling frequencies of the ship, as previously mentioned. Since the encounter frequency between ship and waves remains invariable at the moment, the condition which triggers the parametric rolling motion disappears taking the system out of the instability zone of the Ince-Strutt diagram. Consequently, once the roll of ship reaches a certain angle, no extra energy gain during parametric rolling is transferred to a motion. Energy balance is reached, providing of course there aren't capsizing scenarios.

Also, there must be nonlinear damping present in order for the motion to be limited in amplitude, similar to a quadratic or higher power of the roll velocity. Dissipated energy from damping larger than the extra input energy from parametric resonance tends to stabilize the roll amplitude. It should be stated here based from the findings of this work that the nonlinearity of the GZ curve is more important in the stabilization of parametric roll than nonlinear damping. Finally, cross coupling especially for heave and pitch motions (3 DOF), has an obvious effect on the instant righting arm of a ship, normally more pronounced in head seas.

Review of analytical prediction formulae

Analytical formulae that appear in current industrial guidelines are evaluated in a step-by-step process against various numerical predictions. At an elementary level, it should be confirmed whether the analytical expressions reflect successfully the exact large amplitude dynamics of the assumed Mathieu-type model of ship rolling.

So far it can be said that the probability of parametric rolling has not yet been completely "controlled" and eliminated in design. It is known that nonlinear terms in the rolling equation stabilize parametric rolling reaching steady-state amplitude that is proportional to the square root of the amplitude of restoring fluctuation. It is essential to ensure that the amplitude of parametric rolling oscillation A , which might be generated in an extreme seaway, is kept small (ITTC 2006).

Spyrou (2004) showed that with certain limits depending on the detailed shape of the restoring lever, a third-order polynomial could reasonably represent the exact shape of the initial part of the lever. More specifically, if the amplitude of roll is small to moderate the nonlinear equation of roll in a longitudinal sea that could be used for predicting the steady roll amplitude in the vicinity of principal resonance:

$$\ddot{\eta}_4 + 2\mu\omega_0\dot{\eta}_4 + \omega_0^2(1 - h\cos(\omega_e t - \varepsilon))\eta_4 - c_3\omega_0^2\eta_4^3 = 0 \quad (2-35)$$

The ITTC expressions were based on the following model of roll motion:

$$\ddot{\eta}_4 + 2\mu\omega_0\dot{\eta}_4 + \omega_0^2(1 - h\cos(\omega_e t - \varepsilon))\eta_4 - c_3\omega_0^2\eta_4^3 - c_5\omega_0^2\eta_4^5 = 0 \quad (2-36)$$

This formulation is utilised if the amplitude of parametric roll is moderate to large, upon which a fifth order polynomial is likely to be required for modelling the restoring moment. It essentially enables to “cover” the scenario of the restoring curve initially hardening ($c_3 < 0$) and then softening ($c_5 > 0$). The terms above c_3 and c_5 present nonlinear stiffness coefficients, corresponding the third and fifth order restoring terms, respectively.

Prediction formulae of steady parametric rolling that appear in the ITTC guideline are deduced by the method of harmonic balance. The amplitude A may be expressed as, (ITTC 2006):

$$A^2 = \frac{4}{3c_3} \left[\left(1 - \frac{1}{a}\right) \pm \sqrt{\frac{h^2}{4} - \frac{4\mu^2}{a}} \right] \quad \text{for } c_5 = 0; \quad (2-37)$$

If $c_5 \neq 0$ the following expression of the amplitude could be useful,

$$A^2 = -\frac{3c_3}{5c_5} \pm \sqrt{\left(\frac{3c_3}{5c_5}\right) - \frac{8}{5c_5} \left(-1 + \frac{1}{a} \pm \sqrt{\frac{h^2}{4} - \frac{4\mu^2}{a}}\right)} \quad (2-38)$$

where $a = 4\omega_0^2 / \omega_e^2$. The \pm sign reflects a possibility of a multitude of stable/unstable coexisting solutions deduced from the equation (2-38) where up to four solutions may become possible for the same values of the frequency ratio a . Meaning, it is possible to alternate towards the coexisting higher roll amplitudes, even though the solution of the smallest amplitude is stable.

ABS treats the following severity check problem with the second order differential equation for nonlinear damping by means of numerical integration, which is the modification of (2-35),

$$\ddot{\eta}_4 + 2\mu\omega_0\dot{\eta}_4 + \omega_0^2 f(\eta_4, t) = 0 \quad (2-39)$$

Using a suitable change of variables the formulae (2-39) may be converted into a set of first-order equations. Numerical solution of a system of two first order differential equations in the matrix form can be established by any of the known techniques. In order to be solved numerically, the set of equations is given as follows:

$$\begin{aligned} \dot{\varphi} + 2\mu\varphi + f(\eta_4, t) &= 0 \\ \dot{\eta}_4 - \varphi &= 0 \end{aligned} \quad (2-40)$$

The next step is to assess the influence of the true variation $GZ(\eta_4, t)$ exhibited by a ship due to the so-called wave contouring effect. The transition has to be made from wave crest position to time variable which permits the restoring term to be presented as a periodic function of time. Thus, time-dependent restoring term of the roll equation depending on two dimensional interpolations of the calculated values of the GZ curve can be expressed as:

$$f(\eta_4, t) = \frac{\pm(\eta_4)}{GM_0} GZ(|\eta_4|, t) \quad (2-41)$$

The restoring term as a function of roll angle and time can be manipulated by a step-by-step solution covering all values on the 3-D GZ curves or approximated by a third or higher order polynomial for simplification:

$$GZ(\eta_4) = a_1\eta_4 - a_3\eta_4^3 \quad (2-42)$$

Coefficients a_1 and a_3 can be determined by the characteristics of GZ curve as follows (Taylan, 2007):

$$a_1 = GM, \quad (2-43)$$

$$a_3 = \frac{2GM}{\eta_{4v}^2} - \frac{4A_{\eta_{4v}}}{\eta_{4v}^4}$$

where η_{4v} is the angle of vanishing stability and $A_{\eta_{4v}}$ the area under the GZ curve up to η_{4v} . The above-mentioned equation of roll motion can be solved by a fourth-order Runge–Kutta algorithm using for instance, damping values of $\mu = 0.03, 0.05, 0.075$ and 0.10 , in the absence of model test data. The above procedure is the basis of the severity criterion of parametric roll.

Re-writing the rolling equation (2-9) using asymptotic methods, as another approach (Shin, 2004; ABS, 2004), and dealing with the restoring nonlinearity, while retaining only the linearized damping coefficient μ , results in,

$$\ddot{\eta}_4 + 2\mu\dot{\eta}_4 + \omega_m^2(1 + a_p \cos(\omega_e t))\eta_4 - c_3\eta_4^3 = 0; \quad a_p = \frac{\omega_a^2}{\omega_m^2} \quad (2-44)$$

where c_3 is a third power coefficient used to approximate the nonlinear GZ curve. The corresponding equation in the ABS guideline is identical to eq. (2-36), providing that the 5th-order restoring term is omitted while in the calculation of the natural frequency, GM_m is interpreted as (2-2). Thus, by applying the method of multiple scales, known solution (Sanchez and Nayfeh, 1990) for the steady-state amplitude can be obtained and expressed as,

$$A = \frac{\sqrt{\omega_e - 4\omega_m^2 - 0.5\omega_e \sqrt{\omega_e^2 a_p^2 - 64\mu^2}}}{\sqrt{3c_3}} \quad (2-45)$$

The ABS expression for the amplitude of steady parametric oscillation, after conversion to common symbols, is essentially identical to eq. (2-37) (ITTC, 2006), with one logistic difference however. Coefficient a should be calculated here not for the natural frequency ω_a , but for a modified one, based on the mean metacentric height (Spyrou, 2008).

The roll equation (2-44), as a background for formula (2-45), does not provide sufficient accuracy since it contains an approximation for the GZ curve using a third power polynomial. An expression of type (2-43) could be utilised for approximating the average GZ curve for a number of positions of the wave crest along the ship hull using the method of least squares together with a third order polynomial approximation. Even though, the results might be improved by using a higher order polynomial the new formulae might prove to be especially complex, so the direct numerical integration (2-40) of the rolling equation seems to be preferable at this stage.

3 Formulation of the seakeeping problem

3.1 Potential flow theory

Since roughly four decades ago it is possible to incorporate seakeeping considerations from the beginning of the design by utilizing numerical methods. These numerical methods include linear theories like strip theories up to complete three-dimensional theories, etc.

Formulation of the seakeeping problem is associated with of the potential flow around the hull of a ship advancing and oscillating in waves. The strip theory is also based upon the potential flow theory. This holds that viscous effects are neglected, which can deliver serious problems when predicting roll motions at resonance frequencies. In practice, viscous roll damping effects can be accounted for by empirical formulas.

Following notations are going to address the potential flow problem, which is represented by a set of equations in the unknown Φ (velocity potential). Basically, first step is to develop the exact solution (within the ideal fluid assumption), while the second step is to linearize the potential flow problem. We can define a potential function $\Phi(x, y, z, t)$, as a continuous function that satisfies the basic laws of fluid mechanics: conservation of mass and momentum, assuming incompressible, inviscid and irrotational flow while surface tension may be neglected. This is a prerequisite to obtain a scalar function which is the velocity potential that satisfies the continuity equation within the fluid domain.

A necessary and sufficient condition for irrotational flow is:

$$\nabla \times \vec{V} = 0 \quad (3-1)$$

where ∇ represents gradient operator and \vec{V} is velocity vector. There is a vector identity that states for any scalar, Φ

$$\nabla \times \nabla \Phi = 0 \quad (3-2)$$

This means that the velocity vector of the fluid particles may be represented by the gradient of a velocity potential:

$$\vec{V} = \nabla \Phi \quad (3-3)$$

where $\Phi = \Phi(x, y, z, t)$ is the velocity potential function. Thus, one can assume the existence of velocity potential subject only to the requirement that the fluid motion is irrotational. Note that a vector velocity is obtained from knowledge of a scalar function Φ . The components of velocity in Cartesian coordinates, as functions of space and time, are:

$$u = \frac{\partial \Phi}{\partial x}, \quad v = \frac{\partial \Phi}{\partial y}, \quad w = \frac{\partial \Phi}{\partial z} \quad (3-4)$$

If the velocity components are a function of space alone and are not a function of time we have steady flow. If the fluid is homogeneous and incompressible then the equation of conservation of mass reduces to the equation of continuity:

$$\left(\frac{\partial u}{\partial x} + \frac{\partial v}{\partial y} + \frac{\partial w}{\partial z} \right) = 0 \quad (3-5)$$

where u , v and w denotes the components of the fluid velocity vector.

Using the continuity equation, in terms of the velocity potential it becomes,

$$\left(\frac{\partial^2 \Phi}{\partial x^2} + \frac{\partial^2 \Phi}{\partial y^2} + \frac{\partial^2 \Phi}{\partial z^2} \right) = 0 \quad (3-6)$$

We can substitute in the relationship between potential and velocity and arrive at the Laplace equation, $\nabla^2 \Phi = 0$. Among the various hypotheses the inviscid flow assumption may introduce some limitations, for example, horizontal motions, roll motion and vertical motions of SWATH vessels.

With the velocity potential known the fluid pressure may be determined by Bernoulli equation:

$$p = -\rho \left(\frac{\partial \Phi}{\partial t} + \frac{1}{2} |\nabla \Phi|^2 + gz \right) \quad (3-7)$$

The Bernoulli equation is the most widely used equation in fluid mechanics, and assumes frictionless flow with no work or heat transfer. However, flow may or may not be irrotational. When flow is irrotational it reduces nicely using the potential function in place of the velocity vector. This equation is valid everywhere, not just along a streamline.

After an introduction to the basis of the potential flow, at this point a quick overview will be given as how to tackle the seakeeping problem formulation,

1. Obtain the velocity potential,
2. With the velocity potential it is possible to calculate the fluid velocities,
3. Applying the Bernoulli equation one obtains the fluid pressures (on the hull),
4. Integrating the fluid pressures results in the hydrodynamic forces acting on the ship advancing in waves,
5. Equating the fluid forces with the mass forces (Newton 2nd law) results with the equations of ship motions and structural loads,
6. Equation under (3-5) is solved either in the frequency domain or in the time domain which will be addressed in separate chapters.

Hydrodynamic problem - conventions and coordinate systems setup

Considering a domain of interest for a vessel sailing in the waves, compared with the vessel itself, the domain of the fluid is actually infinite. Geometry of the coordinates of the field of fluid that should be adopted in formulation of the problem can be represented by Fig 3-1. The symbol Vol represents the volume of fluid, which is bounded by the free surface S_F and the wetted body surface S_W on the upper side, S_b by the bottom surface and laterally at infinity S_∞ . Uniqueness of the solution depends of the appropriate boundary conditions.

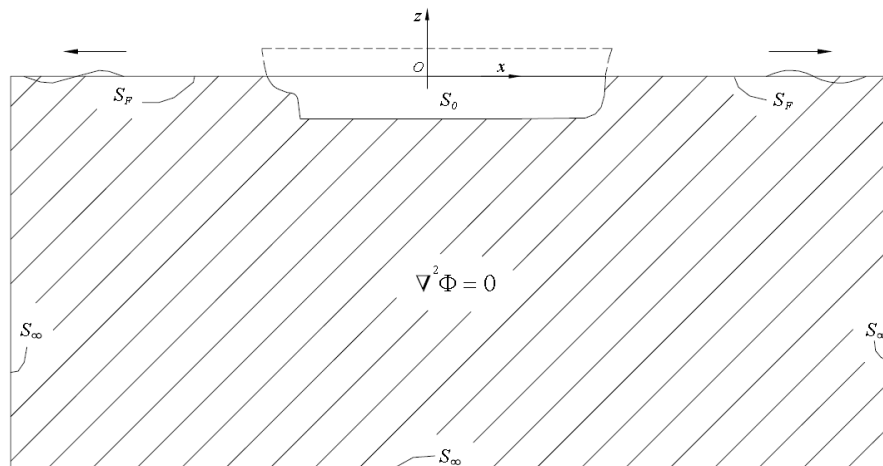


Figure 3-1. Boundary conditions surrounding the fluid domain

To obtain solutions of the Laplace equation two techniques may be employed to determine the potential function Φ . The first technique is to solve directly Laplace's equation with appropriate boundary conditions using either a numerical technique or possibly the separation of variable method. The second and often utilized technique is to investigate some simple functions that satisfy Laplace's equation and then to superimpose these linear functions which is allowable because Laplace's equation is linear, to provide the flow around body of interest. A note on boundary conditions for potential flow is in order. Laplace's equation is second order and requires boundary conditions on complete boundary enclosing a particular region of interest; that is the velocity potential or its derivatives must be known over the entire surface. Consider a flow around a body shown in Fig. 3-1.

The surface and the body (vessel) form the volume of interest Vol . Thus, the physical conditions on these boundaries must be related to appropriate mathematical statements.

Considering the prior definitions, then at each point of the domain the following holds:

$$\nabla^2 \Phi(\vec{x}_0, t) = 0 \quad \vec{x}_0 \in Vol \quad (3-8)$$

This means that when there is a series of simple flow solutions then the solution to more complex flows can be obtained by superposition of the simple flow.

$$p(\vec{x}_0, t) = -\rho \left(\frac{\partial \Phi}{\partial t} + \frac{1}{2} |\nabla \Phi|^2 + gz \right) \quad \vec{x}_0 \in Vol \quad (3-9)$$

To obtain the desired solution of the Laplace's equation it is necessary to impose conditions on all boundaries surrounding the fluid domain. It must satisfy Laplace's equation in the region Vol exterior to S_w , have a zero derivative on S_w and approach the proper uniform stream function potential at infinity. Three orthogonal and right handed coordinate systems will be used (Fig.3-2). The first one is fixed in space $X_0 = (x_0, y_0, z_0)$. Assuming that the ship is moving horizontally with a speed of advance \vec{U} , through a incident harmonic wave, yet another system must be regarded with the coordinates $X = (x, y, z)$ which also advances with the ship forward speed \vec{U} . A third coordinate system $X' = (x', y', z')$ is fixed on the vessel and its origin is coincident with the center of gravity of the vessel, which possess an average speed and oscillatory movements of the ship, so called body fixed system. The unitary vector $\vec{n} = \vec{n}(n_1, n_2, n_3)$ is normal to the surface of the body, directed to the fluid.

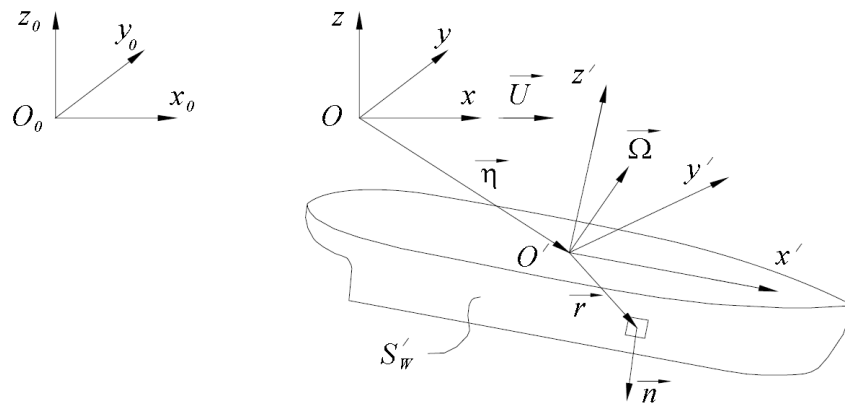


Figure 3-2. Mathematical relationships between the three coordinate systems

Initially, the system of coordinates $X = (x, y, z)$ is coincident with the coordinate system fixed in space $X_0 = (x_0, y_0, z_0)$, but after a time t , the system moves with a $U \cdot t$ distance from the point O_0 , along the axis $-x$, to the point O . The coordinate system $X_0 = (x_0, y_0, z_0)$ of incident harmonic wave is defined through the wavelength λ , amplitude ζ_a and direction β , relative to the axis $-x$ (where $\beta = 180^\circ$ represents a bow wave, as shown in Figure 3-3).

Therefore, the relationship between the two coordinate systems is given by the linear transformation:

$$\vec{x} = (x, y, z) = (x_0 - U \cdot t, y_0, z_0) \quad (3-10)$$

The relationship between the wave frequency and the frequency of the waves against the part of ship is given by:

$$\omega_e = \omega - kU \cos \beta \quad (3-11)$$

where $k = \omega^2 / g$ is the wave number, ω is the wave frequency and ω_e is the encounter frequency.

The rigid body motions in the forward speed reference system consist of:

- Three translations in the directions of x , y and z are surge (η_1), sway (η_2) and heave (η_3) respectively;
- Three rotations around x , y and z are roll (η_4), pitch (η_5) and yaw (η_6) respectively. This is illustrated within the fig. 3-4, given along with conventional directions.

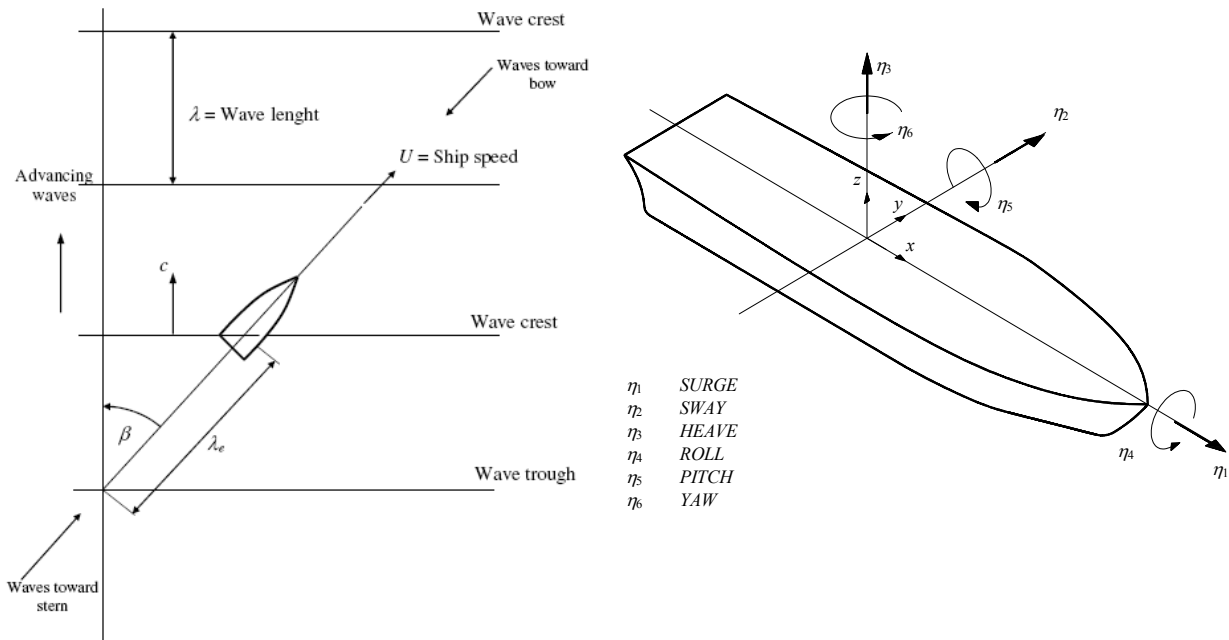


Figure 3-3. Coordinate system of incident harmonic wave Figure 3-4. Rigid body motions of the vessel

3.2 Strip theory – frequency domain solution

The strip theory of Salvesen, Tuck and Falinsen (1970) is based upon the potential flow theory. The strip theory solves the three-dimensional problem of the hydro mechanical and exciting wave forces and moments on the ship by integrating the two-dimensional potential solutions over the ship's length. Interactions between the cross sections are ignored for the zero-speed case. Therefore, each cross section of the ship is considered to be part of an infinitely long cylinder. Viscous effects are neglected, which can deliver serious problems when predicting roll motions at resonance frequencies. In practice, viscous roll damping effects can be accounted for by semi-empirical formulas as will be seen in the following chapters. The strip theory is a slender body theory, so one should expect less accurate predictions for ships with low length to beam ratios. The strip theory however, is still the most successful and practical theory for the calculation of the wave induced motions of the ship

Also, for high-speed vessels and for large ship motions as appear in extreme sea states, the strip theory can deliver less accurate results. The strip theory accounts for the interaction with the forward speed in a very simple way. The effect of the steady wave system around the ship is neglected and the free surface conditions are simplified, so that the unsteady waves generated by the ship are propagating in directions perpendicular to the centre plane of the ship. In reality the wave systems around the ship are far more complex. The strip theory is based upon linearity. This means that the ship motions are supposed to be small, relative to the cross sectional dimensions of the ship. Only hydrodynamic effects of the hull below the still water level are accounted for. So when parts of the ship go out of or into the water or when green water is shipped, inaccuracies can be expected. Also, the strip theory does not distinguish between alternative above water hull forms. Because the added resistance of a ship due to the waves is proportional to the vertical relative motions squared, its inaccuracy will be gained strongly by inaccuracies in the predicted motions (Journee, 2000). Nevertheless, seakeeping prediction methods based upon the strip theory provide a sufficiently good basis for optimization studies at an early design stage of the ship. The equations of motions for six degrees of freedom of a sailing ship, influenced by external loads, are based upon Newton's second law of dynamics. Because of the symmetry of a ship, two uncoupled sets of three coupled equations of motion can be distinguished.

As a result of this formulation in the frequency domain, any system influencing the behavior of the vessel should have a linear relation with respect to the displacement, the velocity and the acceleration of the body. The hydrodynamic mass and damping coefficients and the external wave loads are depending on the amplitude and the frequency of oscillation. The restoring spring coefficients are constant. To calculate the hydrodynamic mass and damping coefficients and the external wave loads in these equations of motions, several approaches of the strip theory can be adopted.

As for the approach utilized in this work the solution of the linear radiation and diffraction problems using a strip theory is assumed harmonic for the unsteady flow. It means that the forced motions and the incident waves (as well as all related responses) are harmonic in time. The radiation and diffraction forces will be represented in terms of coefficients of added mass, damping, and exciting forces. In the so-called strip theory, the ship will be divided in 20 to 30 cross sections (hydrodynamic coefficients associated with each strip are given by the solution of the 2D boundary value problem for the cross sections defining the hull strips), of which the two-dimensional hydro-mechanic coefficients and exciting wave loads can be calculated (3D hydrodynamic problem is reduced to a set of 2D hydrodynamic problems). To obtain the three-dimensional values, these values will be integrated over the ship length numerically. It is assumed that the flow around each strip does not affect the flow on adjacent strips. Finally, the differential equations will be solved to obtain the motions. These calculations are performed in the frequency domain. For the sake of this thesis the formulations presented are somewhat shortened but can be found in detail in

3.2.1 Radiation Forces

Up to this point the hull was assumed slender, however no strip theory simplifications were introduced. In this work in order to avoid the numerical and computational problems associated with the panel's methods, some simplifications in the flow around the hull will be taken into account. A numerically robust code reliable for the calculation of ships hydrodynamic coefficients is considered essential for the application of this theory in the time domain computations to be described in the next chapter. Following the above, a strip theory assumption that the frequency of oscillation is high will be used, therefore the free surface boundary condition may be assumed as 2D. Furthermore, the beam is much smaller than the length, therefore the longitudinal component of the unit vector normal to the hull surface may be neglected ($n_1 \ll n_2, n_1 \ll n_3$) thus,

$$n_1 = 0, \text{ while} \\ n_2, n_3, n_4 = N_2, N_3, N_4$$

so that three components of three-dimensional generalized normal, n_j ($j=2,3,4$), can be replaced with a two-dimensional generalized normal lying in the transverse YZ plane, N_j ($j=2,3,4$), so that,

$$n_5 = -x N_3 \quad \text{and} \quad n_6 = x N_2$$

Thus, the kinematic boundary condition on the body that must be met by potential radiation independent of the speed is as follows:

$$\frac{\partial \varphi_j^0}{\partial N} = i\omega N_j \quad y, z \in c_0 \quad (3-12)$$

As illustrated in figure 3-5, this is a 2D kinematic boundary condition which has to be satisfied on the contour of each cross section along the ship length.

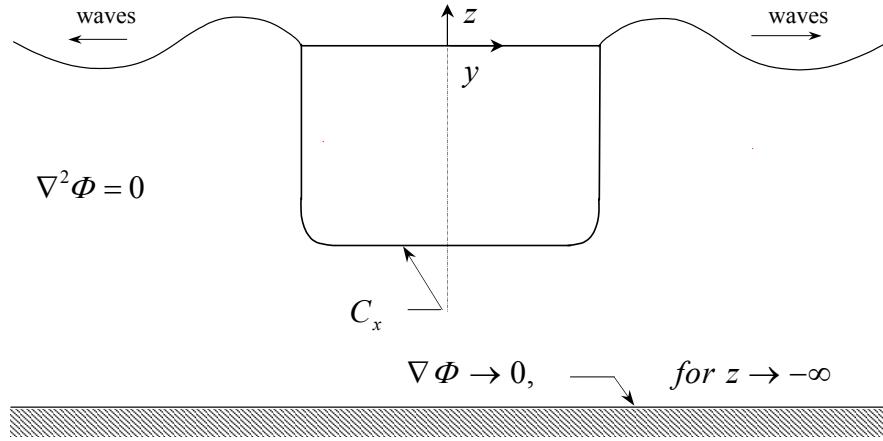


Figure 3-5. Radiation condition on a two dimensional strip

Using the harmonic dependence of the velocity potential, the boundary conditions in free surface for the potential radiation independent of speed can be written as follows:

$$\left(i\omega - U \frac{\partial}{\partial x}\right)^2 \phi_j^0 + g \frac{\partial}{\partial z} \phi_j^0 = 0 \quad \text{for } z = 0 \quad (3-13)$$

To eliminate the effects of three-dimensional boundary conditions the frequency of oscillation is assumed high, thus, the derivative in x -direction can be ignored,

$$\omega \phi_j^0 \gg U \frac{\partial}{\partial x} \phi_j^0 \quad (3-14)$$

The latter hypothesis requires that the encounter frequency is high, i.e., it implies a smaller wavelength to the length of the vessel. This restriction makes this theory applicable only to the higher encounter frequency of meeting and, at first glance, it seems like a very severe restriction.

However, since at the low frequency range the hydrodynamic forces are dominated by the hydrostatic and Froude Krylov components, a less accurate prediction of the radiation forces is not regarded as compromising, in terms of accuracy of the method. To summarize, the conditions that the speed independent radiation potentials must satisfy are as follows:

- Laplace equation

$$\varphi_{yy}^R + \varphi_{zz}^R = 0 \quad (3-15)$$

- Linear free surface boundary condition

$$-\omega^2 \varphi_j^R + g \frac{\partial}{\partial z} \varphi_j^R = 0 \quad \text{for } z = 0 \quad (3-16)$$

- Linear body condition (radiation)

$$\frac{\partial \varphi_j^R}{\partial N} = i\omega N_j \quad j = 1, \dots, 6 \quad y, z \in c_0 \quad (3-17)$$

- Bottom boundary condition

$$\nabla \varphi^R \rightarrow 0, \quad \text{for } z \rightarrow -\infty \quad (3-18)$$

- Appropriate radiation condition at infinite

$$\frac{\partial \varphi^R}{\partial r} - i \frac{\omega^2}{g} \varphi^R = 0 \quad (3-19)$$

Note that φ^R represents the 2D radiation potential for harmonic motions of unit amplitude and it substitutes the ϕ^0 , representing the 3D potential independent of the speed. Therefore, this is the 2D boundary value problem of an arbitrary cross section oscillating on the free surface with harmonic motions of unit amplitude.

The radiation forces acting on a slender ship moving at an average constant speed and oscillating on the free surface are given by representing separately the various components of the force of radiation given by the contributions of six modes of the harmonic oscillatory motion that is:

$$F^R = -\rho \iint_{S_0} \sum_{j=1}^6 \eta_j \varphi_j^R (i\omega n_k - Um_k) ds \quad \text{for } j = 2, 3, 4 \quad k = 1, \dots, 6 \quad (3-20)$$

where k represents the direction of the force and ϕ_j^R is the radiation potential for an oscillatory motion of unit amplitude in the mode j .

For the case of two-dimensional problem of forced oscillations of a cylinder, the expression (3-20) can be simplified by removing the term dependent on the speed and introducing two-dimensional normal. Thus, the integration along the cross section contour C_x represents the 2D radiation force in the k direction due to an oscillatory motion of unit amplitude in the j mode,

$$f_{kj}^{R_{2D}} = -i\omega\rho \int_{C_x} \varphi_j^R N_k ds \quad k, j = 2, 3, 4 \quad (3-21)$$

The force given by the expression $f_{kj}^{R_{2D}} = t_{kj}^{R_{2D}}$ (3-20) can be divided into the real and imaginary part of the following:

$$f_{kj}^{R_{2D}} = \omega^2 a_{kj} - i\omega b_{kj} \quad \text{for } k, j = 2, 3, 4 \quad (3-22)$$

with

$$a_{kj} = -\frac{\rho}{\omega} \operatorname{Re} \left\{ i \int_{C_x} \varphi_j^R N_k ds \right\} \quad k, j = 2, 3, 4 \quad (3-23)$$

$$b_{kj} = \rho \operatorname{Im} \left\{ i \int_{C_x} \varphi_j^R N_k ds \right\} \quad k, j = 2, 3, 4$$

where the coefficients a_{kj}, b_{kj} , are named as added masses and damping coefficients, respectively.

For harmonic motions of arbitrary amplitude we have:

$$F_{kj}^{R_{2D}} = \eta_j^A (\omega^2 a_{kj} - i\omega b_{kj}) \quad \text{for } k, j = 2, 3, 4 \quad (3-24)$$

Finally the time domain representation of the radiation force represented by two components, one in phase with the acceleration of the motion while the other in phase with the velocity of the motion can be written as,

$$\operatorname{Re} \left\{ F_{kj}^{R_{2D}} e^{i\omega t} \right\} = -a_{kj} \ddot{\eta}_j(t) - b_{kj} \dot{\eta}_j(t) \quad (3-25)$$

with the harmonic motion $\eta_j(t) = \operatorname{Re} \left\{ \eta_j^A e^{i\omega t} \right\}$. Radiation force in phase with the acceleration of the motion is equivalent to an inertial force for the translational motions as to a moment of inertia to the rotational motions. A physical interpretation of this term has to do with the additional force required to accelerate this mass of fluid in conjunction with the body and thus, it behaves as if a mass was added. Therefore, the physical meaning of the added mass is an equivalent mass that accelerates together with the rigid body.

Radiation force in phase with the velocity of the motion represents an inviscid damping force that is proportional to the damping coefficient. This damping term is related to the dissipated energy for the generation and radiation of free surface waves due to the harmonic rigid body motions.

For the three-dimensional forces acting on the ship the radiation force in the k direction due to an oscillatory motion of unit amplitude in the j direction is given by:

$$f_{kj}^R = -i\omega\rho \iint_{S_0} \phi_j^R n_k ds + U\rho \iint_{S_0} \phi_j^R m_k ds \quad \text{for } k, j = 1, 2, 3, 4, 5, 6 \quad (3-26)$$

representing the radiation forces acting on a slender ship moving with forward speed and with constant mean harmonic oscillations on the free surface. This expression is similar to that by Salvesen et al. (1970), except from the fact that the terms related to the aft end of the ship (transom

stern) are not included in this code. In this work end terms that are proportional to the ship speed and to the “size” of the transom stern are neglected because, for certain frequencies, they seem to worsen results, as demonstrated experimentally by Meyers et al. (1981). However since the ship investigated possesses large transom stern (one of the features associated with propensity of parametric rolling) this approach has to be revalidated which is one of the tasks considered after the present analysis using the strip theory approach by Prpić-Oršić (1998). Using the strip theory assumptions that the beam is much smaller than the length, a small element of the hull surface may be represented by $ds \cong d\zeta dx$ where dx is along the ship length and $d\zeta$ is along the cross section contour C_x .

The integrations are performed along the length of the ship. The two-dimensional coefficient of added mass and damping, a_{33} and b_{33} are calculated using the "Close-fit" method from Frank (1967). The velocity potential of the vertical oscillatory motion of cylinders is represented by a uniform source distribution along the length of each line segment, of a certain cross-section.

The density of a source is an unknown, determined by satisfying the kinematic boundary condition at the midpoint of each segment of the body, the linearized boundary free surface condition, the bottom boundary condition and the Laplace equation on the outer surface from the body. Once the densities of sources are determined, the velocity potential is easily calculated and the coefficients of added mass and damping are determined by integration along the sections.

Typically, about twenty line segments in half-cross-sections for the calculation of the coefficients of added mass and damping for the motions in the longitudinal plane is considered as sufficient.

3.2.2 Excitation Forces

To tackle the excitation forces it is necessary to solve the hydrodynamic problem of forces acting on the ship advancing with constant forward speed through a field of incident harmonic waves while the ship is restrained at its mean position (no oscillatory motions).

$$F^E = -\rho \iint_{S_0} \left(\frac{\partial(\Phi^I + \Phi^D)}{\partial t} \tilde{n} - (\Phi^I + \Phi^D) U \tilde{m} \right) ds \quad (3-27)$$

This expression shows that the excitation force consists of two parts. One is associated with incident wave potential (wave field pressure) and is commonly referred to as Froude-Krylov force. The remaining part is related to the perturbation on the incident wave field due to the ship presence and is called the diffraction force. Excitation forces are both harmonics in time.

Using the harmonic characteristics of the potential separating the two parts of the exciting force and even breaking it into components in different departments of the system coordinates we obtain that:

$$F_k^D = -\rho \iint_{S_0} (i\omega n_k - U m_k) \Phi^D ds \quad (3-28)$$

$$F_k^I = -\rho \iint_{S_0} (i\omega n_k - U m_k) \Phi^I ds \quad (3-29)$$

where Φ^I and Φ^D represent the incident wave potential and diffraction potential.

The velocity potential can alternatively be represented by:

$$\phi^I(y, z) = \frac{ig}{\omega_0} e^{ik_0 y \sin \beta} e^{k_0 z} \quad (3-30)$$

where $\phi^I(y, z)$ is the complex amplitude of the incident wave potential due to a unit wave acting on the cross sections of the hull. With these expressions for the incident potential assuming geometric simplification of the strip theory the Froude – Krylov forces in each of the directions of the coordinate system are given by:

$$F_1^I = 0 \quad (3-31)$$

$$F_k^I = \zeta_a \int_L e^{ik_0 x \cos \beta} f_k^I dx \quad \text{for } k = 2,3,4 \quad (3-32)$$

$$F_5^I = -\zeta_a \int_L e^{ik_0 x \cos \beta} x f_3^I dx \quad (3-33)$$

$$F_6^I = \zeta_a \int_L e^{ik_0 x \cos \beta} x f_2^I dx \quad (3-34)$$

where f_k^I represents the 2D Froude-Krylov force due to unit amplitude waves. These forces are simple to calculate because the potential of the incident wave is known apriori. The first attempts to calculate the vertical motions of the ship in waves (Froude, 1863 and Krylov, 1896) only considered this component of the excitation force thus assuming that the vessel does not disturb the incident wave. In practice, this hypothesis is valid when the wavelengths are much greater than the ship length. It is also interesting to note that the amplitude of the Froude-Krylov forces is independent of the ship speed.

There are two possibilities for the calculation of the diffraction forces. The first alternative is to directly solve the diffraction boundary value problem to obtain the diffraction potential and calculate the forces similar to the radiation problem. The major difficulty arises from the fact that formally the Laplace equation that needs to satisfy both Φ^I and Φ^D cannot be solved when the vessel is encountered by the bow waves.

The alternative to direct calculation of the diffraction potential is to use the Haskind-Newman relations to represent the diffraction forces in terms of radiation potentials (applies Green theorem). Green theorem states that if φ and ϕ are two solutions of the Laplace equation within a finite volume of fluid bounded by a closed surface S_T , these potentials are related in the following way,

$$\iint_{S_T} \phi \frac{\partial \varphi}{\partial n} ds = \iint_{S_T} \varphi \frac{\partial \phi}{\partial n} ds \quad (3-35)$$

where n is the vector normal to the surface and pointing to the fluid. Combining the expressions (3-12) with equation (3-28), gives the diffraction force in the k direction,

$$F_k^D = -\rho \iint_{S_0} \frac{\partial}{\partial n} \left(\Phi_k^0 - \frac{U}{i\omega} \Phi_k^U \right) \Phi_D ds \quad k = 1, \dots, 6 \quad (3-36)$$

Applying the theorem to the volume of fluid bounded by $S_T = S_0 + S_f + S_b + S_\infty$ results in the diffraction force represented in terms of radiation potential and incident wave potential, using

$$\frac{\partial \phi^D}{\partial n} = -\frac{\partial \phi^I}{\partial n},$$

$$F_k^D = \rho \iint_{S_0} \left(\phi_k^0 - \frac{U}{i\omega} \phi_k^U \right) \frac{\partial \phi^I}{\partial n} dS + \frac{\rho U}{i\omega} \int_{C_A} \phi_j^0 \frac{\partial \phi^I}{\partial n} dl \quad (3-37)$$

where the end term can be omitted as explained earlier. Finally, to obtain expressions for the forces in terms of dimensional quantities it is necessary to adopt a procedure similar to that used in the formulation of the radiation forces. Equations $\phi_j^U = 0$ for $j = 1,2,3,4$ and $\phi_5^U = \phi_3^0$ with $\phi_6^U = -\phi_2^0$ are used to represent the speed dependent potentials, Φ_k^U , in terms of speed independent potentials, Φ_k^0 , the geometric simplification $ds \cong d\zeta dx$ is used to reduce the surface integrals while the 3D unit normal vector is substituted by the 2D unit normal vector resulting in,

$$F_1^D = 0 \quad (3-38)$$

$$F_k^D = \zeta_a \int_L e^{ik_0 x \cos \beta} f_k^D dx \quad \text{for } k = 2,3,4 \quad (3-39)$$

$$F_5^D = -\zeta_a \int_L e^{ik_0 x \cos \beta} \left(x f_3^D + \frac{U}{i\omega} f_3^D \right) dx \quad (3-40)$$

$$F_6^D = \zeta_a \int_L e^{ik_0 x \cos \beta} \left(x f_2^D + \frac{U}{i\omega} f_2^D \right) dx \quad (3-41)$$

where f_k^D is the sectional diffraction force for the incident waves of unit amplitude, given by:

$$f_k^D = \omega \rho \int_{C_x} (iN_3 - N_2 \sin \beta) e^{ik_0 y \sin \beta} e^{k_0 z} \phi_k^R ds \quad k = 2, 3, 4 \quad (3-42)$$

with ϕ_k^R as the 2D radiation potential for forced harmonic motions of unit amplitude in the k mode, while N_2 and N_3 represent the components of the 2D unit vector normal to the cross sections of the hull. The calculation of the dimensional radiation potential ϕ_k^R is performed using the Frank "Close-fit" method. To summarize, the main advantage of using Haskind-Newman relations to calculate the diffraction forces is the reduction of computational effort. A large chunk of the computational effort in the calculations of the ship performance at sea, is associated with solution of the problem of the boundary conditions for each frequency and mode of oscillation that needs to be considered. However, a Haskind-Newman relation basically reduces the computational effort by half.

3.2.3 Restoring Forces

Restoring forces result from combining hydrostatic forces (Bernoulli's equation surface for hull wetted surface) with the ship weight along each of the directions of the coordinate system,

$$F_k^H = -\rho g \iint_{S_w} (z n_k) ds \quad k = 1, \dots, 6 \quad (3-43)$$

Assuming small angular displacements such that higher order terms in the Euler angles can be neglected, the z – coordinate of a point on the hull wetted surface on the forward speed reference system can be expressed as, $z = z' + \eta_3 + y' \eta_4 - x' \eta_5$ where the terms on the right are the coordinates of that point represented in the ship fixed reference system $X' = (x', y', z')$. Introducing this expression in equation (3-43) and assuming some simplifications one can obtain hydrostatic forces linearly proportional to displacement. The simplifications are as follows:

- the hydrostatic pressure is calculated up to the still water surface ($z = 0$),
- the angular motions are of small amplitude,
- ship sides are vertical around the waterline.

With these assumptions the integral in (3-43) can be developed leading to the nonzero hydrostatic forces for ships with lateral symmetry,

$$F_3^H = \rho g \nabla_0 - \rho g A_{wl} \eta_3 + \left\{ \rho g \iint_{A_{wl}} x ds \right\} \eta_5 \quad (3-44)$$

$$F_4^H = \rho g \nabla_0 y_{B_0} + \rho g \left\{ \nabla_0 (z_{B_0} - z_G) + \iint_{A_{wl}} y^2 ds \right\} \eta_4 \quad (3-45)$$

$$F_5^H = -\rho g \nabla_0 x_{B_0} + \left\{ \rho g \iint_{A_{wl}} x ds \right\} \eta_3 + \rho g \left\{ \nabla_0 (z_{B_0} - z_G) + \iint_{A_{wl}} x^2 ds \right\} \eta_5 \quad (3-46)$$

where ∇_0 is the volume of the immersed hull in the condition of static equilibrium with its centre of buoyancy coordinates, while A_{wl} represents static waterplane area.

Combining these equations with the force and moments due to the ship weight results in the restoring forces:

$$F_1^H = F_2^H = F_6^H = 0$$

$$F_3^H = -C_{33}\eta_3 - C_{35}\eta_5 \quad (3-47)$$

$$F_4^H = -C_{44}\eta_4$$

$$F_5^H = -C_{53}\eta_3 - C_{35}\eta_5$$

representing heave restoring force, roll restoring moment and pitch restoring moment respectively.

C_{kj} are the restoring coefficients, namely,

$$C_{33} = \rho g \int_L b d\zeta = \rho g A_{wl}$$

$$C_{35} = C_{53} = -\rho g \int_L \zeta b d\zeta = -\rho g \iint_{A_{wl}} x ds \quad (3-48)$$

$$C_{44} = \rho g \nabla_0 GM$$

$$C_{55} = \rho g \int_L \zeta^2 b d\zeta = \rho g I_{WP} = \rho g \nabla_0 GM_L$$

with GM and GM_L as the transversal and longitudinal metacentric heights and ζ as integrative variable in x direction.

3.2.4 Equations of Motion

The equations of motion resulting from the dynamic balance between external forces (in this case the hydrodynamic forces) and the inertia forces associated with the mass of the ship. The hydrodynamic forces were represented in terms of strip theory in earlier sections. Forces of inertia will now be described in brief.

The Newton's second law states that a force (or moment) is equal to mass (or inertia mass) times the linear (or angular) acceleration of the body. Mathematically, if ρ_B is the specific mass of the body, which depends on the position in space, the force of inertia associated the mass is given by the rate of momentum change, given by:

$$F^M = \frac{\partial}{\partial t} \iiint_{V_B} \rho_B (\dot{\eta} + \dot{\Omega}' \times r) dV \quad (3-49)$$

while the moment of inertia is given by the rate of angular momentum change,

$$M^M = \frac{\partial}{\partial t} \iiint_{V_B} \rho_B r \times (\dot{\eta} + \dot{\Omega}' \times r) dV \quad (3-50)$$

where the velocity of an element of mass in the forward speed reference system $X = (x, y, z)$ is given as $\vec{v} = (\dot{\eta} + \dot{\Omega}' \times r) dV$. The position vector in the body fixed reference system is denoted as r . Remember that the velocity of translation (oscillatory) represented in $X = (x, y, z)$ is $\dot{\eta}$, while $\dot{\Omega}'$ denotes the angular velocity (oscillatory) in the body fixed reference system $X' = (x', y', z')$. The integrations are carried out over the volume of the whole ship V_B .

The specific mass of the body is invariant in time. Assuming small angular displacement, one can arrive at the following representation for the inertia force in the k direction:

$$\{F_k^M\} = \{M_{kj}\} \{\ddot{\xi}_j\} \quad k, j = 1, \dots, 6 \quad (3-51)$$

where $\{M_{kj}\}$ is the mass matrix and $\{\ddot{\xi}_j\}$ is the accelerations vector. Assuming the ship has lateral symmetry, with respect to the longitudinal plane and the centre of gravity is located at $(0, 0, z_G)$ then the mass matrix is,

$$M_{kj} = \begin{bmatrix} M & 0 & 0 & 0 & Mz_G & 0 \\ 0 & M & 0 & -Mz_G & 0 & 0 \\ 0 & 0 & M & 0 & 0 & 0 \\ 0 & -Mz_G & 0 & I_{44} & 0 & -I_{46} \\ Mz_G & 0 & 0 & 0 & I_{55} & 0 \\ 0 & 0 & 0 & -I_{46} & 0 & I_{66} \end{bmatrix} \quad (3-52)$$

with M as a mass of the ship and the moment of inertia coefficients I_{kj} as ($I_{44} = \int_L (y'^2 + z'^2) dm$, $I_{46} = \int_L x'z' dm$, $I_{55} = \int_L (x'^2 + z'^2) dm$, $I_{66} = \int_L (x'^2 + y'^2) dm$). Only coupled centrifugal moment of inertia I_{46} is zero for ships with symmetry around the transverse axis and has a very small value otherwise.

The equations of motion in terms of displacements, velocities and acceleration governing the dynamic equilibrium of forces (and moments) in each of the directions of the coordinate system can be represented as,

$$\sum_{j=1}^6 \left[(M_{kj} + A_{kj}) \ddot{\eta}_j + B_{kj} \dot{\eta}_j + C_{kj} \eta_j \right] = F_k e^{i\omega t} = F_k^I + F_k^D; \quad k=1 \dots 6 \quad (3-53)$$

as seen by using coefficients of inertia, added mass, damping and restoring, respectively.

Equations (3-53) are similar to the governing equations of mass-spring-damper engaged. There are terms of inertia, damping and restoring on left side of the equation and the term of exciting forces on the right. However, there is a substantial difference between these two dynamical systems, because unlike mass-spring-damper, the ship and all governing coefficients depend on the excitation frequency. To avoid this difficulty only the linear solutions in the frequency domain exist.

For vessels with lateral symmetry, coefficients matrix tend to simplify, consequently, reducing the system of six coupled equations (3-53) to a two systems with three equations decoupled from each other. The first set of equations represents the coupled motions of the surge, heave and pitch, as for instance illustrated on figure 3-6,

$$(M + A_{33}) \ddot{\eta}_3 + B_{33} \dot{\eta}_3 + C_{33} \eta_3 + A_{35} \ddot{\eta}_5 + B_{35} \dot{\eta}_5 + C_{35} \eta_5 = F_3 e^{i\omega t} \quad (3-54)$$

$$A_{53} \ddot{\eta}_3 + B_{53} \dot{\eta}_3 + C_{53} \eta_3 + (I_5 + A_{55}) \ddot{\eta}_5 + B_{55} \dot{\eta}_5 + C_{55} \eta_5 = F_5 e^{i\omega t} \quad (3-55)$$

while the other represents the coupled motions of sway, roll and yaw,

$$(M + A_{22}) \ddot{\eta}_2 + B_{22} \dot{\eta}_2 + (A_{24} + Mz_c) \ddot{\eta}_4 + B_{24} \dot{\eta}_4 + A_{26} \ddot{\eta}_6 + B_{26} \dot{\eta}_6 = F_2 e^{i\omega t} \quad (3-56)$$

$$(A_{42} - Mz_c) \ddot{\eta}_2 + B_{42} \dot{\eta}_2 + (A_{24} + I_4) \ddot{\eta}_4 + B_{44} \dot{\eta}_4 + C_{44} \eta_4 + (A_{46} - I_{46}) \ddot{\eta}_6 + B_{46} \dot{\eta}_6 = F_4 e^{i\omega t} \quad (3-57)$$

$$A_{62} \ddot{\eta}_2 + B_{62} \dot{\eta}_2 + (A_{64} + I_{46}) \ddot{\eta}_4 + B_{64} \dot{\eta}_4 + (A_{66} - I_6) \ddot{\eta}_6 + B_{66} \dot{\eta}_6 = F_6 e^{i\omega t} \quad (3-58)$$

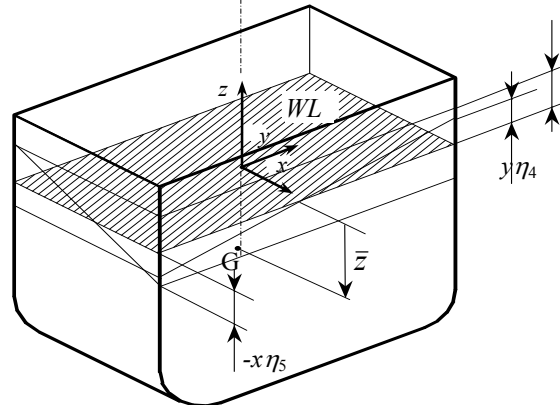


Figure 3-6. Displacement caused by coupling of the heave, roll and pitch motions

The solution of second order linear differential equations are harmonic, therefore the solution of the differential equations (3-53) is obtained by substituting the unknown complex amplitudes in (3-53) and solving the resulting algebraic equations with added mass and damping coefficients matrixes,

$$\mathbf{A}_{kj} \text{ (or } \mathbf{B}_{kj} \text{)} = \begin{bmatrix} A_{11} & 0 & A_{13} & 0 & A_{15} & 0 \\ 0 & A_{22} & 0 & A_{24} & 0 & A_{26} \\ A_{31} & 0 & A_{33} & 0 & A_{35} & 0 \\ 0 & A_{42} & 0 & A_{44} & 0 & A_{46} \\ A_{51} & 0 & A_{53} & 0 & A_{55} & 0 \\ 0 & A_{62} & 0 & A_{64} & 0 & A_{66} \end{bmatrix} \quad (3-59)$$

This chapter presented a frequency domain solution for the problem of the motions on ships advancing in harmonic waves. The solution is based on a strip theory approach, which means that a linear 3D flow is reduced to a 2D flow around the cross sections. The forward speed effects are introduced in a very simplistic manner, and account only to the angle of attack of the hull with the flow at infinite distance.

The simplifications introduced consist of the following:

- For the theory implementation the hull has to be (very) slender, thus the vector normal to the hull surface is 2D which works favorably in the case of C11 containership.
- The frequency of oscillation is high, again very plausible, but in practical terms the high frequency hypothesis is not a problem because at low frequencies the external forces are dominated by Froude-Krylov and restoring forces.
- The incident waves and the motions are of small amplitude (this application is „pushing“ far beyond the acceptable limits of applicability).
- The hull has vertical sides around the still waterline which again is questionable since the hull form of investigated vessel and for that matter similar ones is characterized by the non-vertical sides.
- The omission of the end term due to effects of transom stern was emphasized since the results from the code developed by Fonseca and Guedes Soares (1998) indicated that the inclusion of the end terms tends to worsen the predictions as compared to experimental data. However, since the ship has a very pronounced transom stern a further investigation is advisable using the strip theory code with the inclusion of end terms. Notice that these expressions are valid for the integration of the potential coefficients over the full ship length only. They can not be used for calculating local hydromechanics loads.

Fundamentally, strip theory is valid for long and slender bodies only. In spite of this restriction, experiments have shown that strip theory can be applied successfully to a much broader range of problems but one has to be aware of the capabilities and limits of its use.

3.2.5 Frequency domain results

The reason why C11 post-panamax was chosen relates to the fact that this ship hull form is not only suspicious to parametric rolling but the parametric rolling as a scientific research originates from the accident this vessel suffered approximately 12 years ago. It is therefore presumed that these characteristics are suitable for the scientific exploration of the phenomenon which could identify certain influences of non-linearity in the system and thus exploring the limits of validity of the proposed simulation method. On top of it, not only is this work collated to the own experimental work but also there are existing experimental results from different studies which allowed even better comparisons with numerical results. On the other hand what usually come out are the habitual results that deal with this type of dynamic instability at sea. Thereby given the nature and potential of the

procedure (fast and efficient) it has become increasingly possible to supplement the validation process with the experimental data for parametric resonance.

This section presents the solution in the frequency domain obtained with the computer program based on the strip theory presented in section 3.2. Numerical results are presented in the form of transfer functions of each modes of response as a function of wave frequency. Remember that for each response mode two transfer functions are defined by the ratio of the amplitude of first harmonic response and the first harmonic of the incident wave with the phase shift between these harmonics.

Responses of C11 post-Panamax Container Ship

The case study corresponds to a Froude number of 0.0. The regular waves considered with unitary elevation cover a range of dimensionless frequencies $\omega_0 \sqrt{L_{pp}/g}$ between 0.51 and 5.16, corresponding to wave frequency ω_0 the between 0.1 and 1.0. The ship heading on the waves is 90° (beam waves) for the motions in transverse and horizontal planes or 180° (bow waves) for the motions in the longitudinal plane. The intention is not to get into the exhaustive comparison of the results based on the linear theory but rather to point out where the solution implemented here originates as the basic information for the time domain model presented in Section 3.3. Thus, only the relevant comparisons are presented i.e. responses in the longitudinal plane due to the bow waves and the resonance conditions for the responses in the transverse and horizontal planes.

The method described above is applied here for the prediction of heave and pitch motions in regular head waves on which numerical simulations of vertical motions in regular head seas have been performed by employing the strip theory. The roll motion in head and following seas is induced by the nonlinear kinematic coupling of the pitch and heave motion, and primarily by the temporal variation of the righting lever curve in waves. The heave and pitch responses in terms of non-dimensional amplitudes η_k ($k = 2, \dots, 6$) and the phase shifts θ_{η_k} ($k = 2, \dots, 6$) between the displacements and the wave amplitudes ζ_a are presented in figures 3-7 and 3-8 for regular bow waves as a function of dimensionless wave frequency $\omega_0 \sqrt{L_{pp}/g}$. The heave amplitudes are non-dimensionalised over wave elevation ζ , while the pitch amplitudes are dimensionless with the slope of the wave $k\zeta$. The phase angles are in degrees and represent the delayed response relative to the maximum wave elevation on the longitudinal center of gravity.

It is observed that the calculated amplitudes are showing an expected trend. Moreover, the higher frequencies the short are waves therefore not enough energy is dissipated to excite the ship. The resonant peak in heave is near the natural frequency of the ship. The effects on heave transfer function, increasing the wave height, generate firstly a raise and then a reduction of the second resonance peak, which also tend to be shifted to higher frequencies.

Under these conditions, the encounter frequency in waves of wavelengths comparable to ship length is about twice the natural roll frequency. This two-to-one frequency ratio is assumed to be critical for parametric excitation. The ship responds directly to the wave excitation in the heave and pitch mode and produces an oscillation of the righting lever curve with the frequency of encounter. Linear methods generally tend to overstate the response amplitudes at resonance, here at a wave frequency of about ~ 0.5 rad/s for heave and pitch motions. Consider a wave frequency of ~ 0.45 rad/s which corresponds to a wave-to-ship length ratio of 1.2.

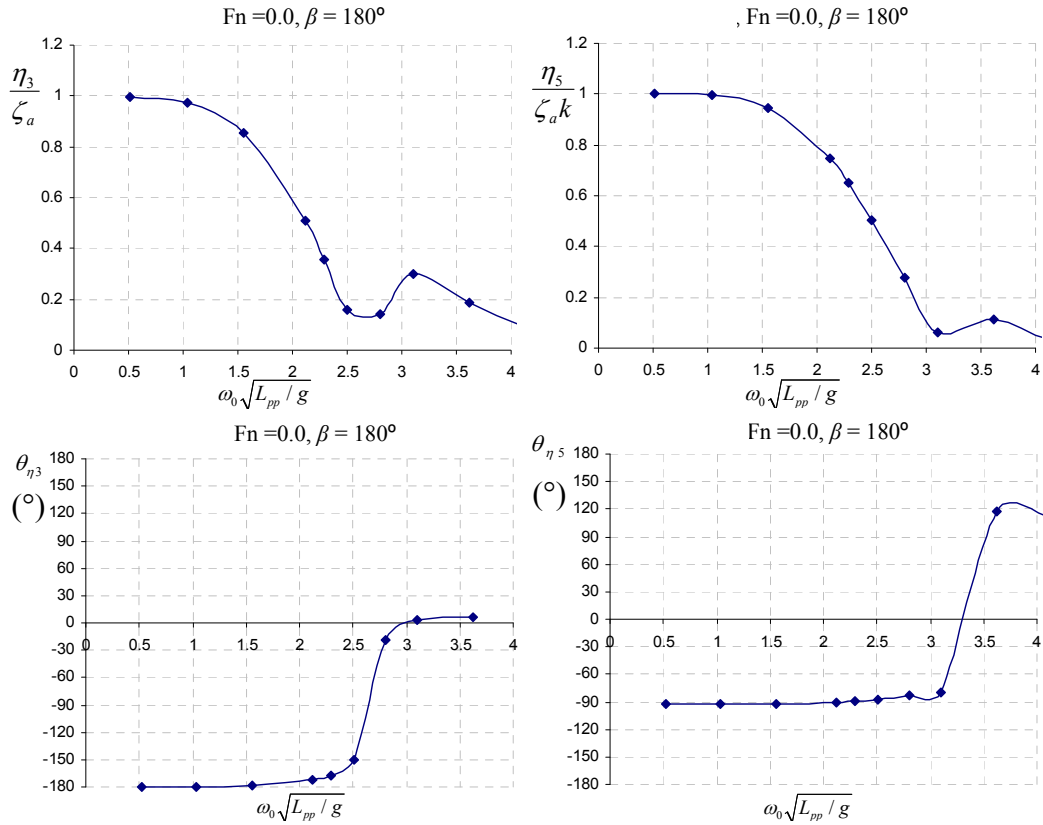


Figure 3-7. Transfer functions for C11 containership in heave and pitch in head seas at zero speed

This frequency is sufficiently far from the resonant wave frequency, so that the results of the linear heave and pitch motion analysis can be employed with confidence. As for the phase angles, the calculated curve compares well with the numerical results expected, i.e., the ship is able to "bypass" the wave at low frequencies practically without the lag.

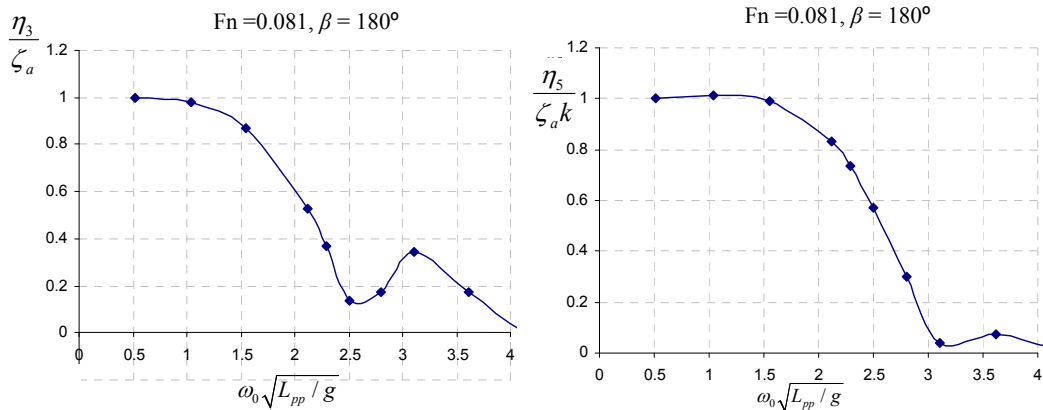


Figure 3-8. Transfer functions for C11 containership in heave and pitch in head seas for 8 knots

Responses in sway, roll and yaw are presented in figures 3-9 and 3-10 for regular beam waves.

However, for the purpose of this work the emphasis is set to the ability of predicting the modal frequency and peak amplitude of response in roll with reasonable accuracy given the nonlinear nature of this response as well as the restoring and damping coefficients for the rolling response.

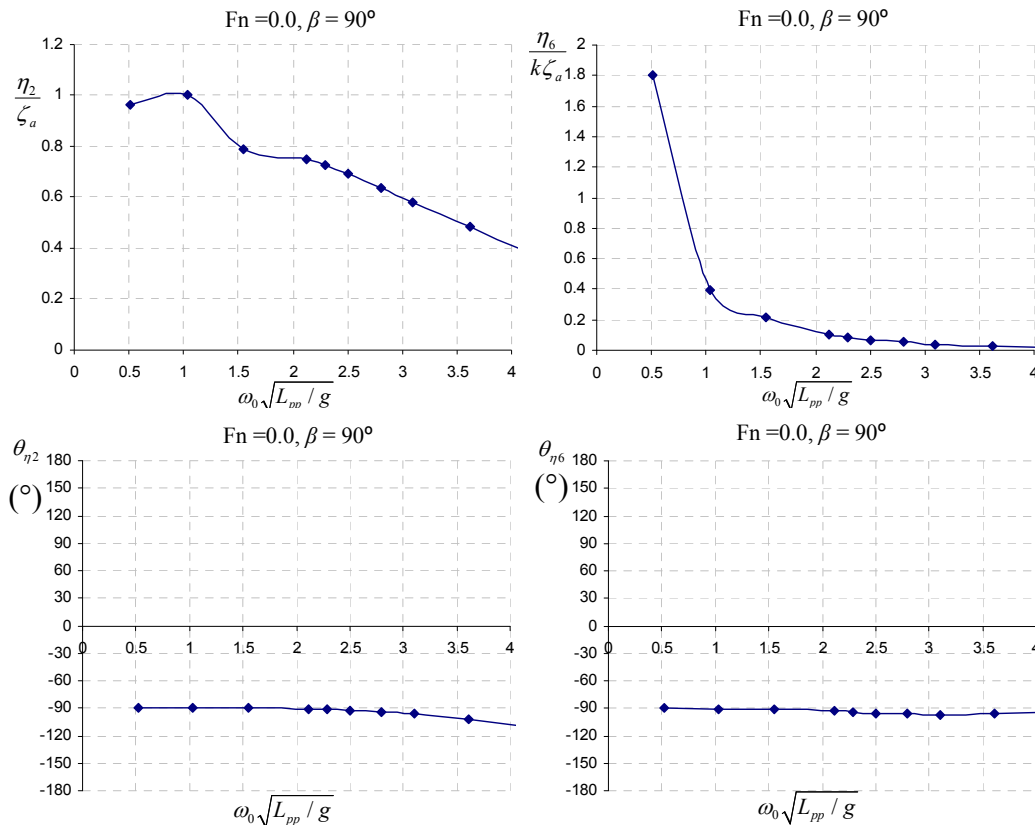


Figure 3-9. Transfer functions for C11 containership in sway and yaw in beam seas at zero speed

The upper bound of the wave excitation amplitude, beyond which the ship becomes dynamically unstable, is governed by both the damping factor and the excitation frequency. It is considered as particularly important to assess those coefficients as it serves to obtain an initial indication of natural roll frequency of the vessel and the expected magnitude of the responses for the resonance condition.

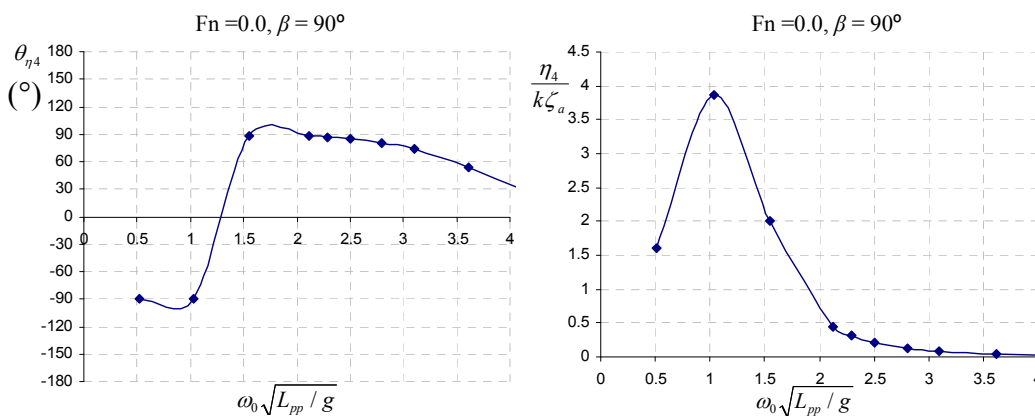


Figure 3-10. Transfer functions for C11 containership in roll motion in beam seas at zero speed

Figures 3-11 and 3-12 demonstrate the variations of the hydrodynamic added mass and damping coefficients in sway, heave, pitch and yaw. The roll added mass and damping coefficients were already presented in figure regarding the memory effects discussion. Differences in the prediction of added mass coefficients are generally limited, while calculation of damping turns out to be a critical issue.

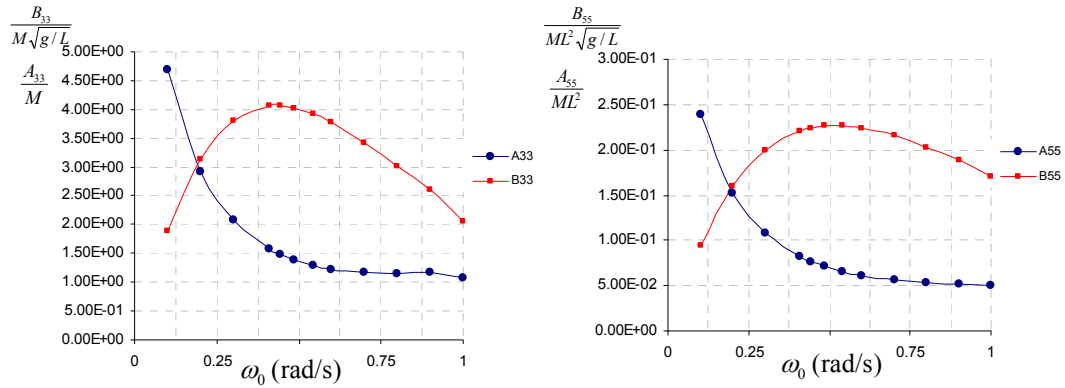


Figure 3-11. Variations of the hydrodynamic added mass and damping coefficients in heave and pitch depending on the various encounter frequencies

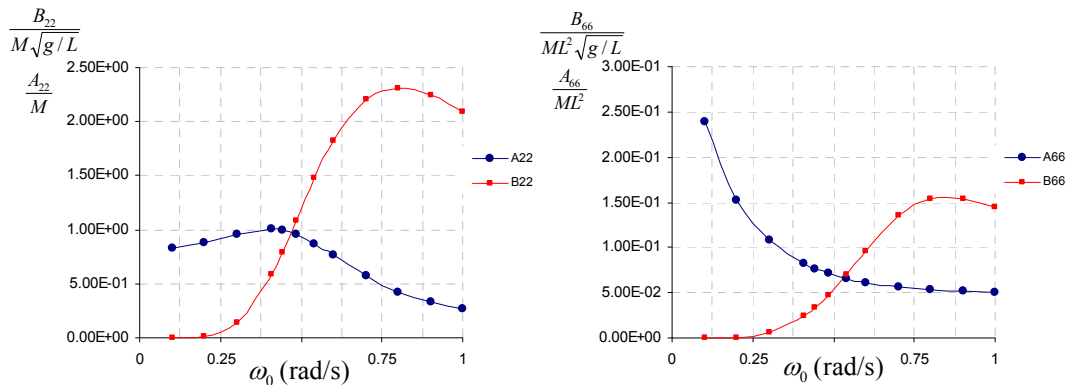


Figure 3-12. Variations of the hydrodynamic added mass and damping coefficients in sway and yaw depending on the various encounter frequencies

The trends of variation appear to be expected with methodology employed in the frequency domain analysis, even if the modules are different and their values seem connected with the motion amplitudes. However, it must be remarked that, when the relative motions between the vessel and the free surface are too large to be considered negligible other highly nonlinear effects, e.g. force due to green water, the results obtained could be questionable; moreover, the validity of the assumption of linear radiation and diffraction forces become arguable in this condition. However, these results obtained by the linear frequency domain implemented in scope of this study showed foreseen trends, both for low and high frequencies.

In the absence of validated experimental data, all the coefficients are assumed as the approved from the theoretical point of view. The experimental data that were conducted as part of the forced oscillation tests are currently being validated within the other group involved with this project (Ribeiro e Silva et al. 2011). It is particularly interesting to assess the correlation of this part of the numerical model with the investigation of the hydrodynamic characteristics of asymmetric cross-sections advancing in regular waves. The code used to obtain the hydrodynamic characteristics is essentially the same as for symmetric cross-sections but the new geometry has to be provided. For that reason forced oscillation tests with hull inclined up to 5° and 10° were conducted. Since the nonlinearity required to capture parametric rolling resides on the fact that at each time instant immersed geometry of each strip realized by the definition of the intersection of the wetted hull surface with the exact two-dimensional elevation of the wave is known, it is imperative to have a precise evaluation of hydrodynamic characteristics for a given cross-section profile.

In conclusion, the trends displayed in all cases presented validate the method and calculation procedure implemented, with regard to the responses in horizontal, transverse and longitudinal planes. Based upon the validations, it is expected that this calculation method can be safely used for conventional mono-hull ships, at least in a preliminary ship design stage.

3.3 Time domain strip theory

3.3.1 Introduction to modeling and simulation of the instabilities in time domain

The birth of modern seakeeping analysis was in the mid 20th century as demonstrated by the landmark papers of Ursell (1949), and St Denis and Pierson (1953). Continual refinements of analysis methods and mathematical techniques, combined with the availability of high performance desktop computers in the late 20th century has made routine seakeeping analysis possible in all design offices. Seakeeping analysis is a much more difficult problem compared with that of calm water resistance, and until fairly recently it has taken a very poor second place in preliminary hydrodynamic design for the majority of vessels. In fact, a vessel's seakeeping characteristics depend on so many interrelating factors that it is virtually impossible to say what will happen if a specific change is made to the hullform without doing reasonably detailed analysis. This is because the answer depends not only on the hullform but also on the wave conditions and the criteria against which the vessel is being assessed.

For that reason a derivative of a strip theory is implemented. Frequency domain methods are simpler and less computationally intensive. Most of these methods use strip theory (Salvesen et al 1970). Basically the vessel's motions are treated as forced, damped, low amplitude sinusoidal motions. Strip theory has many simplifying assumptions, yet is fast and able to produce good results for a wide variety of seakeeping problems. The two main limitations are that vessels must be sufficiently slender (high length to beam ratio) and that the Froude number must not be too high. In formulating the problem of hydrodynamic flow around a ship advancing with oscillatory motion in waves, based on the strip theory method, presented in Section 3.2, it was assumed that the flow is harmonic and the motions are of small amplitude. As explained previously, the free surface boundary condition is linearized around the undisturbed free surface and boundary condition on body surface is expanded around its mean wetted surface. Thus, the inviscid hydrodynamic forces could be decomposed into several independent components, namely the radiation and diffraction forces and the hydrostatic and Froude-Krylov forces. All these forces were therefore considered as linear, and linearity is theoretically valid when the amplitude of the oscillatory motions tends to zero and when the sides of the ship are assumed vertical. Furthermore, the hydrodynamic forces are represented by coefficients which depend on the ship velocity and the encounter frequency. From these forces one can obtain calculated coefficients of added mass, damping and excitation forces. This is a known solution in the frequency domain that together with the use of spectral techniques has great potential in, for example, optimization of hull forms in terms of its dynamic behavior on waves. The main difference between frequency and time domain methods is that for frequency domain methods, the response for a particular frequency is calculated in one step, whereas time domain methods require many thousands of time steps before a regular periodic response is achieved. Hence time domain methods require several orders of magnitude more computing resource than frequency domain methods.

Time domain methods model the wave passing the hull. At small incremental steps in time, the instantaneous net force on the hull is computed by integrating the water pressure and frictional forces on each part of the hull. Using Newton's second law, the acceleration on the hull is computed, this is then integrated over the time step to compute the new vessel velocity and position. Although this procedure sounds relatively straightforward, these methods are still under development in universities and other research establishments and are not routinely used by commercial naval architects. The main problems occur in being able to accurately predict the hydrodynamic forces acting on the hull and the fast computers (even by today's standards) required to run the programs.

What is common about time-domain nonlinear strip method is that the restoring forces and Froude-Krylov forces are evaluated over the instantaneous wetted surface while the bow flare

slamming, bottom impact, green water load by the momentum theory and hydro-elastic effects requires further consideration.

To study the non-harmonic and non-linear responses (large amplitude motions) of the vessel navigating in severe sea states (waves of large amplitude), a linear formulation in the frequency domain is not appropriate. In fact, in severe sea states we are talking about conjunction with a set of nonlinear effects that are highly important for the response of the vessel. In particular, the nonlinear effects considered more significant in terms of importance are:

- Non-linear impulses: associated with the variation of the submerged volume during oscillatory motions of the ship, especially in vessels with a highly non-linear hydrostatic and Froude-Krylov forces (low block coefficient). It is therefore necessary to include the effects of wetted surface variation consequently not being able or for that matter impossible to maintain the linearization of boundary condition around the mean wetted surface of the body;
- Non-linear effects in the potential flow: high slope waves are clearly non-linear, inducing large amplitude oscillatory motions that may jeopardize the hypothesis of linearization of body and the free surface boundary condition and linearization of hydrodynamic forces as well. The parameters that contribute to the nonlinearity in the potential flow are the slope of the incident wave and on the other hand, the inclination of the ship sides in combination with large amplitude motions and high frequency oscillation;
- Viscous effects: mainly associated with the separation of the flow and its boundary layer. Note that the added mass and the damping of the anti-symmetric motions of sway, roll and yaw are modes mostly affected by these viscous effects;
- Effects of green water on deck: the green water effect results from relative motions of large amplitudes between the hull and the waves. In certain scenarios of dynamic instability, this phenomenon may significantly alter the ship motion and should therefore be regarded as relevant.

To correct the limitations of the linear method, while incorporating some of the nonlinearities stated above, a proposed hybrid method is engaged in this study (Riberio e Silva, 2008) using both time and frequency domains, while allowing the simulation of the ship responses at sea. Hybrid approaches (also called “blending methods”) will be examined because of the problems associated with fully non linear computations.

It could be referred to as “pseudo – nonlinear” strip method where the solution is obtained in the time domain. It is noted that for practical reasons, given below, a proposed method is not “fully” in the time domain, since convolution integrals which represent the memory effects of the fluid motion where the impulse responses are integrated for the overall response are not introduced. Note that the previous formulation did not account for the hydrodynamic memory effect. The hydrodynamic load due to the ship motion is a function of its frequency of oscillation. When the ship oscillates, waves will be generated on the free surface. As time increases, these waves will propagate outward from the body, but they continue to affect the fluid pressure and hence the body force for all subsequent times. In the time domain, this force or moment can be represented by a convolution integral of the impulse response function. This formulation was originally developed by Cummins (1962) and Ogilvie (1964) and more recently by Fonseca and Guedes Soares (1998). However, these methods imply that the simplicity of the strip theory method has to be abandoned, since it requires very intense computational time. However it remains to be seen whether it is appropriate to omit those memory effects that consume CPU processing time but may compromise the accuracy of the calculation while taking into account the dominant nonlinear contributions. Still, in terms of practical engineering, the methods utilizing the integration of the impulse responses in time domain are not adopted for the tool to be used, examined and further developed under this investigation.

With these constraints, a much simpler developed formulation upon which to calculate the hydrodynamic forces associated with non-harmonic motions of large amplitude for is required. The vessel’s motion is then determined from the total integrated hull force using rigid body kinematics in a time-domain solver. At each time step, instantaneous wetted surface can be accurately determined and followed by the coefficients and the hydrodynamic forces which are calculated based on the

boundary condition on the body surface at that instant. Thus, at each time instant a set of governing equations in its most simple form is kept, but the parameters A_{kj} , B_{kj} , C_{kj} , F_k^I , F_k^D normally depending on the speed of the vessel and the given frequency of oscillation between ship and the waves also vary with the instantaneous wetted surface of the body, assuming incident wave propagation. Finally, the differential equations of motion, and other nonlinear terms containing, for example the forces exerted by the propeller and rudder, the wind induced forces or the green water must be resolved in the time domain by a numerical integration procedure. Within this chapter a set of formulation that allows calculating the various hydrodynamic forces is presented.

Thus the components of radiation, diffraction, Froude-Krylov and hydrostatic forces exhibiting nonlinear contributions, can be calculated for the ship in its exact position relative to the free surface that varies in time with the profile of the incident wave and the displacement of the ship in six degrees-of-freedom. The use of the wetted surface to determine modal velocities approximates a non-linear body boundary condition.

3.3.2 Hydrodynamic coefficients and forces in regular waves

As already stated, the hydrodynamic model developed by Riberio e Silva and Guedes Soares (2008) implemented within this research is based on the possibility of enabling the calculation of the radiation, diffraction, hydrostatic and Froude-Krylov forces at each time instant for the exact wetted surface hull under the profile of the incident wave. This section provides the formulations for the calculation of these forces under the influence of regular waves (sinusoidal). All these calculations are repeated in each time step of the simulation.

As stated a “blended method” that attempts to capture the most significant nonlinear forces. A blended method treats the large nonlinear forces more exactly while the other forces remain linear. The principal nonlinearity in the hydrodynamic forces derives from the time-varying wetted geometry, which affects the evaluation of all hydrodynamic forces. However, it has been argued that the most important nonlinear forces to capture are the hydrostatic and Froude-Krylov forces on the time-varying wetted geometry. This approach of “bodyexact” hydrostatic and Froude-Krylov forces is taken in the present theory, with all other fluid forces considered linear, thereby separated in the following sections.

3.3.2.1 Radiation coefficients and diffraction forces

As shown before, the hydrodynamic radiation coefficients are obtained by integrating the hydrodynamic pressure over the wetted surface of the hull. In turn, the hydrodynamic pressure is given by a Bernoulli's equation as a function of velocity potential. Therefore, the hydrodynamic solution of the problem involves, essentially, the calculation of velocity potential for the radiation following the boundary conditions imposed.

The problem of linear and three-dimensional boundary condition is formulated and simplified through decomposition of the velocity potential in two separate components: a component with dependence on the forward speed and other term independent of that speed. Then, assuming the ship is slender and that the encounter frequency is high, the three-dimensional boundary condition effects can be eliminated. Still, while elaborating the approach used, it also needs to be stressed out that the added mass and damping coefficients are assumed to be linearly proportional to velocity and acceleration in their response mode. Thus, the hydrodynamic memory effect by Cummins (1962) for the roll motion, expressed as a correction factor to the damping term in roll, is practically negligible for frequencies below 0.5 (rad / s) (Figure 3-13).

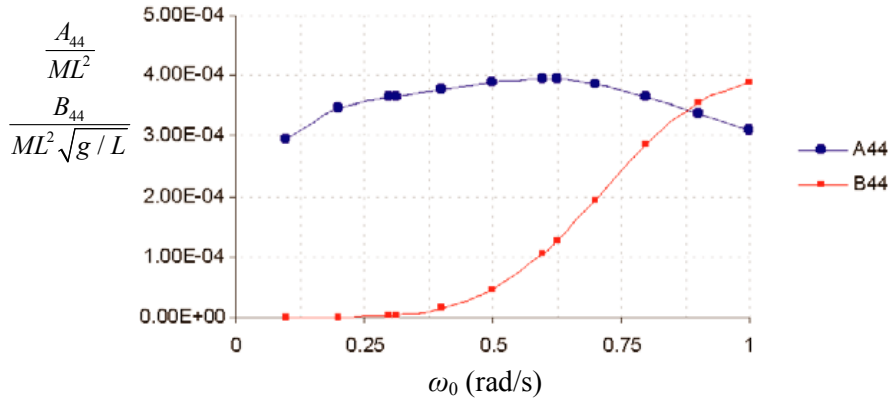


Figure 3-13. Added mass and damping coefficients of roll motion (Ribeiro e Silva et al. 2005.)

Based on this hypothesis for the evaluation on parametric rolling it becomes increasingly possible to use the engineering solution as described above, adding to the claim that wider range of validity (instead of pure strip theory frequency domain application) could be achieved for low oscillation frequencies (long waves), when clearly the radiation and diffraction components are of small influence. For that reason, and judging from the figure 3-13, for ships with conventional forms and contrary to that proposed by other authors, added mass coefficient in roll (considered as one of the most important in this research) will not significantly depend on the antecedent (rather immediate) motion in the fluid in the time domain simulations. However, a component of this force initiated at a certain moment continues to attribute its influence on the system for a period of time. This is referred to as the hydrodynamic memory effect. This claim has to be further established for the C11 post-panamax container ship due to its implications on the results while neglecting the memory effect.

The results obtained are in disagreement with the above stated proposal since the $B_{44}(\omega)$ has an steeper upward stream (Figure 3-14). Although the influence on roll damping expressed as hydrodynamic memory effect due to roll motion is not too large, one should expect results (for instance roll amplitude) characterized by definitely different convergence properties based on the assumptions made on the system memory time duration which allows truncating its expansion on the proposed equations.

In fact, in presence of important nonlinearities associated with the input–output system behavior, the number of terms, which must be taken into account in the series expansion in order to achieve an acceptable system characterization, quickly increases. Those limitations must be identified to obtain models capable of predicting the system dynamic behavior with a good accuracy. The aim however, is not to completely overcome such limitations, rather it is associated with larger computational efforts required and the advantages that a proposed methodology possesses.

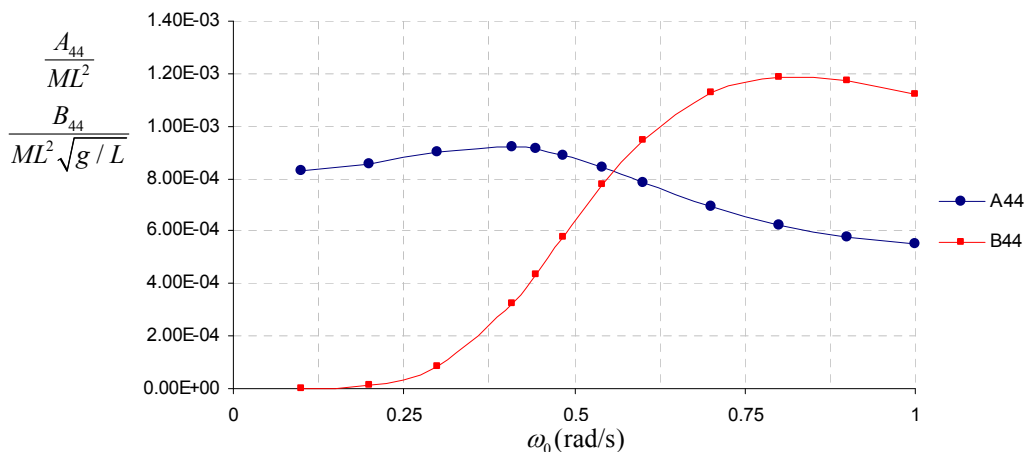


Figure 3-14. Typical variations (for vessels with conventional forms) of the hydrodynamic added mass and damping coefficients in roll depending on the various encounter frequencies

It is important to note, that those limitations are realized especially when compared to the experimental data while identifying suitable procedures for the correction of this approach non-idealities, hopefully compensated with acceptable results of the input/output relationship of a nonlinear dynamic system coupled with the damping model.

Finally, as noted, the coefficients of added mass and damping $A_{kj}(\omega)$ and $B_{kj}(\omega)$ have been deduced under previous section and are given by expressions (3-59) for each mode of response of the vessel in the frequency domain. However, there is a significant difference in how these coefficients should be calculated in the time domain. In the time domain simulations, the added mass and damping coefficients $A_{kj}(\omega)$ and $B_{kj}(\omega)$ are also computed for each cross section and for a given oscillation frequency, using the Frank "Close-fit" method, but now each section has a variable shape regarding the condition of zero potential on the instantaneous wetted surface under the profile of the incident wave. The radiation potential is thus evaluated on the wetted contour c_x of cross sections and not on the mean contour c_0 .

The diffraction force in the present time-domain theory is assumed to be linear. As with the radiation force, the diffraction force could be obtained through the use of a convolution integral. However, using the assumption that there are no significant memory effects in the diffraction problem, the total diffraction force is obtained as a linear superposition of the force due to each frequency component of the defined ambient wave environment.

According to linear decomposition of the global velocity potential assumed in the Chapter 3, for the excitation forces it is necessary to solve the hydrodynamic problem of ship moving with constant speed through a field of incident waves, while the vessel is restricted in its mean position, ie, without oscillatory motions.

The excitation force can be further decomposed into two independent parts: that of Froude-Krylov resulting from the pressure integration of the incident wave field and the diffraction part which represents the effects of disturbance on the incident potential due to the pure presence of the ship. The formulation of these forces was presented in detail previously. In time domain, representation of diffraction force can be obtained directly from the frequency domain results, given by:

$$F_k^D = \text{Re} \left[\left(F_k^D \right) e^{i\omega t} \right] \quad k = 2, \dots, 6 \quad (3-60)$$

where F_k^D is the complex amplitude of the diffraction component, ω is the encounter frequency and Re represents the real part of the expression in brackets. However, given the results obtained by Fan and Wilson (2004), a reported increase of the heave and pitch amplitudes of around 25% given the hull in its exact position relative to the free surface, varying in time with the profile of the incident wave and the displacement of the ship, a nonlinear contribution of diffraction forces was also incorporated.

Diffraction forces formulations were deduced in the previous section and are given by the expressions (3-39) to (3-41). However, as for radiation forces, at each time step considering the instantaneous wetted surface the sectional diffraction forces are calculated. Therefore, the disturbance in the incident potential is evaluated on the wetted contour c_x of cross sections and not on the mean contour c_0 .

3.3.2.2 Froude Krylov forces

Two dimensional (2D) method

With respect to the Froude-Krylov forces associated with the incident wave potential, these were also deduced before and are given by (3-31) to (3-34) for each of the motions. A time domain representation of Froude-Krylov forces on linear harmonic waves can be easily obtained from these expressions integrating the pressure over the entire wetted contour c_x of cross sections and not on the

mean contour c_0 . Thus, it is feasible to obtain Froude-Krylov forces in each mode, represented as a function of incident wave pressure given by,

$$F_k^I = \int_L \int_{C_x} p^I(t, y, z) n_k d\zeta dx \quad \text{for } k = 2, 3 \quad (3-61)$$

$$F_4^I = \int_L \int_{C_x} p^I(t, y, z) (zn_2 - yn_3) d\zeta dx \quad \text{for } k = 4 \quad (3-62)$$

$$F_5^I = \int_L \int_{C_x} x p^I(t, y, z) n_5 d\zeta dx \quad \text{for } k = 5 \quad (3-63)$$

$$F_5^I = \int_L \int_{C_x} x p^I(t, y, z) n_2 d\zeta dx \quad \text{for } k = 6 \quad (3-64)$$

with integrations over the ships length but also over the wetted cross section contour. Incident wave pressure is given by,

$$p^I(t, y, z) = -\rho g \zeta_a e^{k_0 z} \cos(\omega_e t + k \cdot x \cos \beta + k_0 y \cos \beta) \quad (3-65)$$

where ω_e is the encounter frequency, k is the wave number and β represents the heading. However, since the can also be obtained directly from the frequency domain output, calculated at each time instant while considering mean wetted surface S_0 the simpler representation of the Froude-Krylov force looks like,

$$F_k^I = \text{Re} \left[\left(F_k^I \right) e^{i\omega t} \right] \quad k = 2, \dots, 6 \quad (3-66)$$

where F_k^I is the complex amplitude of the Froude-Krylov component and this approach will be adopted. The Froude-Krylov force in the surge mode is approximated by the method proposed by Hutchison and Bringloe (1978), determined by the assumption that the pressure is exerted only at the origin of the ship fixed coordinate system $X' = (x', y', z')$.

Two and a half dimensional (2½D) method

A different approach can be utilized as well. The computational model used is a time domain potential code, capable of fully nonlinear body boundary conditions, while retaining a linear free surface boundary condition. This enables the usage of a free surface Green function. Lifting control surfaces can be modeled within the code. Currently the model is being extended to take into account the free surface deformation and to model the hull itself as a lifting surface.

The fundamental idea of the 2½D method is to solve a series of 2D problems, but use the 3D free surface boundary conditions. Usually this theory is valid for the high speed vessels only, but Holloway and Davis (2001) employed this high-speed strip theory, to develop a time-domain solution on strips fixed in space with a different (downstream) strip of the hull intersecting the plane at each time step. The solution is started at the bow and stepped toward the stern section-by-section. Their method is able to capture hull interactions for the body-exact Froude-Krylov force which is obtained on a sectional basis by integrating the pressures over the time-varying wetted geometry and then integrated over the length of the ship to find the total ship force.

The sectional solution method is based on the transient two-dimensional Green function of Wehausen and Laitone (1960),

$$f(z, t) = \frac{Q(t)}{2\pi} \ln(z - c(t)) - \frac{Q(t)}{2\pi} \ln(z - \bar{c}(t)) - \frac{g}{\pi} \int_0^t Q(\tau) \int_0^\infty \frac{1}{\sqrt{gk}} e^{-ik(z - \bar{c}(\tau))} \sin[\sqrt{gk}(t)] dk d\tau \quad (3-67)$$

where Q is the source strength, and c is the source location and \bar{c} its complex conjugate. The complex velocity $W = u - iv$ is obtained by integrating $\frac{\partial f}{\partial z}$ over all sources. To evaluate the motion of the ship the instantaneous forces on the hull are obtained by integration over its surface, $F_3 = \int_{\text{stern}}^{\text{bow}} f dx$ and $F_5 = \int_{\text{stern}}^{\text{bow}} x f dx$, where $f = -\rho \int_{\text{section}} \frac{\partial \phi}{\partial t} n_z dl$, ϕ is the potential function

describing the flow field, n_z is the vertical component of the unit normal and l is an element of the wetted perimeter. For instance, the overall rigid vessel equations of motion are then (taking an origin at the centre of mass),

$$\left[F_{3,\text{wave}} + F_3(\eta_3, \eta_5) \right] = M\ddot{\eta}_3 \quad (3-68)$$

$$\left[F_{5,\text{wave}} + F_5(\eta_3, \eta_5) \right] = I_5\ddot{\eta}_{53} \quad (3-69)$$

where all components of the hydrodynamic surface force are now on the left hand side of these equations. This formulation slightly differs from conventional strip theory, but is a strip theory in the sense that the three-dimensional problem is again represented as a set of simpler two-dimensional problems.

Assuming the ship to be rigid, the instantaneous acceleration containing significant contributions the hydrodynamic forces acting on the hull, already integrated from the 2D method is then iteratively used to compute the ship motion by numerical integration through time. The inertia forces have their origin subject to the acceleration of the mass of the vessel. Since the mass of the ship is unchanged during the motions there aren't any differences between the formulations of these forces in time domain or frequency domain.

In the present time-domain theory, only the Froude-Krylov pressures are evaluated on the exact wetted surface geometry, as determined by the intersection of the undisturbed incident wave and the instantaneous position of the ship. In the solution of the sectional forces, the wave elevation is evaluated at the (X, Y) position of each vertex of a two dimensional panel on a given section and compared to the Z position of each vertex to determine if the panel is wetted (unlike restoring forces where the geometric simplification assumption of the strip theory $ds \cong d\zeta dx$ is used to reduce the surface integrals). At each time step, it is necessary to determine the position of each 2D panel in coordinates so that the free surface elevation can be evaluated and compared to the panel's Z -value at that (X, Y) location. The transient solutions yield the pressures on the hull surface and the ship motion is computed by integration to find the total forces on the hull and the instantaneous acceleration of the hull. To do so, the following transformation is used where the right end terms present contribution section by section.

$$\begin{pmatrix} X \\ Y \\ Z \end{pmatrix} = [T_w] \cdot \begin{pmatrix} x' \\ y' \\ z' \end{pmatrix} + \begin{pmatrix} \eta_1 \\ \eta_2 \\ \eta_3 \end{pmatrix} \quad (3-70)$$

where

$$T_w = \begin{bmatrix} \cos \eta_5 \cos \eta_6 & \sin \eta_4 \sin \eta_5 \cos \eta_6 - \cos \eta_4 \sin \eta_6 & \cos \eta_4 \sin \eta_5 \cos \eta_6 - \sin \eta_4 \sin \eta_6 \\ \cos \eta_1 \cos \eta_1 & \sin \eta_4 \sin \eta_5 \cos \eta_6 + \cos \eta_4 \cos \eta_6 & \cos \eta_4 \sin \eta_5 \sin \eta_6 - \sin \eta_4 \cos \eta_6 \\ -\sin \eta_5 & \sin \eta_4 \cos \eta_5 & \cos \eta_4 \cos \eta_5 \end{bmatrix} \quad (3-71)$$

Numerically, at each time step a new strip is added at the bow and the stern strip is discarded with capability that provides an accessible simulation that captures the significant nonlinearities due to body-exact Froude-Krylov force. The combined hydrostatic and Froude-Krylov force is assumed to provide the most significant nonlinear contribution to the large amplitude ship motion problem. Given the beam of typical C11 designs, even a small roll angle can lead to large displacement of the outer-hulls, resulting in potentially large changes to the wetted surface geometry. The initial conditions for each simulation should be chosen from the steady state regime corresponding to the initial phase of the waves. In order to set up an appropriate model to describe the nonlinear ship roll motion, we follow the linear order of magnitude analysis by Newman (1978) to identify the leading order forces. In waves of wavelengths comparable to the ship length, the hydrostatic forces and the Froude-Krylov forces are of leading order for heave, roll, and pitch modes. Thus, in the first place, it is important to account for the hydrostatic and Froude-Krylov force contributions in the nonlinear model. For instance, at $F_n = 0$ kts, $\beta = 180^\circ$, $H_w = 8$ m, and $\lambda/L_{pp} = 1$ Froude-Krylov force contributions for both frequency and time domain is shown on figure 3-15.

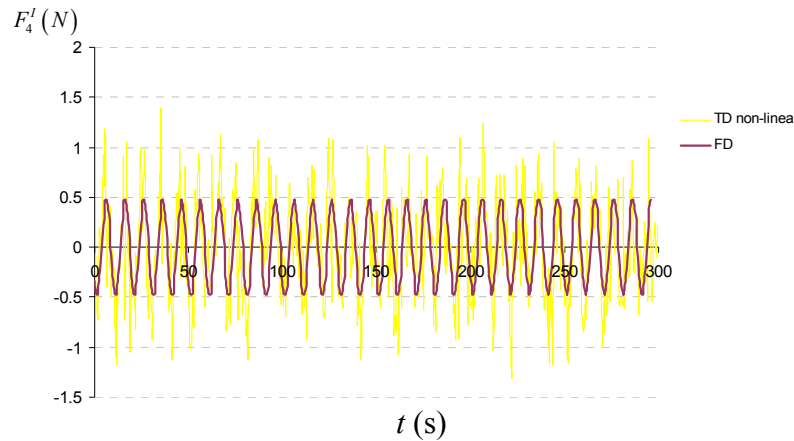


Figure 3-15. Linear and nonlinear simulation of Froude-Krylov force in roll

However, in the motions outcome this is not quite significant. The heave and pitch motion is of far more importance in a sense that those couplings can transfer the energy to roll motion which as a result can become extreme. As evident from the figures 3-16 and 3-17, the linear and non linear contribution of Froude-Krylov forces in heave and pitch are not very differentiated and as such even the frequency domain approximation of Froude-Krylov force covers the simulation quite well.

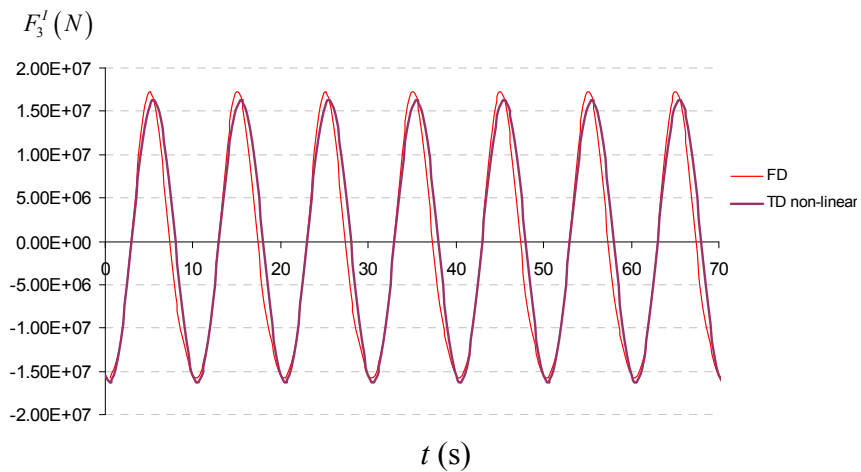


Figure 3-16. Linear and nonlinear simulation of Froude-Krylov force in heave

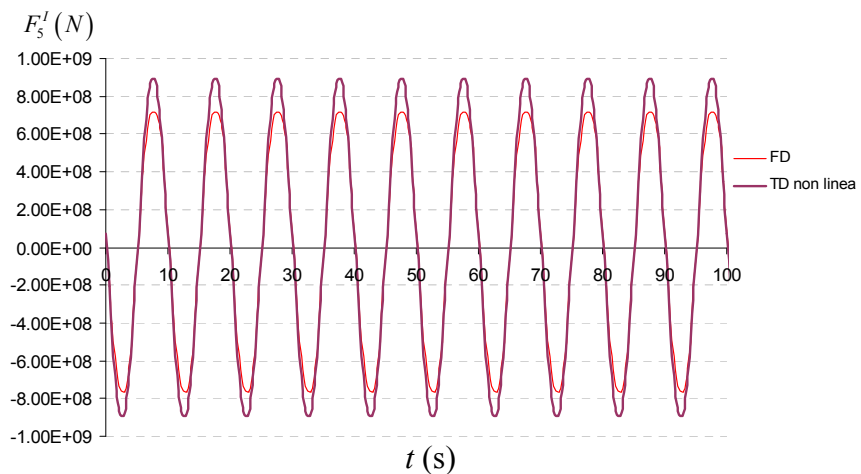


Figure 3-17. Linear and nonlinear simulation of Froude-Krylov force in pitch

For that reason, the forces associated with heave and pitch are at least of one order greater than those associated with the roll motion. We deduce that the nonlinear coupling of heave, roll and pitch motion will affect the roll motion to a higher degree than vice versa.

Bearing in mind above findings with all the nonlinearities included the implemented 2D and 2½D approaches yields the following outlook of the roll displacement time history (figure 3-18). It is evident that the only difference arising from the implementation of both methods is in the shape realisation with the amplitude of roll being almost equal. The particular peaked shape of local maxima (or minima) obtained with 2½D method resembles the nonlinear force in roll as exhibited in figure 3-15, therefore it can be argued that it better matches the physical excitation itself.

To conclude, these procedures imply re-meshing of the hydrodynamic model up to the intersection of the ship with the incident wave elevation at each time instant. Both methods allow introducing nonlinearities in the linear model, evaluating Froude-Krylov forces, which are in fact easy to compute in time domain in their intrinsic nonlinear form, by pressure integration over the instantaneous wetted surface. Due to the numerical instabilities 2½D method implies that integration is carried out using a weighted average of the hull acceleration obtained from the hydrodynamic forces with the acceleration extrapolated over the previous time step. This actually is a step back from the approximated 3D boundary problem even though it presents somewhat improved predictions.

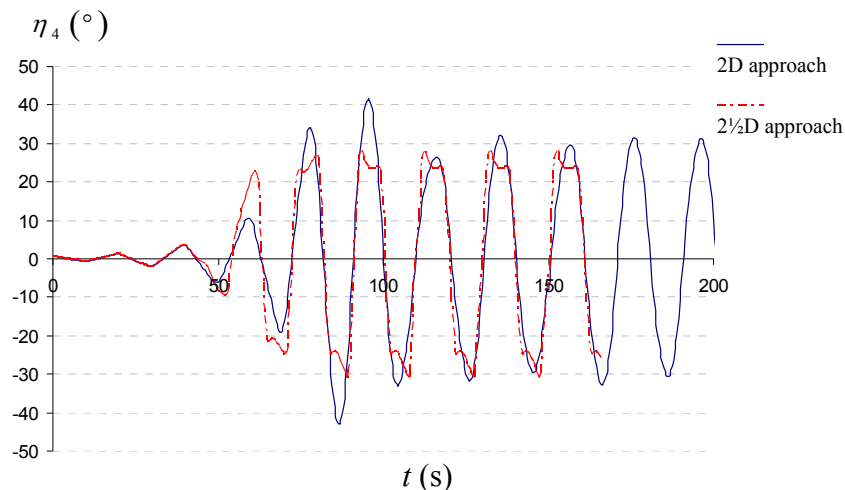


Figure 3-18. Nonlinear outlook of roll displacement with 2D and 2½D methods adopted

Given the fact that the linear Froude-Krylov forces (as seen in figures) cover the nonlinear intricacies in the simulation quite well which is also reported in Malenica et. al (2006) (restoring forces are said to represent largest contribution to nonlinearities, responsible to dictate parametric rolling), parametric rolling phenomena might not be the best fit for the 2½D method application. This might appear quite surprising since even quite crude linear Froude-Krylov approximation with respect to fully nonlinear problem is very accurate. However, it is necessary to keep in mind that rather special parametric rolling conditions are effectuated when diffraction and radiation phenomena will not be very strong meaning that the main wave effects are included in the incident wave field which is covered quite well by Froude-Krylov approximation. This assumption is not valid when Froude-Krylov is not so dominant and other nonlinearities become more important.

The computational speed running in Fortran 90 code through a DOS window of course varies with number of time steps, number of sections and segments utilized but proportionally to the 2D method, which for every “frozen” time instant given the solution is started at the bow and stepped toward the stern section-by-section is up to 20 times more computationally expensive. That fact does not merit the overall method. With respect to its application to design optimization, it has the disadvantage of being more computationally intense than strip theory, but certainly less so than 3D codes.

A utilization of 6 DOF nonlinear boundary-value problems with Det Norske Veritas’ potential flow Rankine-panel method ship motion program WASIM is planned for time domain

parametric roll resonance simulations as a higher fidelity method and for the sake of comparison. Therefore, a standard 2D “blended method” is used, whereby the hydrostatic and Froude-Krylov pressures are calculated on the instantaneous wetted portion of the ship is taken because they are fast and provide results with sufficient engineering accuracy, allowing long time simulations and couplings with other design issues.

3.3.2.3 Hydrostatic restoring forces

The restoring forces result from the combination of hydrostatic forces from the weight of the ship, where the hydrostatic forces can be obtained from the integration of the static pressure component of the Bernoulli's equation along the hull wetted surface.

The hydrostatic pressure is calculated at the mean water line assuming the angular motions are small and that the ship's sides are vertical at around water line. Within the linear theory, the only forces different from zero are related to heave, roll and pitch given by (3-44) to (3-46). However, since the anticipated motions are of large-scale amplitudes, for the time domain simulation knowledge of the ship's position relative to the free surface at each time instant is imperative because the parametric rolling is governed by the time varying restoring term. Restoring coefficients are thus calculated over the instantaneous wetted surface using integration of pressures rather than the traditional techniques of integration of the areas and volumes associated with mean draft. The theoretical approximation originating from the integration of pressures (considering the Green's theorem), as described by Patel and Witz (1984) was adopted in conjunction with the precise definition of segments (marked on Fig. 3-19) in each immersed strip necessary to calculate the hydrostatic pressure distribution of the instantaneous wetted surface.

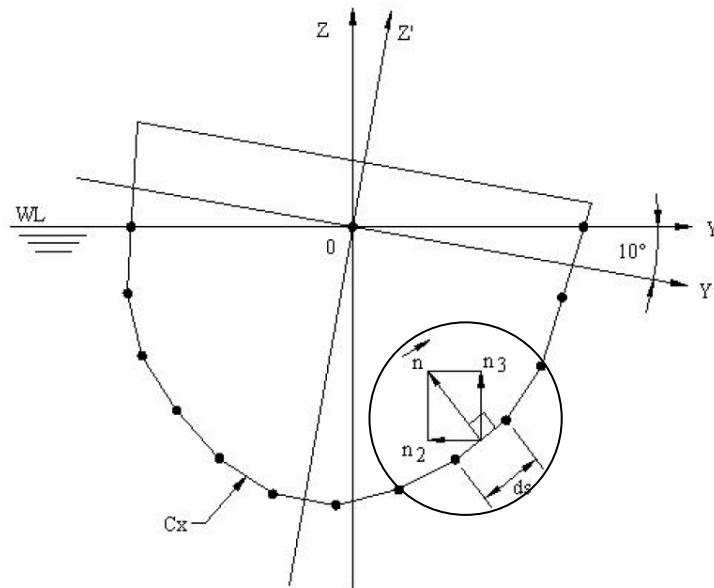


Figure 3-19. Discretization of the segments and the normal vectors along a hull for the purpose of hydrostatic calculations (Ribeiro e Silva et al. 2010.)

As illustrated in figure 3-19, the two-dimensional hydrostatic force and moment calculations are made using the pressure integration technique along each segment (C_x) of each transverse section of the ship hull, rather than using area and volume integration of the ship offsets. The original theoretical approach to the pressure integration technique outlined by Schalck and Baatrup (1990) has been adopted in conjunction with a practical method to generate the segments required to calculate the hydrostatic pressure distribution under either a regular or irregular wave profile.

The expression that gives the hydrostatic forces in various directions was exhibited earlier, therefore assuming the geometric simplification of the strip theory $ds \cong d\zeta dx$ used to reduce the surface integrals one can obtain,

$$F_2^H = \rho g \int_L \int_{C_x} z n_2 d\zeta dx \tag{3-72}$$

$$F_3^H = -\rho g \int_L \int_{C_x} z n_3 d\zeta dx \tag{3-73}$$

$$F_4^H = \rho g \int_L \int_{C_x} (y n_3 - z n_2) d\zeta dx \tag{3-74}$$

$$F_5^H = \rho g \int_L x \int_{C_x} z n_3 d\zeta dx \tag{3-75}$$

where, as shown in Fig. 3-19, C_x represents the wetted contour for each cross sections of the ship while the n_2 and n_3 are the orthogonal projections of the unitary 2D vector normal to each segment of the wetted contour in this cross section.

The hydrostatic contribution however, was limited to the linear solution extracted into the time domain simulations, with the typical righting arm realization when parametric rolling occurs (figure 3-20).

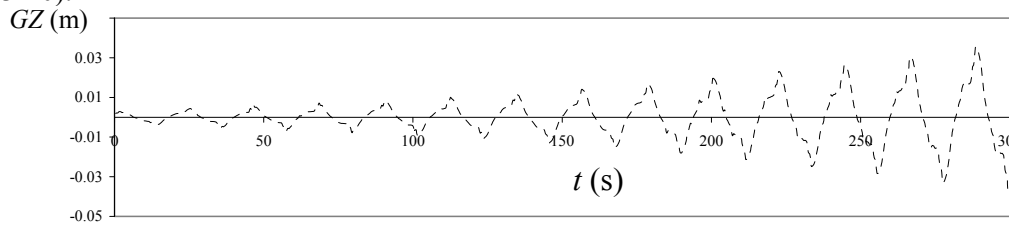


Figure 3-20. Righting arm realization for parametric rolling condition

These results suggest the occurrence of a nonlinear roll resonance, similar to that depicted in the explanatory schematic figure 3-21. The response curve is bended towards the lower frequencies indicating a jump phenomenon marked with dotted lines. The bending towards the lower frequencies is a direct consequence of the non-linear stiffness for the roll motion. It is specifically due to convex character of the GZ curve versus roll angle.

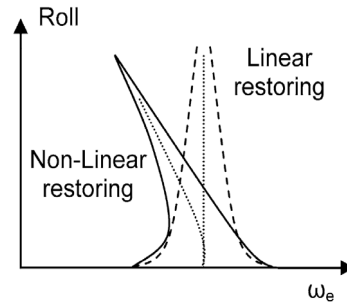


Figure 3-21 Nonlinear effects of restoring.

3.3.3 Equations of motion and time domain responses

The equations of motion represent a dynamic equilibrium between the external forces (in this case wind and hydrodynamic forces) and the associated with the mass of the ship. In this case, the equations of motion are solved by a numerical procedure, all forces being represented in the time domain. In fact, as seen in the previous section the representation of hydrodynamic forces in time is found relatively easily utilizing the results in the frequency domain. Equating the external forces with the inertial forces and the effects of restoring in each of the directions of the coordinate axes one can obtain a set of differential equations of nonlinear motions in time domain.

Owing to complex interactions between the hull and ship generated waves, the governing equations can be written in the form of integro-differential equations. Combining all hydrodynamic forces with the mass forces, using subscript notations, it is possible to obtain six linear coupled differential equations of motion, in abbreviated form, such as (Turk et al.2010),

$$\sum_{j=1}^6 \left[(M_{kj}(t) + A_{kj}(\omega, t)) \ddot{\eta}_j + B_{kj}(\omega, t) \dot{\eta}_j + C_{kj}(t) \eta_j \right] = F_k^I(t) + F_k^D(t) + F_k^P(t) + F_k^R(t) + F_k^W(t) + F_k^{DW}(t); \quad k=1, \dots, 6 \tag{3-76}$$

where the subscripts k, j are associated with forces in the k -direction due to motions in the j -mode ($k = 1, 2, 3$ represent the surge, sway and heave directions, and 4, 5, 6 represent roll, pitch and yaw directions). M_{kj} are the components of the mass matrix for the ship, A_{kj} and B_{kj} are the added mass and damping coefficients, $C_{kj}(t)$ are the hydrostatic (time dependent) restoring coefficients, and F_k are the amplitudes of the exciting forces. $F_k^P(t)$ represents the force exerted by the propeller, $F_k^R(t)$ the force exerted by the rudder, $F_k^W(t)$ wind induced force, and $F_k^{DW}(t)$ denotes the force associated with the green water on deck. The above mentioned forces are only intended as a mean of more complete and better understanding of a proposed methodology but are not a part of the code, apart from the wind force additionally implemented using Blendermann's methodology (1996).

As already mentioned, the solution of equations of motion (3-76) is performed in time by a numerical integration procedure with an appropriate integration step. In each time instant a new position of rigid body is given and intersection of each of the strip on the hull surface with the wetted surface is accurately evaluated.

Forces due to wave excitation (incident wave forces and diffraction forces) and reaction (restoring and radiation) forces due to wave-induced ship motions have to be taken into account. With the model adopted for this case study, radiation and wave excitation forces are calculated at the equilibrium waterline using a standard strip theory (Salvesen et al. 1970), where the two-dimensional frequency-dependent coefficients of added mass and damping are computed by the Frank's close fit method (Frank et al. 1975), and the sectional diffraction forces are evaluated using the Haskind-Newman relations.

The non-linear restoring coefficients in heave, roll, and pitch motions in waves are calculated using a quasi-static approach. In the time domain simulations, maintaining the hypothesis of the linear hydrodynamic model of Silva et al. (2005), the underwater part of the hull is calculated at each time step, together with its geometric, hydrostatic and hydrodynamic properties, represented as follows

$$\Phi = \Phi_U + \Phi_I + \Phi_D + \Phi_R \quad (3-77)$$

where Φ_U denotes the potential of the steady motion in still water, Φ_I is the incident wave potential, Φ_D is the diffraction potential and Φ_R is the forced motion potential.

The forces and moments, calculated using these instantaneous properties, are used to derive the resulting translational and rotational motions. These motions are applied to the hull and the time step incremented. This process is cyclic, the previous time step providing conditions for the current time step. As shown in equations (3-76), a quasi-static approach is adopted to calculate the non-linear restoring coefficients in heave, roll, and pitch motions in waves, in which calculations of significant variations on these restoring coefficients are calculated over the instantaneous waterline.

Finally, all the coefficients are calculated based on the boundary condition on the instantaneous body surface. Using this methodology the parameters $M_{kj}(t)$, $A_{kj}(\omega, t)$, $B_{kj}(\omega, t)$, $C_{kj}(t)$, $F_k^I(t)$, $F_k^D(t)$, $F_k^P(t)$, $F_k^R(t)$, $F_k^W(t)$ and $F_k^{DW}(t)$ depend, among other parameters, on the instantaneous position of the body relative to the free surface.

The intersection of the surface of the hull with the free surface has to be determined at each time instant. For this both surfaces are represented in the coordinate system $X = (x, y, z)$ moving with the average speed of the ship. The contributions of the radiated and diffracted waves are generally very small and can be neglected thus the free surface elevation is dominated by the incident wave profile.

3.3.4 Time domain strip theory in irregular waves

This section is presented to generalize the time domain formulation for the case of the ship moving in irregular waves. The generalization is relatively straightforward if the linear theory to simulate the irregular sea state is considered. Thus the wave elevation of a

stationary and irregular sea state is represented by a superposition (sum) of a large number of harmonic wave components. Assuming that the motion depend on the ship's many non-linear contributions (hydrostatic, Froude-Krylov, diffraction and radiation forces), these parameters are determined from the instantaneous position and speed of the ship, elevation of irregular free surface and the kinematic incident wave field. These calculations are all repeated at each time step of the simulation.

3.3.4.1 Representation of sea state

While the phenomenon of parametric rolling of ships in regular waves has been extensively investigated and solid knowledge has been gained, the particular conditions of this resonance in irregular waves, which represent more realistic sailing conditions, are still under investigation. When observing the sea surface a mariner will see a procession of seemingly random waves (the height visually recorded typically represents the mathematical, significant wave height). Variation in surface elevation over time makes up what is referred to as a time domain series, and for practical analysis it is usual practice to convert this data to a spectral representation of the same data (i.e. frequency domain).

In the previous section, the emphasis was on one or a few regular waves specified in terms of the wavelengths, the amplitudes and the phase factors. The dispersion relation defined the angular frequency. In the first part of this section, waves on the sea surface were assumed to be sinusoidal with constant height, period and direction. The wave height, period, and direction could be treated as deterministic quantities. The only waves in the ocean which resemble what we considered as regular is swell generated by a distant storm. "Swell" describes the natural waves that appear most like monochromatic waves in deep water, but swell, too, is fundamentally irregular in nature. In order to model a sea surface consisting of a wind sea and swell, we must introduce what is commonly referred to as random waves. In reality, wave height and period ranges from one cycle to another as seen on figure 3-22. Visual observation of the sea surface and measurements indicate that the sea surface is composed of waves of varying heights and periods moving in differing directions.

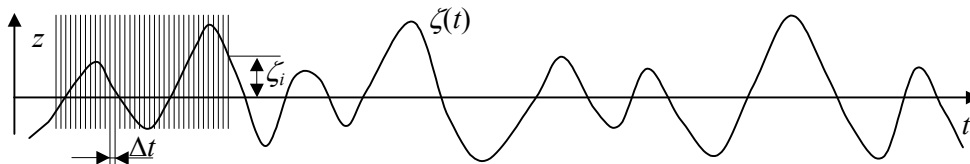


Figure 3-22. Time trace of irregular wave elevation

Therefore, when watching the sea on a windy day, the waves are far from being regular, and it is impossible to keep track of, say an individual wave crest for more than a few periods. Once the fundamental variability of the sea surface is recognized, it becomes necessary to treat the characteristics of the sea surface in statistical terms. This complicates the analysis but more realistically describes the sea surface. The term irregular waves will be used to denote natural sea states in which the wave characteristics are expected to have a statistical variability in contrast to monochromatic waves, where the properties may be assumed constant. Therefore, the gap between the regular and irregular wave conditions has been well recognized and intermediate wave conditions seen as monochromatic waves, namely that of wave groups, have been selected to test, and to provide valuable information at least for the validation purpose due to their combined deterministic and irregular character. Irregular waves generation based on a file with certain number of user pre-defined harmonic wave components is very difficult to implement, so that a pre-defined exact space and time realization of a certain water surface elevation cannot be obtained. Still given the necessity to treat the parametric rolling in realistic conditions an attempt has been made to compare the experimental data with numerical efforts and thus a brief theory of the irregular waves will be presented.

Statistical records analysis shows yet another important feature, and is very helpful from the standpoint of this study relating to the behavior of ships at sea: for extensive areas and periods of 20 minutes or more the wave elevation possesses the stationary statistical characteristics which means that the statistical properties of $\zeta(t)$ are independent of the origin of time measurement. Second, the process $\zeta(t)$ is assumed to be ergodic, which means that any measured record of the process say $\zeta_1(t)$ is typical of all other possible realizations, which permits derivation of various useful statistical information from a single record, eliminating the need for multiple recordings at different sites. To apply these concepts to ocean waves, consider an ensemble of records representing the sea state by $\zeta(t)$ over a finite time T . The most important concept for random waves is the wave spectrum to be defined below. Within the approximations which are built into linear wave theory itself, the spectrum basically gives us all properties we need about the waves, that is, it defines what is called the sea state. Under normal conditions the wave spectrum and hence the sea state is likely to be constant over, say, half an hour. The properties of the sea for a constant sea state is covered by what is denoted short term wave statistics. Short term wave statistics deals with the properties of the individual waves, typically the probability distributions of wavelength, period, height and so on. What we need is a manageable way to describe essential properties of the wave conditions.

According to St. Denis and Pierson (1953) an irregular and stationary sea state can be represented by the sum of a large number of harmonic waves (figure 3-23) where each component has a defined frequency and random phase angle. Whereas the amplitudes and the wave numbers in the sum are constant characteristics independent of where we are, the phase is more arbitrary. Actually it depends on where we choose our origin. Since it is impossible to give a unique definition of where to put an origin in the open ocean, we simply abandon to specify the phase. In random linear wave theory one thus says that the phase is arbitrary, or random. In fact, it turns out to be a good model of the sea surface to consider it made up from a lot of regular plane waves. This model is called random linear wave theory. Spectral approaches are based on the Fourier transform of the sea surface. Indeed this is currently the most mathematically appropriate approach for analyzing a time-dependent, three-dimensional sea surface record. Essentially the wave spectrum implies that the "random" ocean waves can be represented by very many regular wave trains of different amplitude and period, superimposed on one another. Unfortunately, it is exceedingly complex and at present few measurements are available that could fully tap the potential of this method. However, simplified forms of this approach have been proven to be very useful.

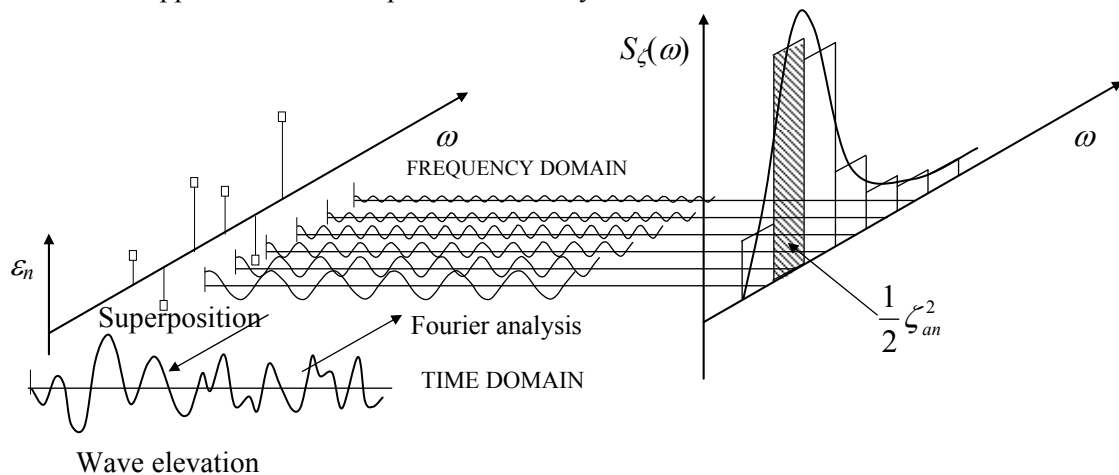


Figure 3-23. The principle of temporal and frequency analysis of wave disturbance

For an irregular sea state the two-dimensional wave elevation is given by:

$$\zeta(x, y, t) = \sum_{n=1} (\zeta_a)_n \cos\{(\omega)_n t + (k)_n (x \cos \beta + y \sin \beta) + \varepsilon_n\} \quad (3-78)$$

where amplitude $(\zeta_a)_n$, frequency ω_n and heading β constitute the profile of wave with random phase harmonic component n . Without going into more details, one assumes that the random phase

angle ε_n is independent stochastic variable, uniformly distributed between 0 and 2π . For deep waters, the frequency and harmonic wave number components are related by the dispersion equation $(\omega)_n^2 = (k)_n g$. The amplitudes of the harmonic wave components, $(\zeta_a)_n$ can be represented by the wave spectrum,

$$(\zeta_a)_n = \sqrt{2S_\zeta(\omega_n)\delta\omega} \quad (3-79)$$

The word spectrum will be known as the Fourier transform of the correlation function. It is possible to derive the wave spectrum starting from the space-time correlation function of the ocean surface, and an assumption about linear wave theory. Correlation function gives an indication of the correlation of the signal with itself for various time lags τ , and so it is a measure of the temporal variation of $\zeta(t)$ with time.

For parameterization, there are many short-term candidate parameters which may be used to define statistics of irregular sea states. Two of the most important parameters necessary for adequately quantifying a given sea state are characteristic height H_S and already mentioned characteristic period T . Other parameters related to the combined characteristics of H_S and T , may also be used in the parametric representation of irregular seas. The significant wave height is without doubt the most important sea state parameter. The concept of significant wave height, which has been found to be a very useful index to characterize the heights of the waves on the sea surface, is introduced by Sverdrup and Munk (1947),

$$H_S = 4.00\sqrt{m_0}, \quad (\varepsilon = 0) \quad (3-80)$$

The standard deviation as a common measure for the variations about the mean is thus a reasonable scale for the surface height variations. For historical reasons it has become a standard to denote four times the standard deviation of the significant wave height. The "old" definition of the significant wave height was the mean of the one third largest waves in the sea, - a definition which is not very easy to apply.

Peak period and mean wave direction which characterize the dominant periodicity and direction of the waves are also introduced. However, these parameterizations of the sea surface in some sense only index how big some of the waves are. When using irregular wave heights in engineering, the engineer must always recognize that larger and smaller (also longer and shorter) waves are present.

The wave spectrum for a given sea state assuming it is a random and stationary process, may be measured by various wave recording devices and the functions we are going to present below have been found to fit the measurements. Various forms of the wave spectrum were suggested that adapt to different conditions and depend on a variable number of input parameters such as wind speed, significant wave height, wave period, shape factors, etc. The JONSWAP spectrum (Hasselmann et al. 1973, 1976) for fetch-limited seas was obtained from the Joint North Sea Wave Project. The relationship between Pierson-Moskowitz and JONSWAP spectra is defined by the somewhat curious expression shown as,

$$S_{JS}(\omega) = S_{PM}(\omega)K_{JS}\phi_{JS}(\omega)$$

$$S_{JS}(\omega) = \alpha \frac{g^2}{\omega^5} e^{(-1,25(\omega/\omega_m)^4)^\gamma} e^{\left(\frac{(\omega-\omega_m)^2}{2\sigma^2\omega_m^2}\right)} \quad (3-81)$$

assuming $\gamma = 3.33$, and a scale factor below the modal frequency $\sigma_1 = 0.07$ with scale factor above the modal frequency $\sigma_2 = 0.09$.

These spectral equations can be used as target spectra whose parameters can be varied to fit observed spectra which may have been measured. In the first situation, the value of the parameterization is in making an educated guess at what the spectrum may have looked like. The value in the second case is for ease of analytical representation. However, very often today engineering analyses are made on the basis of numerical simulations of a specific event by use of a

numerical model. In this case, the model estimates the spectrum and a parametric form is not required. For that reason a discretization of JONSWAP spectrum is developed because there is no analytical way to determine the primitive function of spectral density of the JONSWAP spectrum, therefore a K_{JS} factor must be calculated by a numerical integration method for each of the parameters γ , σ_1 , σ_2 , and ω_m involved in the expression $\phi_{JS}(\omega)$.

$$K = \int_{\omega_{\min}}^{\omega_m} 5 \frac{\omega_m^4}{\omega^5} \left(1 - e^{-1.25 \ln \gamma}\right) \gamma e^{\left(-\frac{(\omega_m - \omega)^2}{2\sigma_1 \omega_m}\right)} e^{-1.25 \left(\frac{\omega_m}{\omega}\right)^4} d\omega +$$

$$+ \int_{\omega_m}^{\omega_{\max}} 5 \frac{\omega_m^4}{\omega^5} \left(1 - e^{-1.25 \ln \gamma}\right) \gamma e^{\left(-\frac{(\omega_m - \omega)^2}{2\sigma_1 \omega_m}\right)} e^{-1.25 \left(\frac{\omega_m}{\omega}\right)^4} d\omega \quad (3-82)$$

where ω_{\min} and ω_{\max} are frequencies that correspond to the minimum and maximum truncation curve of the spectral density through the following conditions:

$$S_{JS}(\omega_{\min}) = S_{JS}(\omega_{\max}) \leq S_{JS}(\omega_m)/100 \quad (3-83)$$

for a truncation order equal to one hundredth of its maximum value.

3.3.4.2 Hydrodynamic forces and coefficients

As suggested for regular waves, the proposed methodology for the irregular waves to calculate all hydrodynamic forces in the time domain while considering immersed geometry of each strip at every time instant is also realized by the definition of the intersection of the wetted hull surface with the exact two-dimensional elevation of the wave, as given by equation (3-78).

Radiation Coefficients

The expressions (3-23), which represent the added mass and damping coefficients in the frequency domain for unit oscillatory motions, are dependent on the encounter frequency and the wave amplitude. The calculation of added mass and damping coefficients in the time domain coupled with forced motions for irregular sea states proposed above is performed considering the spectral peak frequency of the waves.

Hydrostatic Restoring Forces

Hydrostatic restoring forces in irregular waves will be calculated using the equations (3-72) to (3-75). However, the wetted contour of the cross sections, c_x , is now defined by the elevation profile of the irregular waves instead of being defined by the elevation profile of a particular regular wave for each x coordinate of the vessel.

Excitation Forces

The excitation forces in irregular waves also address the contributions of Froude-Krylov and diffraction parts. Starting with the nonlinear contribution of diffraction, this force can also be calculated in irregular waves using the principle of superposition to represent irregular sea state. The calculation of diffraction forces in the frequency domain was presented in previous section. This result is the transfer function of diffraction force shown as a function of Froude number and the heading of the ship with respect to waves. For the expressions (3-32) to (3-34) associated with forced oscillations imposed by irregular sea states the calculation of diffraction forces in time domain can be directly applied with consideration given to spectral peak frequency and the significant wave height in the calculation of the absolute values of these forces. As proposed for the regular waves, the incident potential disturbance should be evaluated over the entire wetted contour of the cross sections, c_x , and not just on the mean contour, c_θ .

To integrate the incident wave field pressure for irregular waves, one would need to superimpose the result from of all harmonic components used to represent the irregular sea state, given by:

$$p^I(t, y, z) = -\rho g \sum_{n=1}^N (\zeta_a)_n e^{(k)_n z} \cos(\omega_n t + k_n x \cos \beta + k_n y \cos \beta + \varepsilon_n) \quad (3-84)$$

Substituting this expression in equations (3-61) to (3-64), it is possible to calculate the Froude-Krylov forces and moments in irregular waves.

3.3.5 Effects of forward speed on hydrostatic and Froude-Krylov forces

This section describes the formulation of the impulse forces which vary significantly when associated with the ships motions advancing with forward speed in waves. It should be noted that the choice of approximate methods described here was influenced by the need to apply these methods in conjunction with the (two dimensional) strip theory in the time domain, presented in earlier sections.

According to the experimental work of Blume and Hattendorf (1982), for ships advancing with forward speed a correction of the immersion in each longitudinal of the coordinate x should be applied as given by,

$$\frac{\zeta_w(x)}{L_{pp}} = -0.442 F_n^4 \left(\frac{1 - 2F_n^2 - 2\frac{x}{L_{pp}}}{2F_n^2} \right) + \left(0.082 + 0.025 \frac{x}{L_{pp}} \right) F_n^2 \cos \left(4\pi \left(\frac{x}{L_{pp}} \right)^2 \right) \quad (3-85)$$

Note that this elevation of the ship wave system, $\zeta_w(x)$, should be superimposed in the equation of the external free wave surface elevation.

Longitudinal Froude-Krylov force in surge

A special treatment of the surge motion considers the influence of periodic quantities on thrust and resistance, and improves surge motion predictions. The Froude-Krylov force in surge can be calculated from the integration of pressures due to the incident wave on the hull (in its mean or instantaneous position) whose three-dimensional velocity potential must be known apriori. However, when performing integration calculations of pressure along the segments in a two-dimensional transverse section, is no longer possible using the time domain strip theory, and alternative approximate methods available in literature such as, by Hutchison and Bringloe (1978), given by:

$$F_1^I(t) = -\rho g \nabla_0 \zeta_a \omega^2 K(k_0) \cos \beta \sin(\omega t) \quad (3-86)$$

Where $K(k_0)$ is the wave number given by,

$$K(k_0) = \frac{\sin \left(\frac{L_{pp}}{2} k_0 \cos \beta \right)}{\frac{L_{pp}}{2} k_0 \cos \beta} \quad (3-87)$$

The calculation of the Froude-Krylov force in longitudinal direction for irregular waves is made considering the spectral peak frequency and significant wave height in the calculation of absolute values of these coefficients.

4 Roll damping contribution

4.1 Introduction

Ship rolling motions is perhaps the most studied ship motion considering the disastrous consequences of failure. Large amplitude ship rolling motions can lead to progressive flooding and may eventually lead to the capsizing or foundering of a ship. The numerical model must take into consideration nonlinearities both in damping and in restoring. Roll motion for ships is more complicated as compared to the other ship motions due to the presence of a non-linear restoring moment and small linear radiation damping. The presence of light damping leads to large amplitude motion when forced at the resonant frequency. As a consequence of the large amplitude roll motion the non-linear viscous damping becomes important and this further adds to the complexity of the analysis. Although a lot of numerical models for parametric roll prediction have been proposed so far, roll damping for large amplitude and influence of roll damping estimation methods on parametric roll prediction have not been investigated nearly enough. The aim is of course, to analyze the nonlinear resonance phenomena in the steady state rolling oscillations of a ship, considering the nonlinearity both in damping moment and in the righting arm.

For the realisation of parametric rolling however, the most important factor is a restoring term. Nonlinearities in the restoring are related to the nonlinear behaviour of the GZ curve. The reliability of the description is based both on the validity of the model and on the values of the relevant parameters that can lead to parametric rolling. On the other hand, the nonlinearity of the damping is associated with frictional resistance and eddies due to appendages.

Presuming parametric rolling is obtained, nonlinear damping effectively controls the bounded roll motion amplitude. So far there have been very few attempts to incorporate the effects of nonlinear damping into analytical model to predict roll motion amplitude. Since parametric excitation can lead to large amplitude roll motion, the effects of nonlinear damping cannot be neglected. Hence incorporating the effects of non-linear damping into stability charts would give a more realistic prospect of predicting roll behaviour. It is the most difficult parameter to estimate because of its complex nature. The quantitative evaluation of roll damping is a difficult task, but estimation of the numerical values of damping is essential in the design of such vessels. Several physical phenomena contribute to roll damping. Moreover, the flow field in the vicinity of the structure in waves is altered by the presence of current or forward speed of the vessel. In addition, the problem cannot be solved directly via numerical modelling (using the fundamental equations of the fluid mechanics). Instead, use of a quasi-analytical and empirical approach has been made: certain simplified mathematical formulations are used to derive the damping function. The price paid is that not all nonlinear damping effects are included properly. To include the fully nonlinear effects of the damping, one could use a coupled system, such as a nonlinear ship motion model with a fully nonlinear viscous flow model. Recently, several viscous flow computations for two-dimensional cross sections have been published, but these are only of limited practical value as the forward speed effects in a ship change the roll damping considerably. However, this can be computationally very time consuming, difficult or even impractical.

In order to incorporate viscous effects in the roll damping moment, use was made of the procedure proposed by Ikeda et al. (1978 a,b,c,d), described by Himeno (1981). However, as Himeno himself acknowledged, we still have not fully understood the roll damping process. With reference being made toward this approach, the linear coefficient takes account of wave generating and frictional damping, whereas the second order coefficient is related to hull eddy and bilge keel damping. Much of the analysis, upon which the various components are based, is taken from analytical semi-empirical models. The difficulty in predicting the roll motion arises from the nonlinear characteristics of roll due to the effect of fluid viscosity. In majority of the researches concerning numerical prediction of parametric rolling, the Ikeda's semi-empirical prediction method

is commonly used for roll damping estimation. However, its accuracy and applicability tested on the prediction of large amplitudes of parametric roll has not been investigated sufficiently. The roll-damping coefficient for a ship hull form has several contributions. These components are considered as (1) skin friction of the hull, (2) eddy shedding from the hull, (3) free surface waves, (4) lift effect damping, and (5) bilge keel damping. The above mentioned forms of damping is presented in a very comprehensive critical analysis of a damping study along with proposed modifications based on the experimental work conducted as a part of this thesis. This subdivision of roll damping may not be hydrodynamically justifiable since hydrodynamic interaction among these components is unavoidable. However, this subdivision is a convenience, which allows computation of the individual components both analytically and experimentally. Schmitke (1978) also set out interesting ways to predict roll damping of the naval ships. Odabasi and Vince (1982) studied the effect of initial angle variations and roll damping on the roll response of a ship by utilizing the asymptotic method developed by Bogoliubov and Mitropolsky. Taylan (2000) presented a nonlinear roll motion model for predicting the roll responses of ships in waves. In this model, nonlinearities are introduced through damping and restoring terms. Together with Pesman et al. (2007) they presented a study of the influence of damping on the roll motion using original Ikeda method.

Haddara and Cumming (1990) emphasised that inviscid damping was a function of forward speed. Thus the magnitude of roll damping with combined waves and steady speed is also an important quantity (Haddara and Zhang, 1994). The slow drift may be approximated by an equivalent steady speed of the ship so that the formulas for wave plus forward speed may be applicable. They suggested a modification of the Ikeda's lift damping formula based on the results of the experiments. Chakrabarti (2001) examined the nonlinear components of roll damping and their empirical contributions. The author presented the empirical formulas derived from a series of model experiments by Ikeda et al. (1978).

As already mentioned, nonlinearities in the damping are related to the damping components different from the wave making and lift, that is, friction, eddy-making and bilge keels. Although theoretical and semi-empirical methods have been proposed in order to evaluate the roll damping, the estimation of the parameters of the model by means of experiments is still a common, and perhaps more reliable, practice. A fitting of the model on experimental data is needed especially when theoretical methods are not available or when the available methods do not give reliable results. Forced roll and free decay (Mathisen et al. 1984, Cardo et al. 1982, Spouge 1990, Hsiu et al. 1990) can usually be used for parameter identification. The former has been shown to be more flexible as they allow the analysis of the dependence of the coefficients on the frequency of the motion, while the results show less scattering (Francescutto et al. 1998). The experimental set-up is much more complicated than what is needed for a simple free decay test. Within the scope of this work an analysis based on free decay curves is conducted due to its more suitable form. It has been shown that both kinds of experiments give nearly the same results, when forced roll tests are performed with an excitation generated by means of mechanical devices (Bertaglia et al. 2003).

Estimated roll damping for the C11 containership by a roll decay test and the Ikeda's semi-empirical prediction method are shown and elaborated in detail in the next chapter. As discussed further in the next section, roll decrement tests were performed and their results used to reduce the uncertainties with respect to the use of data from an empirical model.

4.2 Numerical damping model

One reason that hinders the understanding of the roll damping effect is the nonlinear interaction between the ship body and surrounding fluid (including waves). Roll motions of ships in seaways are relatively weakly damped compared to heave and pitch motions. Therefore, large roll motions may appear near resonance frequencies. Roll damping is caused by wave radiation, tangential viscous shear forces, vortex shedding and induced circulation for the ship with forward

speed. The wave radiation contribution which is modelled directly by the potential flow methods fundamental to all strip methods is insufficient near resonance frequencies. This essentially brings us upon two biggest issues that arise from the non linear damping in conjunction with parametric rolling numerical modelling.

One comes from the fact that parametric rolling phenomenon and consequently its large roll amplitudes and the applicability of roll damping estimation methods have been investigated only to state the influence but not necessarily the accuracy in predicting it. Evaluating damping in any engineering problem when forced at the resonant frequency is extremely difficult. A spot of luck can be traced by the fact that damping effectively bounds the roll amplitude. This is in a way a backward problem since the value of the damping coefficient can be directly linked to the roll amplitude or vice versa. Therefore, it is imperative to examine quantitative prediction of parametric rolling since roll damping significantly affects the roll amplitude and occurrence region of parametric resonance phenomena.

The second arises from the fact that the used time domain "non-linear" potential flow calculations model (Ribeiro e Silva, et al.2005) is pushed far beyond its generally accepted limits of applicability in these circumstances. For a numerical study on the influence of estimation methods for roll damping on parametric roll prediction, it is preferable to utilize a reliable numerical simulation model which can quantitatively predict large amplitude of parametric roll. To validate this numerical model, a model experiment was conducted to measure roll restoring variation, which is a major cause of parametric roll. Basically we are dealing with the uncertainties with respect to the use of numerical 6-DOF ship behaviour model with the weak non-linear effects related to rapid changes in hull geometry around the waterline and the damping model as well. The non-linear diffraction and the non-wave making aspects of the roll damping are neglected; therefore the omission requires correction on basis of empiricism. To summarize, an investigation of the related onset of parametric rolling (not limiting ourselves to the growth up to substantial roll angles), including the effects of non-linear roll damping is undertaken.

When the principal dimensions of the ships are given the most reliable way to obtain the roll damping is through model experiment. However, since most of the time model test data are not available use of a mathematical model is a necessity. To balance numerical accuracy and efficiency, naval architects have developed many parameterized roll damping models. For example, Ikeda summarized by Himeno, suggested the usage of a linearized roll damping coefficient. With the linear strip theory, Himeno improved the theoretical model with his roll damping coefficients, which have, to date, been widely used. Ikeda (2004) proposed prediction methods of roll damping of ships and their application to determine optimum stabilization devices. He has modified his 25 year old empirical formula so that a more accurate formula can be used to determine the damping coefficient of many ships considering forward speed. Critical analysis of the Ikeda method is given along with the proposed formulations and its application on the vessel tested. Separate attention will be given both presenting theoretical model and decay tests.

The equation of the roll motion is coupled with two non symmetrical motions (sway and yaw). Even more, when rolling amplitude becomes large, as is the case for parametric rolling, coupling with the other degrees of freedom (heave and pitch) becomes stronger. Nevertheless, in order to limit the discussion here, the problem of nonlinear roll damping can be written down in simple single degree of freedom form described by a second order differential equation, since the effects of all these couplings on the roll motion can usually be considered as negligible especially when free decay tests are performed since there is no direct excitation of motions different from roll:

$$I_{44} \ddot{\eta}_4 + B_{44} \dot{\eta}_4 + C_{44} \eta_4 = M_{\eta_4} (\omega t) \quad (4-1)$$

in which η_4 is the angular roll motion, dots represent time derivatives, I_{44} is the total moment of inertia in roll, M is the wave exciting moment, ω is the wave frequency and t is time.

The differential equation of rolling can also be written as:

$$(I_{44} + A_{44})\ddot{\eta}_4 + B_{44,1}\dot{\eta}_4 + B_{44,2}\dot{\eta}_4|\dot{\eta}_4| + B_{44,3}\dot{\eta}_4^3 + C_{44}\eta_4 = M_{\eta_4}(\omega t) \quad (4-2)$$

In case of free decay tests the right hand side of the equation equals zero which will be explained further down in this section. The moment of inertia of a vessel is equal to the virtual mass moment of inertia of the vessel in roll motion times the angular acceleration with A_{44} as the added mass moment of inertia of the vessel. The damping coefficient B and the restoring coefficient C are shown as nonlinear quantities. The restoring moment of a ship for rolling motion is the righting moment, which is equal to the righting arm (GZ) times the displacement at any particular angle of inclination and is expressed as,

$$C_{44} = \Delta g GM \quad (4-3)$$

The restoring term in Eq. (4-2) is often given in a polynomial form. The damping term B_{44} may be represented as a series expansion of $\dot{\eta}_4$ and $|\dot{\eta}_4|$ by,

$$B_{44}(\dot{\eta}_4) = B_{44,1}\dot{\eta}_4 + B_{44,2}\dot{\eta}_4|\dot{\eta}_4| + B_{44,3}\dot{\eta}_4^3 \quad (4-4)$$

in which the first term is linear, the second term represents quadratic drag and the third term is cubic. Moreover, the above formulation is usually restrained to first couple of terms consisting of linear term associated with radiation and viscous damping (lift and wave damping) and a quadratic term associated with frictional resistance and eddies behind bilge keels and hard bilge corners. All are considered constant during motion concerned, depending on amplitude $\eta_{4,A}$ and frequency ω .

If the equation 4-2 is divided by $(I_{44} + A_{44})$ we can obtain another expression per unit mass moment of inertia:

$$\ddot{\eta}_4 + 2\nu\dot{\eta}_4 + \alpha\dot{\eta}_4|\dot{\eta}_4| + \beta\dot{\eta}_4^3 + \omega_0^2\eta_4 = 0 \quad (4-5)$$

Since it is difficult to strictly analyze the nonlinear equation stated above it can be represented by the following linearized roll damping coefficient:

$$B_{44}(\dot{\eta}_4) = B_e\dot{\eta}_4 \quad (4-6)$$

where B_e denotes equivalent linear damping coefficient. The roll damping function $B_{44}(\dot{\eta}_4)$ is linearly proportional to the rotation rate $\dot{\eta}_4$ with a constant damping coefficient B_e .

To improve the prediction of roll motions using strip methods, Ikeda carried out a research project to develop a roll damping prediction method which has the same concept and the same order of accuracy as the strip methods which are based on hydrodynamic forces acting on strips, or cross sections of a ship. For these thirty years, the original Ikeda's method developed for conventional cargo ships has been improved to apply many kinds of ships, for examples, more slender and round ships, fishing boats, barges, ships with skegs and so on. In this section a review of the refitted Ikeda (2004) model is presented followed by the proposed corrections based on discrepancies observed in the analysis process.

To begin with, the equivalent coefficient of roll damping components is expressed in terms of its various contributions (Himeno, 1981). The total damping coefficient is obtained from,

$$B_e = B_F + B_E + B_W + B_L + B_{BK} \quad (4-7)$$

in which the component damping coefficients are as follows: B_F equals hull skin friction damping, B_E equals hull eddy shedding damping, B_W equals free surface wave damping, B_L equals lift force damping, and B_{BK} equals bilge keel damping. It is a component discrete type prediction method which was developed by Ikeda et al. In the following section, each component is briefly explained with references.

4.2.1 Frictional Component

Friction damping is caused by skin friction stress on the hull surface of the ship form as the ship rolls. Thus it is conceivable that it is influenced by the waves. The presence of a bilge keel also alters the skin friction.

Frictional component takes 8 to 10% of a total roll damping for about 2 m in overall-length ship model. This component has Reynolds effect (scale effects), as a function of the fluid viscosity and the rate decreases in proportion to ship size and it takes about 1 to 3% for real scaled ships (Figure 4-1).

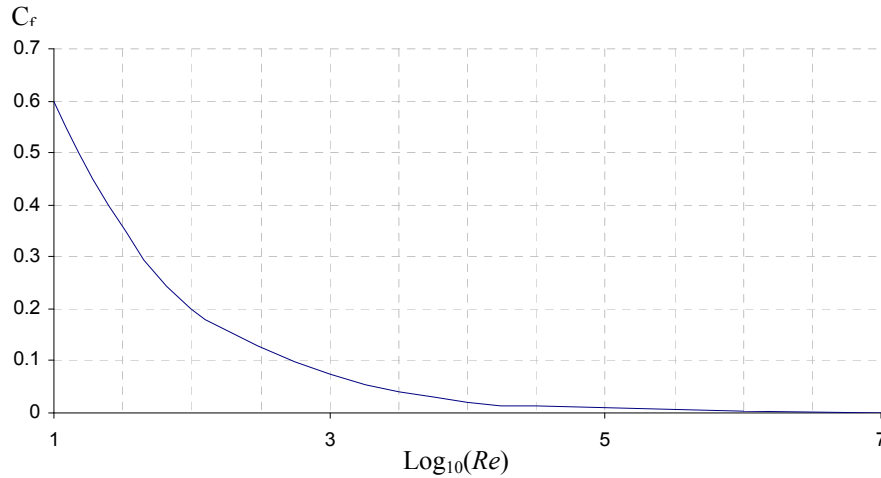


Figure 4-1. Skin friction coefficient as a function of the Reynolds number.

Therefore, the skin friction is higher in the model scale compared to the full scale value and scaling of skin friction by Froude's law is not applicable. Other components of a roll damping do not have a scale effect. Moreover, even if the scale of a ship is changed, the non-dimensional damping coefficient can be used as the same value. For estimation of this component, the following equation which is the modified Kato's equation at $Fn = 0$ by Tamiya's advanced-speed modification is used. The skin friction, slowly but steadily increases with the roll angle.

$$B_F = \frac{4}{3\pi} \rho S_f r_f^3 \eta_4 \omega C_f \left(1 + 4.1 \frac{U}{\omega L} \right) \quad (4-8)$$

In the equation, C_f (the equivalent flat plate frictional coefficient), r_f (the equivalent radius), S_f (the surface area) denote the following equations. According to the above formula, the increment of frictional damping due to ship forward speed is proportional to the speed.

$$C_f = 1.328 \left(3.22 \frac{r_f^2 \eta_4^2}{T \nu} \right)^{-0.5} \quad (4-9)$$

$$r_f = \frac{(0.887 + 0.145 C_B)(1.7d + C_B B) - 2OG}{\pi} \quad (4-10)$$

$$S_f = L(1.75d + C_B B) \quad (4-11)$$

where ν is the coefficient of kinematic viscosity, T is roll period, OG is distance from the water surface to the center of gravity (down ward positive). Adjusting this form to account for the turbulent flow, the formulation for the skin friction damping coefficient has been proposed as (Chakrabarti 2001),

$$B_F = 0.787 \rho S_f r_f^2 \eta_4 \sqrt{\omega \cdot U} \left\{ 1 + 0.00814 \left(\frac{r_f^2 \eta_4^2 \omega}{U} \right)^{0.386} \right\} \quad (4-12)$$

where first term in the above expression, linear and independent of the roll amplitude arises from the laminar flow past the ship. The second term is nonlinear and gives the modification due to turbulent flow. Actually, all the formulations stated here can safely be applied since the ratio of friction damping to total damping is usually quite small almost to the point that it can be ignored.

4.2.2 Wave Making Component

This component takes about 5 to 30% for a general-cargo type ships. However, the component may account to a bigger rate for the type of ships which are characterized by shallow draught and wide section. Wave damping is caused by the free surface waves and is thus a function of the wave parameters. The component at $Fn = 0$ can be calculated by a linear potential theory based on small wave height. Actually, it is computed quite accurately from the linear diffraction/radiation theory and is generally known as radiation damping, B_{w0} . This is the only damping used in the other degrees of freedom with reasonable success in getting satisfactory results.

In the presence of ship forward speed, this damping is modified. A simple analytical expression for this damping may be derived (Ikeda et al., 1978a) for a flat plate by introducing a pair of doublets at the two longitudinal ends. For the effects of forward speed, this component is taken into consideration by using the following modified equation,

$$\frac{B_w}{B_{w0}} = 0.5 \left[\{ (A_2 + 1) + (A_2 - 1) \tanh 20(\Omega - 0.3) \} + (2A_1 - A_2 - 1) e^{\{-150(\Omega - 0.25)^2\}} \right] \quad (4-13)$$

$$A_1 = 1 + \xi_d^{-1.2} e^{(-2\xi_d)} \quad (4-14)$$

$$A_2 = 0.5 + \xi_d^{-1.0} e^{(-2\xi_d)} \quad (4-15)$$

$$\xi_d = \frac{\omega^2 T}{g}, \quad \Omega = \frac{\omega U}{g} \quad (4-16)$$

In addition, the component with the effects of forward speed is computable with an exact potential calculation. Note that the damping coefficient is maximum at $\tau = 1/4$ and asymptotically approaches a constant value at large values of τ . Again, this equation may be applied to those structures which are undergoing a slow drift motion coupled with high frequency motion in waves.

On the other hand it is difficult to imagine modeling an extremely complex phenomenon, such as three-dimensional wave radiation by means of a simple relationship like (4-13). If it is argued, that a prediction of the damping is underestimated, therefore, maximum amplitude of the rolling motion is overestimated, it is possible to make use of the extremely simple methodology proposed considering just to be on a safe side. The results for a slender ship ($C_B = 0.58$) such as C11 container ship shows two peaks at the vicinity of cross sections three and seven as seen on figure 4-2.

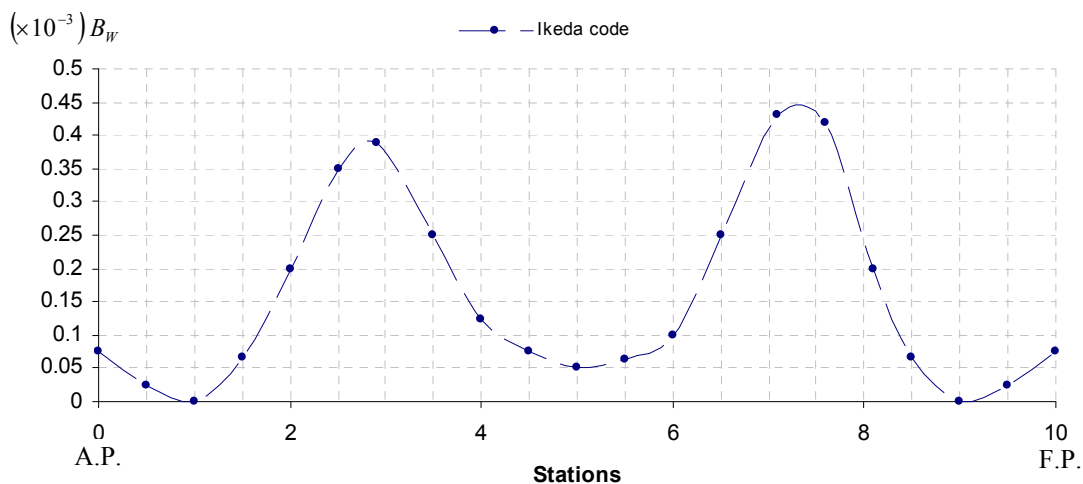


Figure 4-2. Roll damping distribution of wave component.

The Matlab graphical presentation was utilized to simulate the contribution of three-dimensional wave radiation (Fig. 4-3) showing the greatest contributions (red on graph) at the vicinity of cross sections of SS = 3 and SS = 7 on bow and stern parts.

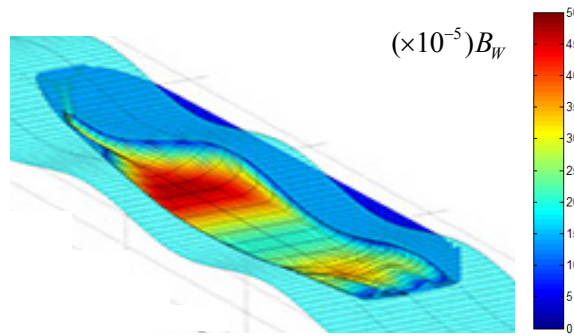


Figure 4-3. Simulated 3D roll damping distribution of wave component.

The reason why the peaks appear on bow and stern parts can be easily understood from the calculated results by a simple prediction formula provided by Kawahara et al. 2009, shown in Figure 4-4. with the characteristics of roll damping coefficient of wave component from Ikeda's experimental work based on two parameters related to the hull shape, area coefficient at a cross section along the hull $\sigma = \frac{A_x}{B_x T_x}$ and half breadth / draft ratio $H_0 = \frac{B_x}{2T_x}$.

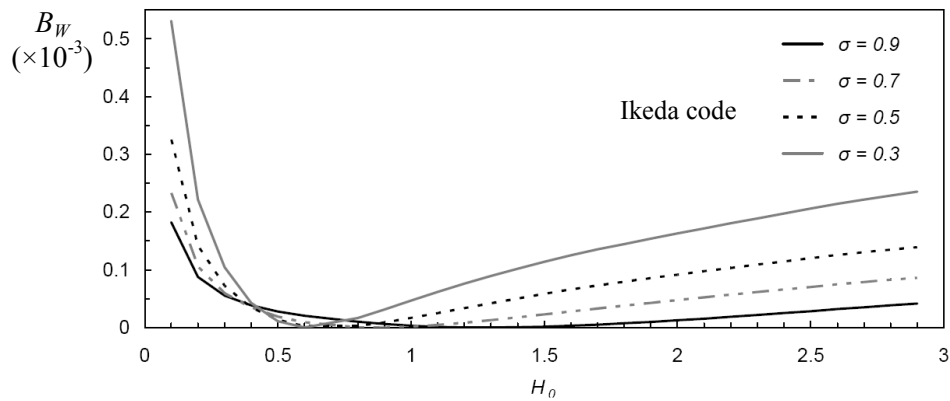


Figure 4-4. Characteristics of roll wave damping coefficient for a two dimensional section.

4.2.3 Eddy Making Component by Naked Hull

The viscous eddy damping considered in roll arises due to separation at the sharp corners and the vortices generated by the flow separation. It is the damping component caused by small separation bubbles or small shedding vortices generated at the bilge part of midship section and large vortices generated at the relatively sharp bottom of bow and stern sections. The main cause is the local two-dimensional vortex shedding from bilge and bottom around bow and stern, where pressure gradient changes rapidly.

Although, vortex shedding flow from oscillating bluff bodies is usually govern by Keulegan-Carpenter number, K_C . Since vortex shedding is not very large the dependence on K_C number is rather small. The eddy-making drag is computed from a formula similar to the velocity squared drag force based on a drag coefficient

$$F = 0.5 \rho C_e S (r \omega \eta_4)^2 \quad (4-17)$$

where r is the radial distance from the center of gravity of the ship to the corner where eddies are shed (local radius). The drag coefficient C_e is obtained from the formula provided for a U shaped or a V shaped hull (Tanaka 1957).

Ikeda performed a forced toll tests on 2D cylinders which are governed by roll damping moment M_R as explained previously,

$$M_R = B_1 \dot{\eta}_4 + B_2 \dot{\eta}_4 |\dot{\eta}_4| \quad (4-18)$$

in which the damping is assumed to have nonlinear form $B_2 \dot{\eta}_4 |\dot{\eta}_4|$ with the coefficient B_2 constant, depending only on the ship hull configuration. Using equivalent linear damping notation we can write in non dimensional form assuming linear proportionality to non dimensional frequency $\hat{\omega}$,

$$\hat{B}_e^* = \frac{B_e^*}{\rho \nabla B^2} \sqrt{\frac{B}{2g}} \quad (4-19)$$

where B is the breath of the section and is displacement of the cylinder. According to the Ikeda hypothesis damping measured in the tank can be represented as the sum of the following components: $B = B_F + B_E + B_W$. It is assumed that the damping of the wave generation B_W^* and that of the frictional shear stress B_F^* are linear contributions integrated into the first term of (4-18). Then, the equivalent linear damping coefficient B_E^* remains defined by:

$$B_E^* = B_2 \eta_4 \omega \Rightarrow \hat{B}_E^* = \frac{B_E^*}{\rho \nabla B^2} \sqrt{\frac{B}{2g}} \quad (4-20)$$

While B_2 is not affected by either η_4 or ω with B_E^* being almost proportional to both, observing the equation (5-20) the conclusion reached by Ikeda appears justified when stated that the damping by vortices generation is both proportional to the square of the frequency and the square amplitude of the rolling motion.

Considering a generic cylinder of length L and draft T equal to the radius, the damping force acting on it can be expressed by introducing a coefficient C_R such as:

$$F_R = 0.5 \rho C_R A V_T^2 \quad (4-21)$$

where

$A = TL$ projected area of the cylinder in the plane orthogonal to direction of rolling motion;

$V_T = \omega(t)T$ instantaneous tangential velocity of rolling motion, with maximum corresponding to the maximum radius;

We can then write,

$$F_R = 0.5 \rho C_R L T^3 \omega(t) |\omega(t)| \quad (4-22)$$

while the moment takes the form of,

$$M_R = 0.5 \rho C_R L T^3 \omega(t) |\omega(t)| T = 0.5 \rho C_R L T^4 \omega(t) |\omega(t)| \quad (4-23)$$

Assuming that the damping moment of the vortex generation is purely quadratic, it coincides with the second term of (5-18), and the quadratic damping coefficient B_2 is represented with the following quantity,

$$B_2 = 0.5 \rho C_R L T^4 \quad (4-24)$$

thus clearly depending on the cylinder geometry and the fluid characteristics. The coefficient C_R can now be expressed as,

$$C_R = \frac{B_2}{0.5 \rho L T^4} \quad (4-25)$$

Based on these considerations, we can finally arrive to the methodology for predicting damping coefficient for eddy generation. The procedure followed by Ikeda to develop an expression for the coefficient C_R provides:

1. identification of the point or points in the occurrence of flow separation,
2. assumption of a certain shape and size distribution of pressures produced by vortices,
3. the integration of pressure over the entire surface of the hull to get the overall damping.

Based on experimental evidence, Ikeda suggested that depending on the shape of the hull we can separate the occurrence of either one or two vortices but their position remains fixed during half period of motion. The condition for the appearance of eddies seems to depend on two parameters

related to the hull shape, area coefficient at a cross section along the hull $\sigma = \frac{A_x}{B_x T_x}$ and half breadth / draft ratio $H_0 = \frac{B_x}{2T_x}$.

The distributions of pressures on the hull sections are all triangular and decreasing monotonously as the distance increases from the corners. The maximum pressure distribution is determined by a pressure coefficient C_P defined as:

$$C_P = \frac{P^*}{0.5 \cdot \eta_4^2 \cdot \omega \cdot r^2} \tag{4-26}$$

where P^* represents the maximum pressure distribution of the instant in which $\eta_4(t) = 0$, while r is the distance from the edges to the roll axis. The pressure passes the maximum value of P^* for the entire section to the fictitious value $P_m = P^* \times 2$ as seen on the figure 4-5, for the calculations on half-section.

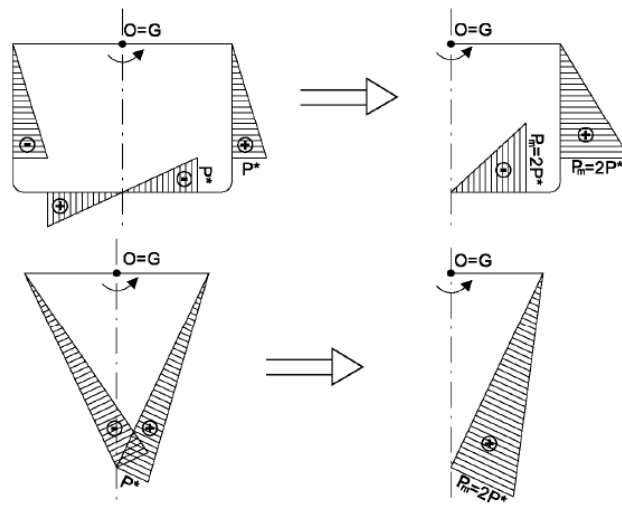


Figure 4-5. Distribution of pressures along the contour of the sections according to the Ikeda method

At this point the damping moment due to the formation of vortices can be obtained by integrating the pressure distribution on the entire wet boundary of the section and multiplying it with an appropriate rolling lever. Hence, for the case of two point separation we have,

$$M_R = LT^2 \frac{P_m}{3} \left\{ \left(1 - \frac{R_b}{T_x} \right) \left(1 - \frac{OG}{T} - \frac{R_b}{T_x} \right) + \left(H_0 - \frac{R_b}{T_x} \right)^2 \right\} \tag{4-27}$$

with,

$$R_b = \begin{cases} 2T_x \sqrt{\frac{H_0(\sigma-1)}{\pi-4}} & \text{for } R_b < T_x \text{ and } R_b < \frac{B_x}{2} \\ T_x & \text{for } R_b > T_x \text{ and } H_0 > 1 \quad (\text{eddy}) \\ \frac{B_x}{2} & \text{for } R_b > H_0 \cdot T_x \text{ and } H_0 \leq 1 \end{cases} \tag{4-28}$$

while for the case of two point separation we can write,

$$M_R = LT^2 \frac{P_m}{3} \left(1 - \frac{OG}{T} - \frac{1}{2} H_0^2 \right) = LT^2 \frac{P_m}{3} \left(1 - \frac{OG}{T} - f_2 H_0^2 \right) \tag{4-29}$$

Combining the two it is possible to obtain the general expression for the eddy making component C_R .

The formula for the eddy-making damping per unit ship length is derived as,

$$B_{E0} = \frac{4}{3\pi} \rho \cdot D_x^4 \cdot \phi_0 \cdot \omega \cdot C_P \cdot C_R \tag{4-30}$$

The pressure distribution caused on the hull surface by the vortex shedding is approximated by the first-order equation, and that pressure value is determined from the measured results of the two-dimensional models which have various shapes of cross-section as seen from the figure before. The proposed formulation for a two-dimensional section is expressed with the following equation,

$$B_E = \frac{4}{3\pi} \rho L d^2 r_m^2 \phi_0 \omega \left\{ \left(1 - f_1 \frac{R}{d}\right) \left(1 - \frac{OG}{d} - f_1 \frac{R}{d}\right) + f_2 \left(H_0 - f_1 \frac{R}{d}\right)^2 \right\} C_p \quad (4-31)$$

in which C_R is computed at incremental ship station. The quantities R_b = bilge radius, OG = distance (positive downward) from O to G , H_0 = half the beam-draft ratio at different stations of the ship (a variable depending on its shape).

$$f_1 = 0.5[1 + \tanh\{20(\sigma - 0.7)\}] \quad (4-32)$$

$$f_2 = 0.5(1 - \cos \pi\sigma) - 1.5 \left[1 - e^{\{-5(1-\sigma)\}}\right] \sin^2 \pi\sigma \quad (4-33)$$

$$C_p = 0.5 \{0.87 e^{-\gamma} - 4 e^{-0.187\gamma} + 3\} \quad (4-34)$$

where γ in the previous equation is the ratio of the maximum relative velocity U_{max} and mean velocity on the hull surface U_{mean} . This can be obtained by the calculation for the Lewis form sections. The criteria used by Ikeda for creating better approximates of Lewis forms sections are given as,

$$H'_0 = \frac{H_0}{1 - \frac{OG}{T_x}} \quad \text{and} \quad \sigma' = \frac{\sigma - \frac{OG}{T_x}}{1 - \frac{OG}{T_x}} \quad (4-35)$$

for the lower portion under the roll axis of the cylinder related to those parameters H_0 and σ of the original section of the cylinder under the water line. However, the Lewis conformal mapping used by Ikeda was identified by several authors as a main obstacle in observed discrepancies between numerical results and experiments especially for novel ship forms (Hamamoto, 2009).

For a 3-dimensional ship form, the above sectional coefficients are integrated over the length of the ship. Thus the section damping coefficient considers the section geometry of the ship along its length. The damping is large near the bow and stern for slender ships while it has a greater contribution near the midship section for a barge-like structure.

In fact, from analysis of the original Ikeda Fortran code published in Himeno (1981), it can be deduced that there is a possibility that the share of center of gravity G may not coincide exactly with point O . In case where the gravity is positioned slightly above or slightly below the waterline, the form generated differs only slightly from that the section itself. On the contrary, if the value of OG is high and therefore center of gravity is far above the waterline, the transformation produces sections which are significantly from that of the starting section. The same applies for the relationship $\frac{OG}{T_x} \gg 0$.

The poor fitting of real forms affects the calculation of most of the coefficients of methodology and in particular the γ parameter. Remember that γ is the ratio of flow velocity at the point of separation for the Lewis form examined and the speed of the flow around a hypothetical sectional circular area equal to the area of the form. Since both speeds are calculated based on the parameters H'_0 and σ' , so in cases where $\frac{OG}{T_x} \ll 0$, γ and therefore C_p is not reliable.

In the original methodology two inconsistencies have also been traced. The first is related to the above noted: the determination of parameter γ which is used to form Lewis sections extended to the center of gravity G . On the other hand, identification points for a flow separation along the contours of the section are generated parametric forms based on the parameters H_0 and σ , extended up to waterline. The second inconsistency is related to expressions for calculating the damping

moments given in (4-27) and (4-29). For both cases of U and V sections, the forces produced by the triangular distributions pressure on the sides and bottom of semi sections can be decomposed into a vertical and horizontal component. The damping moment is given by the sum of sectional moments produced by the different components with respect to the center of gravity of the ship.

While the arm of the vertical components is correctly assessed (for U section $b = \frac{1}{3} \frac{B_x}{2}$ and for V sections $b = \frac{2}{3} \left(\frac{B_x}{2} - R \right)$), the arm of the horizontal components does not seem correct.

Despite the fact that distributions of pressure are being assumed extended to the waterline, the arms used in the case of side triangular distribution approximation (fig. 4-6) are extended until the center of gravity G. For both U and V sections, the arms can be deduced from (3-57) and (3-59) as $b = \frac{2}{3} (T_x - OG)$ when in reality it should be equal to $b = \frac{2}{3} T_x - OG$.

In addition, even the Lewis forms of three parameters can not satisfactorily reproduce forms a bulbous bow sections typical of many ships today. A final serious problem of the methodology can be traced is the case in which the sections are identified as the sections with one point of separation, that are characterized with high ratios B_x/T_x . Typically, this is the case of aft transom, where the damping moment (4-27) can theoretically be vanished. When the condition referred to as a third case on figure, is reached the lines of acting forces produced by the resulting pressure distribution on each side is to go through the G: canceling the arm, consequently the moment as well.

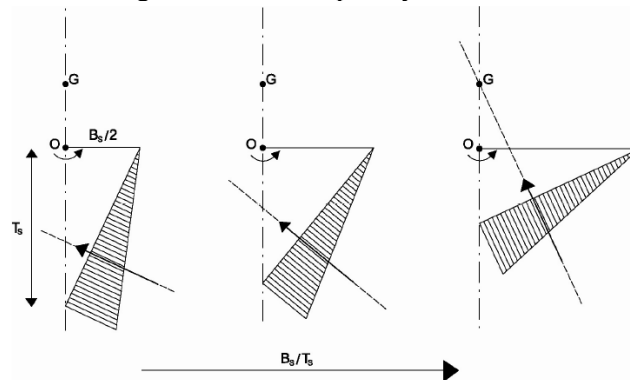


Figure 4-6. Cancellation of damping moment for 2D sections due to the effect of a gradual increase in B_x/T_x ratio with high damping ratio at a point of separation (Dreossi, 2004).

Based on these considerations, the original method was modified in attempt to limit the problems. The changes are described below in brief.

1) Improving the quality of the generated parametric forms. Assuming that the semi empirical relationship for calculating the C_P is reliable, it is sought to improve the quality of the generated parametric forms. This has resulted in the calculation of the coefficient γ , by the replacement of the parameters H_0 and σ with the values of H_0' and σ' derived from real ship sections but extended to the waterline. In addition, for consistency with the experimental results obtained by Ikeda, it is assumed that the sections rolling around the point O, while in the calculation of the damping moment is adopted as reduction point of the forces from the vessels center of gravity G. It requires more verification especially in a sense that original sections have to be printed and overlapped with the Lewis form sections to check the validity of the method.

2) If a calculated component of the viscous roll damping coefficient becomes less than zero, this component will be set to zero. Meaning, in the calculation of the total damping, the damping produced by the sections for which the coefficient C_R is negative needs to be ignored. Therefore, the problem in these cases has been circumvented by requiring C_R to be equal to zero. The approach to the problem is not novel, having been adopted by some Journée implementation of the methodology

of Ikeda in the code to predict the motions Seaway vessel (Journée, 2001). The comparison between the original code and the modified code is presented in the following figure 4-7.

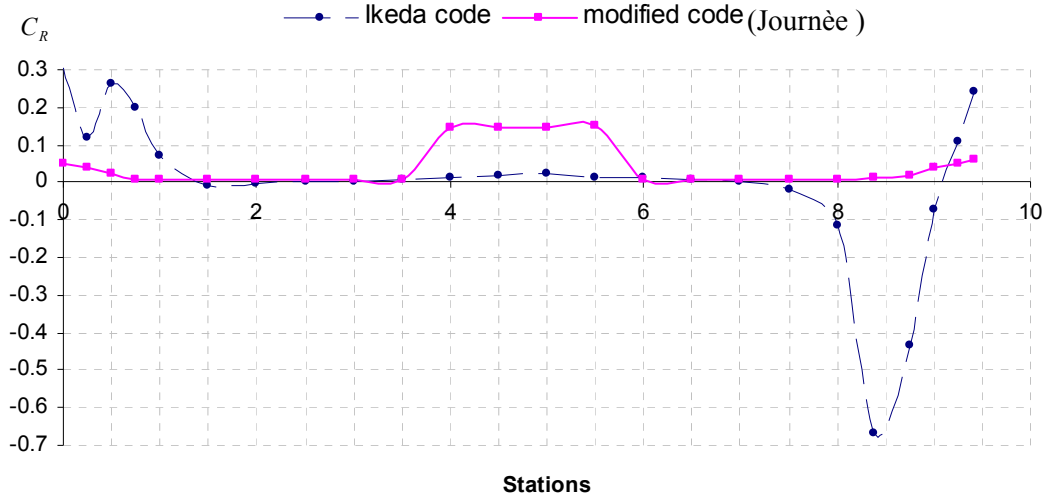


Figure 4-7. Roll damping distribution of coefficient C_R for original and modified methodology.

It is easy to notice the discrepancies in the original code when values of C_R towards bow became very negative.

3) Changing the calculation of the radius at which the separation is supposed to occur. In this case, the procedure is no longer based on the determination of the angle in correspondence to which the function is capable of extreme, but the identification of point in the section where the boundary has the maximum curvature. The relatively simple formulas of Frenet–Serret have been utilized for this purpose.

4) Introduction of a criterion to estimate the accuracy with which the generated Lewis forms approximate the real ship sections. In some cases the Lewis transformation can give more or less ridiculous results. The typical Lewis hull forms, with the regions of the half breadth to draft ratio H_0 and the area coefficient σ to match as presented before, can be distinguished in Journée, 2001.

Not-acceptable forms of ships are supposed to be the re-entrant forms and the asymmetric forms. So conventional forms, bulbous forms and tunneled forms are considered to be valid forms here. To obtain ship-like Lewis forms, the area coefficient σ is bounded by a lower limit to omit re-entrant Lewis forms and by an upper limit to omit non-symmetric Lewis forms. The criteria used to define a parametric form as acceptable (Journée, 2001) can be written as,

$$\frac{3\pi}{32}(2 - H_0) \leq \sigma_0 \leq \frac{3\pi}{32} \left(10 + H_0 + \frac{1}{H_0} \right) \quad \text{for } H_0 \geq 1 \quad (4-36)$$

$$\frac{3\pi}{32} \left(2 - \frac{1}{H_0} \right) \leq \sigma_0 \leq \frac{3\pi}{32} \left(10 + H_0 + \frac{1}{H_0} \right) \quad \text{for } H_0 < 1$$

If a value of σ is outside of this range it has to be set to the value of the nearest border of this range, to calculate the Lewis coefficients. Numerical problems, for instance with bulbous or aft cross sections of a ship, are avoided when the following requirements are full field: $B_x/2 > \gamma D_x$ and $D_x > \gamma B_x/2$.

This choice has the major effect the reduction of the sectional damping for all parametric sections that significantly deviate from the original sections. Given the large difference between original sections and sections of generic parameters in the calculation of maximum speed at the point of separation a possible solution could be to omit potential contributions represented by the second term of V_{max} (Ikeda, 1978b) because it is considered unreliable.

Figure 4-8 shows the sectional distributions obtained with the code modified for this thesis. You may also notice the lower value of damping associated with the bow sections amended in accordance with this logic. Ironically, although the distribution is altered with a more logical

allotment, total value of the eddy making component is only fractionally lower, at least for the C11 container ship.

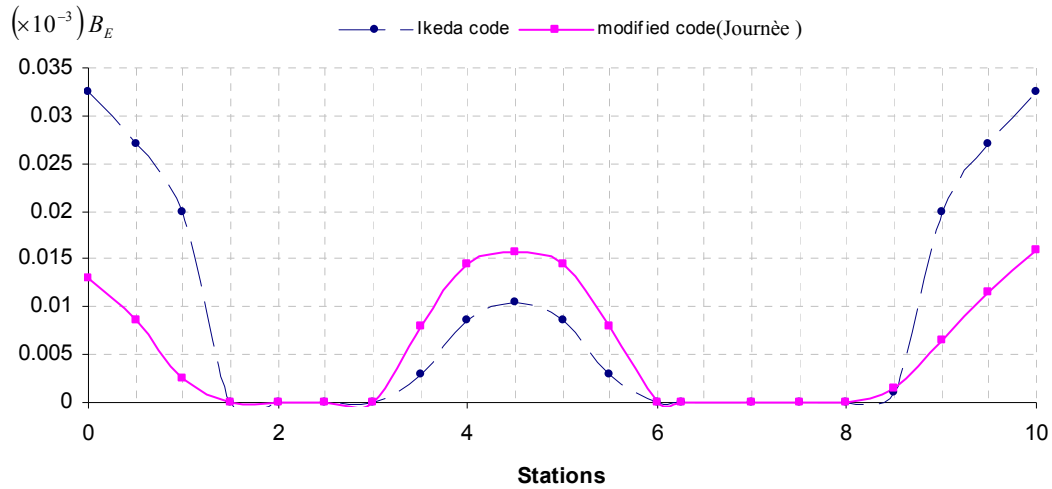


Figure 4-8. Roll damping distribution of eddy making component for original and modified methodology

Considering, the view that it is preferable to have an underestimation of damping rather than a questionable value, which is potentially overestimated; this could be a good incentive but needs to be further experimentally investigated.

Since the roll amplitude is contained in the equation of B_E , the component is nonlinear component for roll amplitude. The eddy making component decreases quickly with the increment of forward speed. Consequently, the eddy damping for a naked ship hull prevails only in the absence of advance speed; it decreases rapidly when the ship moves forward, so that it can be neglected in the high-speed range of $F_n > 0.2$. This fact has also been observed in the experiments by, say, Yamanouchi (1961). In the presence of steady forward speed as stated, the eddy making damping decreases and becomes negligible at a large value of $\omega L/U$. Ikeda et al. (1978) proposed the following empirical formula for an eddy-making damping coefficient in non-zero U . The forward speed effect is approximately expressed with the following equation,

$$\frac{B_E}{B_{E0}} = 0.5 \frac{(0.04K)}{\{(0.04K)^2 + 1\}} \quad \text{where, } K = \frac{L\omega}{U} \quad (4-37)$$

4.2.4 Lift component by naked hull

The lift damping in roll occurs in the form of a lift moment similar to the lift force caused by a ship moving forward with the sway motion. The damping moment M_L due to lift effect can be expressed in the form,

$$M_L = 0.5 \rho L T U k_n l_0 l_R \dot{\eta}_4 \quad (4-38)$$

It should be noted that previous relation is derived for the cases in which the center of gravity of a vessel is on the waterline level doesn't contemplate the cases where $OG \neq 0$. However, Ikeda et al. (1978) modified the values for these levers originally assumed by Yumuro et al. (1970), and proposed another expression covering cases when the roll axis does not pass through the point O. Under quasi-static assumption, the lift component is expressed with the following equation.

$$B_L = 0.5 \rho L T U k_n l_0 l_R \left\{ 1 - 1.4 \frac{OG}{l_R} + 0.7 \frac{OG}{l_0 l_R} \right\} \quad \text{where } \begin{matrix} l_0 = 0.3T, \\ l_R = 0.5T \end{matrix} \quad (4-39)$$

$$B_L = 0.075 \rho L T^3 U k_n \left\{ 1 - 2.8 \frac{OG}{T} + 4.667 \left(\frac{OG}{T} \right)^2 \right\} \quad (4-40)$$

The lift gradient k_n to calculate maneuverability is used and it is expressed in the following equation. In eq. k_n represents the derivative of the lift coefficient of the hull when towed obliquely. The lever l_0 is defined in such a way that the quantity $l_0 \dot{\eta}_4 / U$ corresponds to the incidence angle of the lifting body. The other lever l_R denotes the distance from the point 0 to the center of lift force.

$$k_n = 2\pi \frac{T}{L} + \kappa \left(4.1 \frac{B}{L} - 0.045 \right) \quad (4-41)$$

$$\begin{aligned} \kappa &= 0, \text{ for } C_M \leq 0.92 \\ \kappa &= 0.1, \text{ for } 0.92 < C_M \leq 0.97 \\ \kappa &= 0.3, \text{ for } 0.97 < C_M \leq 0.99 \end{aligned} \quad (4-42)$$

where C_M is the mid-ship cross-section coefficient ($A_M / B \cdot T$) which is less than 1.0. Since the lift damping is a function of U and independent of the frequency ω , it is zero for a ship at zero forward speed. At high forward speeds of a ship, the contribution due to lift to the total damping is quite large. For ship forms such as a container ship in which the roll natural frequency is quite low, lift damping becomes highly important component.

To emphasize the dependence of B_L to position of the center of gravity the equation can be rewritten as,

$$\begin{aligned} B_L &= 0.075 \rho L T^3 U k_n f\left(\frac{OG}{T}\right) \\ \Rightarrow B_L &= B_L \left(\frac{OG}{T} = 0\right) \cdot f\left(\frac{OG}{T}\right) = B_{L0} \cdot f\left(\frac{OG}{T}\right) \end{aligned} \quad (4-43)$$

As noted by Haddara et al. (1994), the formula used by Ikeda to predict the lift coefficient for $OG = 0$ seems to be the result of a readjustment of the Jones formula for lifting surfaces at low aspect ratio. With reference to (4-41) and (4-42), the method requires:

- using an aspect ratio equal to $2T / L$ to presumably take into account the mirroring effect produced by the free surface corresponding to the waterline;
- the addition of a parameter κ , function of the coefficient of the middle section related to the variation of the width of the water lines below the waterline.

To obtain the lift damping value experimentally, one must exclude wave effects by covering the free surface with flat plates or by carrying out the measurement in a low frequency range so that wave damping can be neglected. Since the eddy making damping is negligible for high speeds, it was possible to determine the component of damping due to lift effect by subtracting friction component measured by the total damping. As stated in Haddara et al. (1994), the formula provided by Ikeda often tends to overestimate the damping component to generate lift especially for the high values of the ratio B/T and negative relationship OG/T (center of gravity located above the waterline), therefore trying to improve the predictability of the report.

The most influential parameter recognized in the report related to the quality of the prediction, is the dimensionless coefficient of linear damping, obtaining an expression that highlights the dependence on the Froude number:

$$\begin{aligned} v_L &= \frac{1}{4} \cdot 0.3 \cdot 0.5 \frac{\omega_0}{\sqrt{GM}} \frac{T^3 L^{3/2}}{\sqrt{g}} k_n f\left(\frac{OG}{T}\right) F_n \\ \Rightarrow v_L &= q \cdot f\left(\frac{OG}{T}\right) \cdot F_n \end{aligned} \quad (4-44)$$

At this point, based on the original methodology, it is assumed that the linear contribution on damping originates solely from the terms related to friction, lift and wave generation (figure 4-9) although Pesman et al. (2008) classified friction as nonlinear.

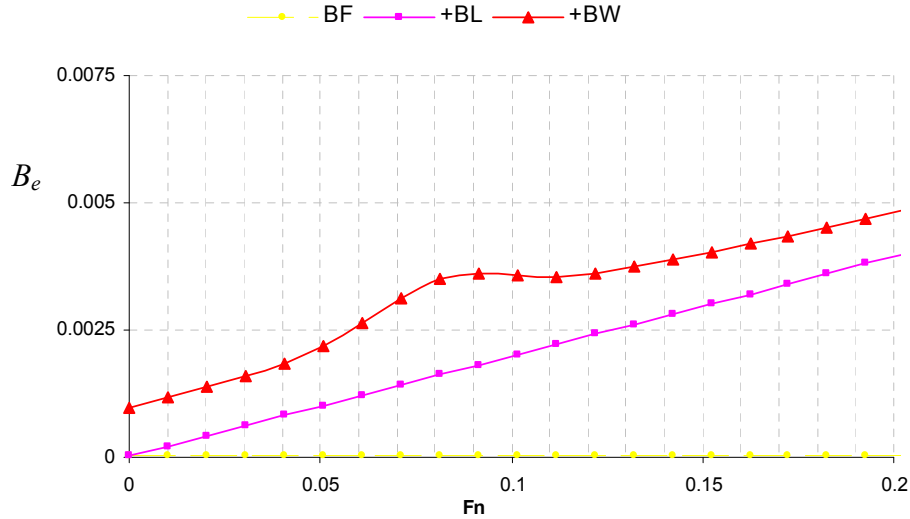


Figure 4-9. General scheme of subdivision of the linear components of damping.

For the analysis, assume that the damping term related to the frictional shear stress can be considered almost constant at different speeds, the term due to the effects of lift has linear upward stream by increasing velocity. The term related to the wave radiation from the hull can be considered constant with speed except in a range of Froude number 0.1 in where, as seen later, grows, reaches a maximum value and finally decreases again yielding the following approximation,

$$v(F_n) = K_{F+W} + K_L \cdot F_n \tag{4-45}$$

The equation is basically a straight line originating from the regression analysis of the experimental data. Ultimately, considering the equation (4-43) with the results of the Ikeda’s experimental data obtained with the means and typology of (4-44) a new function can be derived:

$$f\left(\frac{OG}{T}\right) = \frac{K_L}{q} \tag{4-46}$$

In Table 4-1 the quantities necessary for calculating the f function are considered.

$T(m)$	$L(m)$	∇ (m^3)	$GM(m)$	ω (rad/s)	$B(m)$	C_M	k_N	q	K_L	OG/T	$f(OG/T)$
--------	--------	-----------------------	---------	-------------------------	--------	-------	-------	-----	-------	--------	-----------

Table 4-1. Summary table for lift component $f\left(\frac{OG}{T}\right)$ calculation.

By the analysis suggested, in the absence of further experimental data there are few expressions available for the calculation of the f function. The adopted expression is a modified Dreossi (2004) expression based on the C11 decay tests conducted,

$$f\left(\frac{OG}{T}\right) = \begin{cases} \left[1 - 2.8 \frac{OG}{T} + 4.667 \left(\frac{OG}{T}\right)^2 \right] & \text{for } \frac{OG}{T} > 0 \\ \left[1 + 1.95 \left(\frac{OG}{T}\right)^2 + 2.375 \left(\frac{OG}{T}\right)^4 \right] & \text{for } \frac{OG}{T} < 0 \end{cases} \tag{4-47}$$

is presented plotted against the original Ikeda’s representation using Excel graphical interface on figure 4-10. This basically adds on IF loop in a code but it can be very effective addition.

It should be noted that the above mentioned indicate only the lift component by the naked hull. If the ship has large bilge keels or skag and so on, these appendages may cause more components to consider. In that case, these components can be considered in the same manner.

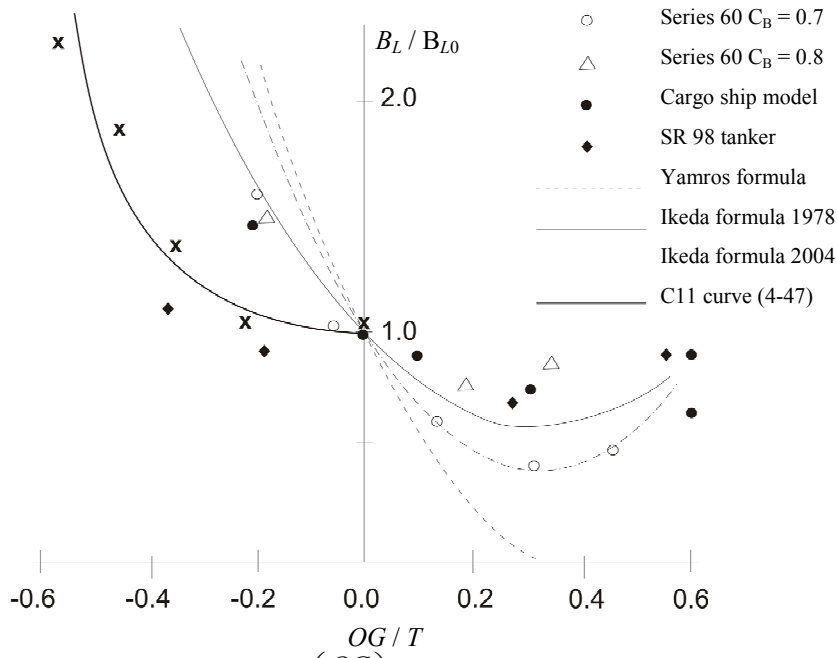


Figure 4-10. Curve of the new function $f\left(\frac{OG}{T}\right)$ given for calculating the lift damping coefficient

4.2.5 Bilge Keel Component

The bilge keel component is usually the largest one in the roll damping. The component creates 50-80% of the total roll damping. The bilge keel is an effective and efficient way to increase the overall damping and thus stabilize excessive roll motion of a ship. The component is created by shedding vortices from the sharp edges of bilge keels due to roll motion. The bilge keel component is divided into normal pressure component on bilge keel and the hull surface pressure component. These contributions vary with the amplitude of roll and the wave frequency not merely in a quadratic nonlinear form, but in a more complicated manner and further that the effect of ship forward speed is not so large as we might expect. The first component is based on the pressure acting on the bilge keel itself, while the second is based on the pressure fluctuation caused by the vortex shedding from the bilge keel on the hull surface. Briefly, it includes the damping of the bilge keels themselves and the interaction effects among the bilge keels, hull and waves.

In Ikeda’s method, the pressure distributions in front and back of a bilge keel are assumed on the basis of the measured ones, and are integrated over the hull surface. This means that the method may be available for any shape of a cross section. Ikeda et al. experimentally found that the magnitude and distribution of the pressure created by a bilge keel significantly depends on K_C .

The normal pressure component on the bilge keel is given by the following equation, expressed in terms of an equivalent drag coefficient C_D ,

$$C_D = \left(22.5 \frac{b_{BK}}{r\pi f \eta_4} + 2.4 \right) \tag{4-48}$$

$$B_{BKN} = \frac{4}{3\pi} \rho r^3 l_{BK} b_{BK} \eta_4 \omega f^2 \left(22.5 \frac{b_{BK}}{r\pi f \eta_4} + 2.4 \right) \tag{4-49}$$

where f is the modification coefficient about the bilge radius expressed by the following equation,

$$f = 1 + 0.3e^{-160(1-\sigma)} \tag{4-49}$$

while, r is the distance from the center of rolling to the bilge keel, b_{BK} and l_{BK} are the width and length of a bilge keel, and η_4 is the roll amplitude. The hull surface pressure component is calculated by integrating the pressure distribution that a presence of bilge keel causes along the hull surface.

Admission to the reliability of the expression of the drag coefficient obtained experimentally by Ikeda aside, the first criticism can be leveled at the methodology concerns. In calculating the distance between the fin and roll axis and in general throughout the sectional procedure, by adopting the approximate radius r_k it does not take into account the real geometry of the problem, that is the real point of connection between anti-roll fin and the hull. A second problem is related to the choice of arm used in the calculation of the damping moment produced by each fin. Using the arm as the distance r , with the original methodology, it assumes inlinement through the roll center. Although this is certainly the best geometric solution to maximize effective damping of bilge keels, in practice and in the nature of fluid dynamics construction will sometimes require the installation positions with different orientations.

Trying to improve the predictive capabilities, the method is implemented as function of the calculation of frictional damping on the vector notation. Again, for the different sections a local reference system has been defined similar to that shown in Figure 4-11. Therefore, two kinds of algorithms can be used in damping program. First is the simplified estimation method where only the aft and fore station of the bilge keel longitudinal position have to be specified. Second is the method in which the attachment condition of a bilge keel can be more correctly taken into consideration (the exact position of bilge keel attachment to the hull should be specified, meaning bilge keel doesn't have to be horizontal).

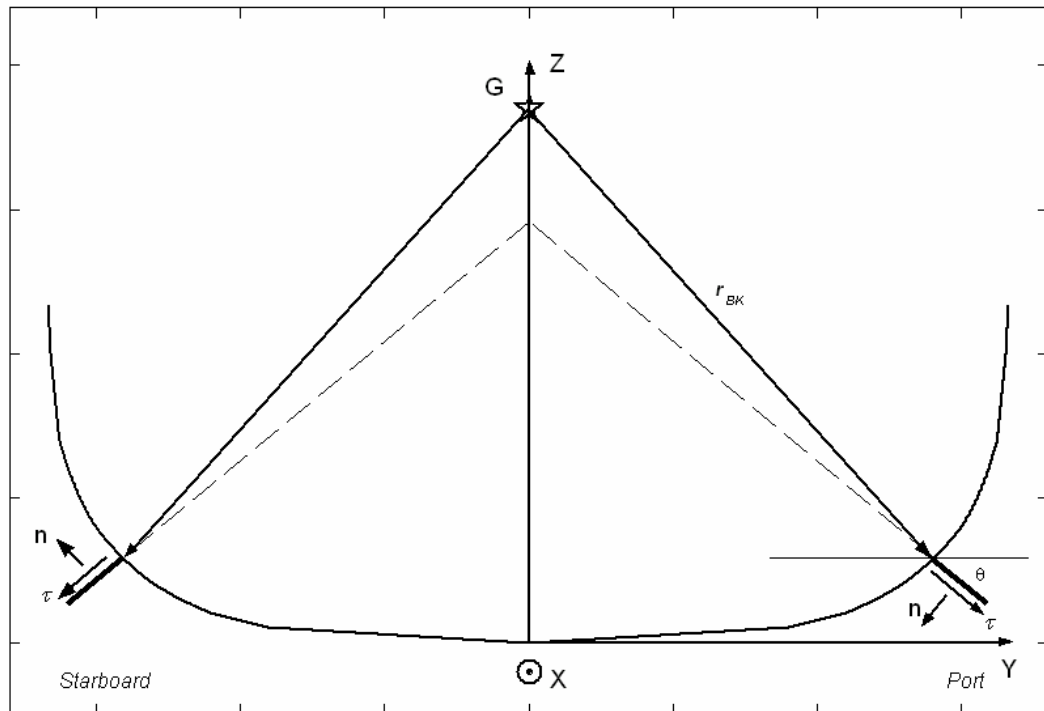


Figure 4-11. Geometry for calculating sectional damping coefficient due to normal force of the anti-roll fins.

Another small change made to the original methodology for calculating that subcomponent of the damping factor has led to the change of f (eq. (4-49)) Ikeda introduced to adjust the forecasts obtained for sections by very solid results from experiments. The correction factor f , in the calculation of the coefficient of drag has been revised in light of CFD simulations of rectangular sections with anti-roll fins - typical of FPSO vessels performed by Yeung et al. (1998). After the comparison of coefficients of quadratic nonlinear damping obtained by Yeung with those provided by the original code, the eq. (4-49) can be replaced with:

$$f = 1 + 0.8 e^{-160(1-\sigma)} \quad (4-50)$$

It will be interesting to see whether this approximation can be set as valid along with damping assessment as a whole using CFD simulation, which is one of the objectives after the present work.

On the other hand, the pressure component of damping per unit length due to hull surface was obtained from the pressure measurement on a 2-dimensional hull surface, which was caused by the presence of the bilge keels.

$$B_{BKH} = \frac{4}{3\pi} \rho r^2 T^2 \eta_4 \omega f^2 \left\{ - \left(-22.5 \frac{b_{BK}}{r\pi f \eta_4} - 1.2 \right) A_2 + 1, 2B_2 \right\} \quad (4-51)$$

where

$$A_2 = (m_3 + m_4)m_8 - m_7^2$$

$$B_2 = \frac{m_4^3}{3(H_0 - 0,215m_1)} + \frac{(1 - m_1^2)(2m_3 - m_2)}{6(1 - 0,215m_1)} + (m_3m_5 + m_4m_6)m_1 \quad (4-52)$$

Values m_1 to m_8 can be traced in original methodology (Ikeda et al. 1978). The bilge circle radius R_b and the mean distance r from the roll axis to the bilge keel are given by equation (eddy), thus r equals,

$$r = T \left\{ \left(H_0 - 0.293 \frac{R_b}{T} \right)^2 + \left(1 - \frac{OG}{T} - 0.293 \frac{R_b}{T} \right)^2 \right\}^{1/2} \quad (4-53)$$

The hull-pressure damping decreases slightly with forward speed. This amount, however, will compensate the increment of normal force damping due to the lifting effect, since it is known that total damping of bilge keels does not vary much. We just have to remember here that the nature of bilge-keel damping changes from being nonlinear to being more nearly linear as ship speed increases (Himeno, 1981).

The additional part of the bilge keel contribution comes from the wave damping of bilge keel, however it can be noted that for bilge keels with ordinary beam of $b_{BK} B/60$ to $B/80$, we can safely neglect the wave effect of bilge keels, since the contribution of this component is usually quite small compared to the viscous damping caused by bilge keels.

4.3 Roll damping calculation

The damping components that were introduced in the preceding sections can be summed up to give the total damping of ship rolling using either eq. (4-7) or the following:

$$B_e = B_F + B_E + B_W + B_L + B_{BKN} + B_{BKH} + B_{BKW} \quad (4-54)$$

The expressions presented in the preceding section provide five main contributions to the total damping in roll. In all cases the effect of current or forward speed has been shown explicitly with additional formulations. The empirical formulas have been derived from many experiments with flat plates, cylinders, ships and barge models. However, as with any such empirical formulations, the formulas are based on experimental data on particular ship shapes and generalization to all shapes may pose some problems. Some of the problems were realized and consequently attempt was made to modify the original method introducing some new aspects.

Here we discuss the general properties of the prediction procedure and the damping components. When the ship is stationary, only the lift term B_L becomes zero, while the other terms are predicted as in the strip method, integrating sectional values along the longitudinal axis of the ship. In addition to the components above, also surface tension effects should be considered (Bass et al. 1998, Contento et al. 1994). However, according to (Francescutto, 2002) the effect of surface tension is difficult to be considered from a practical point of view because it depends strongly on the condition of the painted surface of the model as well as on that of the water surface. If the ship is fitted with bilge keels, vortex shedding at the edges of the bilge keels represents an additional efficient dissipation means. In the modified methodology, all components except the relative component of lift are values obtained from two-dimensional sectional coefficients subsequently

integrated over the entire length of hull or appendages. The advantage from this calculation procedure is the possibility of having knowledge of a sectional distribution of damping.

If the ship moves with a certain non-zero forward speed, roll is damped, in addition, by a damping moment associated to lift effects arising on the hull, however, the modification to the individual components is made for the ship as a whole, thus we cannot obtain the sectional longitudinal distribution of the roll damping (which is possible in the absence of forward speed as seen in figures 4-12abc).

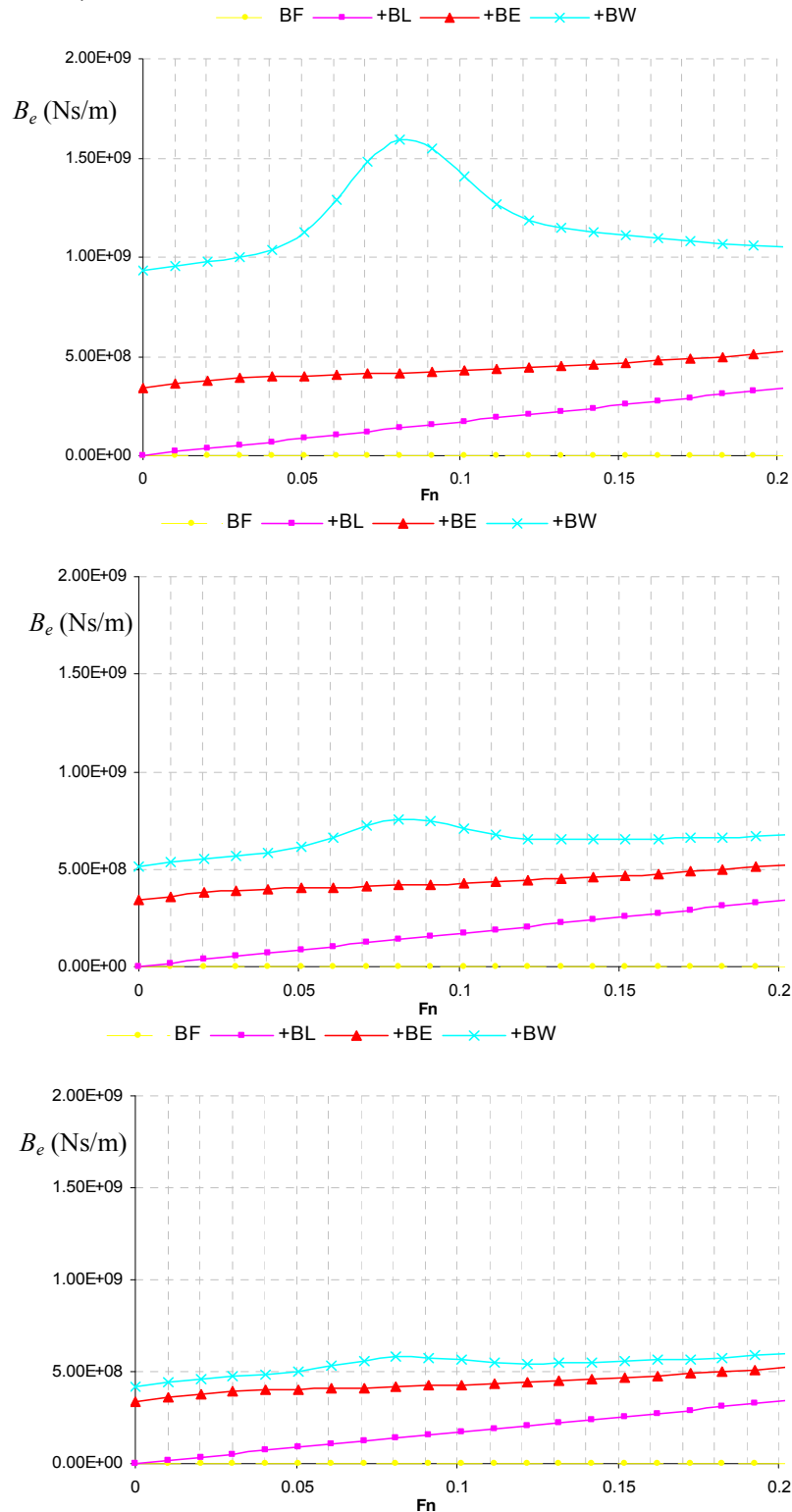


Figure 4-12abc. Comparison of the bare hull damping components for the 3 cases of wave radiation damping, B_{w0} with respect to velocity

The effects attributable to such forward speed are reproduced by means of multipliers applied to individual components only after integration over the surface of the hull. As noted previously the modifications introduced are applied mainly to inception of the longitudinal distributions in conjunction to hull form approximation which presents an important problem for the future study. Note that what also affects the damping estimation is a correct assessment of the wave radiation damping, B_{w0} . It has been rather puzzling to find three quite distant values using the linear diffraction/radiation theory from seakeeping code (4-12a, 4-13a), the coefficient obtained from Chakrabarti (2001) for the model with almost the same principal dimensions (4-12b, 4-13b) and the approximation method from Himeno (4-12c, 4-13c) compared with the measurements by Takaki and Tasai (1973). This may be because the wave component of the roll damping intricately depends on frequency and locations of roll axis. Therefore, if more accurate prediction is needed, the calculated wave damping from potential theory should be used.

An example of the computed damping coefficients for a container ship is shown in Figure 4-12abc for a bare hull and for the bilge keel installed in figure 4-13abc. The chosen roll amplitude was 20° , wave length equals ship length, heading 180° and the bilge keel positioned in between stations 4 to 6 with breadth of 0.5 m.

The total damping shown in Fig. 4-13abc includes the five damping terms discussed above. The individual contribution of the five components to this damping coefficient in roll vs the Froude number is illustrated for the container ship and agrees with the expected physical behavior of the damping model. The wave damping component for the Chakrabarti (2001) is comparatively small. The wave component using the linear diffraction/radiation theory is on the contrary quite large. It is found that the forward speed increases the lift component significantly. The most important contribution at zero forward speed is the eddy-making damping coefficient. However, with the increment of forward speed eddy-making damping coefficient typically decreases. The presence of the bilge keel provides a steady increase in the damping coefficient. Although bilge-keel damping is shown as nearly constant in figure 4-13abc, the linear part increases as Fn becomes large. Damping due to bilge keels shall be assumed to be an additional damping term with respect to the bare hull condition, and not a multiplicative factor. Hence, although data in figure 4-13abc could serve as an interesting reference concerning the overall influence of fitting of bilge keels for this particular ship, it is not suitable for being used as a prediction means in case of this ship (or any other for that matter) until there is a possibility to validate it with the proper decay tests with bilge keels installed.

To separate contributions from linear and nonlinear damping an illustration is given on figure 4-14. As already indicated previously the separation consists of linear part of the damping attributed solely to the terms of the lift and wave-making, and partly by friction. The non-linear part instead is governed by the contributions of eddy making and bilge keels, and the remainder of the friction term.

Comparisons of these damping components are shown in figure 4-15 as a function of the roll amplitude. Adding to the statement for the bilge keels related to the figure (Fn) values of bilge keel damping in the limiting case $\eta_4 = 0$ increases but the slopes of the corresponding curves decrease as Fn increases. From this figure it is even more obvious to separate contributions from linear and nonlinear damping based on the above mentioned subdivision. Utilizing the same conditions of $\lambda/Lpp = 1$, heading 180° and the bilge keel positioned in between stations 4 to 6 with breadth of 0.5 m, the calculations are preformed while the Froude number was set at zero.

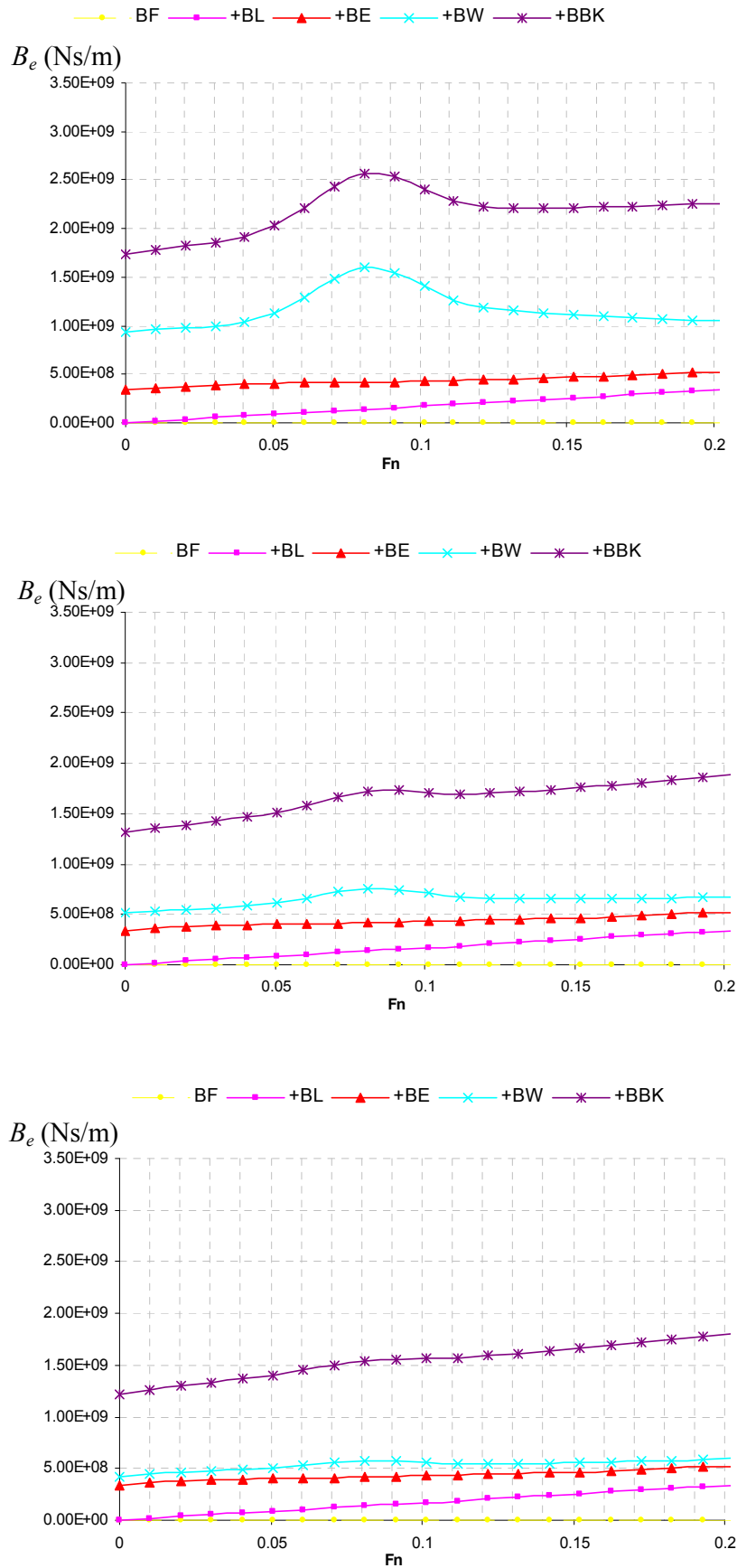


Figure 4-13abc. Comparison of the damping components for the 3 cases of wave radiation damping B_{w0} with the bilge keel with respect to velocity

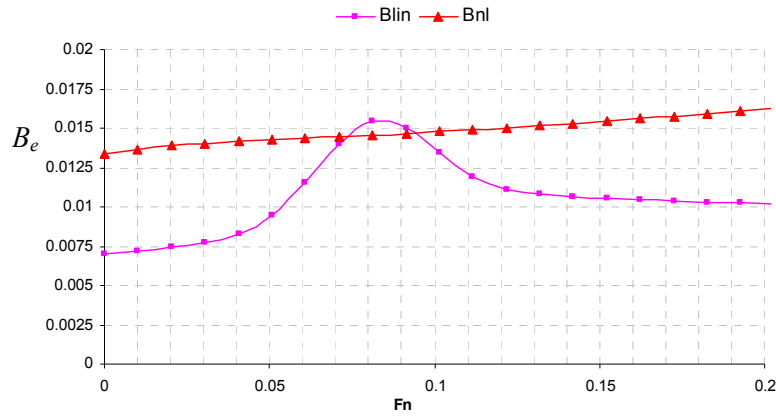


Figure 4-14. Schematic view of roll damping components with advance speed

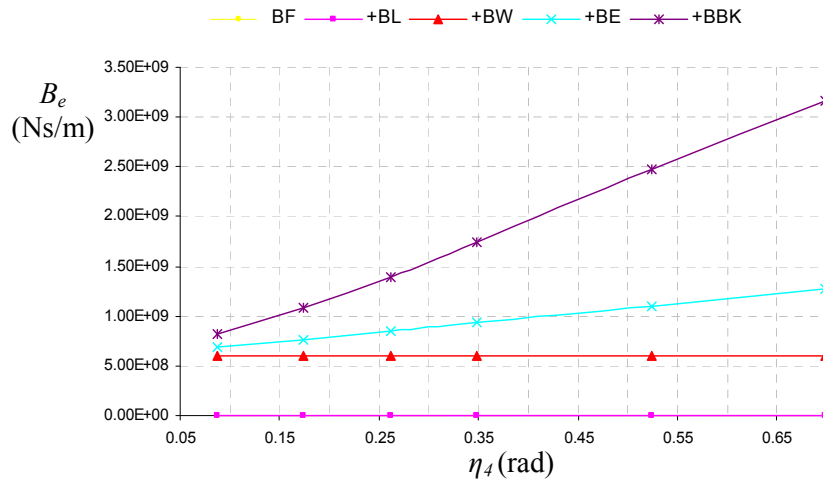


Figure 4-15. Schematic view of roll damping components with respect to roll amplitude

On the following figure (4-16), by implementing the calculations this time for the speed of 8 knots the apparent distinction is related to the lift component (gradually increases with forward speed) and to the wave radiation from the hull which can be considered constant with speed except in a range of Froude number 0.1 where it grows (a “bump” on figure 4-14) before finally decreasing.

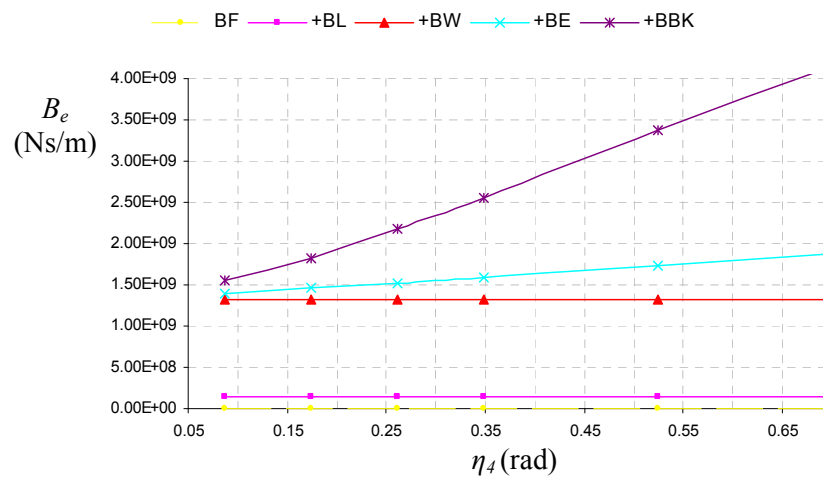


Figure 4-16. Nonlinear effect of roll damping components for speed of 8 kts

The terms B_F and B_{BK} also depend on the frequency as shown in figures 4-17 and 4-18, although they appear to be linear with respect to the amplitude. Even though they were originally defined as being nonlinear, the coefficients vary with Reynolds number in the case of B_F and with the period parameter in the case of B_{BK} which can rationalize previous statement.

Considering scale effects, the almost linear damping like B_L and B_W are of course independent of it. It can be considered as in the case of an oscillatory flat plate that damping contributions B_E and B_{BK} that are generated by separating bubbles may not be affected by the scale difference between model and ship. Therefore only the frictional damping suffers from the scale effect.

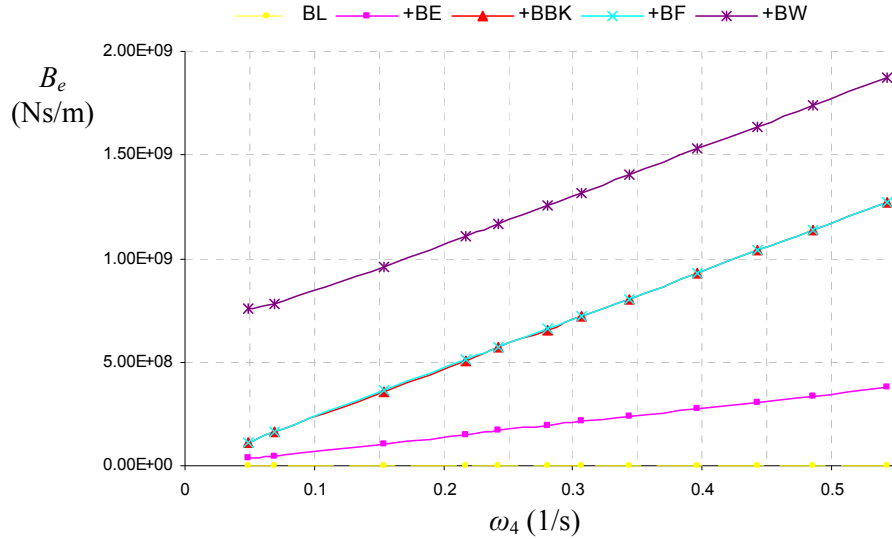


Figure 4-17. Effect of roll frequency on roll damping components for 0 kts

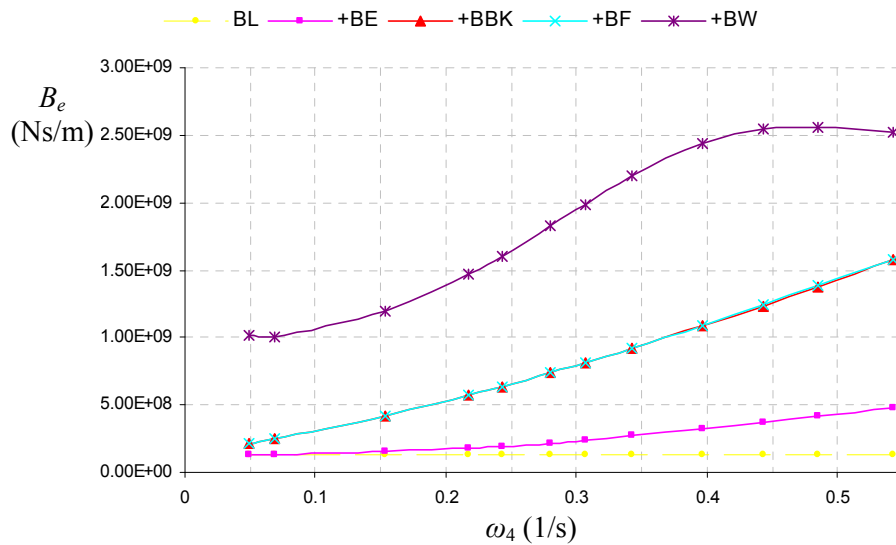


Figure 4-18. Effect of roll frequency on roll damping components for a ship with advance speed of 8 kts

The roll predictions from these calculations can be considered adequate only when compared to the roll decrement tests but the method should prove to be fairly robust. Although it is still necessary to improve the prediction method for component damping, at present an adequate set of prediction formulas can be adopted for ordinary ship hull forms. The difference between the case of a bilge keel and no bilge keel was shown. In this case the bilge keel almost doubles the total damping in roll for the container ship. Unfortunately, at this stage it has to be mentioned that as a part of this research decay tests with bilge keel installed were not performed which makes the task of validating the numerical code more onerous. This can be realized from the fact that based on extensive literature survey Ikeda's method overestimates the roll damping but even from the preliminary code performance it could be related to the bilge keel component. A notion can be deduced stating unreliability concerning the absence of experimental tests while fitting the model with bilge keels.

Since the viscous component of a roll damping changes according to the change in roll amplitudes (especially B_{BK} as illustrated in fig. 4-15), total roll damping is nonlinear. However, since

this nonlinearity strongly appears only for roll amplitudes, one can use the technique of equivalent linearization for energy in a roll motion period. The roll damping coefficient B_{44} is a function of roll amplitude η_4 , and it becomes increasingly difficult to solve roll motion equation. For the case of regular sea, the iteration method for roll amplitude is used for a frequency domain roll calculation.

In the case of irregular seas, to predict the ship response in short-term irregular seas, the energy-spectrum analysis based on the principle of linear superposition has been applied. Let the energy spectrum of the incoming long-crested waves be denoted by $S_w(\omega)$. Then we can obtain the energy spectrum of the ship response $S(\omega)$ in the form,

$$S(\omega) = |A(\omega)|^2 \cdot S_w(\omega) \quad (4-55)$$

The frequency ω of the waves can be transformed into the encounter frequency ω_e of the ship. The response amplitude operator $A(\omega)$ represents the ship response per unit magnitude of input wave. In particular, it becomes $\phi_0 > kh_a$ (k is the wave number) in the case of roll response. The equation system is nonlinear when $A(\omega)$ depends on the amplitude of the wave and thus on the spectrum $S_w(\omega)$. Several attempts have been made to treat this nonlinearity. The most simple way is to take the $A(\omega)$ value as that in the case of the wave height ($2h_a$) equal to the significant wave height, $H_{1/3}$. This corresponds to assumption that the roll damping caused by viscosity (B_E, B_{BK}, B_F) is constant, equal to the actual value associated with a roll amplitude ϕ_0 corresponding to the prescribed wave height. The ω -dependence of the roll damping, in this case, is taken into account explicitly. This rather simple way can eventually be applied to predict transitional time domain roll motion using convolution integration method.

Obviously the roll damping of a vessel is an important parameter in the assessment of parametric roll. A relevant characteristic is the fact that it decreases with decreasing speed. In the lower speed range it is dominated by the non-linear eddy and bilge keel damping components. At moderate and higher speeds the linear lift damping of the hull becomes a dominant factor (Ikeda et al. (1978), Dallinga et al. (1998)). In other words the risk on parametric roll decreases with increasing speed. Other means that increase the ships roll damping also decrease the risk on parametric rolling. Fin stabilizers are effective as well, but only at some forward speed.

In summary, an empirical correction for roll damping in strip methods still appears to be the best choice in practice, although alternative schemes could be deployed as well. The input file name of the following program is "DAMPIN.DAT", an output file name is "DAMPOUT.DAT", and both files are text files. The input file is written the calculated condition those are hull data, forward speed, roll amplitude, wave period and wave direction (roll period). On the other hand, for the output file, the conditions of calculation, the calculated roll damping coefficient and its components are written.

5 Numerical implementation of seakeeping model for parametric rolling assessment

5.1 Introduction

In section 3.2 the problem of linear boundary condition was formulated for the flow around the ship advancing in waves and the solution presented in the frequency domain for the calculation of ship motion is based on the strip theory. In section 3.3 non-linear modeling of instabilities in the time domain is presented whose solution is obtained from hydrodynamic coefficients previously calculated in the frequency domain.

This chapter describes the numerical implementation of the methods and computer code presented in previous chapters, validated with the experimental readings. Initially, it has to be stated the main particulars of the ship subject to the investigation were already presented along with some calculations referring to the chapters elaborated, especially various stability characteristics analytically exerted with the propensity for the occurrence of parametric resonance. In terms of numerical simulations one begins by obtaining the solution in the frequency domain, since this solution is a prerequisite to reach the solution in time domain. Next is the validation of program in the time domain through a systematic study of influence on operating parameters (the characteristics of waves, the forward speed and load condition of the vessel) in the realization of phenomenon of parametric resonance in longitudinal and slightly oblique waves for the vessels under investigation. This PhD dissertation used as a starting point the existing code from the Technical University of Lisbon which was expanded and improved and as such it will be presented in brief. The original program was fully automated, broadened, upgraded and modified taking into account the decay tests to address nonlinearities in damping. With the new program the scope of the process widens extensively, enabling the validation of simulation program of parametric resonance for the irregular waves in particular. Also, it supports the validation of methods and program for the analysis of the influence of nonlinear components of the motion. Even more, this chapter explains in detail how the non-linear effects are introduced in the equations of motion, which characterize the solution in the time domain and discusses the effects of coefficients and the nonlinear forces considered. The non-linear components are considered as a non-linear impulse, given by contributions of hydrostatic and Froude-Krylov forces and viscous responses in the transversal plane. These nonlinear forces are included in the equations of motion in the time domain combining the linear terms with nonlinear terms. The emphasis here is on the interrelated roll damping of a vessel acting as an important parameter in the assessment of parametric roll for developing reliable performance-based criteria. A completely new module is introduced since roll damping significantly affects on not only roll amplitude but also the occurrence region of parametric roll, thus accurate estimation of roll damping in this work is treated as crucial for quantitative prediction (using this time domain software) of parametric roll.

5.2 Implementation of time domain strip theory and numerical computing schemes

The formulations and methods developed and presented in previous chapters were implemented in computer programs to obtain numerical solutions. In this section these programs developed in Fortran and C++ programming language are briefly described.

The various programs worked independently from reading the input data and calculating the linear (frequency domain) and nonlinear (time domain), motions in regular or irregular waves. However, the set of program enabled step by step calculations while getting a lot of partial and intermediate results. The input data for the motions are hull geometry, the loading condition of the

vessel (mass, position of center of gravity and radius of gyration around the center of gravity, etc.), the ship's speed, heading angle with respect to the waves and the characteristics of waves.

The hull geometry includes the complete immersed hull and the entire hull above the waterline. Note that in the events of large amplitude motions and subsequent immersion of the ship's deck, the deck geometry to the center line should also be included therefore eventually even superstructure acting as a flow obstacle. To set this geometry, a finite number of cross sections (strips) along the length of the ship are predefined associated with two-dimensional strips. Generally, 21 sections are considered as sufficient to achieve a fair hydrostatic and hydrodynamics representation of the hull while also recommending a smaller spacing between sections in areas of hull tapering, i.e. the bow and stern. A subroutine capable of reading hull geometry was developed in GF format ("Geometry File") that is used in hydrostatic calculation of commercial programs such as AutoHydroTM and GHSTM. Cross sections are represented by points distributed by half-sections, because it is assumed that the ship has symmetry in the x - z plane. These points are then "mirrored" with respect to x - z plane and then successively applied (in each step of integration) to linear and rotational motions around the reference axes.

In purpose of calculating the restoring hydrostatic coefficients using the integration of pressures method over the various segments of each strip maximum 128 points are required to describe the shape of each half-section. The calculations of the hydrodynamic coefficients and exciting forces, requires about 10 points considered as sufficient to describe most cross sections forms. All longitudinal positions of cross-sections (x) as the points coordinates on the same sections, are represented in coordinate system fixed on the ship $X = (x', y', z')$.

The waves can be either regular or irregular. In case of regular waves, it is necessary to set the wave frequency and the slope of the wave. In case of irregular waves, it is required to choose an energy spectrum of the sea state, as explained previously. Information regarding the peak period of sea state must also provided together with the significant wave height, or the variance of the sea state.

The flowcharts with all the major steps involved in the calculations of non-linear motions in the frequency and time domain represent processes performed by calculating the entire set of programs are presented in Ribeiro e Silva, (2008).

There were several substantial drawbacks with the application of this procedure. As the numerical procedure is gradually explained the first thing that comes to mind is the onerous work needed (a month) to get results just for the longitudinal regular seas. All the statements about the relative simplicity and robustness of the method especially when it comes to computational efficiency, fall below target, because all the programs are separate entities and completely independent of each other. To illustrate the former procedure one has to start with the frequency domain solution, i.e. the calculation of added mass and damping coefficients and the calculation of radiation and excitation forces. Excitation forces include diffraction forces and Froude-Krylov forces calculated as a function of the incident wave frequency. Additionally, restoring hydrostatic forces represented by the linear restoring coefficients are also calculated. All these forces combined together with the inertia forces form the equations of motion (linear) in the frequency domain, to calculate the transfer functions of motions in regular waves. The response derived, such as acceleration or relative motion can also be easily calculated. With transfer functions of the responses and using the energy spectrum of the irregular sea state it is possible to compute the response spectra and some statistics of the responses.

Considering the overall set of computations, this is a hybrid method, where some of these calculations are performed in the frequency domain and partly in the time domain. The reason lies in the fact that the time domain method uses the hydrodynamic coefficients and hydrodynamic excitation forces calculated for a given incident wave frequency.

In the time domain, one starts by iteratively defining the intersection between hull surfaces with the free surface for each time step of simulation. After each instantaneous wetted cross section is set, the coefficients of restoring hydrostatic forces, hydrodynamic radiation coefficients and

excitation forces are calculated. These results of course depend on the geometry of the vessel, the position of the waves relative to the hull and the ship speed.

The next step is to solve nonlinear equations of motion in time domain of advancing ship with solution at each time step performed by the method of numerical integration consisting of Runge-Kutta 4th order differential equations. At each time step all the components resulting in dynamic equilibrium of forces are calculated. The main results of the simulation are the absolute motions. However, if necessary based on kinematic relations other results can be extracted (relative motions and accelerations at certain points). The simulated registries are treated in various ways to quantify several response characteristics. For responses in regular waves, the peaks can be calculated (maximum absolute values), the average values of the records and the average values of the positive and negative peaks. For responses in irregular waves, energy spectrum and a series of statistics of responses, such as mean values, the variances and the average periods, significant heights, and the distribution of maxima and minima.

The second phase can be referred to as cyclic routine leading to the solution of equations of motion in time. In each simulation cycle, the displacements and velocities of the ship are extrapolated for the next time instant. With this information at hand, and with the elevation of irregular wave profile it is possible to compute the relative motion between the ship and waves. Next step is to calculate the distribution of nonlinear sectional forces along the length of the ship. These include the hydrostatic, Froude-Krylov and viscous contribution. Subsequently, sectional forces are integrated over the length of the ship and used to derive global forces on the vessel to be inputted into the equations of motion. By obtaining the dynamic equilibrium the solution of the equations of motion results in accelerations. These are used to extrapolate the displacements and velocities for the next time instant governing the relative position of ship with respect to waves. This is indeed a rather simple procedure but as previous paragraph indicates the governing set of equations of motions at certain time instants directly depends just on the previous one, thus neglecting the preceding motion mathematically expressed as convolution integral explaining so called memory effects. This assumption based on the calculation in the previous chapter for a C11 has been questioned and it remains to be validated.

To sum it up, a listing of all programs that make up for the seakeeping calculations of a ship in waves are collected and presented for a viewer. The programs for calculating the hydrodynamic coefficients and diffraction forces for two-dimensional symmetric sections were developed by Fonseca and Guedes Soares (1998) and starting from it the existing code inherits exactly the same algorithm but since it accounts for existing ship position with respect to waves encountered it is therefore simply applied for asymmetric sections (of course instantaneous submerged intersection is of paramount importance). As for other programs, Ribeiro e Silva (2008) has developed time domain routine and irregular wave's features.

ADDAMP_NS → Calculates the added mass and damping coefficients of asymmetric two-dimensional bodies oscillating at free surface by a Frank "Close-Fit" method, using a strip theory.

FEDIFRA_NS → Calculates the diffraction forces and Froude-Krylov forces, depending on the oscillation frequency for the asymmetric two-dimensional bodies oscillating at free surface by a Frank "Close-Fit" method, using a strip theory.

SOLVE_NS → Combines the two above to obtain responses.

ARCHIMEDES → Calculates the restoring forces and Froude-Krylov forces for a given ship, as a function of instantaneous mean free surface of the hull under the profile of the incident wave, using the integration of pressures method for an incident undisturbed wave field. From these pressures sway and heave forces, roll, pitch and yaw moments are calculated for the hydrostatic restoring and Froude-Krylov. Note that by changing a parameter file of input data, the implemented method can consider the integration of the pressures along the instantaneous wetted contour of the cross sections, x_c , as oppose to the mean contour, c_0 , at each of the cross sections across the hull.

ROLLDAMP → Calculates the damping coefficients in the frequency domain for roll motion by the components method of Ikeda et al. (1978). Alternatively the damping coefficients domain for

roll motion can be calculated by the Miller method (1974) and then introduced MOTION_NS manually in the program described below.

MOTION_NS → Calculates the transfer functions of linear in the frequency domain for a given ship, utilizing strip theory.

DATAHYST → Analyzes records and identifies all the simulated maximum and minimum together with the time instants at which they occur, calculates the mean value, variance, zero up-crossing period, significant amplitudes and heights.

DATASPECTR → Calculates the response spectra and some statistics of the responses for irregular two-dimensional sea states.

RANDWAVES → Program creates time series of free surface elevation from a given spectral representation of regular waves, whose harmonic components are defined by their amplitudes and phase angles. The sea conditions created is one temporal and spatial random realization and may have different spectral representations alternatives.

SHIPATSEA → Program that makes the simulation and calculates surge, sway heave, roll, pitch and yaw motions in the time domain. The simulations can be performed considering restoring coefficients variable in the time domain, defined at each time instant around the instantaneous free surface (wave profile) or, alternatively, defined around the mean free surface (still water). These two options are also extended to the process of calculating hydrodynamic coefficients. Therefore, the simulations can be performed considering the hydrodynamic coefficients and excitation forces for a given wave profile, calculated for asymmetric strips, defined around the instantaneous free surface or, alternatively, considering hydrodynamic coefficients of added mass and damping in still water, calculated for symmetric strips, defined around the mean free surface. The program can also consider either regular or irregular waves, with the two-dimensional irregular waves corresponding to several alternative spectral forms.

The type of simulation, the time increment and duration of the simulation are pre-chosen by the user. The computational effort depends heavily on the nonlinearities considered and the number of harmonics component introduced to represent the sea state. If one chooses a type of simulation where only the restoring forces are non-linear and if the predetermined number of harmonic component is relatively small (while maintaining a good representation of the irregular wave), the computational time can be considerably less, but it raises the accuracy issues.

There are some additional features that were not utilized within this study.

However what seems to be the biggest strength of the proposed methodology was in reality the biggest shortcoming. Although the code was computationally efficient the procedure to obtain the results was extremely cumbersome. Actually, all these programs by both authors work independently.

If necessary, the tabular presentations of the file in question can be presented upon request for completeness. However, an extra calculation in Excel with numerous data transfer is not only impractical and error prone but also extremely time consuming. The original idea based on the proposed use of a strip theory calculation routine under such conditions highly favored due to the fact that these are easily accessible routines, which require relatively small computation effort for practical engineering applications at the initial design stage, due to the complex execution in reality didn't work. The idea was to undertake actions which could result in a "multi-objective flexible automation" procedure from the simulation results itself or even more so as a result to a possible linkage with ship systems. For that reason the derived time variant added mass, damping, and excitation forces in time domain simulation are recoded in Fortran and more intuitively linked with frequency domain outcome from which they originate but this time at exact underwater sections where the velocity potential is required to satisfy the instantaneous boundary conditions. Therefore, the radiation forces, the Froude-Krylov forces and the diffraction forces in the time domain is calculated using the newly coded transfer functions of these forces from the frequency domain.

This partly addresses the "automation" term. Whereas it was possible to run a single simulation for one ship speed, one wave frequency, one wave height and a one heading restrained to the longitudinal seas, new program makes it possible to run simulations with a simple command line

that contains user defined number of previously mentioned parameters. Therefore, it is enabled to obtain a full scatter of records for a desired range of ship speeds, wave frequencies, wave heights and headings. The unavoidable data handling was coded in C++ and batch programming. However, the final user, preferably an engineer engaged in early design stage has a very simple and efficient task to perform. Newly developed user interface isn't going to be presented since the emphasis is on theory implemented.

The fact that these are easily accessible routines and the introduction of Flags which dictate the level on nonlinearity makes it flexible. What also makes it flexible is the added feature (Flag 5) which enables the program switch to take into account the decay tests results. The original program was modified to address the damping nonlinearity by introducing the concept of linear plus quadratic plus (cubic) term. If the decay tests are conducted for the ship investigated this is the advisable procedure.

The new damping program based on modified Ikeda's method is also coupled with the Shipatsea program. However, since the damping investigation is a large part of this investigation this program is also intended to work separately from the motions program. Therefore, with the term "multi-objective" it is meant that a variety of problems can be addressed and implemented with the whole incorporated and complete software package.

The following list of programs and the calculation procedures are done entirely by the author during the course of this research. The first list is the set of programs that work within the optimization procedure of interaction between the frequency and time domain simulations. However, what is required is an appropriate folder structuring. All these programs constitute of about 2500 lines of the code. It was necessary to use the base programming instead of using Excel macros or similar in order to greatly reduce computational time by optimizing several procedures.

IKEDADAMP → Calculates the damping coefficients in the frequency domain for roll motion by the components method of Ikeda et al. Originally, the code was utilized using Miller method but the fact that scientific community generally uses the Ikeda method it was modified in that manner. The primary idea was to modify the existing *ROLLDAMP* program. *ROLLDAMP* program based on the authentic Ikeda method was built by Fonseca (1998) but its form proved insufficient when comparing the results from basin, therefore a completely new module was built which runs simultaneously with the motions program. The idea was abandoned for two reasons. One was the possibility to create a program that works independently from the package for the purposes of the damping investigation. The other comes from the fact that the *ROLLDAMP* program originates from mid 90's at time when the present hull forms were not introduced and since that time a lot of propositions to modify Ikeda's strip theory came up especially in the wake of novel forms damping estimations. Therefore, a hybrid concept is implemented also referred to as "blending method". Both programs are utilized with *ROLLDAMP* in the frequency domain while the *IKEDADAMP* in the time domain, but not in a way to be superimposed by each other rather compounded, thus enabling the advantages of both. By this it is implied that *ROLLDAMP* program serves as "static" facilitator. The new module runs with the ship motions program in a way that the program originally starts with the damping values (named "static") from the *ROLLDAMP* program but after establishing steady state it recalculates damping values (named "dynamic") using roll amplitude as a variable for a new run simulating the non linearities in a damping process. Adding a time variable component such as roll amplitude as a damping function in conjunction with the comprehensive Ikeda's method makeover makes it rather compelling.

The flowchart of the presentation above is given in figure 5-1.

The damping is hydro-dynamically unsolved apart from the CFD methods so in this hybrid approach one is able to treat the problem quasi-nonlinearly and enhance model predictions of the influence that may be attributed on damping with respect to the roll amplitudes.

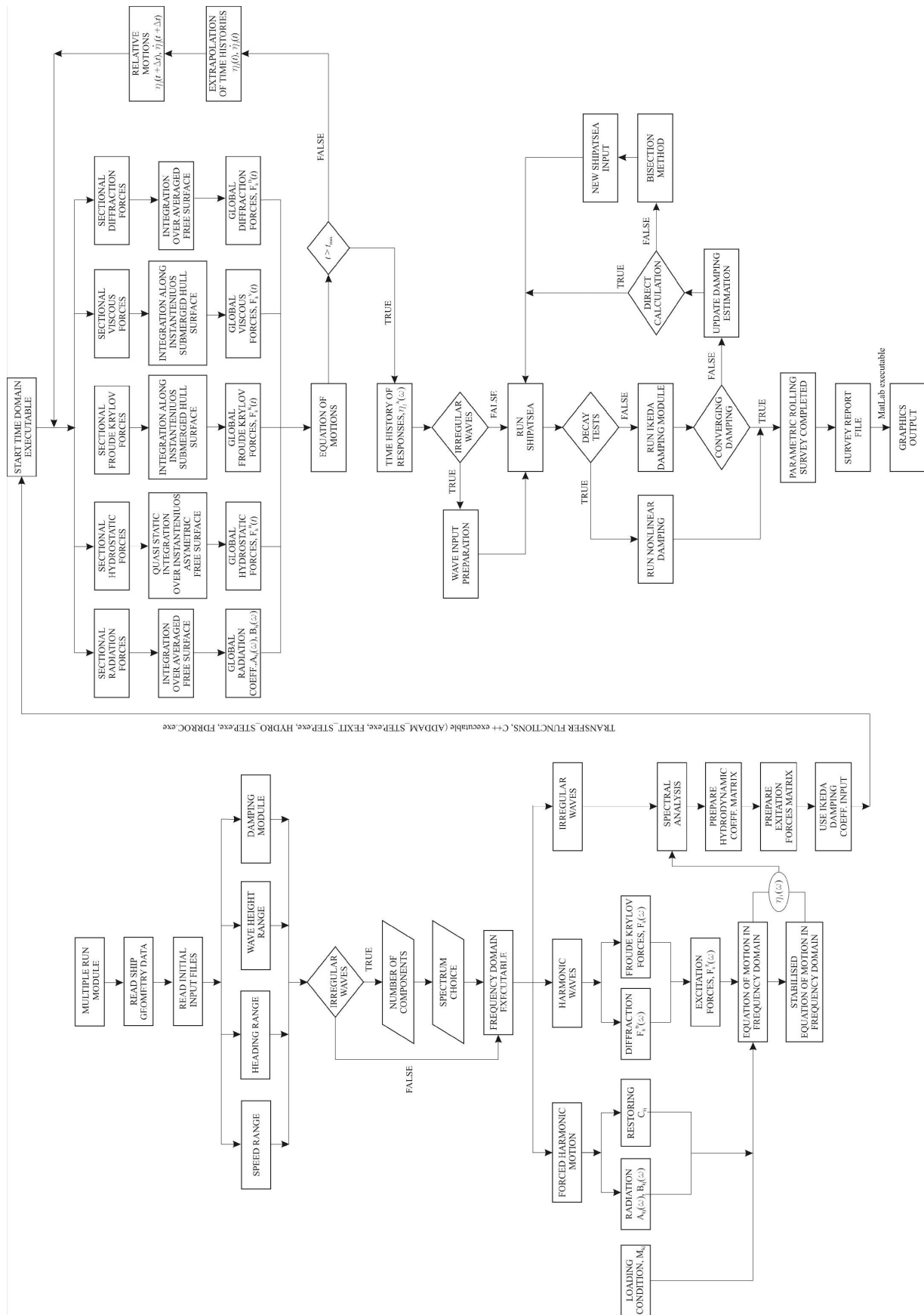


Figure 5-1. Numerical model code flowchart

The first attempts were carried out using a different approach exercising the convergence method in estimating the damping coefficient. This proposed procedure is of course very general, too

general to be of specific guidance for any particular problem, and consequently practical implementation usually demands great care in the choice of approximations. Although it was speed efficient, in a series of results it showed that because of restrictions proposed usually some cases from the simulation couldn't converge thus forming an unrealistic result. This immediately leads to a poorly indicated phase as these initial errors tend to propagate through each of the phases of determination process and in general lead to a poor or incorrect solution. However, good choice of approximated boundaries still makes it a computationally efficient tool. Whereas it is often the case that certain uniform estimates can be had, it is equally often also true that these best available bounds are none too strong. The overall impediment is of course the nonlinearity. The second approach was a bit more difficult in terms of employment and execution but both convergence method and direct calculation is applicable.

SHIPATSEA_D → This is a modified *SHIPATSEA* program that deals with linear + quadratic + (cubic) concept of damping representation. What was already thoroughly explained in previous chapter is in practice implemented here. The program abandons the equivalent linear damping form based on Ikeda's method and uses one of the proposed damping representations. For this case study linear + quadratic model was chosen. The damping coefficients from decay tests have to be supplied in a separate DAT file.

5.3 Preliminary results in time domain simulations

Linear strip theory, due to its simplicity and to the minimal computational effort required, is still the most employed model used for the prediction of ship responses in an incident wave field. Several researchers have focused their studies on methodologies capable of including nonlinear effects in the solution of the seakeeping problems, as the interest for motions and loads in heavy weather, when nonlinear effects become no more negligible, is remarkably increased in the years.

A nonlinear time domain seakeeping analysis has been performed for ships advancing in head, bow and oblique seas with regular waves. A hybrid approach has been employed, solving the unsteady hydrodynamic problem in the frequency domain and the equations of motion in the time domain. This procedure transfers radiation and diffraction forces, supposed linear, from frequency to time domain, where nonlinear Froude-Krylov and hydrostatic forces are computed considering the actual hull wetted surface at each time step. It is obvious however, that strip theory calculation method is pushed far beyond its generally accepted limits of applicability in these circumstances, in particular with respect to its restriction on the assumption that motions are small. For high-speed vessels, for ships with length to beam ratios lower than 3.0 and for ships with a significant influence of submerged cross-sections or bulbous bows, more or less inaccurate results can be expected. Because of using a linear theory, less accurate results can be expected for large motions in extreme sea conditions. However, some of these restrictions are related to the strip theory method it-self. In that case one is dependent on other computing techniques (damping treatment) or model experiments.

5.3.1 Mathematical model implementation for head waves

The hybrid approach to the prediction of ship responses in time domain is divided into two steps: the frequency domain (presented) and the time domain analysis. The first step allows evaluating the radiation and the diffraction forces, solving the unsteady hydrodynamic problem for a given number of meaningful arbitrary frequencies. The latter solves the equations of motion in time domain, gauging at each time step Froude-Krylov and hydrostatic forces by integration of the hydrostatic pressure over the actual hull wetted surface under the incident wave profile. Implicitly, this methodology assumes that nonlinear contributions related to radiation and diffraction forces are small compared with those related to Froude-Krylov and hydrostatic forces. Hence the firsts are supposed linear, while the latter are evaluated fully nonlinear. Since added mass and damping are

frequency dependent whereas ship motions are directly evaluated into the time domain and nonlinear effects are included, a theory presented in Chapter 3.3 is applied in order to transfer the radiation forces from frequency domain to time domain.

In the case of transient problem in the time domain, the solution of the equations of motion advancing in time starts from an initial time which can be set for example the still situation (zero initial velocity). The solution in time domain was formulated in Chapter 4, based on equations of linear motion (3-52), and these are solved by the Runge-Kutta fourth order method. At the initial instant ($t = 0$) is necessary to establish the conditions of motion (displacement and velocity) corresponding to this moment. In the computer program the possibility to start the motion from a certain initial value was implemented also user defined. For the roll motion this initial value may be representative of a given transverse slope (inclination) associated with the wind action (Blendermann, 1996) capable of triggering the phenomenon of parametric resonance in longitudinal waves.

For the other motions as already explained in the program capabilities (in especially for heave and pitch) it is also possible to start the motions based on their solutions in the frequency domain. That is to say that at time $t = 0$, solution in frequency domain and the solution in time domain coincide.

Considering a ship as an unconstrained rigid body subjected to gravity, radiation, diffraction, Froude-Krylov and hydrostatic forces the motion is solved in the time domain by a numerical procedure. Different time domain formulations have been proposed in order to include nonlinear effects in the solution of the problem. Depending on the desired simulation, the equations of motion (3-53) involve a series of hydrodynamic coefficients. In a simplified simulation of parametric resonance only considered nonlinearities are those of the restoring coefficients in heave roll and pitch. Depending on the degree of complexity set for a given incident wave frequency, the added mass A_{kj} , damping coefficients B_{kj} , diffraction and Froude-Krylov force, could be either kept constant during time simulation or not. Diffraction forces are obtained simply transforming in the time domain the corresponding frequency domain terms. Froude-Krylov and hydrostatic forces, which in the frequency domain are considered relative to the mean hull shape and linearized, can here be estimated considering the actual wetted hull body surface, known at each time step.

At this point, a procedure timeline can be displayed. In order to establish and set up the experiment, the first run on the original code was performed so that the occurrence regions of parametric rolling are identified. Bearing in mind the experiment costs (limited number of runs) the basin must get a rather precise request to analyze conditions of interest so that the code and the procedure can eventually be worked out. The analysis starts with the regular head waves. If the parametric resonance is observed it is necessary to exert and retrieve the peak condition for the phenomenon (in terms of polar plots it is almost the gravity center of shaded area corresponding to the actual parametric rolling outcomes) in order to facilitate experimental setup.

Following the theory presented, a computer code was implemented with the features necessary to predict ship motion instabilities, particularly utilized for a design wave and forward speed that could lead to the occurrence of parametric rolling. An investigation was undertaken to determine whether head-sea parametric rolling could have been the cause of the vessel's extreme motions. Based on previous investigations, the conditions upon which head wave parametric rolling resonance is likely to occur, such as the effects of the encounter period, the wave height and the encounter angle on parametric rolling amplitude were clarified. In order to run simulations the program is set up by tuning the parameters so that parametric rolling can be expected, such as, the natural period of roll is equal to approximately twice the wave encounter period and the wave length is in the order of the ship length (between 0.8 and 2.0 times L_{pp}). Wave height needs to exceed a critical level and roll damping needs to be small. The duration of each regular wave simulation record should be long enough for steady state ship motions to be established.

For this specific case the chosen wave length to ship ratio varies from 0.8 to 1.4. The investigation was carried out for wave heights ranging from 4 m to 10 m. Finally, all the calculations have to be checked for the forward speed dependence up to the maximum achievable speed (within

operational range). More specifically, forward speeds will be considered up to 20 knots with the increment of a 1 knot. By varying each of these parameters, significant amplification of roll motion is observed and studied. The complete numerical results of motions exerted by a longitudinal regular head waves are displayed in Turk et al. 2009 and Ribeiro e Silva et al. 2010, in particular elevation $\zeta(t)$, surge $\eta_1(t)$, sway $\eta_2(t)$, heave $\eta_3(t)$, roll $\eta_4(t)$, pitch $\eta_5(t)$ and yaw $\eta_6(t)$ motion from these preliminary outings.

The simulations have shown that until the wave height of 6 m is reached parametric rolling does not occur. The very first condition (Figure 5-2) upon which the parametric rolling resonance is evident, corresponds to forward speed of 7 knots, wave height of 6 m, and the wave length equal to ship length (wave period $T_W = 12.95$ s) (Turk et al. 2009).

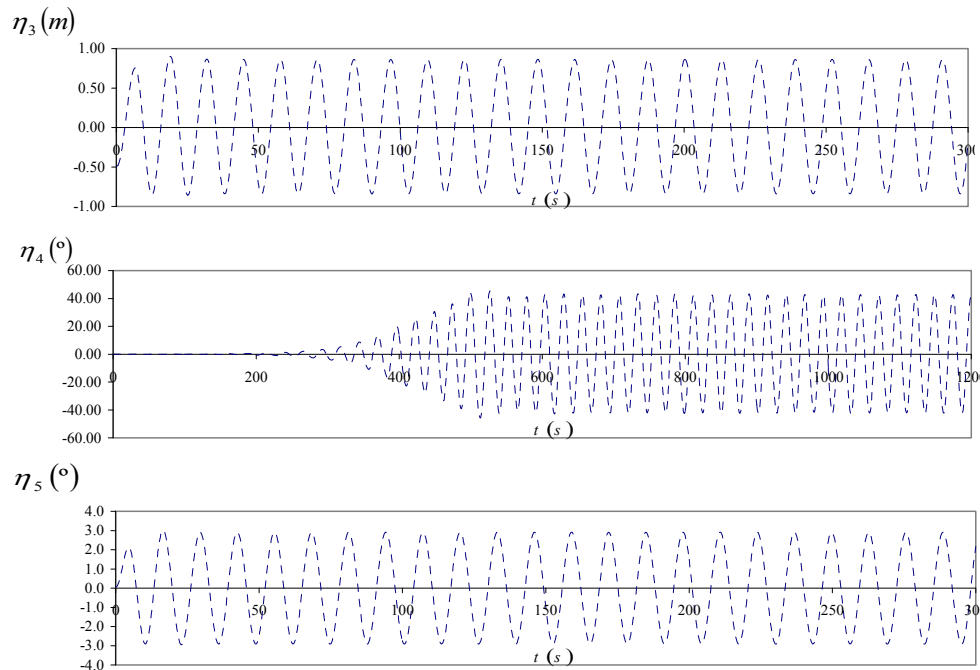


Figure 5-2. Development of parametric rolling in regular waves ($H_W = 6$ m, $T_W = 12.95$ s, speed 7 knots)

Phase diagrams of the roll motion equation may also be obtained from each case analysed as seen is figure 5-3. This is rather important as a starting point where upon all the simulations following similar parameters can be closely observed and fine tuned. Parametric rolling usually occurs within the enclosed range of the encounter periods, the wave heights and the encounter angles and because of it one assumes that this specific case on fig. 5-2 is incipience of “regional” (in terms of shaded parts of polar plots) occurrence of parametric roll. On the contrary, if an isolated event based on arbitrary conditions is traced, that can almost certainly be attributed to the numerical errors in the simulations.

It can be deduced that sway and yaw motion is negligible in comparison to heave, roll and pitch motions. When the frequency of encounter (excitation frequency) is near the pitch frequency, the pitch mode is excited if the encountered wave amplitude (excitation amplitude) is small. As the excitation amplitude increases, the amplitude of the pitch mode increases until it reaches a critical small value. As the excitation amplitude increases further, the pitch amplitude reaches a saturated value, and all of the extra energy is transferred to the roll mode. Furthermore, heave and pitch motions accompanying parametric rolling in regular waves are such that a significant rise of roll amplitude is associated with small decrease in heave and a very small decrease in pitch. This is relevant for establishing a pattern upon which the range of parametric conditions for such a resonant effect can be sustained and monitored. Seeing the figure 5-2, it is also possible to deduce and verify that the roll and pitch motion are well synchronized with the approaching wave.

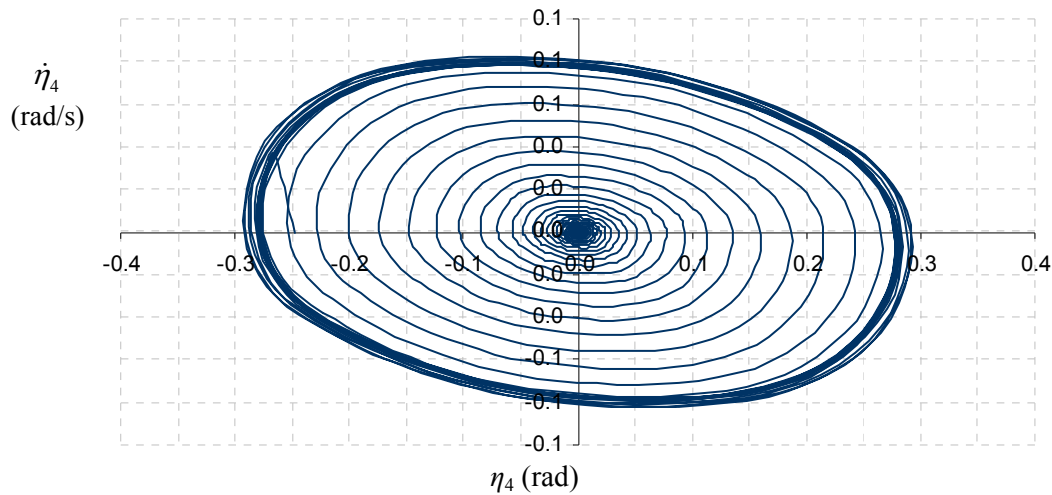


Figure 5-3. Phase diagram of the roll motion ($H_W = 6$ m, $T_W = 12.95$ s, speed 7 knots)

The results can also be interpreted as such that given the right combination of wave height, wave period, natural rolling period and speed the three sets of parametric rolling can be identified in head-sea for a classic case of wave length equal to the ship length. It is important to outline the parametric conditions upon which they can take place and even more important the “occurrence groupiness” effects which represents whether those parameters are in relative vicinity. In other words, not a significant change in wave height, wave period, natural rolling period and speed between those set of conditions can be accountable for a sustainable or prolonged parametric rolling given possible unfavourable ship handling tactics.

By analyzing the numerical results obtained, there are two aspects that have to be considered the most important ones. First is the parametric condition that precedes all the other ones upon which the parametric rolling effect develop ($H_W = 6$ m, $T_W = 12.95$ s, speed 7 knots). The second is the parametric set-up where for the particular speed the highest amplifications of roll motion are observed and preferably for an extended range of wave heights (for instance, $H_W = 7-8$ m, $T_W = 12.95$ s, speed 7-9 knots).

Given the extensive literature survey it is not coincidence that a period of $T_W = 12.95$ s corresponding to wave to ship length of 1, was chosen as simulation exemplar. That is not to say that the other frequencies aren't vulnerable but the focus on $T_W = 12.95$ s was deliberate given the definition itself (ABS, 2004) explaining parametric rolling. It has to be noted that this simulation corresponds well with information reported onboard this vessel in Oct. 1998 during the accident. Furthermore, the conditions upon which parametric rolling took place and the amplitudes of the roll as well, are in relative agreement with the experimental results published in France et al. (2001).

5.3.2 Mathematical model implementation for following waves

Since the original procedure was constrained only to the longitudinal seas what is left is the parametric rolling survey regarding following waves excitation. In principal, although the physical excitation is similar and theoretically challenging as well, the parametric rolling due to the following waves has received much smaller dissemination of the scientific community. The reason is very simple. Even though the parametric resonance originates from the following wave's excitation of fishing vessels modern hull forms and its exploitation is very much in tune to the vastly more expensive floating structures like post-panamax containerships.

However, as for head waves, the simulation did detect parametric rolling and that is in correspondence to the reported, even dating from the 1950s (Cummings, 1959). The resonant effect only occurs for the wave length to ship length ratio of 0.8 corresponding to the period of $T_W = 11.59$ s, starting from the case of zero knots. The energy put into the pitch and heave motion by the wave excitations may be partially transferred into the roll motions by means of nonlinear coupling among

these modes; consequently roll motion can be indirectly excited. As compared to heave and pitch motions, which are reaching stabilised solutions for a small number of oscillations, the induced roll motion has firstly a transitory phase and then the rolling amplitude slowly increases until the steady state is reached. Figure 5-4 shows an expanded view of the roll and pitch response in regular waves.

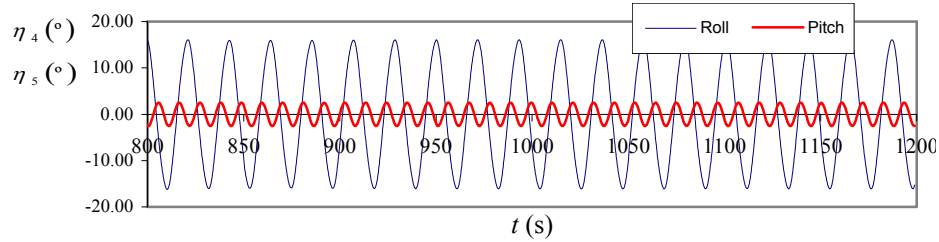


Figure 5-4. Expanded view of roll and pitch motions at largest roll

Positive pitch values mean the vessel is pitched down by the bow. Also, it can be seen from figure 5-4 that there are two pitch cycles for each roll cycle, and that the model is always pitched down by the bow at maximum roll. That is, when the model is at maximum starboard roll it is pitched down by the bow, when upright at zero heel it is pitched down by the stern, and when at maximum port roll it is pitched down by the bow again. Throughout the test program, this relationship between pitch and roll motions existed whenever parametric roll was induced. Similarly as with head waves investigation these results are already published by Turk at al. 2011 and will be omitted from this work.

The simulation records are systemized and presented in table 5-1.

Folder destination	speed (kts)	heading	λ/L_{pp}	height	roll amplitude	roll amp. rounded	B44 Ikeda	indication
..lc11ext\TDM\Speed_0_kts\Heading_0\LvLpp_0.80\H_4	0.00	0.00	0.80	4.00	0.00	0.00	0.00	-
..lc11ext\TDM\Speed_0_kts\Heading_0\LvLpp_0.80\H_5	0.00	0.00	0.80	5.00	0.00	0.00	0.00	-
..lc11ext\TDM\Speed_0_kts\Heading_0\LvLpp_0.80\H_6	0.00	0.00	0.80	6.00	0.00	0.00	0.00	-
..lc11ext\TDM\Speed_0_kts\Heading_0\LvLpp_0.80\H_7	0.00	0.00	0.80	7.00	13.50	10.00	363000000.00	+
..lc11ext\TDM\Speed_0_kts\Heading_0\LvLpp_0.80\H_8	0.00	0.00	0.80	8.00	21.81	20.00	552000000.00	+
..lc11ext\TDM\Speed_0_kts\Heading_0\LvLpp_0.80\H_9	0.00	0.00	0.80	9.00	39.30	40.00	929000000.00	+
..lc11ext\TDM\Speed_0_kts\Heading_0\LvLpp_0.80\H_10	0.00	0.00	0.80	10.00	38.42	40.00	929000000.00	+
..lc11ext\TDM\Speed_1_kts\Heading_0\LvLpp_0.80\H_4	1.00	0.00	0.80	4.00	0.00	0.00	0.00	-
..lc11ext\TDM\Speed_1_kts\Heading_0\LvLpp_0.80\H_5	1.00	0.00	0.80	5.00	0.14	0.00	0.00	-
..lc11ext\TDM\Speed_1_kts\Heading_0\LvLpp_0.80\H_6	1.00	0.00	0.80	6.00	0.06	0.00	0.00	-
..lc11ext\TDM\Speed_1_kts\Heading_0\LvLpp_0.80\H_7	1.00	0.00	0.80	7.00	2.19	0.00	0.00	-
..lc11ext\TDM\Speed_1_kts\Heading_0\LvLpp_0.80\H_8	1.00	0.00	0.80	8.00	37.18	40.00	918000000.00	+
..lc11ext\TDM\Speed_1_kts\Heading_0\LvLpp_0.80\H_9	1.00	0.00	0.80	9.00	36.42	40.00	918000000.00	+
..lc11ext\TDM\Speed_1_kts\Heading_0\LvLpp_0.80\H_10	1.00	0.00	0.80	10.00	27.96	30.00	737000000.00	+
..lc11ext\TDM\Speed_2_kts\Heading_0\LvLpp_0.80\H_4	2.00	0.00	0.80	4.00	0.02	0.00	0.00	-
..lc11ext\TDM\Speed_2_kts\Heading_0\LvLpp_0.80\H_5	2.00	0.00	0.80	5.00	0.44	0.00	0.00	-
..lc11ext\TDM\Speed_2_kts\Heading_0\LvLpp_0.80\H_6	2.00	0.00	0.80	6.00	0.00	0.00	0.00	-
..lc11ext\TDM\Speed_2_kts\Heading_0\LvLpp_0.80\H_7	2.00	0.00	0.80	7.00	14.55	10.00	381000000.00	+
..lc11ext\TDM\Speed_2_kts\Heading_0\LvLpp_0.80\H_8	2.00	0.00	0.80	8.00	32.91	30.00	724000000.00	+
..lc11ext\TDM\Speed_2_kts\Heading_0\LvLpp_0.80\H_9	2.00	0.00	0.80	9.00	26.44	30.00	724000000.00	+

Table 5-1. Summary table for parametric rolling realizations in following waves.

The similar pattern is noticeable for the ship speed of 1 knot, however the highest amplification of roll motion is shifted toward lower wave heights. That trend is transcended to the last evidence of the parametric rolling in following waves which can be traced to the speed of 2 knots, where at wave amplitude of 5 m dies out. This actually supports the theory stating that such an effect cannot be sustained for a prolonged range of ahead speeds and it usually vanishes at certain threshold wave heights due to the energy balance between damping and change of stability.

It should be noted that these results originate from the methodology proposed by Ribeiro e Silva (2008). However, the optimisation of methodology and the code was already applied having a fully automatic routine at hand. Although the physical content remained the same, some of the procedures were updated while some features added. As a result of the automation the following summary output is presented in the table 5-2. The table corresponds only to the $\lambda/L_{pp} = 1$, and the results for other wave frequencies are at present omitted. The shaded cells depict the parametric rolling outcome for the 180° heading, with the highest amplification traced and colored in red.

phase relationships which indicate its phase. A new list of equivalent damping's is calculated from the updated set of phase relationships and the procedure is repeated. In this way the procedure converges towards a set of reflections which will give strong indications for new phases in the early stages of phase generation with the simple weighted formula. Starting from the presumption that the best available bounds are none too strong, pre-calculated damping values using a new program were set as reference variables with the roll amplitudes as the determining factor. In this particular case the values were set for roll amplitudes of 5°, 15°, 25°, 35° and 45°. During the simulation the phase relationships acting over boundaries of 10°, 20°, 30°, and 40° were exercised. In other word, the equivalent damping was updated using pre-calculated values for the roll amplitudes as nonlinear variables, depending whether over or under the boundary range they fall. The notation is mostly either self-explanatory or else standard. For instance, if the recorded roll amplitude is 31° then the values of 35° are taken for the next simulation run. The procedure is iterative until the results efficiently converge within the acceptable approximated boundaries. However during the execution it was found that no matter the number of iterative simulations taken, some outcomes are unrealistic or infeasible.

It is already established that the parametric rolling is observed associated with the grouped set of conditions extending in the range of 3 to 6 subsequent ship speeds. Several random realisations were chosen to demonstrate the proposed methodology. To start with, case study “test No. 10” is chosen along with the immediate and following neighbouring condition responsible for the PR realization. Table 5-3, shows the complete set of velocities associated with the specific parametric condition ($T_W = 12.95$ s, $H_W = 8$ m) which corresponds to $\lambda/L_{pp} = 1$. Parametric rolling is simulated within the range of 7-13 knots. However, there was uncharacteristically large roll amplitude detected (shaded), confirmed even on the experiment, as the major difference of roll amplitude η_4 of about 20° suggest.

Folder destination	speed (kts)	heading	λ/L_{pp}	height	roll amplitude	roll amp. rounded	B44 Ikeda	indication
..lc11ext\TDM\Speed_0_kts\Heading_180\LvoLpp_1.00\H_8	0.00	180.00	1.00	8.00	0.00	0.00	0.00	-
..lc11ext\TDM\Speed_1_kts\Heading_180\LvoLpp_1.00\H_8	1.00	180.00	1.00	8.00	0.00	0.00	0.00	-
..lc11ext\TDM\Speed_2_kts\Heading_180\LvoLpp_1.00\H_8	2.00	180.00	1.00	8.00	0.00	0.00	0.00	-
..lc11ext\TDM\Speed_3_kts\Heading_180\LvoLpp_1.00\H_8	3.00	180.00	1.00	8.00	0.00	0.00	0.00	-
..lc11ext\TDM\Speed_4_kts\Heading_180\LvoLpp_1.00\H_8	4.00	180.00	1.00	8.00	0.00	0.00	0.00	-
..lc11ext\TDM\Speed_5_kts\Heading_180\LvoLpp_1.00\H_8	5.00	180.00	1.00	8.00	0.01	0.00	0.00	-
..lc11ext\TDM\Speed_6_kts\Heading_180\LvoLpp_1.00\H_8	6.00	180.00	1.00	8.00	0.02	0.00	0.00	-
..lc11ext\TDM\Speed_7_kts\Heading_180\LvoLpp_1.00\H_8	7.00	180.00	1.00	8.00	53.94	40.00	1010000000.00	+
..lc11ext\TDM\Speed_8_kts\Heading_180\LvoLpp_1.00\H_8	8.00	180.00	1.00	8.00	45.04	40.00	1040000000.00	+
..lc11ext\TDM\Speed_9_kts\Heading_180\LvoLpp_1.00\H_8	9.00	180.00	1.00	8.00	43.26	40.00	1010000000.00	+
..lc11ext\TDM\Speed_10_kts\Heading_180\LvoLpp_1.00\H_8	10.00	180.00	1.00	8.00	41.66	40.00	966000000.00	+
..lc11ext\TDM\Speed_11_kts\Heading_180\LvoLpp_1.00\H_8	11.00	180.00	1.00	8.00	18.01	20.00	674000000.00	+
..lc11ext\TDM\Speed_12_kts\Heading_180\LvoLpp_1.00\H_8	12.00	180.00	1.00	8.00	13.63	10.00	539000000.00	+
..lc11ext\TDM\Speed_13_kts\Heading_180\LvoLpp_1.00\H_8	13.00	180.00	1.00	8.00	4.23	5.00	482000000.00	+
..lc11ext\TDM\Speed_14_kts\Heading_180\LvoLpp_1.00\H_8	14.00	180.00	1.00	8.00	0.01	0.00	0.00	-
..lc11ext\TDM\Speed_15_kts\Heading_180\LvoLpp_1.00\H_8	15.00	180.00	1.00	8.00	0.00	0.00	0.00	-
..lc11ext\TDM\Speed_16_kts\Heading_180\LvoLpp_1.00\H_8	16.00	180.00	1.00	8.00	0.00	0.00	0.00	-
..lc11ext\TDM\Speed_17_kts\Heading_180\LvoLpp_1.00\H_8	17.00	180.00	1.00	8.00	0.00	0.00	0.00	-
..lc11ext\TDM\Speed_18_kts\Heading_180\LvoLpp_1.00\H_8	18.00	180.00	1.00	8.00	0.01	0.00	0.00	-
..lc11ext\TDM\Speed_19_kts\Heading_180\LvoLpp_1.00\H_8	19.00	180.00	1.00	8.00	0.01	0.00	0.00	-
..lc11ext\TDM\Speed_20_kts\Heading_180\LvoLpp_1.00\H_8	20.00	180.00	1.00	8.00	0.10	0.00	0.00	-

Table 5-3. Summary of parametric rolling survey for regular head waves ($H_W = 8$ m, $T_W = 12.95$ s)

After adopting the convergence method the roll amplitude distribution is much smoother and more realistic while the difference in roll amplitude for the experimentally tested condition falls to approximately 9°, effectively reducing the roll amplitudes for $\eta_4 = 10.37^\circ$ which is 50% improvement. The biggest influence as seen on table 5-4 is for the 7 knots with the roll amplitudes reduction of $\eta_4 = 21.26^\circ$. The last two parametric conditions actually increased the amplitudes for about $\eta_4 \approx 4^\circ$ proving that the method is not one-sided in terms of being bounded towards lowering amplitudes only.

Folder destination	speed (kts)	heading	λ/L_{pp}	height	roll amplitude	roll amp. rounded	B44 Ikeda	indication	delta
..lc11ext\TDM\Speed_7_kts\Heading_180\LvoLpp_1.00\H_8	7	180	1	8	32.68	30	898000000	+	21.26
..lc11ext\TDM\Speed_8_kts\Heading_180\LvoLpp_1.00\H_8	8	180	1	8	34.67	30	898000000	+	10.37
..lc11ext\TDM\Speed_9_kts\Heading_180\LvoLpp_1.00\H_8	9	180	1	8	44.02	40	1010000000	+	0.76
..lc11ext\TDM\Speed_10_kts\Heading_180\LvoLpp_1.00\H_8	10	180	1	8	43.33	40	966000000	+	1.67
..lc11ext\TDM\Speed_11_kts\Heading_180\LvoLpp_1.00\H_8	11	180	1	8	22.54	20	674000000	+	4.53
..lc11ext\TDM\Speed_12_kts\Heading_180\LvoLpp_1.00\H_8	12	180	1	8	18.12	20	657000000	+	4.49

Table 5-4. Summary of parametric rolling survey for regular head waves ($H_W = 8$ m, $T_W = 12.95$ s) with damping blending method

This was a successful example of the proposed routine, however as seen on the following example the method can also underperform. The technical difficulties at hand therefore concern the

possibility of wild (but, say, bounded) oscillations. Continuing our discussion from the beginning about the possible ways strong convergence breaks down, the table 5-5, represents the three runs (0 knots, 180° heading, $\lambda/L_{pp} = 0.8$, $H_W = 7-10$ m) in attempt to feasibly converge up to a realistic roll amplitude. As seen on the end of the table three cases have successively converged with the difference of amplitude rounded to zero. On the other hand simulations associated with $H_W = 8$ m are oscillating in between of $\eta_4 \approx 23 - 45^\circ$ range. The oscillation stabilizes for the manually imputed Ikeda’s damping values (to test the convergence) as function of roll angles in between $\eta_4 \approx 32 - 36^\circ$, however the proposed convergence cannot reach it. In such cases the mean values of oscillation could be amenable, albeit this is extremely simple presumption. All this suggests the possibility of identifying more general circumstances in which extra information available for convergent sequences can be useful. A possible solution would be to implement basic bisection method to weigh the contribution (even genetic algorithm technique) of non converging outcomes (random generator) thus enabling rapprochement between two “incompatible” operators. This type of simulation ineptitude (behavior), however, is in vast minority constituting in about 3% of all simulations. The reason is that some simulations (usually peaked simulations of a certain grouped parametric rolling realization) are oversensitive to the equivalent damping terms and relatively small variations are consequently pushing the roll amplitudes back and forth.

Folder destination	speed (kts)	heading	λ/L_{pp}	height	roll amplitude	roll amp. rounded	B44 Ikeda	indication	delta
..lc11ext\TDM\Speed_0_kts\Heading_180\LvoLpp_0.80\H_7	0.00	180.00	0.80	7.00	19.73	20.00	552000000.00	+	
..lc11ext\TDM\Speed_0_kts\Heading_180\LvoLpp_0.80\H_8	0.00	180.00	0.80	8.00	39.41	40.00	929000000.00	+	
..lc11ext\TDM\Speed_0_kts\Heading_180\LvoLpp_0.80\H_9	0.00	180.00	0.80	9.00	36.32	40.00	929000000.00	+	
..lc11ext\TDM\Speed_0_kts\Heading_180\LvoLpp_0.80\H_10	0.00	180.00	0.80	10.00	35.20	40.00	929000000.00	+	
..lc11ext\TDM\Speed_0_kts\Heading_180\LvoLpp_0.80\H_7	0.00	180.00	0.80	7.00	21.14	20.00	552000000.00	+	1.41
..lc11ext\TDM\Speed_0_kts\Heading_180\LvoLpp_0.80\H_8	0.00	180.00	0.80	8.00	23.12	20.00	552000000.00	+	16.29
..lc11ext\TDM\Speed_0_kts\Heading_180\LvoLpp_0.80\H_9	0.00	180.00	0.80	9.00	36.68	40.00	929000000.00	+	0.35
..lc11ext\TDM\Speed_0_kts\Heading_180\LvoLpp_0.80\H_10	0.00	180.00	0.80	10.00	35.63	40.00	929000000.00	+	0.43
..lc11ext\TDM\Speed_0_kts\Heading_180\LvoLpp_0.80\H_7	0.00	180.00	0.80	7.00	21.14	20.00	552000000.00	+	0.00
..lc11ext\TDM\Speed_0_kts\Heading_180\LvoLpp_0.80\H_8	0.00	180.00	0.80	8.00	45.65	40.00	929000000.00	+	22.53
..lc11ext\TDM\Speed_0_kts\Heading_180\LvoLpp_0.80\H_9	0.00	180.00	0.80	9.00	36.68	40.00	929000000.00	+	0.00
..lc11ext\TDM\Speed_0_kts\Heading_180\LvoLpp_0.80\H_10	0.00	180.00	0.80	10.00	35.63	40.00	929000000.00	+	0.00

Table 5-5. Summary of parametric rolling survey for regular head waves ($H_W = 8$ m, $T_W = 11.59$ s) with damping blending method

The best example to illustrate the comparatively good behaviour of these simulations is by looking at the figures showing the C11 response in regular waves of varying frequencies for the head sea condition. These figures illustrate the susceptibility of the C11 hull to parametric rolling over a wide frequency range and the recorded maximum roll angles. Differences are obvious as the updated methodology not only exhibits smoother layout but also decreases the roll amplitudes in average close to 11%. More evidence to support the claim is presented further below in the figure 5-5.

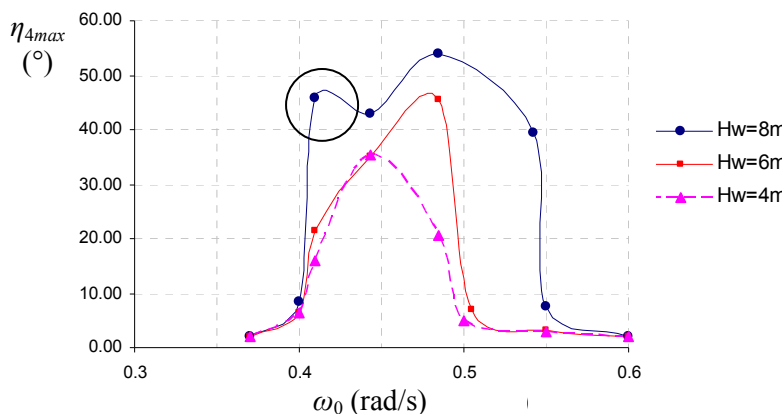


Figure 5-5. Regular wave parametric roll response for C11-class ship (original methodology)

Also, the bump evident on figure 5-5, for $H_W = 8$ m is unrealistic, as one would anticipate the biggest rolling amplitudes in the vicinity of $\lambda/L_{pp} \approx 1$ ($\omega_0 \approx 0.485$ rad/s), with the incident wave above a threshold or critical amplitude for parametric roll to be initiated and sustained. The roll amplitudes spreading around $\omega_0 = 0.485$ rad/s should decrease while frequencies in the range under $\omega_0 = 0.385$ rad/s and over $\omega_0 = 0.575$ rad/s exclude the possibility of parametric resonance.

The bump on the figure 5-6 is greatly reduced as the maximum roll amplitudes for the $\lambda/L_{pp} = 1.2$ ($\omega_0 = 0.442$ rad/s) are slightly higher than for $\lambda/L_{pp} = 1.4$ ($\omega_0 = 0.41$ rad/s) which is to be expected. Also the highest amplitudes are observed for the $\lambda/L_{pp} = 0.8$ ($\omega_0 = 0.554$ rad/s) already deduced as the general trend validated with all the parametric rolling experimental tests. The good choice of approximated boundaries makes it quite an efficient tool.

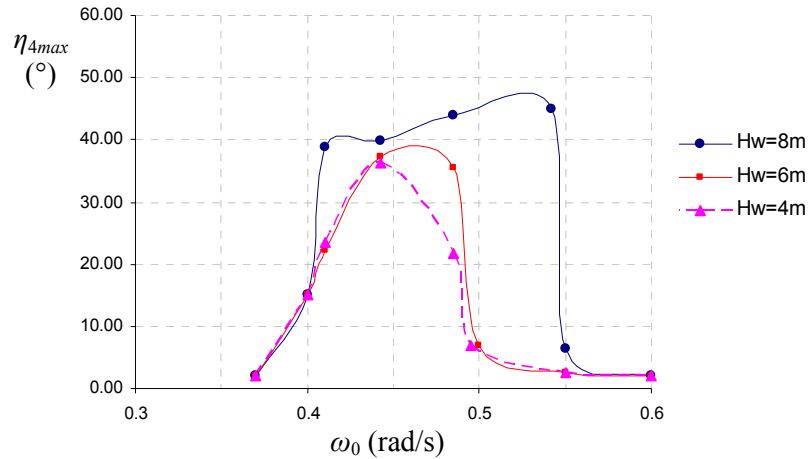


Figure 5-6. Regular wave parametric roll response for C11-class ship (updated methodology)

The width of the regular wave response curve suggests that the C11 hull form is likely to encounter parametric rolling in certain irregular seas as well.

Figure 5-7 shows the mean of 1/10th highest roll amplitudes plotted against the (significant) wave height for regular head seas. The risk of parametric roll in head seas with the most unfavourable wave period tuning selected (the specific parametric condition ($T_W = 12.95$ s, which corresponds to $\lambda/L_{pp} = 1$) is presented, as a function of the occurrence of parametric roll for each significant wave height.

The wave height and ship speed can not really be disengaged. The wave height in conjunction with the wave period will define the maximum sustainable speed at which the vessel will be able to navigate with the full power use. The maximum sustained speed line represents the lowest sustained speed for each given wave height.

Figure 5-7, depicts the situations where risk can be present, although it should be taken as relatively conservative, still a fairly good indication is given. The fully shaded area corresponds to the bounded realization of parametric rolling (PR) extended between the lower and upper curve for the speeds that enable it.

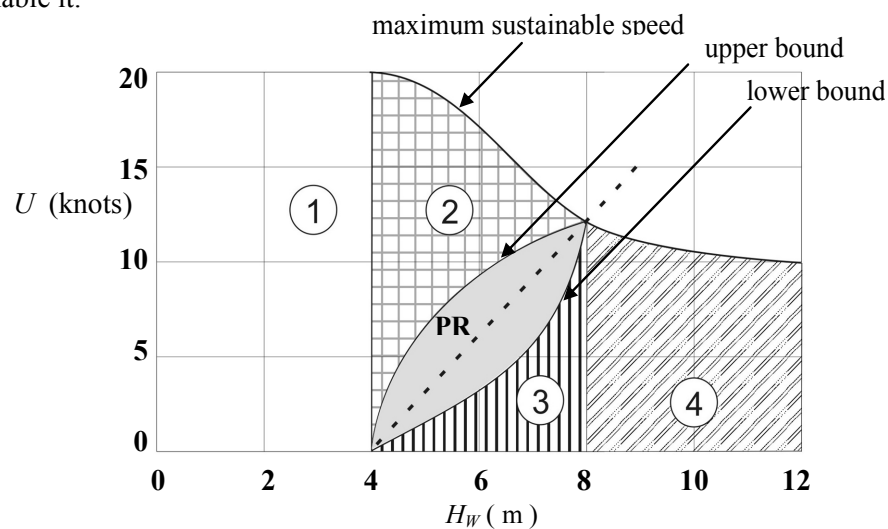


Figure 5-7. Risk of parametric as a function of significant wave height and sustained speed

The region ① specifies that the parametric excitation under the wave height of 4 m is unfeasible. The region designated at ② shows that a potential risk of parametric roll, is avoided due to the possibility of maintaining higher sustainable speed. Taking into account the results obtained, translated into ship handling tactics if headed into the seas, the master should keep increased speed to reduce the risk although problems may be encountered when speed is reduced voluntary. The area under ③ suggests that the parametric roll will not occur due to low speeds but that can be misleading since those speeds as designated here are unlikely in realistic sailing experience. The area under ④ is “safe” since the parametric rolling is only possible for the speeds above the maximum sustained speed line.

The previous figure shows clearly that high sustained speed reduces the risk of parametric roll. Taking into account the results obtained, translated into ship handling tactics, the vessel should have remained in beam seas during the storm or, if headed into the seas, should have increased speed to reduce rolling. All of these manoeuvres are contrary to normal heavy weather ship handling practice and counter-intuitive for masters.

Different conditions can be adopted as well. This means that higher sustained speed could be reached in more favourable wave periods at the same wave height. Lets take a look at the cases corresponding to the $\lambda/L_{pp} = 1.2$ ($\omega_e = 0.442$ rad/s) and $\lambda/L_{pp} = 1.4$ ($\omega_e = 0.41$ rad/s). The shaded area of parametric rolling is upped toward a higher ship speeds which is actually convenient since the part of the area becomes truncated by the maximum sustained speed line. The worse scenario is for the $\lambda/L_{pp} = 0.8$ ($\omega_e = 0.542$ rad/s) where the parametric rolling area is shifted toward higher wave heights (~10 m) but also for the lower speeds (1-7 knots) which may be dangerous since it falls within normal heavy weather ship handling practice intuitive for the masters.

If for instance the heading is altered to the 150° the whole parametric rolling realization is shifted left as the numerical code for the wave height of 4 m, yields parametric rolling in range of 3-7 knots. This is to be expected since the oblique wave provides stronger roll excitation in the first place. All those conditions can be plotted as well but due to the extensive nature of this work are at present omitted.

The expected roll amplitude for the head waves can be plotted over the wave height as well, as seen on Fig. 5-8. It is observed that up to a wave height of 4.0 m, no roll motion is excited. Interestingly though, in the interval from 4.0 m to 4.3 m both, zero amplitude and large amplitude motions are possible, which brings us back to the stability charts from Mathieu equation. Beyond the wave height of 4.3 m there exist only stable motions with large amplitudes.

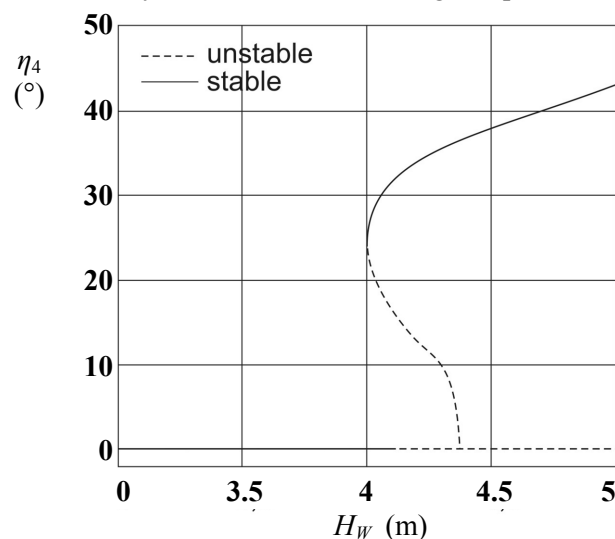


Figure 5-8. Stable and unstable realizations of roll responses

Different conditions can be also implemented here as for instance, the heading altered to the 150° dislocates the whole parametric rolling realization left starting at the wave heights of nearly 3 m while also narrowing the double solutions of boundary value problems.

As the numerical optimization enables different headings, similar can also be illustrated in Fig. 5-9 and 5-10, for a bow waves ($150\text{-}210^\circ$) set up for $T_w = 12.95$ s ($\lambda/L_{pp} = 1$) where one can see that the threshold significant wave height (wave height for which parametric roll will start) increases by increasing ship speed with the highest risk in range from 7-13 knots. Note that the parametric rolling possibility for the waves of $H_w = 4$ m exists only for the bow quartering waves.

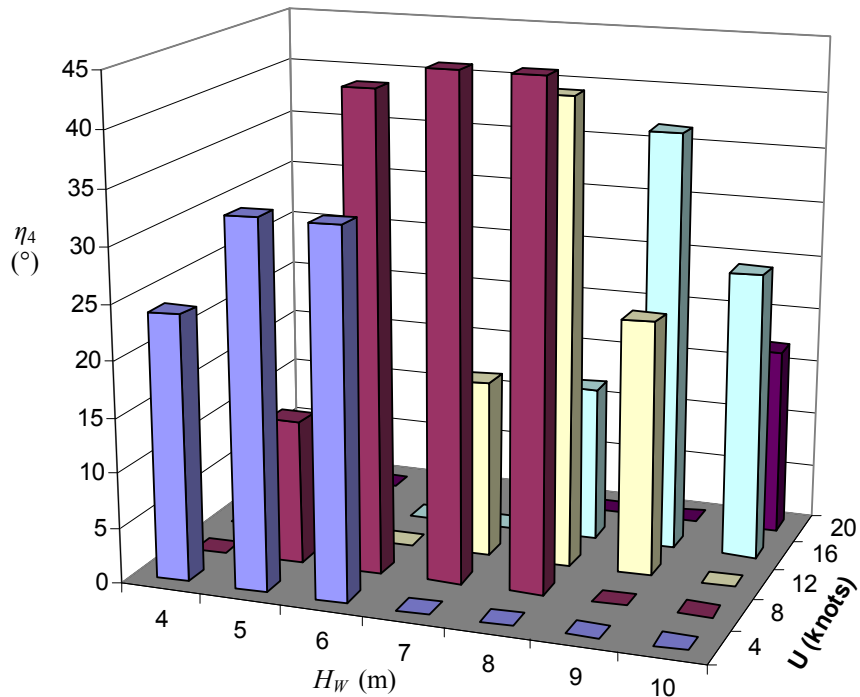


Figure 5-9. Maximum roll responses for bow waves for $T_w = 12.95$ with updated methodology

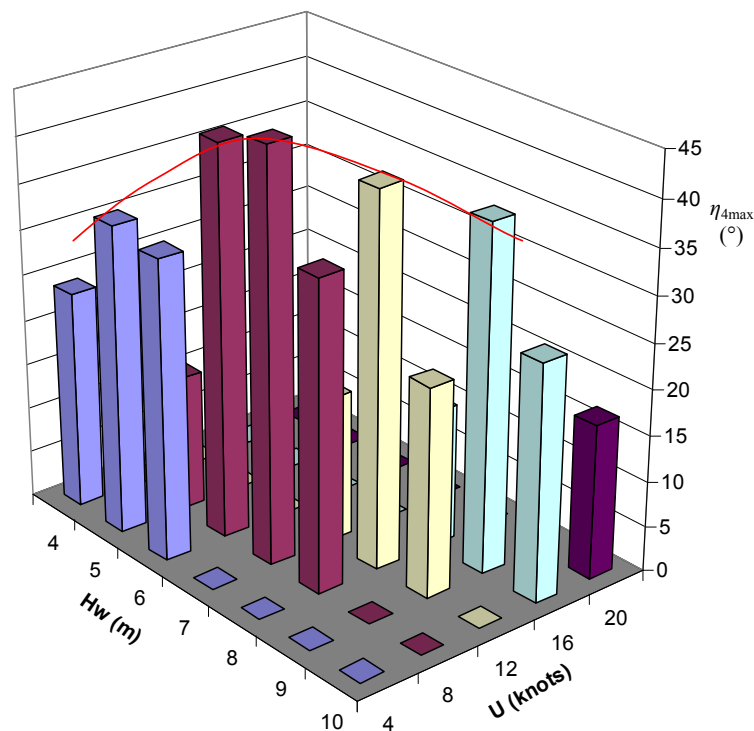


Figure 5-10. Quantitative validation of regression fit for the occurrence regions of parametric rolling

Also, the growth of roll amplitudes should increase with the wave height but as already mentioned the simulations reaches the threshold value somewhere in the range of $H_w = 9$ m, consequently decreasing roll angles. This is given more illustrative on figure 5-10. Figure 5-10 also shows calculated regression fit (red line) of the highest observed amplifications of roll angles for each ship speed even though a better approximation would be to a surface chart presentation.

In each line on the figure 5-11 linear regression fits are reported only as qualitative indications of the trend, and there is no intention to provide any means for extrapolation. The sudden drop at around $H_w = 8 - 9$ m is somewhat contrary to the reported by Levadou et al. 2004, where threshold significant wave height increases progressively with increasing ship speed.

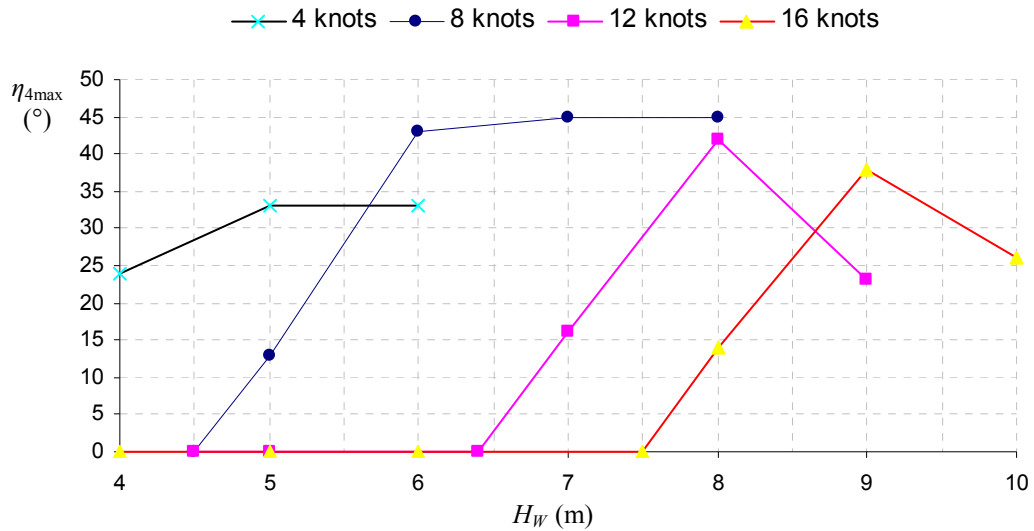


Figure 5-11. Linear fitting for varying speeds with roll responses as a function of wave heights

The same can be applied for the stern waves (330-30°) set up. The physical mechanism that triggers it is little bit different as are the results (figure 5-12).

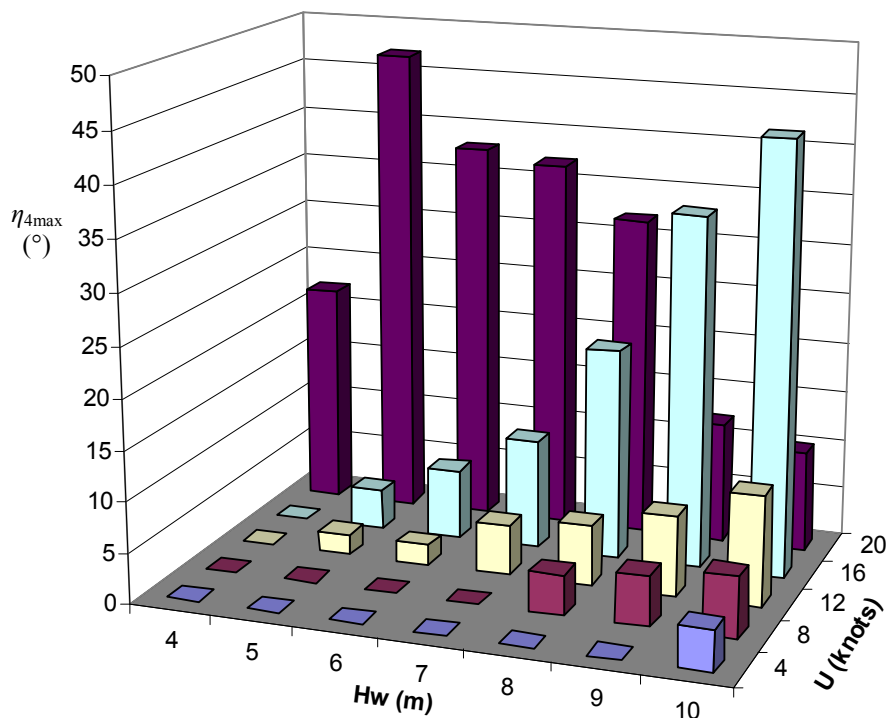


Figure 5-12. Maximum roll responses for stern waves for $T_w = 12.95$ with updated methodology

Since the wave height of 8 m was established as a threshold value for parametric rolling the influence of heading is going to be investigated and presented (figure 5-13).

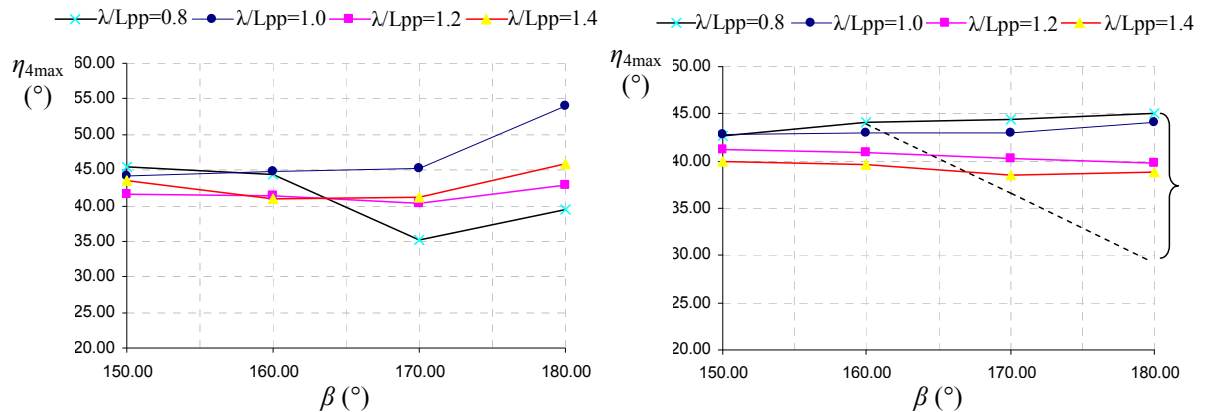


Figure 5-13. Comparison of roll response from both original and modified methodology for different headings

Note that these are the highest observed amplitudes and pattern for mean amplitudes can be different. The dotted line on the graph presents un-converging solution ranging from $\eta_4 \approx 28 - 45^\circ$ for a heading of 180° , as was already previously explained while explaining the method and pointing to the perceived disadvantages. The results however would be converging toward higher values when a suitable convergence sequence is implemented.

The modified procedure enables agreeable comparison to the report from France, 2003., both in magnitude and trend, as roll angles slightly increase at increasing relative headings, with the greater values associated with the $\lambda/L_{pp} = 0.8$, also confirmed by the experiments. The higher roll excitation encountered in head seas is likely related to the wave shapes as they move along the ship and their influence on GM variations.

As before, the concept can be applied for the stern waves (330° - 30°) set up. The propensity and effects of parametric rolling have been considered from all the various aspects that contribute it, therefore, one can conclude that the convergence method greatly enhances the performance of the numerical simulation both on the qualitative and quantitative properties of solutions.

The simulations were performed ranging from:

- » Heading (150° - 210° and 330° - 30°) with the increment of 10° ,
- » Wave heights (4-10 m) with the increment of 1 m,
- » Wave to ship length ratio (λ/L_{pp} of 0.8-1.4) with the increment of 0.2,
- » Ship speeds (0-20 knots) with the increment of 1 knot,

which makes roughly 4700 total simulations. The operated range of headings is taken as such where parametric rolling has a dominant presence. At the bow or the stern quartering waves the effect of beam rolling, pure loss of stability, etc becomes more influential to the point where it's impossible to distinguish between them. A possible mechanism that yields large roll angles is loss of stability in case of lower metacentric height. Unfortunately there was no time to cover this aspect in the present work. Risk of loss of stability in following and stern-quartering seas in cases of very low encounter frequency could also be investigated in the future in order to provide a complete picture of the operational risk related to extreme roll behavior. The plot in figure 5-14 shows a histogram of the individual roll motion cycles during the whole seaway simulation. It is evident that occurrence number decreases for about 7.5% while also the roll amplitudes are in general decreased especially looking at the most extreme cases. This latter outcome provides a better resemblance to the realistic sea scenarios.

This kind of histogram representation can be utilized either for the whole irregular seaway simulation or for the individual roll motion cycles during the 1-hour simulation of a designated condition.

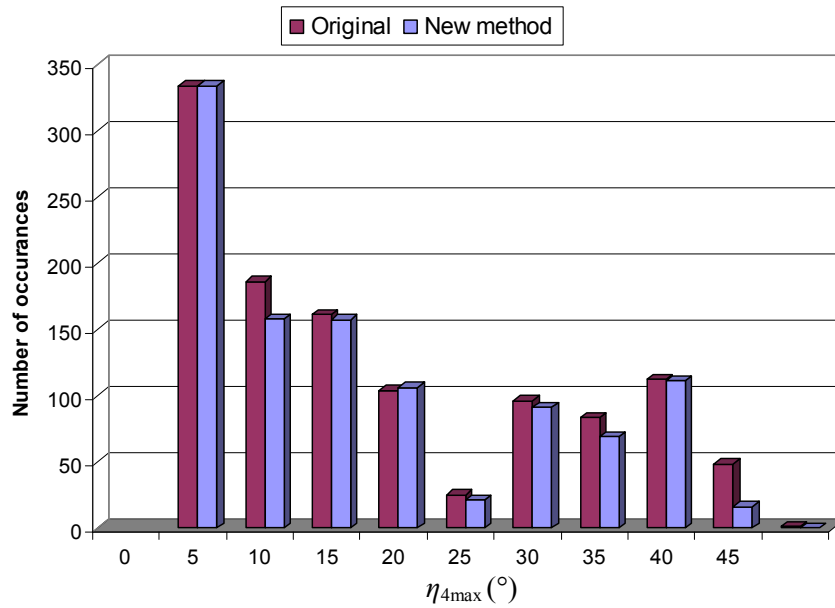


Figure 5-14. Comparison of number of occurrences from both original and modified methodology for all simulations

5.5 Graphical visualizations of the parametric rolling simulations

Following the theory presented and implemented within the incorporated numerical schemes, the parametric rolling survey in regular waves, already experimentally verified, is consolidated within graphical representations of simulations engaged. As mentioned above, those simulations are needed in conjunction with the polar diagrams as a written version of the operational guidelines for the Master to mitigate or avoid parametric rolling. Polar diagrams can be produced for different sea states and loading conditions.

In order for the simulations to be more plausible and visually more enhancing the 3D “Matlab simulink” program was created. The program constitutes of two subroutines, the first utilises the data gathering while the second enables 2D polar representation. A better visualisation is certainly possible but that is left to the experts.

The first set of polar plots of the results for regular waves case obtained from the new damping module integrated and utilized with the above proposed methodology is deliberately associated with the $\lambda/L_{pp} = 1$ typically pointed out as the condition that exerts most severe parametric rolling condition.

Based on the results that’s not entirely true with respect to peak roll amplitudes ($\lambda/L_{pp} = 0.8$ yielded highest amplitudes as confirmed by experiments) but it is based on the propensity towards parametric rolling as seen from figures 5-15 to 5-18.

The figures 5-15 to 5-18 present the 2D polar plots of the motions as a function of heading and speed, for a designated wave height. Note that red color tendency epitomizes the highest calculated amplitudes.

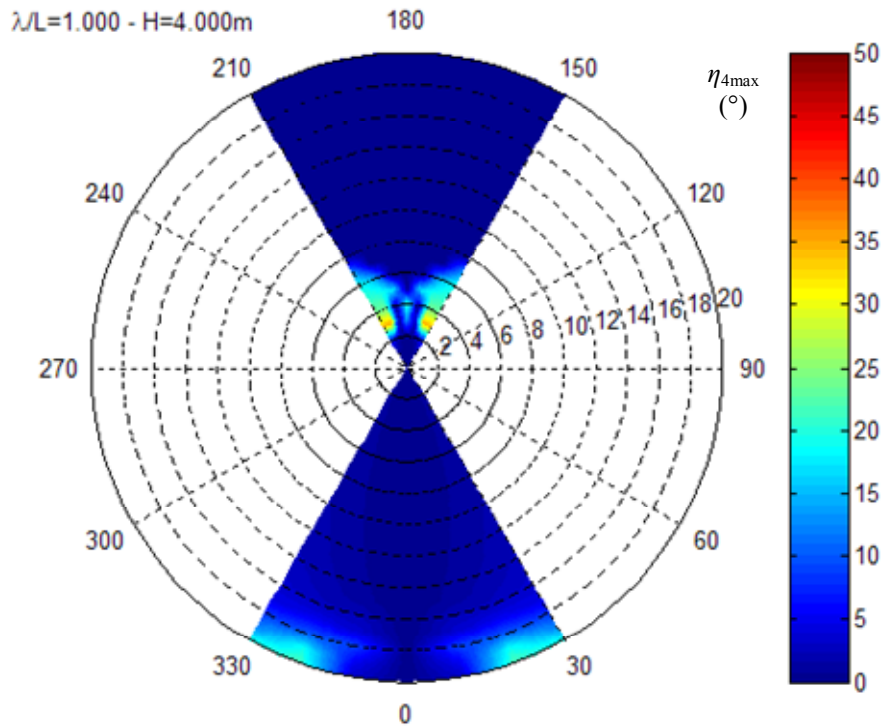


Figure 5-15. Numerical evidence with polar plots (GM1) of parametric rolling for ($H_w = 4$ m, $T_w = 12.95$ s).

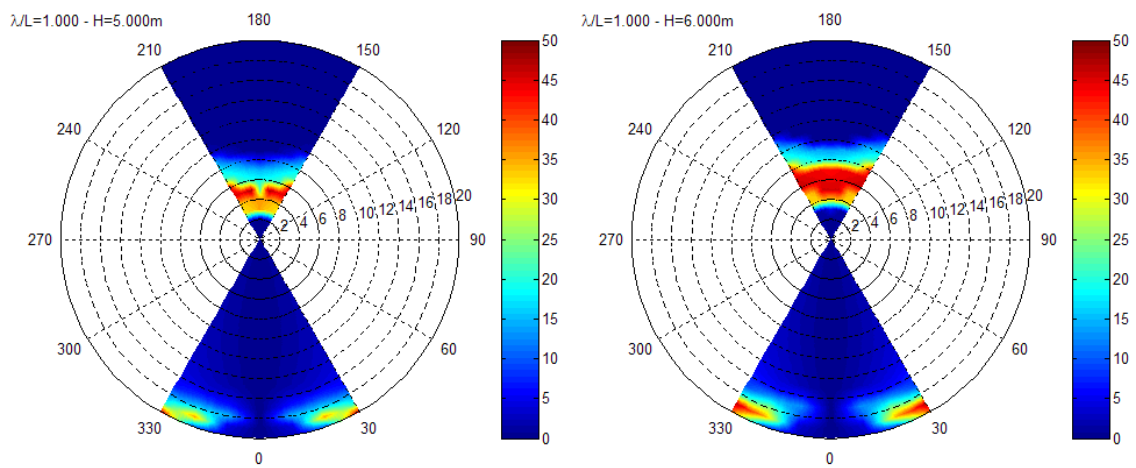


Figure 5-16. Numerical evidence with polar plots (GM1) of parametric rolling for ($H_w = 5 / 6$ m, $T_w = 12.95$ s).

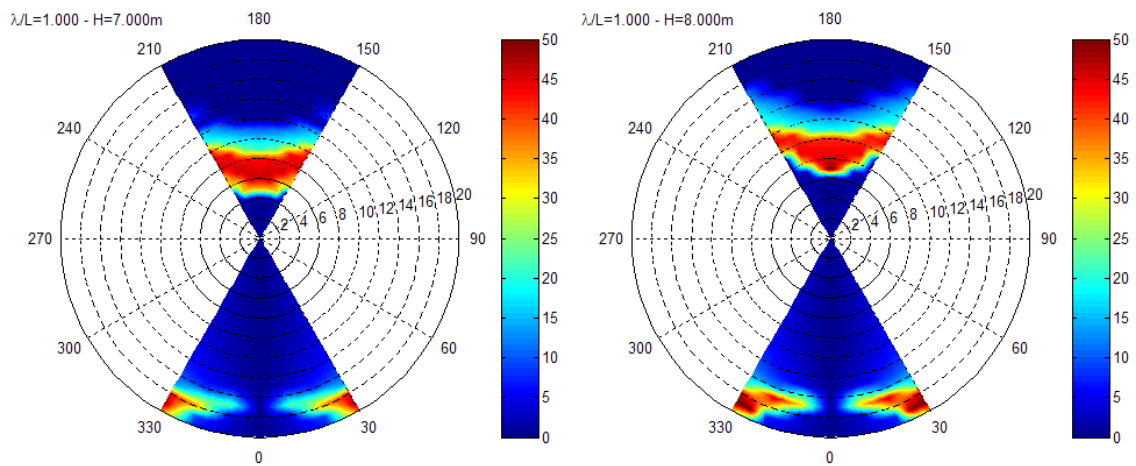


Figure 5-17. Numerical evidence with polar plots (GM1) of parametric rolling for ($H_w = 7 / 8$ m, $T_w = 12.95$ s).

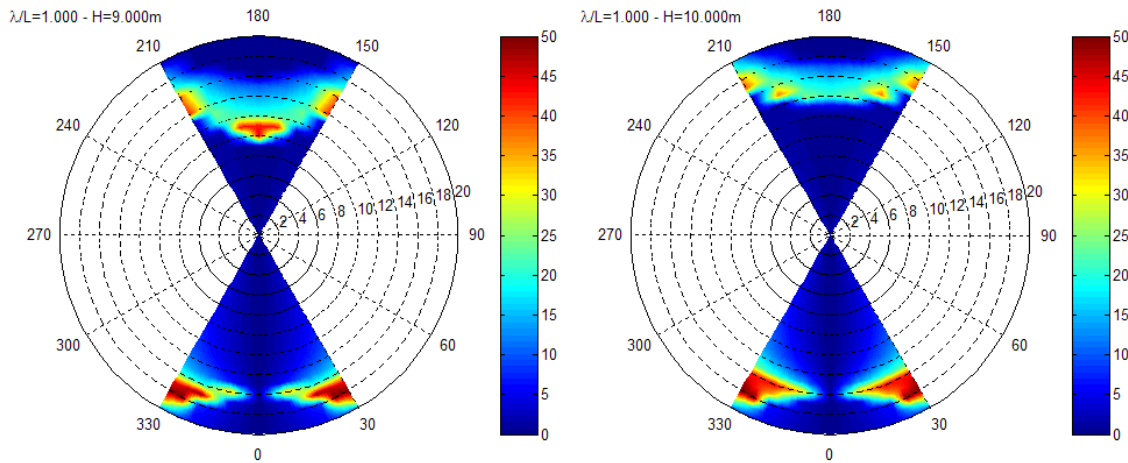


Figure 5-18. Numerical evidence with polar plots (GM1) of parametric rolling for ($H_W = 9/10$ m, $T_W = 12.95$ s).

Following the figure (5-19) summarize all the above presented as a 3D polar plot. A very intuitive outlook is enabled showing the full range of the parametric rolling realization. One can imagine the “cloud” inside this cylinder as a potential danger zone that should be avoided with appropriate ship handling. As one of the goals of the present study is to present an example of useful operational guidance by means of polar plots, extreme roll behavior is predicted for the above range of headings.

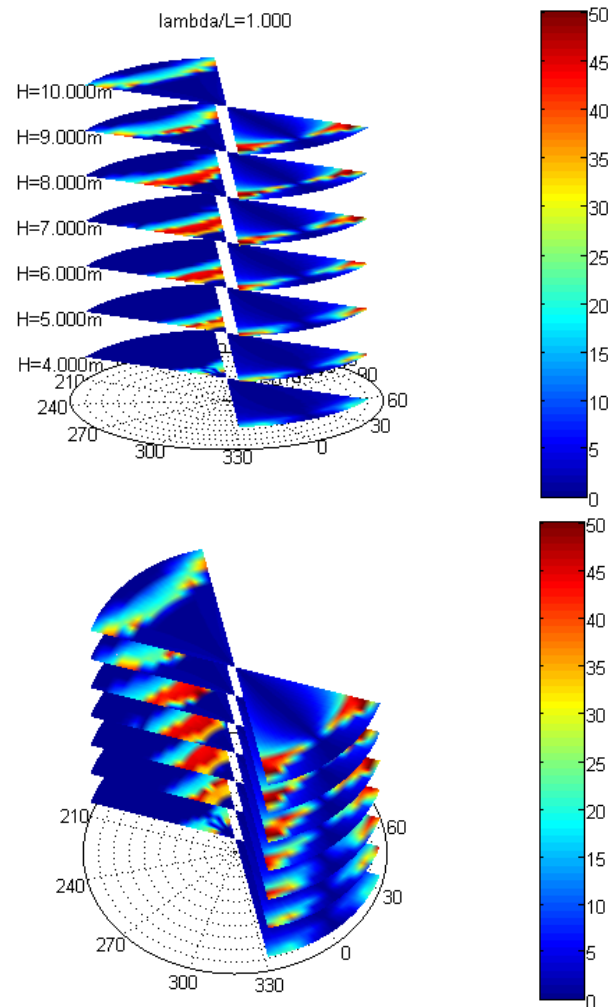


Figure 5-19. Numerical evidence with 3D polar plots (GM1) of parametric rolling with $T_W = 12.95$ s.

The next set of polar plots (fig. 5-20 to 5-22) represents the results obtained for the other wave frequencies.

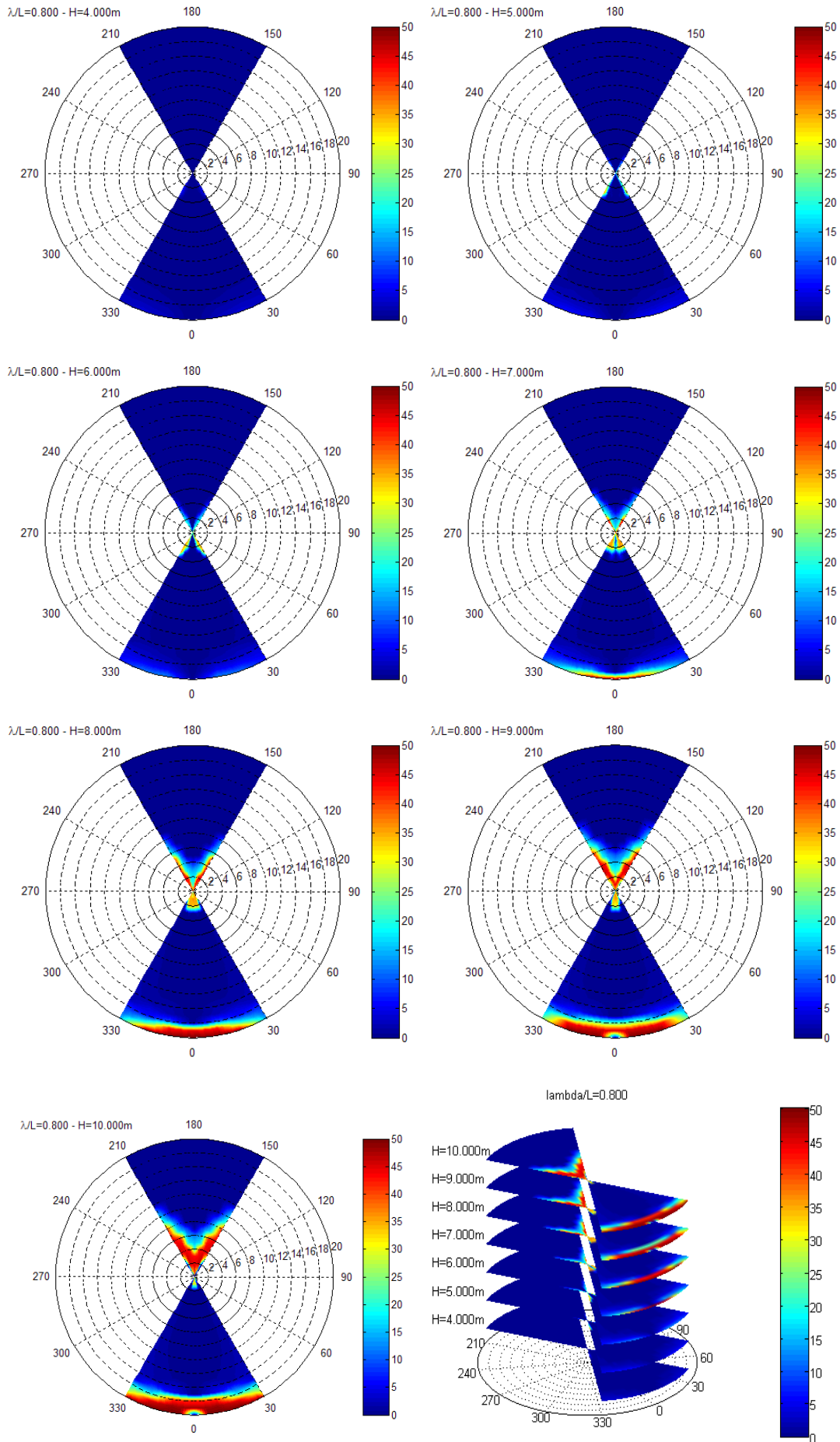


Figure 5-20. Numerical evidence with 2D and 3D polar plots (GM1) of parametric rolling with $T_W = 11.59$ s.

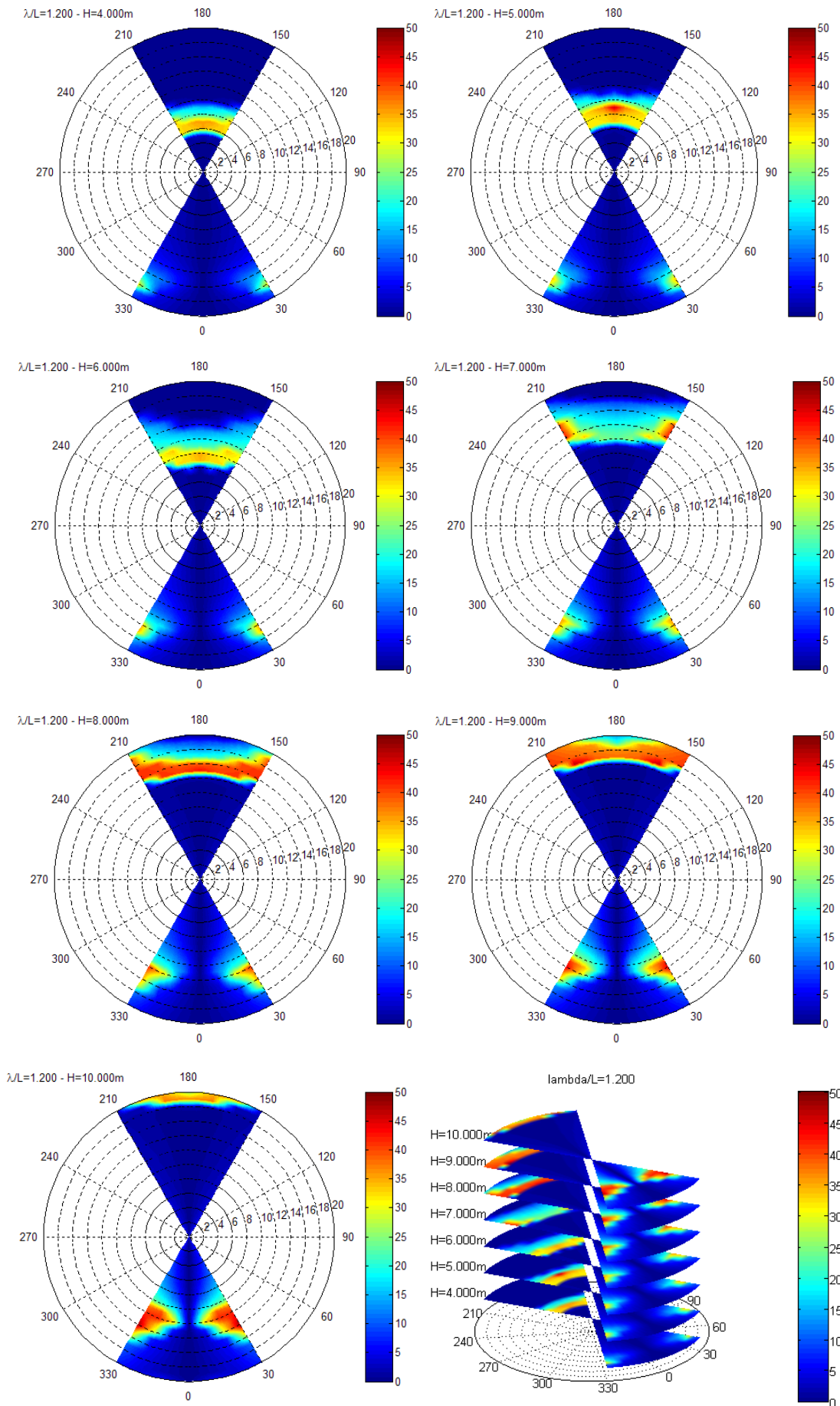


Figure 5-21. Numerical evidence with 2D and 3D polar plots (GM1) of parametric rolling with $T_W = 14.19$ s.

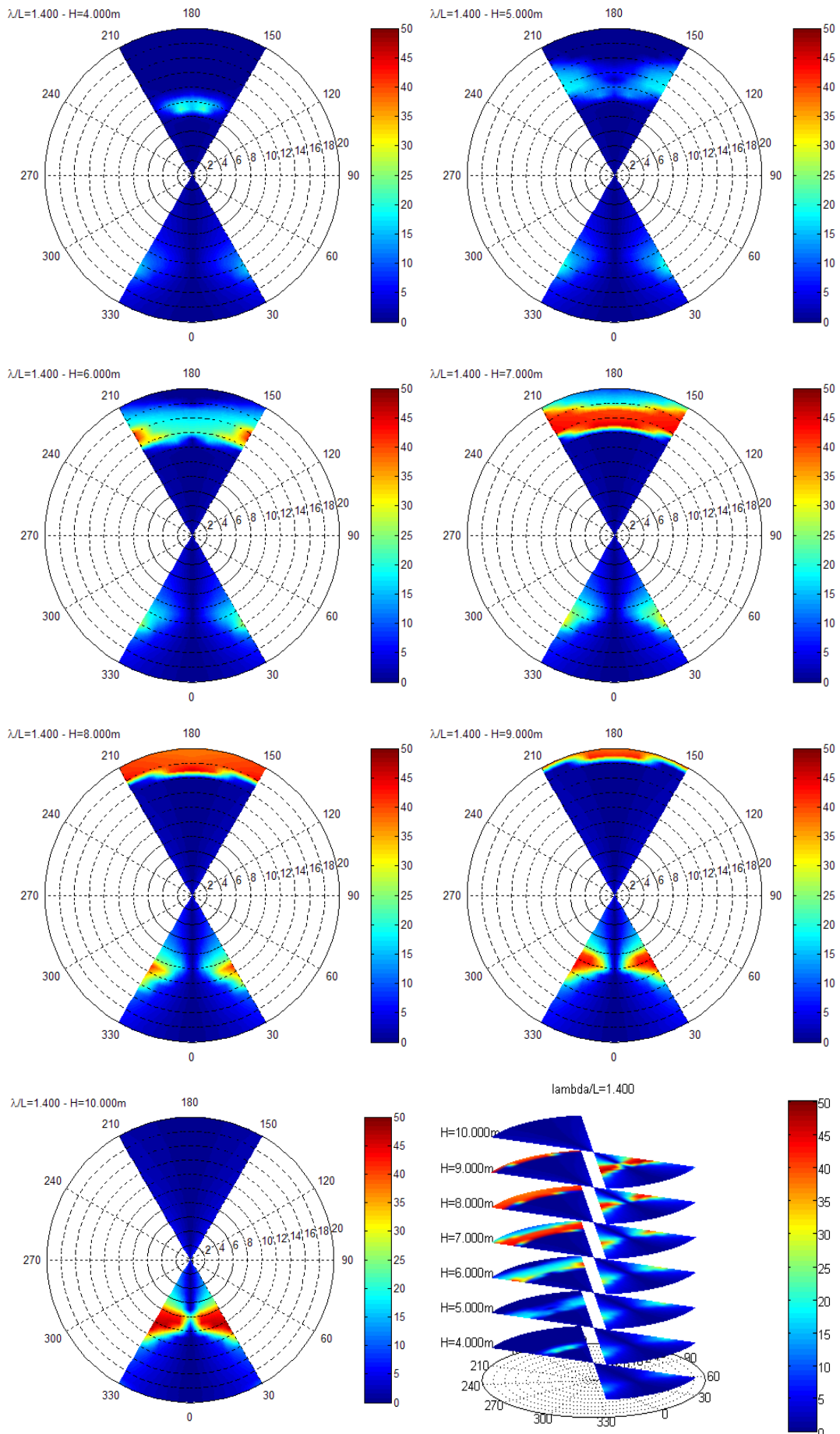


Figure 5-22. Numerical evidence with 2D and 3D polar plots (GM1) of parametric rolling with $T_W = 15.33$ s.

Aside from severe rolling in head seas, other significant results of the investigations were decreased roll response with smaller wave frequencies, but also with the greater vessel speed (in general). Taking into account the results obtained, translated into ship handling tactics, the vessel should have remained in beam seas during the storm or, if headed into the seas, should have increased speed to reduce rolling. All of these manoeuvres are contrary to normal heavy weather ship handling practice and counter-intuitive for masters. Furthermore, for the realistic operational guidance the simulations would have to be presented for all headings, what ever cause they originate from. It would not be wise to propose a change in heading to avoid one problem and encounter another one.

6 Experimental setup and program

6.1 Introduction

Following the procedural timeline, the first action that was taken after the first run of simulations were worked off and systemized as above, was the execution of the experiments conducted as a crucial part of this work. This represents relevant information. On one side it coincides with the effort to get the exact speed of the ship which will most likely cause parametric rolling for a given condition. That speed is in a way a “design speed” for parametric rolling and thus can be taken as a starting point for the model tests preparation that will be taking place. As already stated, it is imperative that before the experiment itself, such conditions are predicted in order to calibrate test instruments and devices, wave generation etc. for measuring the movements of the ship.

Also, the experiments are going to be debriefed here since they account to important validation for the tune up of the damping model via decay tests which will be presented in the next chapter.

In order to verify such capability, the criteria should be applied for the case when existence of parametric roll is certain, such as conditions from (France, et al., 2003). One such case involving the C11-class container carrier at a speed of 10 knots in a wave height of 8.4 m and a wave circular frequency of 0.44 rad/s was successfully reproduced in (Belenky, et al., 2003). Although the pointed range of speeds for head waves could be anywhere in range of 7-11 knots the experimental validation of the proposed methodology and the software’s developed for the case of regular head waves will be executed for the ship velocity of 8 knots. Similarly the following wave’s scenario is going to be tested for 0 knots. Given the explanations above it is time to move on describing the experimental setup.

As a part of a HydraLab III project there is an ongoing experimental investigation that took place in CEHIPAR (Canal de Experiencias Hidrodinámicas del Pardo), Spain where the above presented numerical results can be evaluated and verified. The tank has a length of 150 meters, width of 30 meters, and a depth of 5 m and is equipped with a flap type wave maker and an overhead towing carriage (figure 6-1). The wave maker is located in one of the 30 m sides. Its 60 flaps with independent motion, together with the use of wall reflection allows the generation of all types of waves with a good quality and inside a wide useful area.

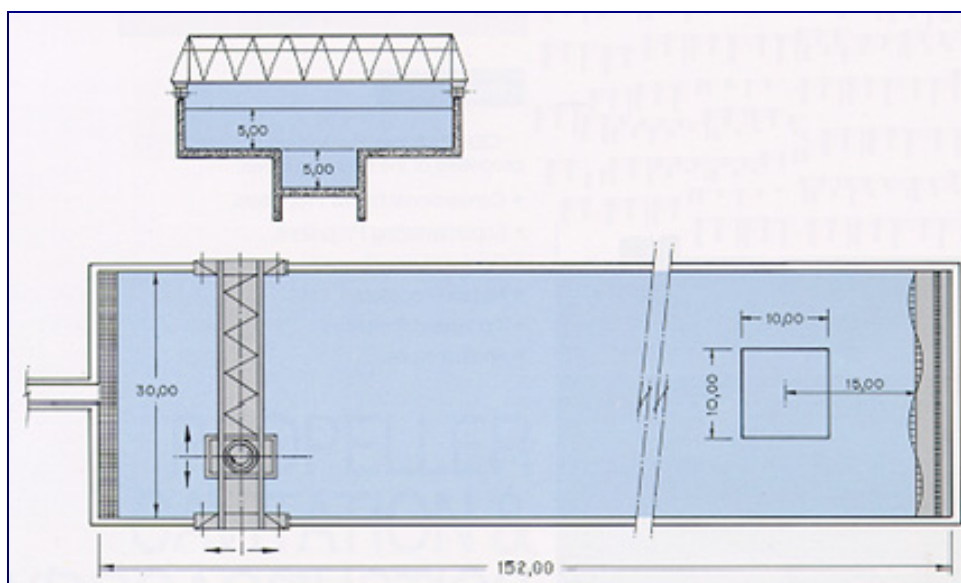


Figure 6-1. Basin with wave maker and CPMC (Computerized Planar Motion Carriage)

The set-up for the experimental analysis started with the so called “design speed” for parametric rolling. The preliminary work conducted in the basin included building the model, wave

calibrations, free roll decay tests, forced oscillation tests before all other tests associated with parametric rolling investigation. The whole experimental setup is going to be presented in brief.

This experimental research programme aims to gather reliable data on parametric rolling hydrodynamic characteristics to be compared with the corresponding numerical results obtained from the modified strip theory model. This extensive experimental programme has been divided in 4 main groups of tests:

1. Free heave, roll and pitch tests in both regular and irregular waves;
2. Captive tests in waves;
3. Forced oscillation tests;
4. Roll decay tests in both calm water and waves.

This work focuses on items 1 and 4. As already debriefed the question that was asked for the experiments that are described later is whether a good correlation in experimental and computational results for the heave, roll and pitch hydrodynamic coefficients (added mass and damping) calculated using the strip theory will be obtained. In respect to the planning of activities, attention has been paid to keep the time allocated to a maximum of 16 runs per day including all activities.

As shown, this strip theory approach is capable of reproducing parametric rolling and thus to be applied employing different techniques for the frequency domain analysis. However, nonlinear simulations are strongly conditioned by the evaluation in the frequency domain of linear radiation and diffraction forces and errors in these calculations could affect the correct assessment of nonlinear effects. So the question to be answered by the other group of project participants is whether under parametric rolling conditions good correlation can be obtained between experimental and computed values of heave and pitch hydrodynamic coefficients (added mass, and damping) using the strip theory calculation method. As stated, these hydrodynamic coefficients were already tested within previous projects under the tutorship of Prof. Guedes Soares and as such are considered adequate. However, by means of the forced oscillation tests of a segmented model (figure 6-2) it is expected to gather more sufficient and reliable hydrodynamic data to answer the question above.

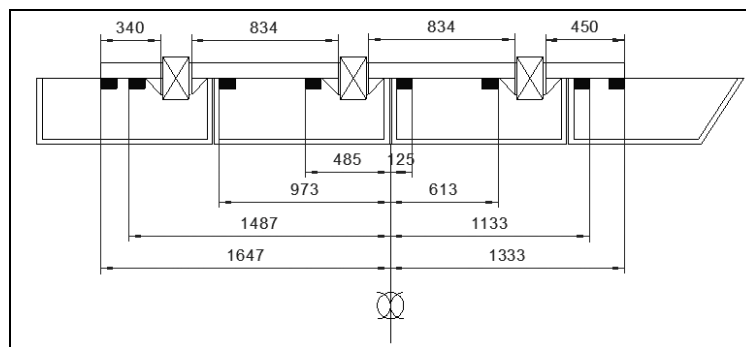


Figure 6-2. The graphical representation of the model, distances are in millimetres

It is especially aimed at asymmetric sections, therefore to obtain the roll restoring moment captive model tests were conducted at two different speeds and 3 different heeled positions (0° , 5° and 10°). Likewise, the second group of activities, forced oscillation tests, were conducted for the same heel angles as well. The tests consisted of forcing the model to execute harmonic pitch and heave motions while being towed along the tank at several speeds and above indicated heeled positions. The main objective is said to be obtaining the data on radiation forces for the validation of the numerical program that is under development to predict and adequately simulate parametric rolling (Ribeiro e Silva et al. 2010.). In this group of activities, tests were carried out for the vessel seen on figure 6-3, in various decay and wave encounter conditions.



Figure 6-3. Experimental setup for the parametric rolling tests

6.2 Roll decay experiments in both calm water and waves

The mechanism consists of two, three or more infrared cameras that observe the movements of a series of diodes (LED's) mounted on the model. The roll damping coefficient can be determined by the difference in the two adjacent wave peaks (or valleys) of the free roll oscillation (with a finite initial departing angle) in calm water.

The tests conducted in Cehipar can be divided into two main groups:

- a) decay tests in calm water,
- b) decay tests in waves;

A systematic presentation of the decay test is shown in table 6-1,

N°	GM	Wave N°	SHIP				MODEL			Heading (°)	File
			H (m)	T (s)	V (kn)	V (m/s)	Hs (m)	Tp (s)	V (m/s)		
1	1				0.0	0.00	0.000	0.00	0.00	180	DECAY_TEST_GM1_V=0kts DECAY_TEST_GM1_V=7.97kts
2	1				8.0	4.10	0.000	0.00	0.51	180	
3	1	3	8	12.95	0.0	0.00	0.123	1.61	0.00	180	
4	1	3	8	12.95	7.8	4.00	0.123	1.61	0.50	180	
468	1	11	4	11.59	8.0	4.10	0.062	1.44	0.51	180	
469	1	12	4	12.95	8.0	4.10	0.062	1.61	0.51	180	
470	1	13	4	14.90	8.0	4.10	0.062	1.85	0.51	180	
471	1	14	4	15.33	8.0	4.10	0.062	1.90	0.51	180	
302	2				0.0	0.00	0.000	0.00	0.00	0	TESTS302-305
303	2				3.9	2.00	0.000	0.00	0.25	0	
304	2				8.0	4.10	0.000	0.00	0.51	0	
305	2				11.7	6.00	0.000	0.00	0.74	0	
306	2				15.6	8.00	0.000	0.00	0.99	0	
307	2				19.4	10.00	0.000	0.00	1.24	0	
308	2	13	4	14.90	0.0	0.00	0.062	1.85	0.00	0	
472	2	11	4	11.59	1.9	1.00	0.062	1.44	0.12	0	
473	2	12	4	12.95	3.9	2.00	0.062	1.61	0.25	0	TESTS473
474	2	14	4	15.33	5.8	3.00	0.062	1.90	0.37	0	TEST474

Table 6-1. Summary of the decay tests conducted (provided by Cehipar)

Both will be analysed and applied within the research of validating 6 DOF numerical model and propensity to parametric rolling. By comparing this experimental result with numerical results with roll damping estimated from roll decay model test and the Ikeda's prediction method, the influence of roll damping estimation methods on parametric roll prediction was examined.

As already said, the energy dissipation associated to wave radiation represents a minor part of the overall damping especially at large rolling amplitude. Hence friction and eddy making are the two most important components to be considered in case of roll at zero speed. Both frictional effects and eddy making dissipation are associated to the water's viscosity (wave making damping, on the other hand, can be captured by the potential flow modelling). Experiments are carried out under "Froude similarity law" and, as a consequence, "Reynolds similarity law" is not fulfilled: this means that

possible scale effects could be present if the model is too small, i.e. if the Reynolds number at model scale is too small compared to the full scale Reynolds number. According to (Francescutto 2002, Hutchison 1991) the eddy making component of damping is expected not to be affected by (significant) scale effects. On the other hand, again referring to same and with also Journée (2001) the frictional component of roll damping could be significantly affected by scale effects. Unfortunately (from the safety point of view) the model scale frictional damping, when transformed to full scale under Froude similarity, is expected to be larger than the actual frictional damping at full scale (this is almost exactly the same phenomenon occurring in standard calm water resistance tests concerning the frictional component of the ship's resistance). On the other hand the fortunate aspect of the problem is that usually the frictional damping contribution to the overall damping moment is significant only for small rolling angles, whereas the almost-scale-effects-free eddy making damping becomes dominant at large rolling angles.

The first group of experiments consisted of the decay tests in calm water by varying model speed. The analysis of free roll decays represents the easiest means (though not necessarily an easy one) to obtain suitable mathematical models representing energy dissipation for the roll degree of freedom. Results from roll decay analysis are used to predict the ship rolling amplitude when tests in regular waves at the required wave steepness cannot be carried out due to limitations in the maximum generable wave height in the towing tank.

Two approaches of analysing decay tests will be presented together with results using modified Ikeda's method. The problem in assessing correct values for the damping coefficient using standard procedure with the linear plus quadratic model can be summarized within two prerequisite actions. One is the problem of fitting the time series using certain averaging techniques because the signal is scrambled. The other comes from the fact that the signal, although theoretically averaged to zero in reality possesses certain deviation. To correct this non mean zero a Roberts (1982) procedure was employed which will be explained in brief.

Therefore, before starting with the roll extinction analysis data must be preprocessed by smoothing the output and reducing data to zero mean. This action is not always mandatory but it is required when the input signal is affected by non-zero mean and high noise frequencies. After this first part of the analysis, that mostly involves subjective / qualitative judgments, it is possible to make a step forward by post-processing the scatter plots from the decrement analysis by means of suitable parametric models in order to obtain numerical estimates of the coefficients of the model especially for the damping function. Finally, a systematic comparison of linear / nonlinear damping coefficients, as well as a systematic comparison of the equivalent linear damping at different amplitudes can be used to disclose possible trends associated to speed effects.

6.2.1 First group of decay tests

6.2.1.1 Signal filtering technique

Before running these types of data analysis from decay tests certain filtering techniques have to be considered. Random noise can greatly affect the result of certain types of analysis. Two important examples are: quantification of peaks in the signal (noise can shift the location of the peak, and leads to systematic overestimation of the height of the peak), and differentiation (noise is amplified by differentiation). Since random (or 'white') noise is distributed over all frequencies, and signal is typically limited to low frequencies, a reduction of high frequency components will improve the signal/noise ratio.

The most common mean of the averaging technique use is done by Butterworth filter design as a class of IIR (Recursive) Filters. The Matlab code utilised was provided by the CENTEC and the first approximations were conducted using the n^{th} order Butterworth low-pass filter with what looked like sufficient accuracies. Recursive filters, whose output at a given time depends both on the current

and previous inputs and on previous outputs, can generally have performance that is superior to nonrecursive filters with the same total number of coefficients. Low-pass filtering is another term for the smoothing as an operation which removes high-frequency fluctuations from a signal.

Function $[b,a] = \text{butter}(n, \omega_n)$ designs an order n lowpass digital Butterworth filter with normalized cutoff frequency ω_n . It returns the filter coefficients in length $n + 1$ row vectors b and a . Recursive digital filters always have a time lag between input and output. Solution for the time lag problem is to filter twice, second time in reverse direction, but its not necessary. Digital filters require constant sampling interval which may be a problem, and lastly it is not (yet) clear to me how the Matlab implementation deals with boundary conditions. In the Matlab libraries it is stated that for higher order filters, numerical problems due to roundoff errors may occur when forming the transfer function using the $[b,a]$ syntax.

Upon consulting an expert in signal processing alternative implementation of filtering is deployed using Matlab code, namely frequency sampling-based finite impulse response filter design (fir2 nonrecursive filter). A filter is usually specified in terms of its frequency response. The commonest requirement is that the filter should pass frequency components of the input signal lying within a certain band (the passband), and stop, or at least attenuate, components within the stopband(s). The filter type which can be designed by the applet is a low pass filter, where the passband extends from zero frequency to some chosen "cutoff" value. The applet uses the window or Fourier transform method. The filter order primarily determines the width of the transition band: the higher the order, the narrower is the transition between the passband and stopband, giving a sharper cutoff in the frequency response.

A drawback for the filter obtained by this technique is the non-causality. A "non-causal" filter is one which requires not only the current and previous input values ($x_n, x_{n-1}, x_{n-2}, x_{n-3}, \dots$) but also future input values ($x_{n+1}, x_{n+2}, x_{n+3}, \dots$). Non-causal filters can be used where a complete record of the sampled input signal is available which holds true in our case and makes it more compelling. The filter coefficients are obtained by applying an inverse fast Fourier transform to the grid and multiplying by Hamming window function. The key idea, in other words, is to iterate between the space of coefficients and the space of functions $H(f)$, until a Fourier conjugate pair that satisfies the imposed constraints in both spaces is found.

Filter $h = \text{fir2}(n = 50, f, m)$ returns row vector h containing the $n+1$ coefficients of an order n FIR filter. In this case designs a 50th-order lowpass filter and overplots the desired frequency response with the actual frequency response using convolution. The frequency-magnitude characteristics (figures 6-4 and 6-5) of this filter match those given by vectors $f = [0 \text{ Fg } \text{Fg} \ 1]$ and m , where f is a vector of frequency points in the range from 0 to 1 and Fg defines upper boundary frequency of the low-pass filter. The first point of f must be 0 and the last point 1. The frequency points must be in increasing order. The m is a vector containing the desired magnitude response at the points specified in f . An example is shown on the following figures expressed as the frequency response of a digital filter that can be interpreted as the transfer function evaluated at $z = e^{j\omega}$. You can always write a rational transfer function returned as a complex frequency response $H(e^{j\omega})$ of a digital filter.

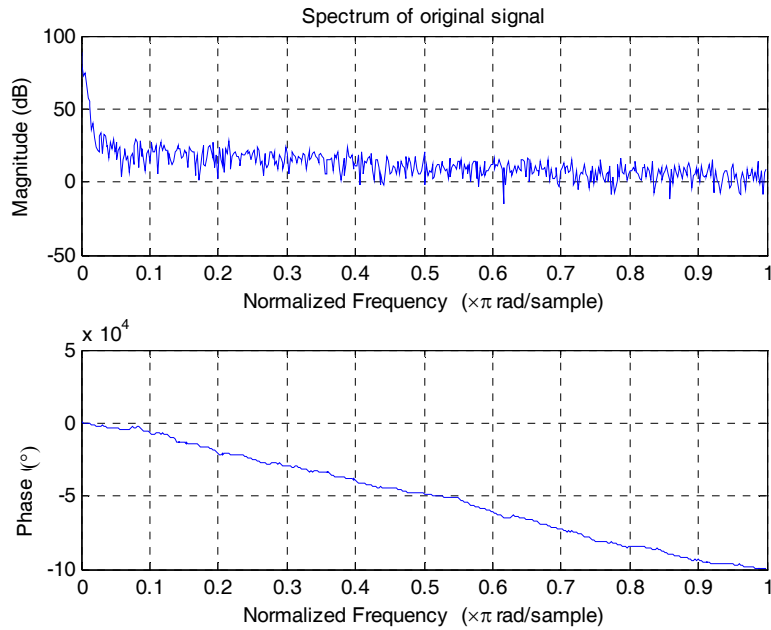


Figure 6-4. Spectrum of the original and filtered signals

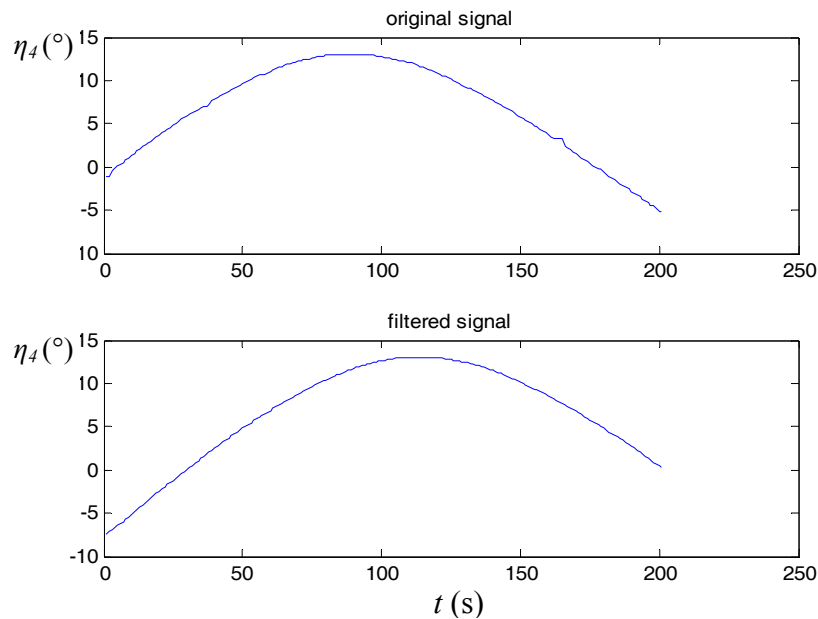


Figure 6-5. Roll amplitude response with both the original and filtered signals

This is typically an interactive trial and error process. Recursive filters (“butterworth”), feeding as they do on their own output, is not necessarily stable. If the coefficients are badly chosen, a recursive filter can have exponentially growing, so-called homogeneous, modes, which become huge even after the input sequence has been turned off. This is not good. The problem of designing recursive filters, therefore, is not just an inverse problem; it is an inverse problem with an additional stability constraint. The goodness of a filter is best based on visual inspection of the results. Also note that it depends on the subsequent steps in the analysis too. For instance, a good filter for peak detection may be one which reduces noise to 1% of the signal. The same filter may not be good for differentiation, because the noise in the derivative is still too high. Filters for differentiation typically need a lower cut-off frequency. An example of TEST302 is given in figure 6-6 along with the close up on figure 6-7. Tests 302 to 307 are conducted in calm waters heading 0° by varying speed from 0 kts to 20 kts.

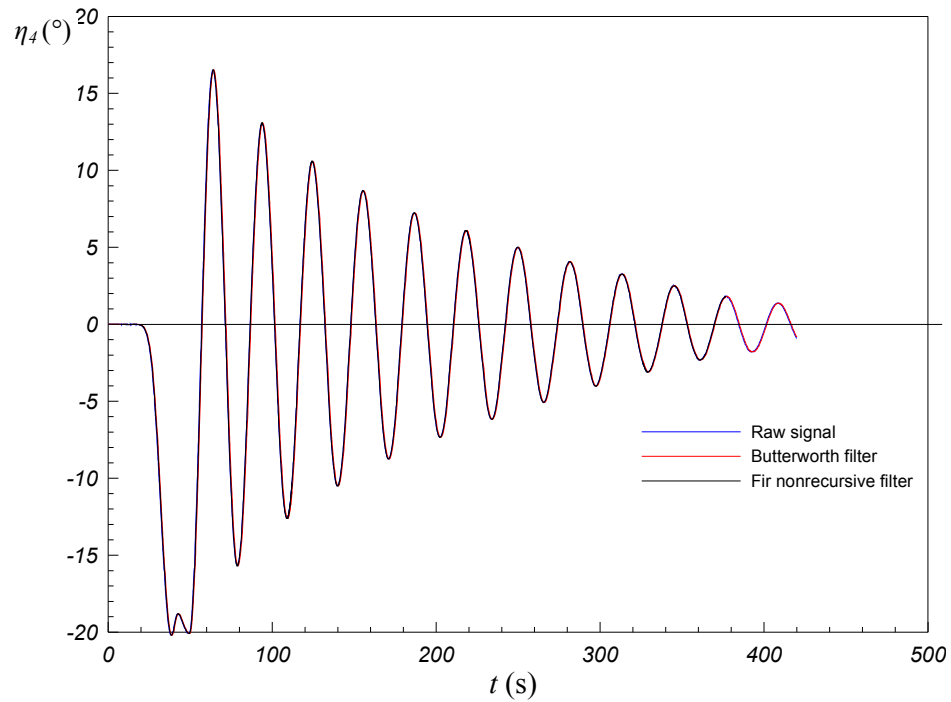


Figure 6-6. Filtering of TEST 302

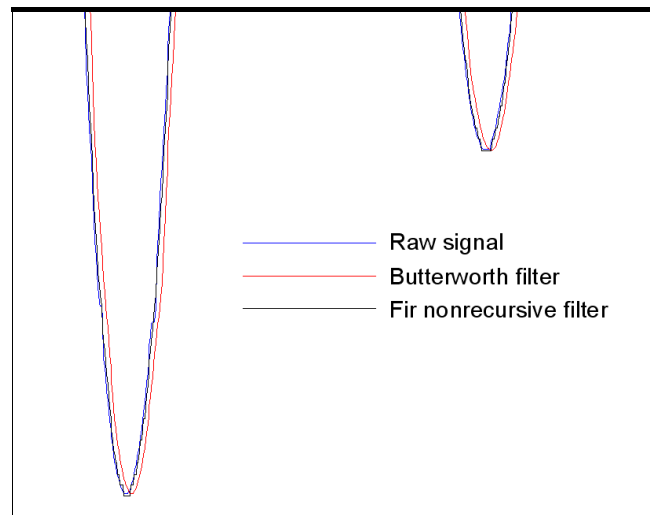


Figure 6-7. Close-up of TEST 302 filtering

The butterworth method is good at getting the general shape of the desired filter, and good where “flatness” is a desired goal. However, the nonlinear mapping between ω and f makes it difficult to design to a desired shape for a cut-off, and may move cut-off frequencies from their desired places. Since the flat regions of the signal present less important information the non-recursive filter looks better around peak values of the signal which proved to be valuable when evaluating damping coefficient using linear plus quadratic model.

6.2.1.2 Roberts non- zero mean correction

The second issue detected in the processing of the decay tests is the existence of non zero mean. As already mentioned the Roberts procedure (1982) is implemented. Some pre-processing of the data is necessary to remove a small very low frequency component or mean drift which is introduced by the roll measuring device mounted in the model. The drift was removed by first fitting separate polynomials through the positive and negative peaks as illustrated on figure 6-8a. From the positive peak fit, estimates $\hat{b}_j (j = 1, 2, \dots)$ were obtained of the magnitudes of the intermediate

negative peaks. Similarly, from the negative peaks polynomial estimates $\hat{a}_j (j = 1, 2...)$ were found for the magnitudes of the intermediate positive peaks. The j -th positive peak a_j was then corrected by forming the average of a_j and \hat{a}_j , that is,

$$a_j(\text{avg}) = \frac{a_j + \hat{a}_j}{2} \tag{5-80}$$

Using the same analogy the negative peak values were also corrected. The effect of this correction is illustrated by fig 6-8b.

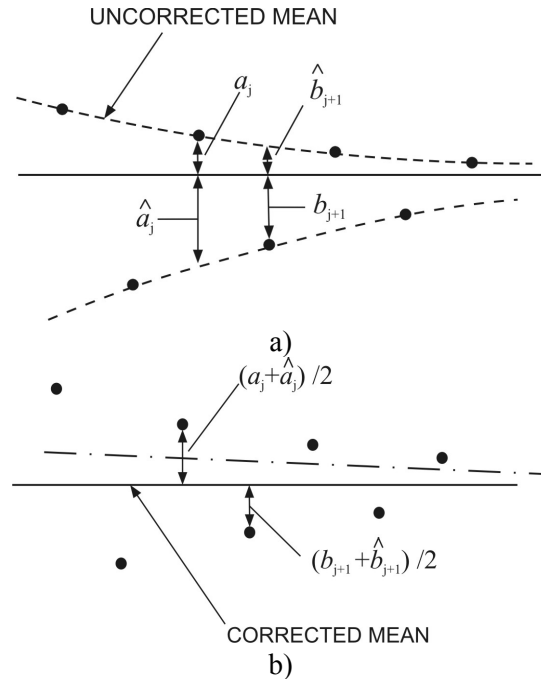


Figure 6-8. Drift removal a) polynomial fitting to positive and negative peaks b) corrected peak values

Using the methodology provided, an example is shown (TEST302 → calm water decay test without advance speed). On figure 6-9a the original positive and negative peaks data (table 6-2) is presented along with calculated polynomial fits, respectively.

Time(s)	ORIGINAL PEAKS FILE		MODIFIED PEAKS FILE	
	η_4 (°)	Abs(η_4) (°)	Abs(η_4) (°)	η_4 (°)
64	16.50	16.50	17.50	17.50
79	-15.70	15.70	-15.10	15.10
94	13.10	13.10	13.50	13.50
109	-12.60	12.60	-12.20	12.20
125	10.60	10.60	11.00	11.00
140	-10.50	10.50	-10.00	10.00
156	8.68	8.68	9.12	9.12
171	-8.74	8.74	-8.33	8.33
187	7.24	7.24	7.62	7.62
203	-7.33	7.33	-6.99	6.99
218	6.08	6.08	6.40	6.40
234	-6.17	6.17	-5.85	5.85
250	5.00	5.00	5.31	5.31
266	-5.07	5.07	-4.79	4.79
282	4.07	4.07	4.30	4.30
298	-4.01	4.01	-3.83	3.83
314	3.25	3.25	3.39	3.39
329	-3.09	3.09	-2.98	2.98
345	2.51	2.51	2.59	2.59
362	-2.32	2.32	-2.37	2.37

Table 6-2. Summary of the decay tests conducted

As seen from figure 6-9b, when plotting the absolute values of negative peaks, it clearly does not follow the path of the positive fitted peaks, actually being higher. This is the evidence of mean drift which can produce a substantial error when calculating damping coefficients.

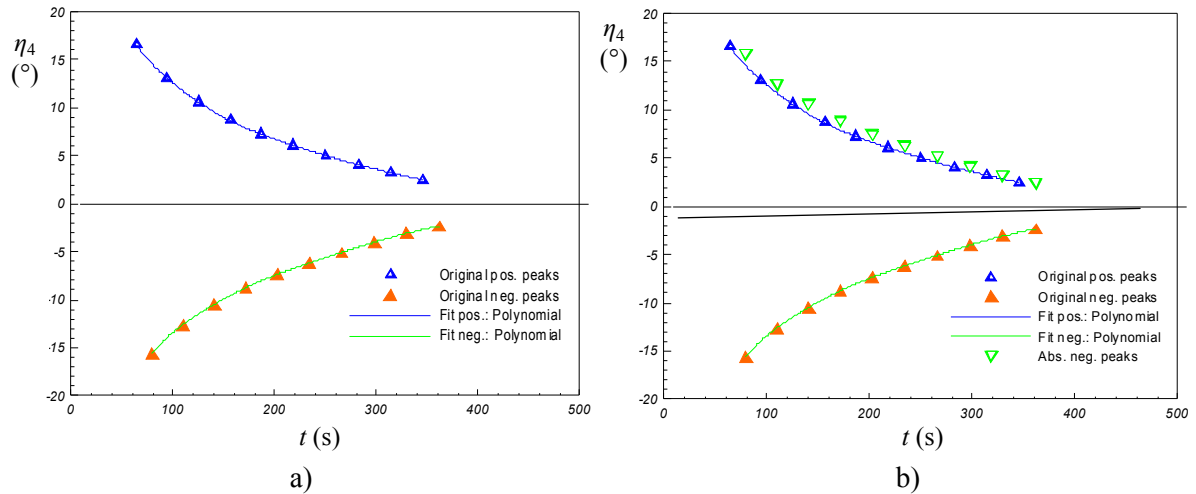


Figure 6-9. Application of drift removal procedure for TEST302

Theoretically, the right zero mean is closer to the negative peaks but not simply vertically translated. In reality however, it follows the slightly oblique line given in figure 6-9b. The comparison of the corrected data cross-referenced to the original data is presented in figure 6-10. Finally, plotting the absolute values of negative modified peaks clearly shows an inlinement with the positive peaks and thus the removal of a small very low frequency component or so called mean drift. This procedure has to be undertaken for all decay tests conducted as a part of this study.

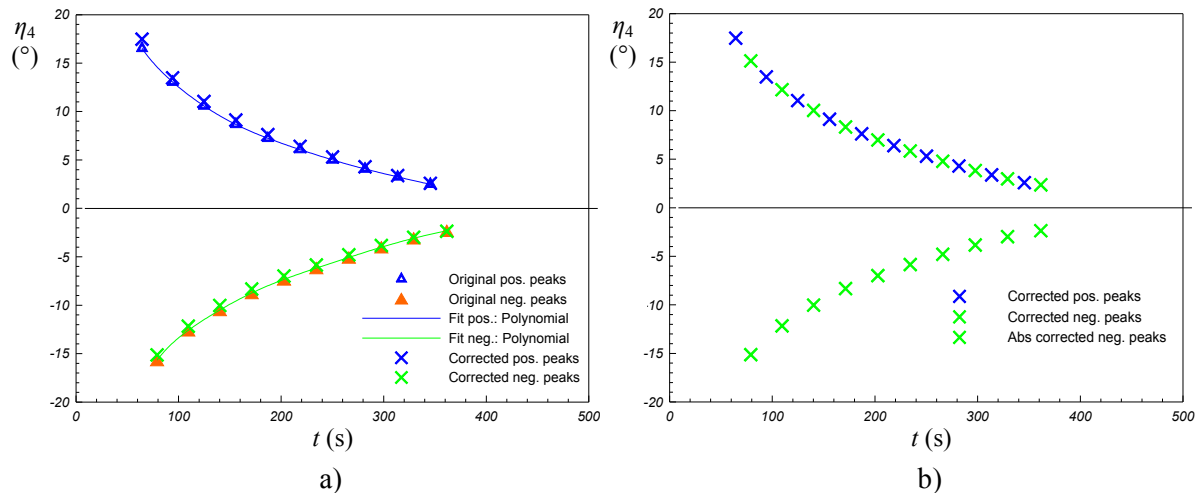


Figure 6-10. Results of the drift removal procedure for TEST302

6.2.2 Second group of decay tests with different loading condition

The second group of tests consisted on two decrement tests in calm waters, nominally at heading of 180°. Since there are no waves, in reality it makes no difference. The two tests were conducted for speeds of 0 and 8 knots, respectively. The difference however is a loading condition, this time ballast condition with GM1 = 0.993 m. Since the parametric rolling test performed, were associated with the conditions of the previous decay tests, what actually can be identified as main part of the interest is the relative ratio of the equivalent damping corresponding to the each loading conditions. What makes those tests unique is the fact that they were repeated, albeit with the different initial inclination. Figure 6-11 shows the comparison between raw and filtered signals. Note that filtered signals are coming with a time delay.

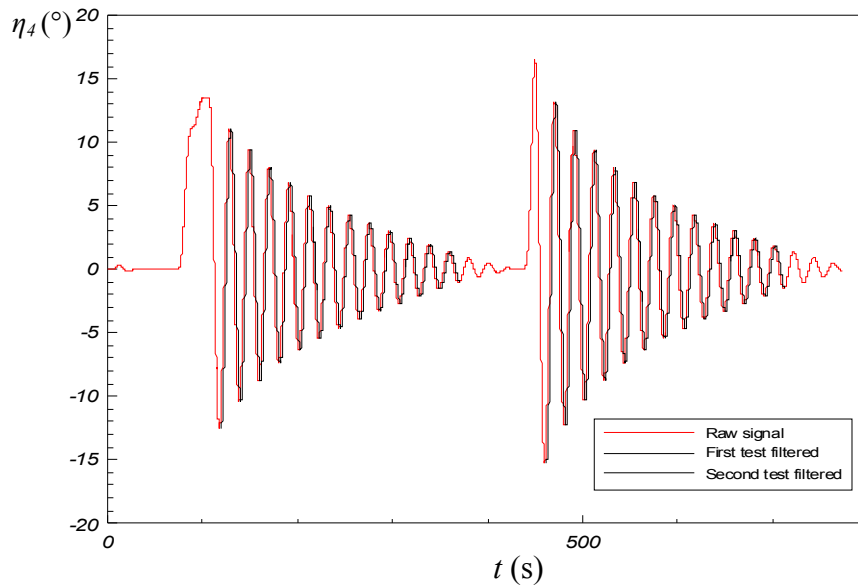


Figure 6-11. Time trace of decay test for 0 knots with filtering

Slightly different approach is utilized by not implementing Roberts’s procedure. As seen from the figures dispersion around mean values for both tests appears to be not significant (figures 6-12 and 6-13).

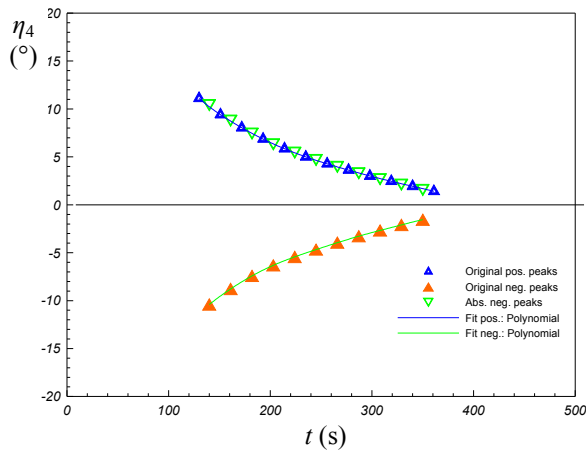


Figure 6-12. Checking of drift removal procedure for 0 knots (1 run)

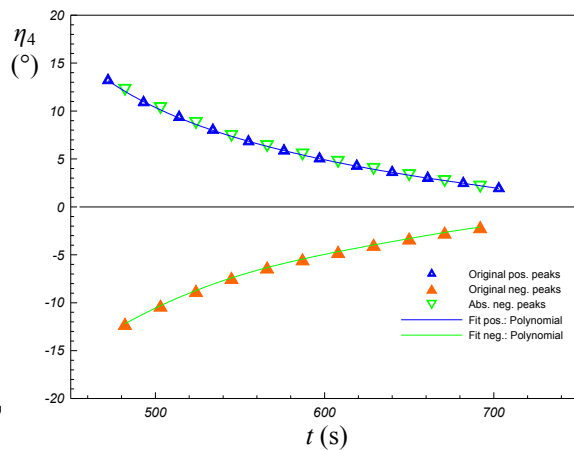


Figure 6-13. Checking of drift removal procedure for 0 knots (2 run)

6.2.3 Third group of decay tests in waves

The final group of roll decrement tests was conducted in waves. Utilizing a "classical" way of analyzing roll decay curves by means of the so called decrement curve was in vain from the start. Analyzing decay tests in calm water is considered as the easiest mean (though certainly not an easy one) to obtain suitable mathematical models representing energy dissipation for the roll degree of freedom. While it was found challenging to tackle those tests an attempt to use a method of this type for the waves proved rather cumbersome. The problem in waves is that a mathematical model of 1-DOF cannot suitably represent coupling between the motions that occurs as evident from the readings illustrated for the TEST 470 on figure 6-14.

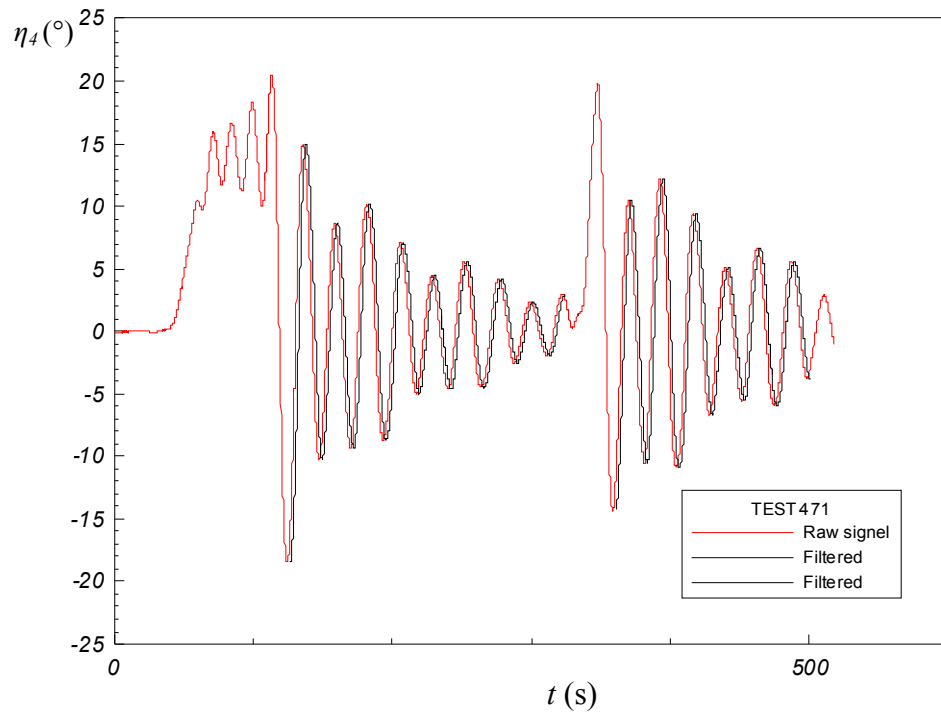


Figure 6-14. Decay test 470 with filtering

For the rest of the tests it's impossible to get the damping (tests: 308, 469, 472B, 473, 473B and 474) since there are no evident behavior of damping as seen from figure 6-15.

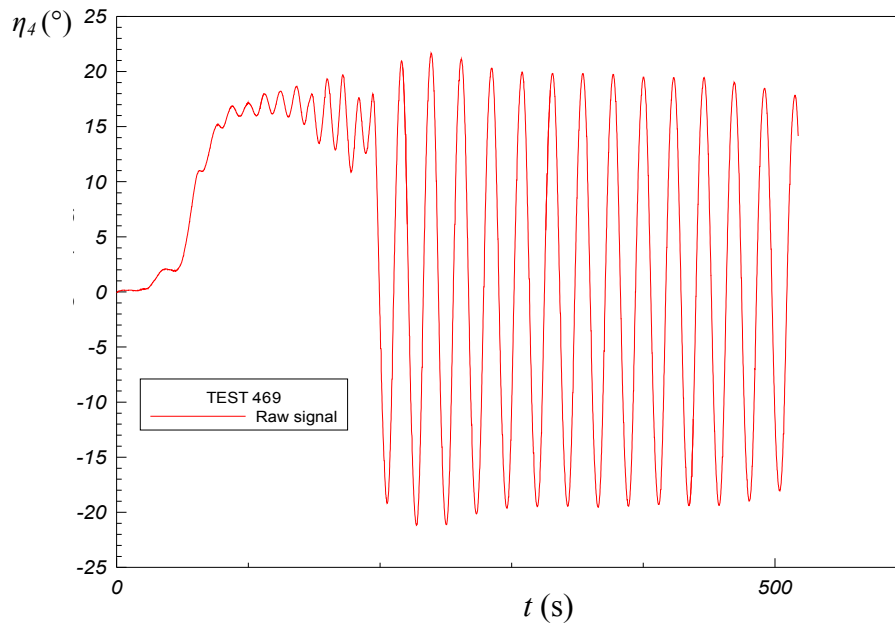


Figure 6-15. No damping for decay test 469

After subsequent analysis it was established that although these tests were originally designated as the decay tests the conditions upon which they are performed correspond to the parametric rolling condition, for instance TEST 469 on table 6-3.

N°	GM	Wave N°	H (m)	T (s)	V (kn)	V (m/s)
469	1	12	4	12.95	8.0	4.10

Table 6-3. Particulars of decay test 469

What is being considered is exactly the steady state realization of the parametric rolling since the ship is already inclined and released from the perceptible angle. Therefore, adequate signals that correspond to the parametric rolling condition (with the transient phase) and the one from the decay tests (sans transient state) can be assimilated. What is evident from this examination is actually the quintessence of this research.

The damping parameter that essentially dictates the amplitude of rolling is impossible to trace without any rate of decay possible to identify and to retrieve. It can be referred to as a “resonant damping” which is further proof of the difficulty in assessing it correctly. In an oscillating system such as this, as damping increases, the amplitude of the system at the resonance frequency decrease and the resonance frequency also decreases. The damping is, to put it simpler, derived from internal friction; a damped oscillator moves slower than an undamped one. If the oscillator travels slower, it takes longer time to complete an oscillation.

Looking back at the basics, if ω_0 is taken to be a constant then ω_d is seen to be a decreasing function of the damping coefficient B_{44} . The mechanical response for an oscillator is typically a time-varying function of position. It doesn't matter if oscillator is forced or not. The resonant frequency will be the same either way, since the resonant frequency is found by solving for the natural (that is, unforced) response. The problem of damping factor as a measure of damping performance in resonant frequencies is its qualitative assessment, in other words finding a rate at which “something” dissipates energy. These physical connections invariably promote amplitude growth and are often difficult to inspect due to the nature of the process, with changes in damping particularly difficult to characterize.

Out of necessity, what is left is to use the decay tests preformed in calm water. However, this approach, although nonlinear in nature (and thus better than linearized results), has its own limitation: it does not account for possible dependencies of the coefficient on roll oscillation frequency. This could create serious problems when ships are not in calm water. In those more realistic situations, ships roll with a wider spectrum of frequencies. The damping coefficient derived from a single (natural) frequency may simply be not sufficient. Even if a more realistic damping coefficient could be measured from the amplitude variation in specified incident waves, this approach is very inefficient: such measurement must be carried out for different ship hulls in different environments.

6.3 Free parametric rolling tests in both regular and irregular waves

6.3.1 Parametric rolling experiments in regular waves

The preceding sections have introduced the theoretical background, the numerical procedure and the programs that were used to evaluate the non-linear instabilities in ships. Any mathematical model code that is used to estimate ship motions requires validation of its results to demonstrate reliability in future conditions. The first part of the tests focused on the initial setup and parametric rolling tests in regular waves, reporting of parameters such as the wave height, heading, moments and forces. The tests No 5 to 16 correspond to head case scenario and the tests No 309 to 320 to the following wave's parametric rolling experiments (table 6-4).

Nº	GM	Wave N°	SHIP				MODEL			Heading (°)	File	Max Roll
			H (m)	T (s)	V (kn)	V (m/s)	H (m)	T (s)	V (m/s)			
5	1	15	6	5.77	7.97	4.10	0.092	0.72	0.51	180	TEST5	32.15
6	1	16	6	6.45	7.97	4.10	0.092	0.80	0.51	180	TEST6	23.88
7	1	17	6	7.07	7.97	4.10	0.092	0.88	0.51	180	TEST7	1.3
8	1	18	6	7.63	7.97	4.10	0.092	0.95	0.51	180	TEST8	0.53
9	1	19	8	5.77	7.97	4.10	0.123	0.72	0.51	180	TEST9	33.43
10	1	20	8	6.45	7.97	4.10	0.123	0.80	0.51	180	TEST10	25.32
11	1	21	8	7.07	7.97	4.10	0.123	0.88	0.51	180	TEST11	1.91
12	1	22	8	7.63	7.97	4.10	0.123	0.95	0.51	180	TEST12	0.84
13	1	23	10	5.77	7.97	4.10	0.154	0.72	0.51	180	TEST13	35.72
14	1	24	10	6.45	7.97	4.10	0.154	0.80	0.51	180	TEST14	27.27
15	1	25	10	7.07	7.97	4.10	0.154	0.88	0.51	180	TEST15	1.83
16	1	26	10	7.63	7.97	4.10	0.154	0.95	0.51	180	TEST16	0.76
Calibración olas												
309	2	15	6	11.59	0.0	0.00	0.092	1.44	0.00	0	TEST309	35.78
309B	2	7	2	11.59	0.0	0.00	0.031	1.44	0.00	0	TEST309b	0.13
309v	2	15	6	11.59	1.0	0.51	0.092	1.44	0.06	0	TEST309v	35.79
310	2	16	6	12.95	0.0	0.00	0.092	1.61	0.00	0	TEST310	35.793
311	2	17	6	14.19	0.0	0.00	0.092	1.76	0.00	0	TEST 311	31.53
312	2	18	6	15.33	0.0	0.00	0.092	1.90	0.00	0	TEST312	25.96
313	2	19	8	11.59	0.0	0.00	0.123	1.44	0.00	0	TEST313	35.74
313B	2	11	4	11.59	0.0	0.00	0.062	1.44	0.00	0	TEST313B	[]
314	2	20	8	12.95	0.0	0.00	0.123	1.61	0.00	0	TEST314	38.19
315	2	21	8	14.19	0.0	0.00	0.123	1.76	0.00	0	TEST315	34.06
316	2	22	8	15.33	0.0	0.00	0.123	1.90	0.00	0	TEST316	26.34
317	2	23	10	11.59	0.0	0.00	0.154	1.44	0.00	0		
318	2	24	10	12.95	0.0	0.00	0.154	1.61	0.00	0		
319	2	25	10	14.19	0.0	0.00	0.154	1.76	0.00	0		
320	2	26	10	15.33	0.0	0.00	0.154	1.90	0.00	0		
Calibración olas												

Table 6-4. Summary of parametric rolling experiments with emphasis on different loading condition (provided by Cehipar)

The first check was made for the regular head waves with the specific parametric condition ($T_W = 12.95$ s, speed 8 knots) which corresponds to $\lambda/L_{pp} = 1$. The length of such a wave is already established as being equal to the ship length to maximize the effect of stability change in waves, but the wave height has to be assigned by varying wave heights ($H_W = 6, 8, 10$ m). Time records of the tests 6, 10 and 11 are also shown in figures 6-16, 6-17 and 6-18, respectively.

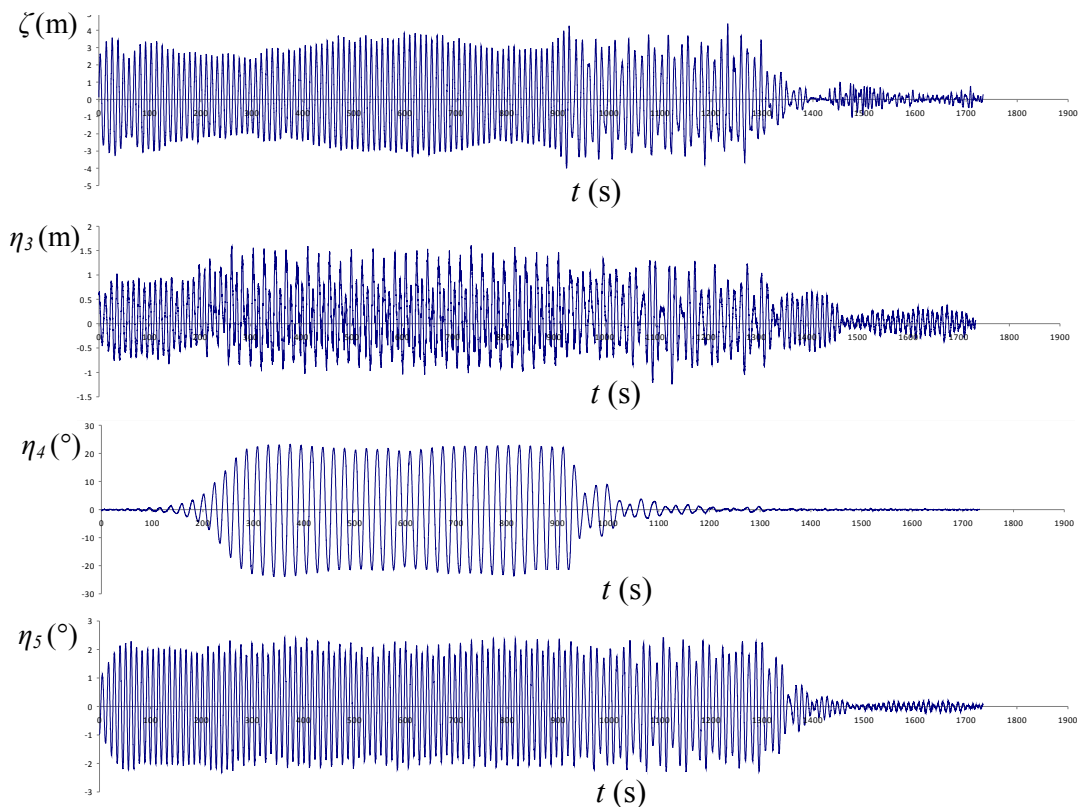


Figure 6-16 Development of parametric rolling in experiments with regular waves ($H_W = 6$ m, $T_W = 12.95$ s, speed 8 knots)

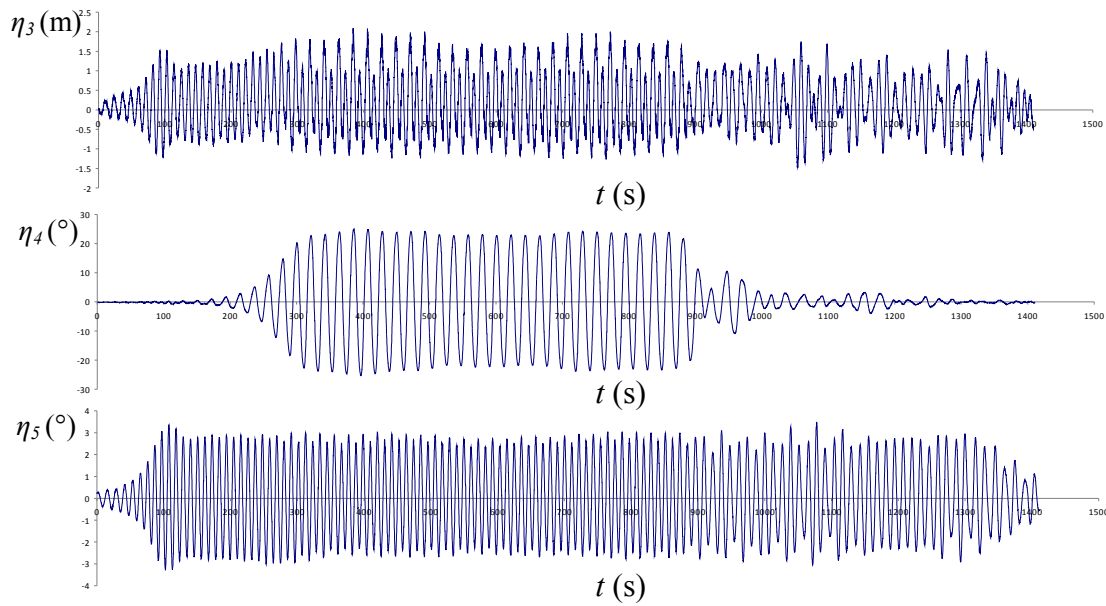


Figure 6-17. Development of parametric rolling in experiments with regular waves ($H_W = 8$ m, $T_W = 12.95$ s, speed 8 knots)

On the other hand, adopting the same condition but for different wave period $T_W = 14.19$ s (wave length to ship ratio of 1.2), didn't exhibit any parametric rolling characteristics (Figure 6-18). This can easily be explained since it was found that parametric rolling as a resonant phenomenon for the regular wave's scenario is more inclined to regularly exhibit the parametric rolling due to wave's "groupiness" effect, of course influenced by the wave frequency as witnessed here. Comparison of figures 6-16 and 6-17 bluntly demonstrates the physical mechanism that drives parametric rolling excitation. On figure 6-18 the mean amplitude of heave variation for the parametric rolling case is 1.5 m, while the mean pitch amplitude is around 2.5° . The figure 6-18 reveals a mean calculated value of heave variation of 2 m, with the mean pitch amplitude of around 3.9° . Normally, as the excitation amplitude increases, the amplitudes of heave and pitch mode increase until it reaches a critical saturated value. However for resonant phenomena, as the excitation amplitude increases further, all of the extra energy is transferred to the roll mode enabling the parametric rolling to take place. This explains why the mean pitch and to a slightly lesser extent heave amplitudes in parametric resonance are decreased compared to the values on figure 6-18, since the system energy is channelled towards roll motion.

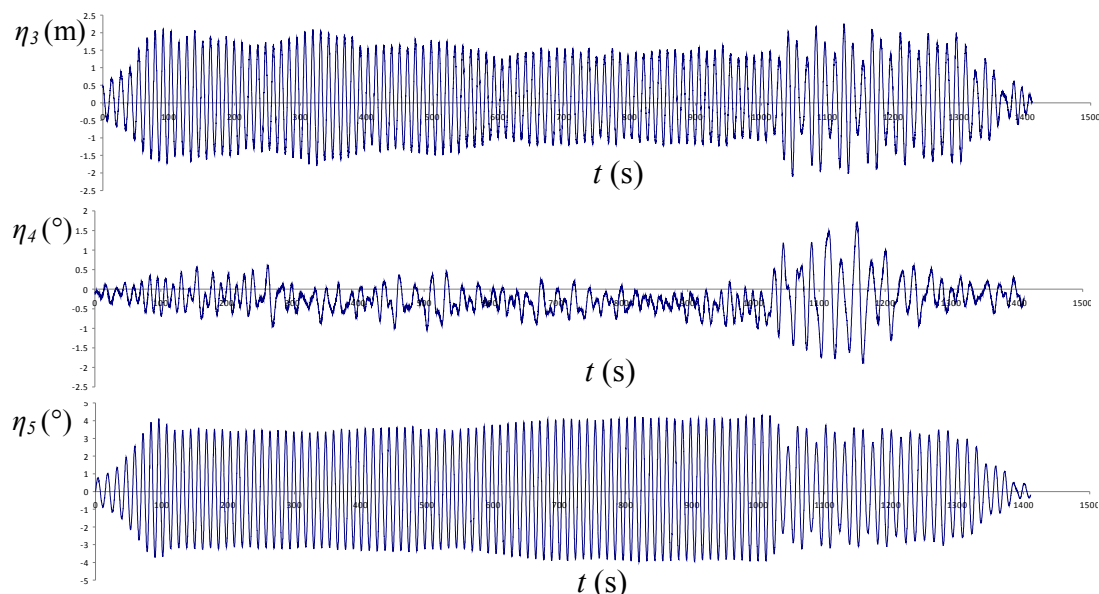


Figure 6-18. No parametric rolling in experiments with regular waves ($H_W = 8$ m, $T_W = 14.19$ s, speed 8 knots)

Following waves

The “design speed” for parametric rolling in following waves taken as a starting point for the model tests was set as zero knots. The parametric rolling was observed at the wave frequency of $\omega_0 = 0.542$ rad/s. The results obtained from the regular following waves are presented in scope of this paragraph.

At first it was very odd to find that parametric rolling is sustained for all the wave frequencies tested. However, as explained during the previous paragraph the theoretical background which sets a sequence of components for parametric rolling condition to initiate is very complex. During the analysis it was found that the second group of the decay tests which were associated with following waves was operated at different metacentric height (table 6-4, second column $GM1$ and $GM2$) for the purpose of evaluating the contribution of loading condition on the resonance effect.

Resulting from the multiple inter-dependence of physical parameters, the excitation coefficient depending on the variation of the metacentric height on following waves has emerged as the most important one, responsible for the simulation outcome, particularly related with the partial energy transfer to the roll mode of motion due to the surplus of the roll moment (higher arm). Therefore, these simulations were recalculated using the appropriate geometrical set up (consequent change of displacement, VCG and GM). A total of 8 tests for $GM2 = 0.990$ m were carried out for the above mentioned condition and the complete list of results is summarized in table 6-4. For instance, the corresponding test No. 314 is also presented on figure 6-19.

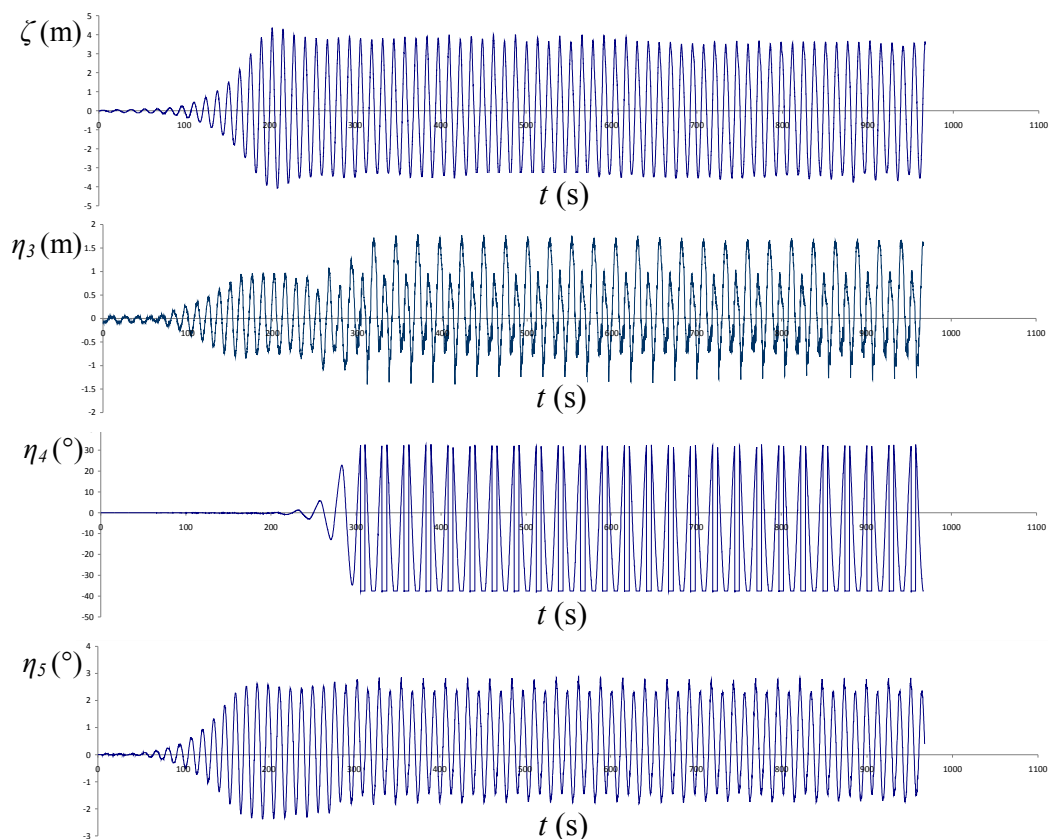


Figure 6-19. Experimental development of parametric rolling in experiments with regular following waves ($H_W = 8$ m, $T_W = 12.95$ s, speed 0 knots)

6.3.2 Parametric rolling experiments in polychromatic waves

Prior to investigating irregular waves a set of experiments was designed to assess polychromatic waves. It is interesting to see the characteristic of parametric rolling for such a specific condition lying in between regular and irregular waves. They are essentially irregular waves but constituting of limited number of harmonic components. It presents series of ship model tests that

have been designed and conducted with the aim to generate necessary experimental data for the validation of numerical simulation tools and to gain experience on the behaviour of the ship in resonance conditions that is assumed necessary towards the understanding and identification of the specific conditions of parametric rolling in irregular head waves.

Therefore, it may be considered as a “bridge” connecting two similar yet different realizations of parametric rolling, with the gap between the regular and irregular wave conditions recognized. These intermediate wave conditions, namely that of wave groups, have been selected to test and to provide valuable information at least concerning qualitative validation purposes due to their combined deterministic and irregular character.

These tests were the most extensive ones. Therefore, a total of 40 tests were performed with the different set up of polychromatic waves (3-7 components) and of different headings (160°-180° and 0°-20°). The idea of having these extended tests was to establish a link, rather the pattern upon which the physical behaviour from the regular to irregular excitation is differentiated. The following table 6-5 lists the complete free polychromatic wave’s tests.

N°	SHIP			MODEL			MODEL			Heading (°)
	GM	Wave N°	H (m)	T (s)	V (kn)	V (m/s)	H (m)	T (s)	V (m/s)	
17	1	29	8	12.95	7.96968	4.1	0.12307692	1.60625	0.508542412	180
18	1	30	8	12.95	7.96968	4.1	0.12307692	1.60625	0.508542412	180
19	1	31	8	12.95	7.96968	4.1	0.12307692	1.60625	0.508542412	180
20	1	32	8	12.95	7.96968	4.1	0.12307692	1.60625	0.508542412	180
21	1	33	8	12.95	7.96968	4.1	0.12307692	1.60625	0.508542412	180
22	1	34	8	12.95	7.96968	4.1	0.12307692	1.60625	0.508542412	180
23	1	29	8	12.95	8.16	4.20	0.123	1.61	0.52	170
24	1	30	8	12.95	8.16	4.20	0.123	1.61	0.52	170
25	1	31	8	12.95	8.16	4.20	0.123	1.61	0.52	170
26	1	32	8	12.95	8.16	4.20	0.123	1.61	0.52	170
27	1	33	8	12.95	8.16	4.20	0.123	1.61	0.52	170
28	1	34	8	12.95	8.16	4.20	0.123	1.61	0.52	170
28a	1	34a	8	12.95	8.16	4.20	0.123	1.61	0.52	170
29	1	29	8	12.95	8.36	4.30	0.123	1.61	0.53	160
30	1	30	8	12.95	8.36	4.30	0.123	1.61	0.53	160
31	1	31	8	12.95	8.36	4.30	0.123	1.61	0.53	160
32	1	32	8	12.95	8.36	4.30	0.123	1.61	0.53	160
33	1	33	8	12.95	8.36	4.30	0.123	1.61	0.53	160
34	1	34	8	12.95	8.36	4.30	0.123	1.61	0.53	160
34a	1	34a	8	12.95	8.36	4.30	0.123	1.61	0.53	160
321	2	35	8	11.59	0.00	0.00	0.123	1.44	0.00	0
322	2	36	8	11.59	0.00	0.00	0.123	1.44	0.00	0
323	2	37	8	11.59	0.00	0.00	0.123	1.44	0.00	0
324	2	38	8	11.59	0.00	0.00	0.123	1.44	0.00	0
325	2	39	8	11.59	0.00	0.00	0.123	1.44	0.00	0
326	2	40	8	11.59	0.00	0.00	0.123	1.44	0.00	0
327	2	35	8	11.59	0.00	0.00	0.123	1.44	0.00	10
328	2	36	8	11.59	0.00	0.00	0.123	1.44	0.00	10
329	2	37	8	11.59	0.00	0.00	0.123	1.44	0.00	10
330	2	38	8	11.59	0.00	0.00	0.123	1.44	0.00	10
331	2	39	8	11.59	0.00	0.00	0.123	1.44	0.00	10
332	2	40	8	11.59	0.00	0.00	0.123	1.44	0.00	10
332a	2	40a	8	11.59	0.00	0.00	0.123	1.44		10
333	2	35	8	11.59	0.00	0.00	0.123	1.44	0.00	20
334	2	36	8	11.59	0.00	0.00	0.123	1.44	0.00	20
335	2	37	8	11.59	0.00	0.00	0.123	1.44	0.00	20
336	2	38	8	11.59	0.00	0.00	0.123	1.44	0.00	20
337	2	39	8	11.59	0.00	0.00	0.123	1.44	0.00	20
338	2	40	8	11.59	0.00	0.00	0.123	1.44	0.00	20
338a	2	40a	8	11.59	0.00	0.00	0.123	1.44	0.00	20

Table 6-5. List of all experimental polychromatic waves tests (provided by Cehipar)

As seen on the table 6-5, each test number corresponds to a certain wave number that comprises one wave generation of different harmonic components. Therefore, the aim is to evaluate the parametric rolling realization from lets say somewhat distant wave generations. The complete list of waves is presented on the following table 6-6.

The dominant component (an analogy to significant wave height from irregular waves) is $H_W = 8$ m and $T_W = 12.95$ s, while the others are predefined creating a wave profile from 3 to 7 harmonic components.

Nº	NOMBRE	H1	T1	H2	T2	H3	T3	H4	T4	H5	T5	H6	T6	H7	T7
29	POLI01	8.00	12.95	0.50	11.95	0.50	13.95								
30	POLI02	8.00	12.95	0.50	11.95	0.50	13.95	0.25	10.95	0.25	14.95				
31	POLI03	8.00	12.95	0.50	11.95	0.50	13.95	0.25	10.95	0.25	14.95	0.125	9.95	0.125	15.95
32	POLI04	8.00	12.95	2.00	11.95	2.00	13.95	2.00	10.95	2.00	14.95				
33	POLI05	8.00	12.95	1.00	11.95	1.00	13.95	1.00	10.95	1.00	14.95				
34	POLI06	8.00	12.95	0.50	11.95	0.50	13.95	0.50	10.95	0.50	14.95				
34a	REGULAR03	8.00	12.95												
35	POLI07	8.00	11.59	0.50	10.59	0.50	12.59								
36	POLI08	8.00	11.59	0.50	10.59	0.50	12.59	0.25	9.59	0.25	13.59				
37	POLI09	8.00	11.59	0.50	10.59	0.50	12.59	0.25	9.59	0.25	13.59	0.125	8.59	0.125	14.59
38	POLI10	8.00	11.59	1.00	10.59	1.00	12.59	1.00	9.59	1.00	13.59				
39	POLI11	8.00	11.59	0.50	10.59	0.50	12.59	0.50	9.59	0.50	13.59				
40	POLI12	8.00	11.59	0.25	10.59	0.25	12.59	0.25	9.59	0.25	13.59				
40a	REGULAR13	8.00	11.59												

Table 6-6. List of all theoretical polychromatic waves (provided by Cehipar)

The waves are generated from by the wave maker. The wave maker is located in one of the 30 m basin sides. The wave maker is powered by six hydraulic pumps with a total output of 551 kW. On the opposite side of the wave maker there is a wave beach of very good absorbing characteristics.

Its 60 flaps with independent motion, together with the use of wall reflection allows the generation of all types of waves with a fairly good quality and inside a wide useful area. However, even with relatively modest number of comprising components it was impossible to create an exact duplicate of the desired wave calibration. Therefore, the outlook of the wave profile used in the numerical simulations had to be adjusted to the immediate realisation from the basin. For that reason actual wave profile as seen corrected on the table 6-7 had to be implemented in calculations by using appropriate wave height, wave period and consequently phase shift of each contributing harmonic component.

Nº	NOMBRE	H1	T1	H2	T2	H3	T3	H4	T4	H5	T5	H6	T6	H7	T7
29	POLI01	0.123	1.606	0.008	1.482	0.008	1.730								
		0.132		0.018		0.018									
	error(%)	7.25		134.00		134.00									
	Alturas corregidas	0.115		0.003		0.003									
30	POLI02	0.123	1.606	0.008	1.482	0.008	1.730	0.004	1.358	0.004	1.854				
		0.130		0.020		0.017		0.005		0.006					
	error(%)	5.63		160.00		121.00		30.00		56.00					
	Alturas corregidas	0.117		0.003		0.003		0.003		0.002					
31	POLI03	0.123	1.606	0.008	1.482	0.008	1.730	0.004	1.358	0.004	1.854	0.002	1.234	0.002	1.978
		0.128		0.019		0.016		0.005		0.007		0.001		0.002	
	error(%)	4.00		147.00		108.00		30.00		82.00		-42.80		-14.72	
	Alturas corregidas	0.118		0.003		0.004		0.003		0.002		0.003		0.002	
32	POLI04	0.123	1.606	0.031	1.482	0.031	1.730	0.031	1.358	0.031	1.854				
		0.120		0.038		0.039		0.028		0.042					
	error(%)	-2.34		22.85		25.78		-9.49		36.50					
	Alturas corregidas	0.126		0.025		0.024		0.034		0.023					
33	POLI05	0.123	1.606	0.015	1.482	0.015	1.730	0.015	1.358	0.015	1.854				
		0.127		0.032		0.026		0.015		0.020					
	error(%)	3.19		108.00		69.00		-2.50		30.00					
	Alturas corregidas	0.119		0.007		0.009		0.016		0.012					
34	POLI06	0.123	1.606	0.008	1.482	0.008	1.730	0.008	1.358	0.008	1.854				
		0.127		0.019		0.014		0.010		0.010					
	error(%)	3.19		147.00		82.00		30.00		30.00					
	Alturas corregidas	0.119		0.003		0.004		0.006		0.006					

Table 6-7. List of actual measured polychromatic waves generated in the basin (provided by Cehipar)

One of the ways to evaluate actual time history of the characteristic wave profile is by applying the fast Fourier transform. A common use of Fourier transforms is to find the frequency components of a signal buried in a noisy time domain signal. Accordingly, the wave elevation time history is processed to identify the frequency components by looking at the original signal. Converting to the frequency domain, the discrete Fourier transform of the noisy signal is thus found by taking the fast Fourier transform (FFT). The corresponding algorithm evaluates enough frequency components to reconstruct the finite segment that was analyzed. As seen on the figure 6-20 based on the Test No. 29 referred to as POLI01 in a model scale, a measured and the adjusted signal is presented. The signal corrupted with zero-mean random noise can be interpreted with the amplitude spectrum of the $\zeta(t)$. After the procedure is implemented for all the tests and calibrated waves the first group of tests is associated with the head waves as systemized in table 6-8.

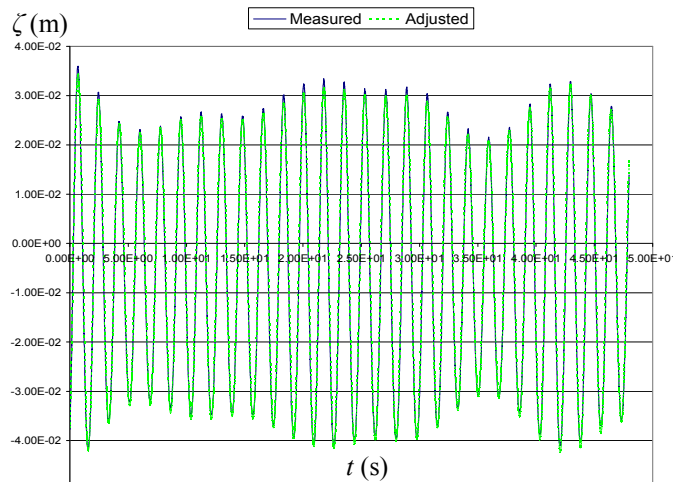


Figure 6-20. Comparison of the measured and adjusted wave signal

N°	GM	Wave N°	SHIP				MODEL			Heading (°)	File
			H (m)	T (s)	V (kn)	V (m/s)	H (m)	T (s)	V (m/s)		
17	1	29	8	12.95	7.96968	4.1	0.12307692	1.60625	0.508542412	180	TEST17
18	1	30	8	12.95	7.96968	4.1	0.12307692	1.60625	0.508542412	180	TEST18
19	1	31	8	12.95	7.96968	4.1	0.12307692	1.60625	0.508542412	180	TEST19
20	1	32	8	12.95	7.96968	4.1	0.12307692	1.60625	0.508542412	180	TEST20
21	1	33	8	12.95	7.96968	4.1	0.12307692	1.60625	0.508542412	180	
22	1	34	8	12.95	7.96968	4.1	0.12307692	1.60625	0.508542412	180	

Table 6-8. Polychromatic head waves tests (provided by Cehipar)

6.3.3 Parametric rolling experiments in irregular waves

Investigation of the conditions in which parametric rolling occurs in irregular head and oblique waves, with forward advance speed, considering the same significant wave heights and modal wave encounter frequencies recorded during the most critical test of parametric rolling in regular head waves was investigated. Repetition of the tests with the same spectral energies but with different wave realizations in space and time was conducted.

During the polychromatic wave’s analysis, it was established, albeit on the small sample, that for the parametric rolling to actualize a sufficiently long quasi-regular excitation needs to be sustained. A total of 6 tests were performed with the different wave set up for different headings (160°-180° and 0°-20°). The idea of having these tests was to prove a pattern observed from the polychromatic tests upon which the physical correlation between the regular and irregular excitation is essential for the parametric resonance to actualise. The following table 6-9 lists the complete free irregular wave’s tests.

N°	GM	Wave N°	SHIP				MODEL			Heading (°)
			H _w (m)	T (s)	V (kn)	V (m/s)	H _w (m)	T (s)	V (m/s)	
35	1	27a	8	12.95	7.97	4.10	0.123	1.61	0.51	180
36	1	27a	8	12.95	8.16	4.20	0.123	1.61	0.52	170
37	1	27a	8	12.95	8.36	4.30	0.123	1.61	0.53	160
339	2	30a	4	14.19	0.00	0.00	0.123	1.76	0.00	0
340	2	30a	4	14.19	0.00	0.00	0.123	1.76	0.00	10
341	2	30a	4	14.19	0.00	0.00	0.062	1.76	0.00	20

Table 6-9. Lists of the complete free irregular wave’s tests

Once the critical conditions for the regular waves are identified, the vessel was then tested for equivalent conditions in irregular waves having an appropriate number of harmonic components. As encounter conditions constantly change when irregular waves are considered, the next batch of tests consisted of testing different wave realizations in space and time.

7 Analysis of roll damping experiments

7.1 Theoretical background of the fitting procedure used for the analysis of roll decrement tests

Roll decay tests performed were used to reduce the uncertainties with respect to the use of data from an empirical model for a numerical study on the influence of estimation methods for roll damping on parametric roll prediction. Although a lot of numerical models for parametric roll prediction have been proposed so far, roll damping for large amplitude and influence of roll damping estimation methods on parametric roll prediction presents an even greater difficulty.

In the case fitting procedures on experimental data on analytical approximations, usually based on the curve of maxima (Spouge, 1990), or on fully numerical approaches, usually based on the full time history can be adopted.

Dalzell (1978) proposed an approximation to the conventional linear plus quadratic ship rolling model. The author replaced the linear plus quadratic damping model with a mixed linear plus cubic approximation able to represent the experimental data as well as the linear-plus-quadratic model. Quite the opposite Mathisen et al. (1984) reported a better approximation of the damping behaviour of ship rolling by means of the linear-plus-quadratic model.

Cardo et al., (1982) considered two models for damping moment. In the first model, there is linear dependence on the roll angle and a mixed linear-plus-quadratic dependence on the roll velocity. In the second model there is quadratic dependence on the angle of roll and a linear-plus-cubic dependence on the roll velocity. The difficulty was caused by the fact that the coefficients of the models always appear in a coupled form. The chosen fitting procedure, despite the use of the same analytical approximation, can lead to results which can also be quite different when there is non negligible nonlinearity both in the righting arm and in the damping.

Roberts (1982) studied the same problem, by formulating some simple expression for the stationary response distribution. For the case of linear damping it was found that the motion was unstable if the damping factor was sufficiently small. The inclusion of a quadratic damping term in the equation of motion was shown to limit the unstable motion predicted by the linear damping assumption more so than the linear plus cubic model.

A much more general and reliable methodology for the evaluation of parameters, based on the direct numerical integration of the differential equation, can be used as proposed by Contento et al. (1994). In this methodology the problem of parameters identification is seen as a multi-dimensional optimization problem (the number of dimensions coincides with the number of free parameters). The function to be minimized is the sum of the squared residuals between the experimental decay curve and the decay curve predicted by the mathematical model. For this task usual minimization routines are available. This method is very powerful, because it can handle any type of proposed model, while the shortcoming of this method is related to the computational effort associated with the numerical integration algorithm.

Many models are able to reproduce well, with a suitable choice of coefficients, the behaviour of the ship in a free decay experiment. The approach used in the present work is the parametric fitting of the amplitude dependent equivalent linear damping performed assuming that the oscillation frequency is, with good accuracy, almost independent from the rolling amplitude. Slightly different from what can usually be found in literature can be adopted as well due to the fact that the variation of the frequency with the roll amplitude can be explicitly taken into account. This would however require an analytical description of the restoring term usually implemented by the 1 DOF models when the roll amplitude dependence of the oscillations frequency, is mainly associated with nonlinearities of roll restoring. The goal is to obtain the roll amplitude dependence of the equivalent linear damping coefficient which is mainly associated with nonlinearities of damping. In order to understand the theoretical background of the analysis of roll decays it is necessary to start with some

fundamental considerations. The first one concerns the dynamic modeling of free roll motion with a 1-DOF approach. Experimental roll decay data can indeed be described, quite often, by an uncoupled nonlinear differential equation having the following general form:

$$I_{44} \cdot \ddot{\eta}_4 + B_{44}(\dot{\eta}_4) + \Delta \cdot \overline{GZ}(\eta_4) = 0 \quad (7-1)$$

where η_4 (rad) is the roll angle, dots represent derivatives with respect to time, I_{44} (kg m²) is the total roll moment of inertia including the effect of hydrodynamic added inertia (A_{44}), $B_{44}(\dot{\eta}_4)$ (Nm) is the damping moment function assumed to be dependent only on the instantaneous roll velocity $\dot{\eta}_4$, Δ (N) is the ship displacement and $GZ(\eta_4)$ (m) is the ship righting lever. The two most commonly used general models for the nonlinear damping representation are:

a) the mixed “linear” with respect to roll angle and “linear-quadratic” with respect to roll velocity,

$$B_{44}(\eta_4, \dot{\eta}_4) = 2\nu\dot{\eta}_4 + \alpha_1\dot{\eta}_4|\eta_4| + \alpha_2\dot{\eta}_4|\dot{\eta}_4| = 0 \quad (7-2)$$

b) the mixed “quadratic” with respect to roll angle and “linear-cubic” with respect to roll velocity,

$$B_{44}(\eta_4, \dot{\eta}_4) = 2\nu\dot{\eta}_4 + \beta_1\eta_4^2\dot{\eta}_4 + \beta_2|\dot{\eta}_4|^3 = 0 \quad (7-3)$$

If we consider that the inclination angles are moderate, (wet deck is not submerged), and knowing that the angle dependence cannot be easily separated from the velocity dependence these two models are simplified governing the two typical nonlinear models that are usually found in literature:

a) “linear-plus-quadratic” model,

$$B_{44}(\eta_4, \dot{\eta}_4) = 2\nu\dot{\eta}_4 + \alpha\dot{\eta}_4|\dot{\eta}_4| = 0 \quad (7-4)$$

b) “linear-plus-cubic” model,

$$B_{44}(\eta_4, \dot{\eta}_4) = 2\nu\dot{\eta}_4 + \beta\dot{\eta}_4^3 = 0 \quad (7-5)$$

The more used approach to the problem consists of considering a damping moment that has a linear component plus another one proportional to $\dot{\eta}_4|\dot{\eta}_4|$ of roll angular velocity. Probably all model basin in the world follows this approach to assess the damping from a decay test. However, a few years ago Cehipar basin adopted a new technique of approximating decay curve with exponential fitting function considering full time series. The results will be verified using a linear plus quadratic model for the damping and a subsequent equivalent linearization. We can actually write the eq. (7-1) after dividing it by I_{44} to get the more usual form of linear + quadratic + cubic model,

$$\begin{aligned} \ddot{\eta}_4 + 2\nu\dot{\eta}_4 + \alpha\dot{\eta}_4|\dot{\eta}_4| + \beta\dot{\eta}_4^3 + \omega_0^2 \cdot r(\eta_4) &= 0 \\ 2\nu\dot{\eta}_4 + \alpha\dot{\eta}_4|\dot{\eta}_4| + \beta\dot{\eta}_4^3 &= \frac{B_{44}(\dot{\eta}_4)}{I_{44}} \quad ; \quad \omega_0^2 = \frac{\Delta \cdot GM}{I_{44}} \quad ; \\ r(\eta_4) &= \frac{GM(\eta_4)}{GM} \quad ; \quad GM = \left. \frac{dGZ}{d\eta_4} \right|_{\eta_4=0} \end{aligned} \quad (7-6)$$

Analytical approximate techniques have been widely used in the past to obtain approximate analytical closed form solutions of particular cases of (7-6) (Cardo et al 1982, Bulian, 2004). In this work we will follow a different idea, which is based on the “classical” way of analyzing roll decay curves by means of the so called decrement curve.

The fundamental assumption of the theoretical background that will follow is that, in a limited time window Δt centered at a time \tilde{t} , the nonlinear model (7-6) can be effectively replaced or approximated by a linear equivalent model as follows:

$$\ddot{\eta}_4 + 2\nu\dot{\eta}_4 + \alpha\dot{\eta}_4|\dot{\eta}_4| + \beta\dot{\eta}_4^3 + \omega_0^2 \cdot r(\eta_4) = 0 \rightarrow \ddot{\eta}_4 + 2 \cdot \nu_{eq} \cdot \dot{\eta}_4 + \omega_0^2 \cdot \eta_4 = 0$$

$$\text{in } \left[\tilde{t} - \frac{\Delta t}{2}, \tilde{t} + \frac{\Delta t}{2} \right] \quad (7-7)$$

The idea is, therefore, to obtain quantification of the coefficient ν_{eq} (Himeno, 1981) from the analysis of roll decays in order to finally obtain an estimation of a series of parameters that, as will be discussed later in detail, will characterize the damping function of the nonlinear model. In place of a term-by-term comparison, therefore, it will probably be reasonable to define an equivalent extinction coefficient ν_{eq} with the clear analogy with the equivalent linear damping coefficient B_e . However, this approach, although simple and nonlinear in nature (and thus better than linearized results), has its own limitation: it does not account for possible dependencies of the coefficient on roll oscillation frequency. The approach that could be used in the future work is slightly different from what can usually be found in literature and is applied for this research due to the fact that in the present analysis the variation of the frequency with the roll amplitude is not explicitly taken into account. That would imply using the equivalent natural frequency, for instance $\omega_{0,eq}$ approximating the frequency equal to the amplitude dependent damped roll frequency. The parametric fitting of the amplitude dependent equivalent linear damping is usually performed assuming that the oscillation frequency is, and with good accuracy, almost independent from the rolling amplitude.

It is extremely important to underline that the simplification /substitution (7-7) is not uniquely defined and it is therefore necessary to better specify how the equivalent linear damping coefficient ν_{eq} shall be determined. In this work we start by introducing error functions as follows:

$$\chi_d^2(\nu_{eq}) = \int_{\tilde{t}-\frac{\Delta t}{2}}^{\tilde{t}+\frac{\Delta t}{2}} \left[2 \cdot \nu_{eq} \cdot \dot{\eta}_4(t) - \left(2\nu\dot{\eta}_4(t) + \alpha\dot{\eta}_4(t)|\dot{\eta}_4(t)| + \beta\dot{\eta}_4^3(t) \right) \right]^2 dt \quad (7-8)$$

Then we define ν_{eq} as the quantity that minimize the error functions in (7-8), thus, by imposing a zero gradient, we get:

$$\frac{\partial \chi_d^2}{\partial \nu_{eq}} = 0 \Rightarrow \nu_{eq} = \frac{1}{2} \cdot \frac{\int_{\tilde{t}-\frac{\Delta t}{2}}^{\tilde{t}+\frac{\Delta t}{2}} \left(2\nu\dot{\eta}_4(t) + \alpha\dot{\eta}_4(t)|\dot{\eta}_4(t)| + \beta\dot{\eta}_4^3(t) \right) \cdot \dot{\eta}_4(t) dt}{\int_{\tilde{t}-\frac{\Delta t}{2}}^{\tilde{t}+\frac{\Delta t}{2}} \dot{\eta}_4^2(t) dt} \quad (7-9)$$

Definitions in (7-9) are quite general and it is probably worth mentioning that this way of thinking has significant similarities with the statistical linearization (Robert et al. 1990). Moreover, the introduced definition for the equivalent linear damping is substantially equivalent to what is done when the equivalent linear damping coefficient is defined on the basis of equivalent energy dissipation per cycle from the nonlinear damping and the equivalent linear damping terms.

Consider a general roll decay curve, such as that reported in Nayfeh et al. 1979: time instants t_i and t_{i+1} are assumed to correspond to consecutive local extremes η_{4i} and $\eta_{4(i+1)}$ of the roll time history.

With reference to figure 7-1, the idea is to assume that, in each half roll cycle, the roll behaviour can be approximate by the following linear differential equation:

$$\ddot{\eta}_4 + 2 \cdot \nu_{eq,i} \cdot \dot{\eta}_4 + \omega_0^2 \cdot \eta_4 = 0 \quad \text{in } [t_i, t_{i+1}] \quad (7-10)$$

assuming the change of coefficient $\nu_{eq,i}$ from half cycle to half cycle. According (7-10), and remembering that

$$\forall i \quad \eta_4(t_i) = \eta_{4i} \quad \wedge \quad \dot{\eta}_4(t_i) = 0 \quad (7-11)$$

the roll decay for the i -th half cycle can be approximated, in principle, by the following analytical solution:

$$\eta_4(\tau) \approx e^{(-v_{eq,i} \cdot \tau)} \cdot (A \cdot \cos(\tilde{\omega}_i \cdot \tau) + B \cdot \sin(\tilde{\omega}_i \cdot \tau))$$

with

(7-12)

$$\tau = t - t_i \quad ; \quad A = \eta_{4i} \quad ; \quad B = \frac{v_{eq,i}}{\tilde{\omega}_i} \cdot \phi_i \quad ; \quad \tilde{\omega}_i = \sqrt{\omega_0^2 - v_{eq,i}^2}$$

Assuming that the system is lightly damped, as it is usually the case, then $\frac{v_{eq,i}}{\omega_i} \ll 1$ and (7-

12) can be approximated by

$$\eta_4(\tau) \approx e^{(-v_{eq,i} \cdot \tau)} \cdot \eta_{4i} \cdot \cos(\tilde{\omega}_i \cdot \tau)$$

$$\dot{\eta}_4(\tau) \approx -e^{(-v_{eq,i} \cdot \tau)} \cdot \eta_{4i} \cdot \tilde{\omega}_i \cdot \sin(\tilde{\omega}_i \cdot \tau)$$
(7-13)

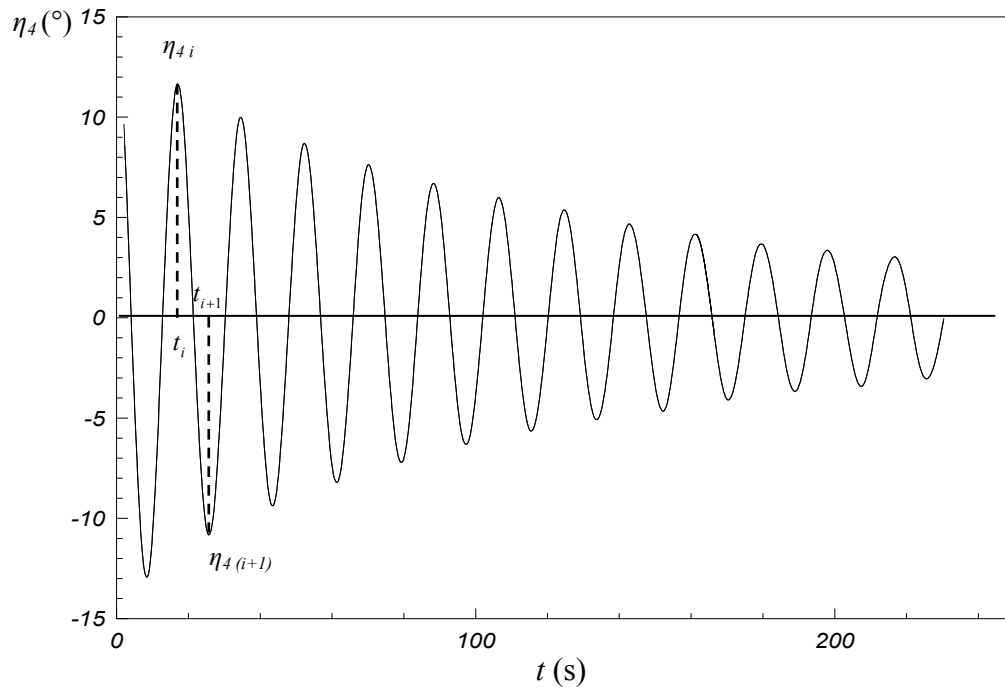


Figure 7-1. Example of roll decay curve

According to the assumption that (7-13) is a good representation of the roll decay in the time interval $[t_i, t_{i+1}]$ it follows that the characteristic parameters $v_{eq,i}$ and ω_0 can be determined as:

$$v_{eq,i} \approx \frac{1}{t_{i+1} - t_i} \ln \left(\frac{|\eta_{4i}|}{|\eta_{4(i+1)}|} \right)$$
(7-14)

$$\tilde{\omega}_i \approx \frac{\pi}{t_{i+1} - t_i}$$

Note also that, under the assumption of lightly damped system,

$$\ln \left(\frac{|\eta_{4i}|}{|\eta_{4(i+1)}|} \right) \approx \frac{|\eta_{4i}| - |\eta_{4(i+1)}|}{|\eta_{4i}|} \ll 1$$
(7-15)

Moreover, considering that the reduction $|\eta_{4i}| - |\eta_{4(i+1)}|$ of the roll envelope in half roll cycle is sufficiently small, it is possible to associate the characteristic parameters $\nu_{eq,i}$ and ω_0 to the average roll envelope A_i for the i -th half roll cycle, calculated as:

$$\begin{aligned} A_i &= \frac{|\eta_{4i}|}{t_{i+1} - t_i} \int_0^{t_{i+1} - t_i} e^{(-\nu_{eq,i} \cdot \tau)} d\tau = |\phi_i| \cdot \frac{1 - e^{(-\nu_{eq,i} \cdot (t_{i+1} - t_i))}}{\nu_{eq,i} \cdot (t_{i+1} - t_i)} = \\ &= \frac{|\eta_{4i}| - |\eta_{4(i+1)}|}{\ln|\eta_{4i}| - \ln|\eta_{4(i+1)}|} \underset{\frac{|\eta_{4i}| - |\eta_{4(i+1)}|}{|\eta_{4i}|} \ll 1}{\approx} \frac{|\eta_{4i}| + |\eta_{4(i+1)}|}{2} \end{aligned} \quad (7-16)$$

Using the roll decay test as shown on figure 7-1, roll motion values ϕ_i can be extracted upon which following calculations can be made,

$$\eta_{4m} = \frac{|\eta_{4i}| + |\eta_{4(i+1)}|}{2} \quad (7-17)$$

$$\Delta\eta_4 = |\eta_{4i}| - |\eta_{4(i+1)}| \quad (7-18)$$

Denote η_{4i} as an absolute value of roll angle for the i -th extreme. By integrating the roll equation over a half period and equating the energy dissipated by damping to the work done by the restoring moment, the following expression for the roll decrement as a function of the mean roll amplitude can also be obtained by following,

$$\Delta\eta_4 = \pi\kappa\eta_{4m} + \frac{4}{3}\alpha\eta_{4m}^2 + \frac{3\pi}{8}\beta\omega_0\eta_{4m}^3 \quad (7-19)$$

$$\Delta\eta_4 = a\eta_{4m} + b\eta_{4m}^2 + c\eta_{4m}^3 \quad (7-20)$$

The coefficients a , b , c are known as the extinction coefficients and based on the above equations we can obtain a relation to the damping coefficients,

$$a = \pi\kappa$$

$$b = \frac{4}{3}\alpha \quad (7-21)$$

$$c = \frac{3\pi}{8}\beta\omega_0$$

or

$$2\nu = \frac{B_{44,1}}{(I_{44} + A_{44})} = \frac{2a\omega_0}{\pi} = 2\kappa\omega_0$$

$$\alpha = \frac{B_{44,2}}{(I_{44} + A_{44})} = \frac{3}{4}b \quad (7-22)$$

$$\beta = \frac{B_{44,3}}{(I_{44} + A_{44})} = \frac{8}{3\pi\omega_0}c$$

Use of linear plus quadratic model for this procedure is advisable. From the above equations it should be noted that the extinction coefficient can adversely be linked to only partly proportional segments of a specified damping coefficient whether it is independent on roll amplitude or it varies with it.

As a result of this analysis (eq. 7-14 and 7-15), for each experimental decay test, it is possible to obtain a scatter plot of the quantities $\nu_{eq,i}(A_i)$. The last step to be performed is to link the experimentally determined estimations of $\nu_{eq}(A)$ with the original nonlinear model (7-6) using definitions (7-9). To accomplish this task it is first necessary to provide an explicit analytical form for

damping, using a typical expression that has shown by experience to be able to handle both the bare hull condition and the case of models fitted with bilge keels is the linear plus quadratic plus cubic in velocity model, namely:

$$B_{44}(\dot{\eta}_4) = 2 \cdot \nu \cdot \dot{\eta}_4 + \alpha \cdot \dot{\eta}_4 |\dot{\eta}_4| + \beta \cdot \dot{\eta}_4^3 \quad (7-23)$$

The model (7-23) has three free parameters, i.e. ν , α and β . However, the case of the reduced linear plus quadratic model, i.e. (7-23) with $\beta = 0$, is often sufficient. In general, the form of the damping model is selected after a visual observation of the behavior of the experimentally determined curve of $\nu_{eq}(A)$.

The next step is to calculate ν_{eq} using (7-9) but approximating the roll behavior in each half cycle with a harmonic motion with constant amplitude equal to the average roll amplitude A in each half roll cycle (7-16), and frequency equal to the amplitude dependent damped roll frequency. According to this approximation, and considering (7-23) we obtain the following results:

$$\begin{aligned} \eta_4(\tau) &\approx A \cdot \cos(\tilde{\omega}(A) \cdot \tau) \\ \dot{\eta}_4(\tau) &\approx -A \cdot \tilde{\omega} \cdot \sin(\tilde{\omega}(A) \cdot \tau) \\ \tilde{\omega}(A) &= \sqrt{\omega_0^2(A) - \nu_{eq}^2(A)} \\ \nu_{eq}(A) &= \frac{1}{2} \cdot \frac{\int_0^{2\pi/\tilde{\omega}(A)} (2\nu\dot{\eta}_4(\tau) + \alpha\dot{\eta}_4(\tau)|\dot{\eta}_4(\tau)| + \beta\dot{\eta}_4^3(\tau)) \cdot \dot{\eta}_4(\tau) d\tau}{\int_0^{2\pi/\tilde{\omega}(A)} \dot{\eta}_4^2(\tau) d\tau} = \\ &= \nu + \frac{4}{3\pi} \cdot \alpha \cdot (\tilde{\omega}(A) \cdot A) + \frac{3}{8} \cdot \beta \cdot (\tilde{\omega}(A) \cdot A)^2 \end{aligned} \quad (7-24)$$

The whole procedure for the estimation of the parameters of the nonlinear model (7-6) considering (7-23) can be summarized as follows:

- 1) Determine extremes η_{4i} and corresponding time instants t_i from an experimental roll decay time series (after appropriate filtering of the raw measured signal);
- 2) For each half cycle determine:
 - The average amplitude A_i (7-16);
 - The equivalent linear damping coefficient $\nu_{eq,i}$ to be associated to A_i (7-14);
- 3) Fit the analytical model (7-24) to the experimental scatter plot of $[\nu_{eq}(A)]_{\text{exp}}$ through a least square fitting in order to obtain the damping model coefficients ν , α and β (if necessary). For this fitting it is actually convenient to consider ν_{eq} as a function of the variable $z = \tilde{\omega}(A) \cdot A$.

From the least square fitting of the analytical models for damping to the experimental data it is possible to have confidence intervals associated to the fitted parameters and it is also possible to have an estimation of the prediction bounds for the fitting, i.e. a quantification of the residual dispersion of experimental data with respect to the assumed model.

Each figure reports also the values of the root mean squared error (RMSE) in order to give an order of magnitude of the residual dispersion of data with respect to the selected fitting model. The RMSE as reported in the figures has been calculated as:

$$RMSE = \sqrt{\frac{\sum_{j=1}^{N_{data}} (y_{\text{exp},j} - y_{\text{fit},j})^2}{N_{data} - n_{par}}} \quad (7-25)$$

where N_{data} is the total number of data, n_{par} is the number of free parameters (degrees of freedom), $y_{exp,j}$ is the j-th experimental value and $y_{fit,j}$ is the value as obtained from the fitting. In the case of the fitting of damping model in bare hull condition the number of degrees of freedom is 3 where the free parameters are ν , α and if needed β .

The model is inclined to a chosen angle and then released. To register motion during the tests an optical tracking system is often used. This system allows measuring the motion of a model without affecting them. However, this was another issue that significantly stalled the analysis process. Since the original results haven't been nearly as accurate even producing negative damping (quadratic term) a suspicion has been raised that the measurements have been affected by an additional bearing damping. The magnitude of sliding friction is a constant value independent of surface area, displacement or position, and velocity. However, a system being acted upon by Coulomb damping is nonlinear because the frictional force always opposes the direction of motion of the system. Furthermore, because there is friction present, the amplitude of the motion decreases or decays with time. In case of forward speed one would expect some additional frictional effect of bearings. Indeed the resistance itself and the surge force induced by waves create a moment orthogonal to the bearing axis, which is something that bearings usually "don't like", so they reply with extra friction. To make it short, at least presented here, different aspect of the analysis process such as filtering and mean drift were targeted as the responsible for those outcomes. Coulomb force was inappreciable that the additional term in linear plus quadratic equation, summed to the quadratic part was neglected and subsequently discarded in the analysis process.

7.2 Decay tests processing for the first group of tests

When all the prerequisites are fulfilled the post processing of the roll decrement tests is implemented. The results of TEST302 are presented in correspondence to the theory previously explained. Indeed, the resonant rolling amplitude of a ship in longitudinal waves having frequency close to twice the natural roll frequency is approximately inversely proportional to the equivalent linear damping calculated at the stationary rolling amplitude. An overestimation of the roll damping from model experiments could cause an underestimation of the actual rolling amplitude of the full scale ship or vice versa, with obvious consequences regarding the actual level of safety of the ship.

The nonlinear damping model can be suitably implemented in any seakeeping code to properly manage the roll response both in regular and irregular waves. A certain amount of practical experience is required to properly manage experimental data before processing. It involves a correction of the decay record by reducing the duration of the input signal, consequently cutting the data of low amplitude oscillations. The analysis is significantly affected by the maximum roll amplitudes lower than one to two degrees since dispersion of experimental data becomes significant. In other words scattering of the low amplitude oscillations data can significantly affect regression coefficients that must be read from interpolation curve (usually root mean square error) since the results of the analysis and fitting of the decrement curves by considering data from different conditions give an order of magnitude of the residual dispersion of data with respect to the selected fitting model.

Note that also the first maximum is usually affecting the analysis (and thus the first "extreme"). In the analysis of the obtained roll decays the first half roll cycle has been neglected for a series of reasons. Since the initial part of each experimental record shows a steady heel equal to the initial roll angle it was not easy to associate a precise time instant to the beginning of the roll decay. On the other hand the relevant magnitudes and time instants of occurrence can clearly be associated to the remaining extremes.

A distortion of the first half roll cycle can also be noticed in the process of analysis, and unfortunately not a negligible one. This can be attributed to the induced parasitic effect of the experimental arrangement (Figure 7-2).

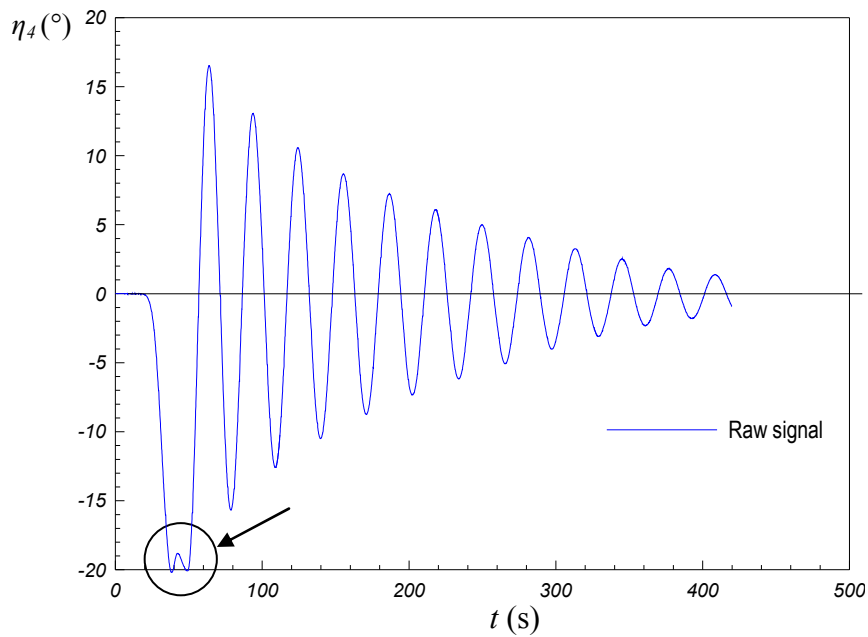


Figure 7-2. Influence of the first half roll cycle

While comparing the remaining part of the record (lets call it “valid”) to the beginning of the decay a qualitatively slower steadier roll oscillation was observed. Furthermore, the remaining part of the decay has the vortex shedding already initiated as oppose to the first half roll peak which can be considered as a transient in the developing of the fluid field from the “stand still” condition, hence a situation is not fully comparable. Due to the neglecting of the first half roll cycle the first available peak is roughly at around 15° with an actual value around 20° which is the first major drawback since the ultimate goal was to associate the decay tests to the conditions leading to parametric rolling with amplitudes considerably higher then the ones available.

With reference to equations (7-14, 7-16, 7-24) the results of the analysis and fitting of the decrement curves are reported on figure 7-3, using the linear plus quadratic plus cubic model $\ddot{\eta}_4 + 2v\dot{\eta}_4 + \alpha\dot{\eta}_4|\dot{\eta}_4| + \beta\dot{\eta}_4^3 + \omega_0\eta_4 = 0$.

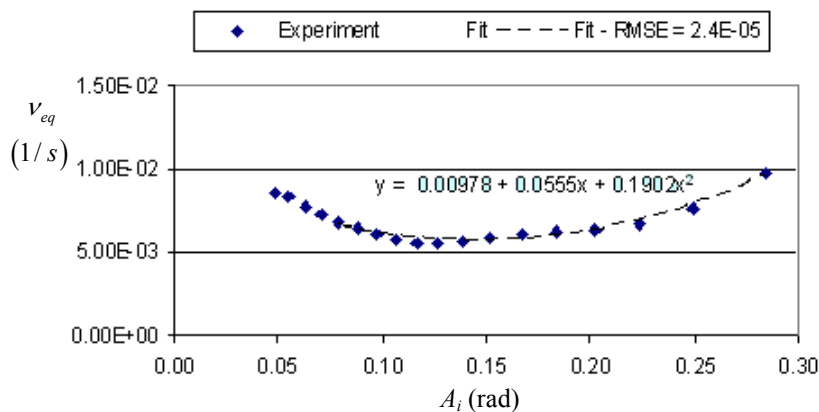


Figure 7-3. Linear + quadratic + cubic model for decay test 302

In case of bare hull condition an additional cubic term was required to obtain a good fitting of the data (figure 7-3). The reason is mainly to be sought in the fact that $v_{eq}(A)$ requires larger rolling amplitudes to show a significant derivative with respect to the amplitude A . It could be guessed that this behavior is associated to retardation in the vortex shedding in bare hull condition. As a consequence, larger rolling amplitudes are necessary, in bare hull condition, to initiate a significant vortex shedding from the hull alone. The equivalent linear damping $B_{44eq} = 4.44E+08$ Ns/m was obtained (table 7-1).

Linear+Quadratic+Cubic Model				
I44+A44 =	3.139E+10	I44 =	1.1E+10	
m =	76056430	77957400		
GMt =	1.973			
w =	0.2165561	0.2151776		
T =	29.014127	29.2	Assuming	I44+A44 = 3.18E+10
2miu =	9.79E-03	a1 =	7.14E-02	b44_1 = 3.07E+08
alpha =	5.55E-02	a2 =	7.41E-02	b44_2 = 1.74E+09
beta =	1.90E-01	a3 =	4.85E-02	b44_3 = 6.01E+09
Check				
B44_eq =	4.44E+08	Assuming	0.350408 = phi_m	
B44_cr =	1.37E+10			
xsi =	3.25E-02			
U= 0.0 m/s				
B44_eq =	4.44E+08			
b44_1 =	307167977			
b44_2 =	1.743E+09			
b44_3 =	6.009E+09			

Table 7-1. Linear + quadratic + cubic model for decay test 302

However, this type of the model seems to have limited extrapolation capabilities, therefore better types of modeling should be sought in bare hull condition in order to avoid unreasonable increases of damping at large rolling angles outside the range of tested rolling amplitudes with the consequent underestimation of roll amplitude at peak. This is due to the fact that linear + quadratic + cubic model enables better approximation and more precise fitting based on the known experimental data but may fail short outside of the tested range from decays. As you may guess the problem of extrapolation of damping models to rolling amplitudes significantly larger than the maximum rolling amplitude used in roll decay experiments has a substantial influence on parametric rolling estimation. Moreover, this problem could become serious especially in bare hull condition where the use of a cubic damping coefficient that leads to a significant growth of damping, as the amplitude of roll increases, is necessary in order to fit the experimental data.

Several alternative schemes have been used as well:

- 1) Standard logarithmic decrement method of successive peaks by considering successively both maxima and minima
- 2) Decrement of successive peaks including both maxima and minima
- 3) Decrement of successive maxima
- 4) Decrement of successive minima

These files can be examined and processed by the Grapher software to obtain the regression model (figures 7-4 and 7-5). The theory implemented is explained in Bhattacharrya and Blagoveshchensky. The quadratic damping model has been assumed during this analysis, since the linear plus quadratic plus cubic model utilized with this theory exhibited unrealistic behavior. As seen from figures standard logarithmic decrement method has an unusual orientation which would actually imply underestimated values of damping associated with larger amplitudes. This is to illustrate the importance of the scattering of the low amplitude oscillations data which significantly affects regression coefficients that must be read from the interpolation curve.

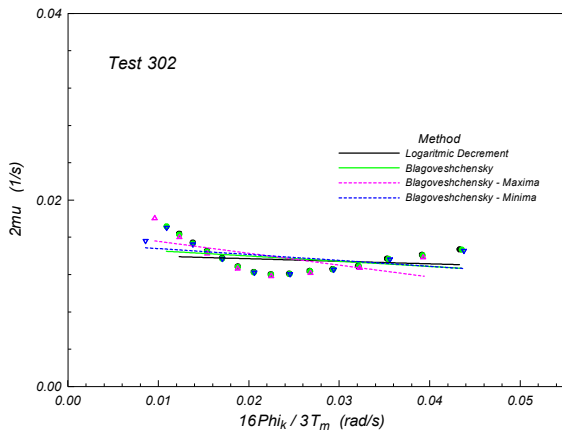


Figure 7-4. Dimensional roll damping evaluation by means of different methods (lin+quad)

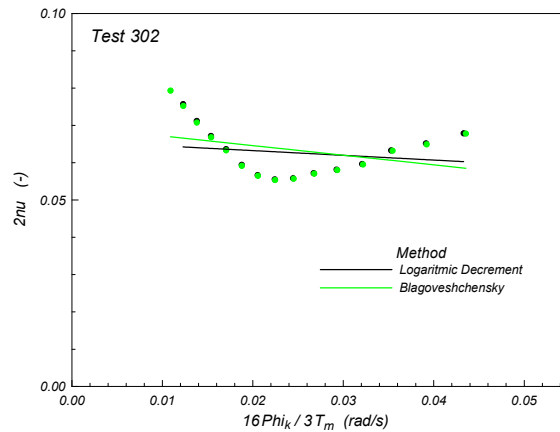


Figure 7-5. Non-dimensional roll damping evaluation by means of different methods

With proper correction of the decay record by reducing the duration of the input signal (figure 7-6 and 7-7) regression model can assume more realistic appearance. This model has better extrapolation qualities, however, the sensitivity on the length of the signal raise the global level of uncertainty associated to the analysis of roll decay tests (not negligible). Hence, due attention should be paid when planning, carrying out and analyzing this type of tests in order to reduce sources of error.

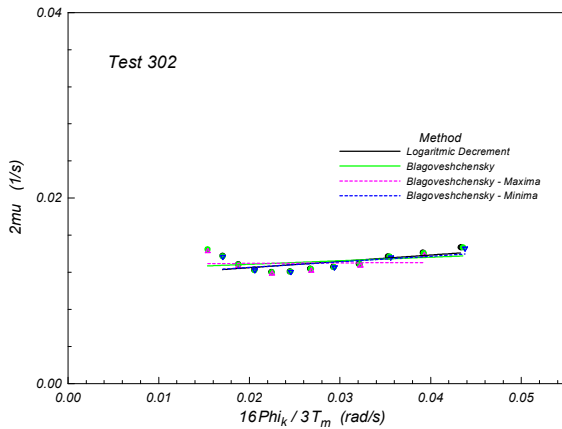


Figure 7-6. Dimensional roll damping evaluation by means of different methods (lin+quad)

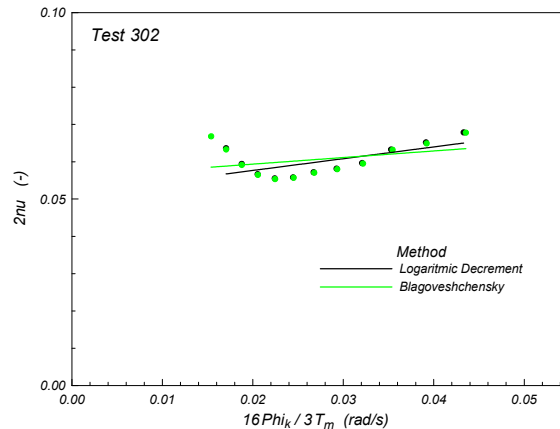


Figure 7-7. Non-dimensional roll damping evaluation by means of different methods

Using linear + quadratic model with reference to equations (7-17 to 7-22) the equivalent linear damping $B_{44eq} = 3.90 \cdot 10^8$ (Ns/m) was obtained as seen in table together with the Fortran output with extinction coefficients (table 7-2).

Linear+Quadratic Model				Parameter	Uncertainty
I44+A44 =	3.139E+10	I44 =	1.1E+10	A(1) =	.000000 .000000
m =	76056430	77957400		A(2) =	.089817 .000000
GMt =	1.973			A(3) =	.001000 .000281
w =	0.2165561	0.215917		A(4) =	.000000 .000000
T =	29.014127	29.1	Assuming	I44+A44 =	3.16E+10
				Chi-squared =	.959765E+01
2m _{iu} =	1.24E-02	a1 =	9.01E-02	b44_1 =	3.89E+08
alpha =	7.50E-04	a2 =	1.00E-03	b44_2 =	2.35E+07
Check				Full covariance matrix	
B44_eq =	3.90E+08	Assuming	0.350408	= phi_m	
B44_cr =	1.36E+10				.00E+00 .00E+00 .00E+00 .00E+00
xsi =	2.86E-02				.00E+00 .00E+00 .79E-07 .00E+00
					.00E+00 .00E+00 .00E+00 .00E+00
U= 0.0 m/s				Damping coefficients	
B44_eq =	3.90E+08			Linear term =	1.238216E-02
b44_2 =	23537355			Quadratic term =	7.498361E-04
b44_1 =	390187604			Cubic term =	0.000000E+00
				Kapa = B44/B44cr	2.858967E-02

Table 7-2. Linear + quadratic model for decay test 302

The analysis of the decrement curves allowed having a first impression of the behavior of the experimental results. The solution however, would be to provide a more quantitative assessment of the fitted models necessary to analyze the obtained fitted coefficients from each condition. Meaning, the test should be repeated to collect more data and possibly more scatter since the dispersion of experimental data especially at smaller amplitudes is quite significant. Moreover, it would be possible to aggregate $\nu_{eq,i}(A_i)$ and ω_0 coming from different roll decays performed on the same model in the same conditions with possibly changing initial heel angle. Technically, this is not entirely true due to the fact that although we are speaking of the tests performed in same conditions equivalent natural frequency $\omega_{0,eq,i}(A_i)$ changes from half cycle to half cycle. The aggregation of data could be an important aspect to the selection of the roll decrement approach for the determination of the nonlinear damping due to the fact that perfect repeatability of initial conditions for different decays is not possible. Still even if the tests are treated separately it could give us more indication as to the selection of the damping model.

Unfortunately the range of available rolling amplitudes from decays does not allow us to draw a definite conclusion on this point. If we are strictly dealing with the analysis of the decay tests alone the reader should concentrate on the inner part of the tested range. On the other hand, for the parametric rolling validation the decay tests should be considered with caution because they are to some extent governed by the a-priori selection of the damping model and its prediction of the tails of the curves at large rolling amplitudes.

This may sound a bit unreasonable since it is exactly what the aim of the research was, but it poses the well known problem of the extrapolation of damping models out of the tested range from decays.

According to the obtained results, a damping model in bare hull condition showing a linear asymptotic behavior at large rolling amplitudes for the equivalent linear damping coefficient could be advisable.

Upon obtaining the damping coefficients using any of the proposed models another approach to verify the results has been implemented in order to enable the comparison between time series from experiment, this time with the record obtained by the Runge Kutta 4th order method. Using the damping coefficients it is possible to reconstruct time series and blend it to the original signal.

As can be seen on figure 7-8, small disagreement is evident, but it's worth noting that the envelope of maxima, both for the roll displacement and for roll velocity, is well reproduced. Only the time instants at which maxima occur are shifted. This behavior could be considered as an evidence of the decoupling between the main effect of the parameter that modifies the oscillation frequency and the main effect of parameter modifying the envelope of maxima. The disagreement that arises in the first cycle of roll is associated with the initial instantaneous rolling period which is very long due to the fact that the initial angle is close to the vanishing angle.

However, a good compliance is clearly visible especially looking at general trend of the signals frequencies and flatter regions with slight discrepancies noticeable at the peak values. This can in fact be easily explained because the record obtained by the Runge Kutta 4th order method approximates the time record without mean drift removal, thus not suitable for a correct damping estimation. Unfortunately since the procedure of fixing non-zero addresses only the peak values (based on the "classical" way of analyzing roll decay curves by means of the so called decrement curve) it is not feasible to make a comparison with the full time series. Still, it gives a good indication of both the software and method validity at the start of the analysis process.

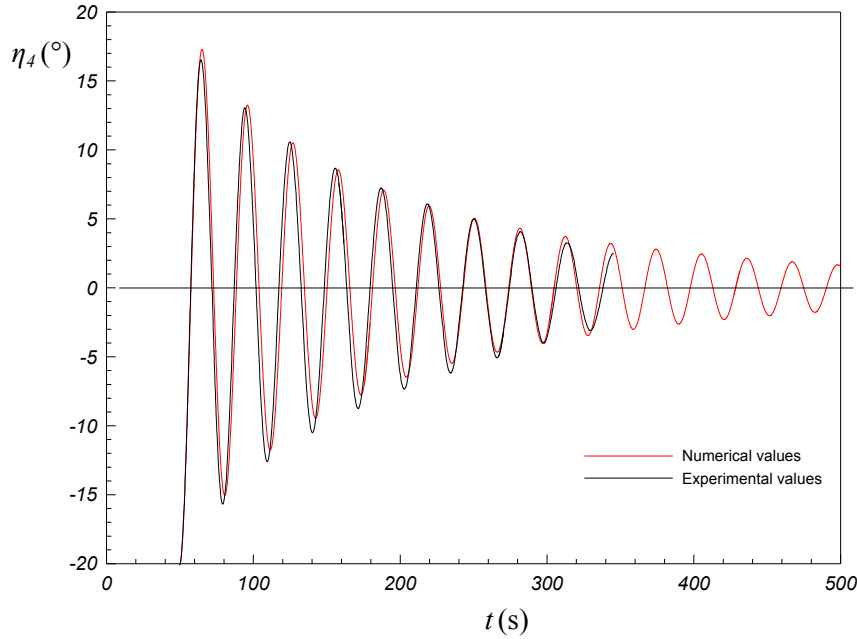


Figure 7-8. Comparison between time series from experiment and time series obtained by Runge Kutta method

7.2.1 Alternative exponential fitting technique

Fortunately, to eliminate some of the uncertainties a possibility to have an alternative tool using the Cehipar approach that handles the damping evaluation differently considering the full time series proved very valuable. In the following the theory will be explained in brief using basin nomenclature respectively. Solution of the homogeneous equation, of the motion recorded in the extinction test is:

$$\ddot{x} + 2\omega_0\mu\dot{x} + \omega_0^2x = 0 \tag{7-26}$$

with an exponential solutions of the type $\alpha e^{\beta t}$.

Exponent values β are real or complex depending on the value of the dimensionless damping. If the value is less than one ($\mu^2 < 1$) we have what is called a sub critical damping and β values are two complex conjugates with negative real part so that the solution is of type:

$$x = x_0 e^{-t/\tau} \cos(\omega_n t + \varepsilon), \quad x = x_0 e^{-\omega_0 t \zeta} \cos(\omega_0 t \sqrt{1 - \mu^2} + \varepsilon) \tag{7-27}$$

where the amplitude x_0 and phase ε are two parameters that can be obtained from the initial conditions of displacement and velocity. The motion that occurs corresponding to a given initial position and velocity in the absence of external forces (homogeneous equation) can be seen in the figure 7-1.

The motion is an oscillation with a frequency $\omega_n = \omega_0 \sqrt{1 - \mu^2}$ but with amplitude that decays exponentially with time. The rate of decline is greater the higher the parameter μ and is determined by what is known as "time constant" τ that is inversely related to the dimensionless damping. It should be noted that we could consider the possibility of a negative value, but that would imply an infinitely growing motion, something physically impossible in the absence of external forces.

This type of motion is called exponentially damped oscillatory motion. To characterize defined as follows:

- *Natural or resonance frequency.* The frequency ω_0 that corresponds to $\sqrt{C/A}$, where C is the recovery constant and A is the mass (inertia) plus the added mass (inertia). This frequency

would be the frequency of oscillation for the movement considered if there is no damping (i.e. if $\mu = 0$).

- *Natural or resonance frequency with damping.* This is the frequency that really oscillates the system without external excitation in the presence of damping. From the above equation we see that this frequency corresponds to $\omega_0\sqrt{1-\mu^2}$. In many cases μ is small enough so that the natural frequency with and without damping are virtually identical.
- *Dimensionless damping coefficient.* Parameter μ determines the rate of decay or damping of the amplitude versus time. By contrast, the value of B is called dimensional damping. Both are related by $B = 2\omega_0\mu A$.
- *Time constant.* The exponential that determines the damping can be written as $e^{-t/\tau}$, where the parameter $\tau = 1/(\omega_0\mu)$ is called the time constant or "decay time".

When the dimensionless damping is greater than one, the two solutions of β are real and negative having an exponential that tends to zero without oscillations. It could be indicated that the rolling usually has a small damping so that extinction occurs with oscillations, while the pitch and heave are often close to the critical damping and damped quickly.

The extinction trials are traditionally analyzed using what is called logarithmic decrement. This traditional method made sense when the calculation was more complicated, but with modern systems it is more convenient to adjust the theoretical function defined as $x = x_0 e^{-\omega_0 t \mu} \cos(\omega_0 t \sqrt{1-\mu^2} + \varepsilon)$ with the values recorded in the time series using any least squares algorithm. With proper initial estimates, any algorithm converges quickly to the correct solution.

With this method more robust estimates are obtained for using the total measured points and not just the extreme values. An example of TEST 302 using this approach is given in figure 7-9.

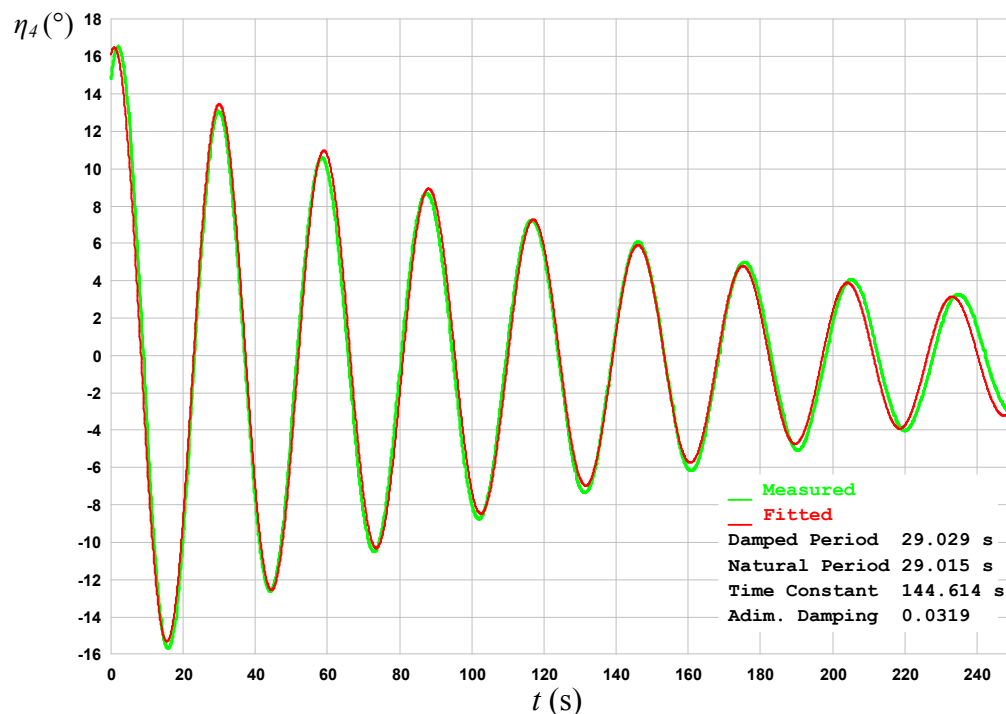


Figure 7-9. Decay test 302 processed by the exponential fitting method

On table 7-3, the results for this set of experiments are presented.

Test 302 U=0 knots		Test 305 U=11.7 knots	
Natural Period	29.015 s	Natural Period	28.425 s
Non dimensional Damping	0.0319	Non dimensional Damping	0.0481
$\omega =$	0.217 rad/s	$\omega =$	0.221 rad/s
$I_{44}+A_{44} =$	3.139E+10 kgm ²	$I_{44}+A_{44} =$	3.013E+10 kgm ²
$B_{44} =$	4.337E+08 Ns/m	$B_{44} =$	6.407E+08 Ns/m

Test 303 U=3.9 knots		Test 306 U=15.6 knots	
Natural Period	28.969 s	Natural Period	28.105 s
Non dimensional Damping	0.0337	Non dimensional Damping	0.0481
$\omega =$	0.217 rad/s	$\omega =$	0.224 rad/s
$I_{44}+A_{44} =$	3.129E+10 kgm ²	$I_{44}+A_{44} =$	2.945E+10 kgm ²
$B_{44} =$	4.575E+08 Ns/m	$B_{44} =$	6.334E+08 Ns/m

Test 304 U=8 knots		Test 307 U=19.4 knots	
Natural Period	28.763 s	Natural Period	27.778 s
Non dimensional Damping	0.037	Non dimensional Damping	0.0858
$\omega =$	0.218 rad/s	$\omega =$	0.226 rad/s
$I_{44}+A_{44} =$	3.085E+10 kgm ²	$I_{44}+A_{44} =$	2.877E+10 kgm ²
$B_{44} =$	4.987E+08 Ns/m	$B_{44} =$	1.117E+09 Ns/m

Table 7-3. Decay tests processed by the exponential fitting method

But of course there is a drawback to this method as well. It only represents the damping in equivalent terms (though more precisely) but loses advantage compared to the linear plus quadratic (or similar) presentation which is more in the nature of nonlinear damping behavior. The nonlinear damping model as already stated can be suitably implemented in any seakeeping code to account for the roll response both in regular and irregular waves.

7.2.2 Summary of the results: Discussion and doubts

The results of the first set of experiments are systemized and crosschecked for the purpose of comparison and validation of the proposed methods. The results corresponding to the TESTS 302-307 as a function of the ship speed in figure 7-10 are presented in terms of the equivalent linear damping as oppose to the usual presentation in terms of non dimensional damping. The reason being is that those values are directly inputted into the ship motions program and thus easier to manipulate.

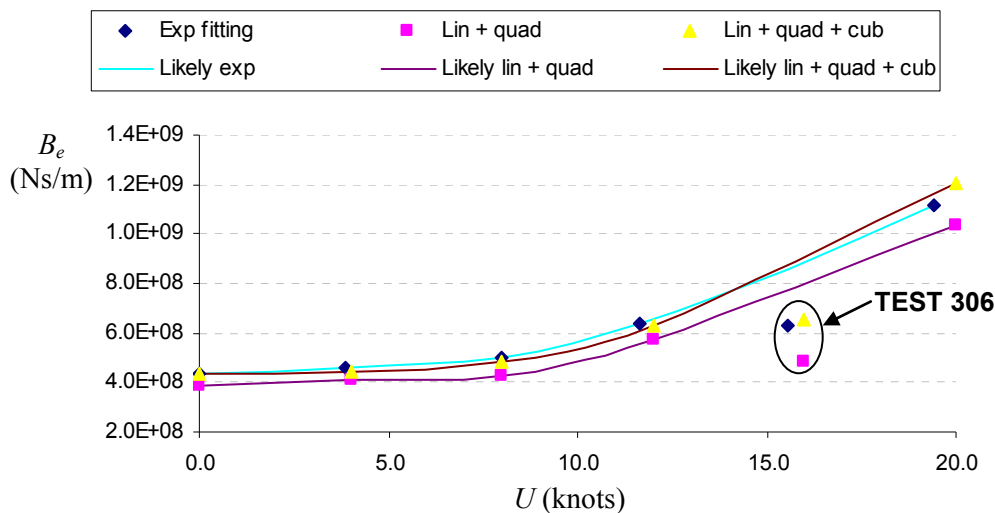


Figure 7-10. Comparison of results by utilizing different models for decay tests 302 to 307

However, for the scope of the work it could be presented in a more traditional way. There were total of 6 tests performed by varying model speed. The aim was to obtain damping coefficients for the remaining speeds which can be suitably implemented into the seakeeping code to assess the rolling amplitude responses especially for the parametric rolling conditions. As seen from the figure 7-10 all the tests apart from TEST 306 (16 kts) are corresponding to the theoretical predictions, i.e. damping is increasing with the increment of speed. Since there were three models implemented for the damping assessment and all are pointing the same it can be concluded that the TEST 306 was for some reason messed up. As such, it will be discarded from subsequent analysis. This is why the curves from the figure 7-10 are referred to as “likely” since the term “fitting” which would more acceptable didn’t include TEST 306.

The figure shows very good agreement between all models utilized. In particular, linear plus quadratic plus cubic model compared with the exponential fitting model are almost overlapping. The linear plus quadratic model although simpler in nature comes within 10% of the results obtained from the other two models. It has to be said that the results based on the "classical" way of analyzing roll decay curves by means of the so called decrement curve highly depend on a preliminary visual observation of the experimentally obtained curves of the amplitude dependent equivalent linear damping $\nu_{eq,i}$. For the two classical ways a Roberts procedure was implemented to remove mean drift and although it is a very common procedure one could argue it is still the tempering of the original signal. However, using the Roberts procedure enhanced the performance of the classical models for more than 15%.

Furthermore, looking back at the entire sets of tests processed clearly shows unusual behavior at the beginning tail of the curves (figures 7-3 and 7-6) associated with the low amplitude responses based on the experimental data. For this reason alone a standardized procedure of neglecting peak amplitudes lower than 2° is an absolute necessity. Still one has to be careful not to cut the signal too short, consequently subduing the information related to the nonlinear behavior of the damping process.

From all the literature survey nothing similar was traced. The first assumption as already stated involved a possible existence of the additional bearing damping so called Coulomb force which is in phase with roll velocity. The physical consequences on the outcome of the experimentally obtained curves of the equivalent linear damping coefficient $\nu_{eq,i}$ to be associated to A_i would be logical since the bearing damping affects the lower amplitudes more. This is due to the fact that the ship oscillates with the reduced roll velocity at the smaller peak angles (for instance as it stops at the peak value of 2° it doesn’t have the same momentum as the 16° while it accelerates on the other side). Meaning the additional bearing damping generated in this range of amplitudes is more difficult to overcome. However, the basin provided the assurance that this effect can be considered as negligible. Nevertheless, as evidenced from the curves it would appear that damping associated with the low amplitudes is unreasonably high. Looking at it the other way, one could argue that the values associated with the absolute amplitudes in range of 3° to 7° are severely underestimated. As a pure speculation, it may be interpreted as a pure loss of stability in that range of inclination (underestimated damping) associated with specific hull form (pronounced bow flare, flat transom stern and nonvertical ship sides near the waterline) of the C11 post-Panamax containership. Such ships have wide deck beam to store large number of containers and in the same time, the underwater hull is streamlined to minimize the resistance (Prpić-Oršić et al. 2007).

The fundamental dynamics that create this kind of behavior is considered as reasonably clarified mostly associated with restoring term but the sudden loss of damping as the vessel reaches roll angles of approximately 5° could shed more light at the problem as well. A possibility that the ship loses “damping ability” due to its uncharacteristic and novel form could certainly exist and it would trigger the excessive roll motion even stronger. It is highly unlikely that all tests are being mishandled while executed. This is definitely another aspect that needs to be investigated in the aftermath.

A suggestion would be to perform forced oscillation tests but not on the ship in the upright position but inclined up to suspect angles. The suspicion raised can also be eased with the additional decay testing (not likely) or by analyzing decay records from other ships for the sake of verifying the procedure. To conclude this part a choice of the type of the model to account for the extrapolation outside of the tested range from decays associated with typical parametric rolling amplitudes has to be elaborated. A linear + quadratic model was assumed not because it is the easiest to implement while modifying the numerical model of the ship motions, but because the experimental data is showing a linear asymptotic tendency at large rolling amplitudes for the equivalent linear damping coefficient $\nu_{eq,i}$.

On the contrary, for the linear + quadratic + cubic model the use of a cubic damping coefficient leads to a significant growth of damping as the amplitude of roll increases. It could be stated that, apart from the very last peak, the quantity $\Delta\eta_4/\eta_{4m}$ is going to infinite as it moves towards small amplitudes, and this still indicates some dry friction effect in the bearings as discussed (ruled out by the basin). It can be seen that $\Delta\eta_4/\eta_{4m}$ is not linear, therefore a linear + quadratic damping model is not applicable due to the odd behavior at small (actually not very small) rolling amplitudes. Still with the possibility of tuning the model (certain amount of practical experience) to the results of the other two models and with better extrapolation capabilities as elaborated it seems as a right choice. However, without the possibility of tuning the linear + quadratic model it is highly advisable that an alternative scheme is deployed.

Another reason for its implementation lies on the fact that an overestimation of the roll damping from model experiments could cause an underestimation of the actual rolling amplitude of the ship, with obvious consequences regarding the actual level of safety of the vessel. Considering worse case scenario and the lowest values obtained for this type of the model it is advisable to be on the safe side especially dealing with this number of uncertainties encountered along the analysis process. Using the linear + quadratic model a separation of the linear and quadratic coefficients enables enhancement of the damping prediction. Normally, a damping coefficient is utilized by its equivalent term obtained from Ikeda's method or similar, but with the dispose of the decay tests it's possible to treat it in its nonlinear nature. Therefore, an assessment of both the linear and quadratic contributions for the entire range of speeds of interest is presented on figures 7-11 and 7-12.

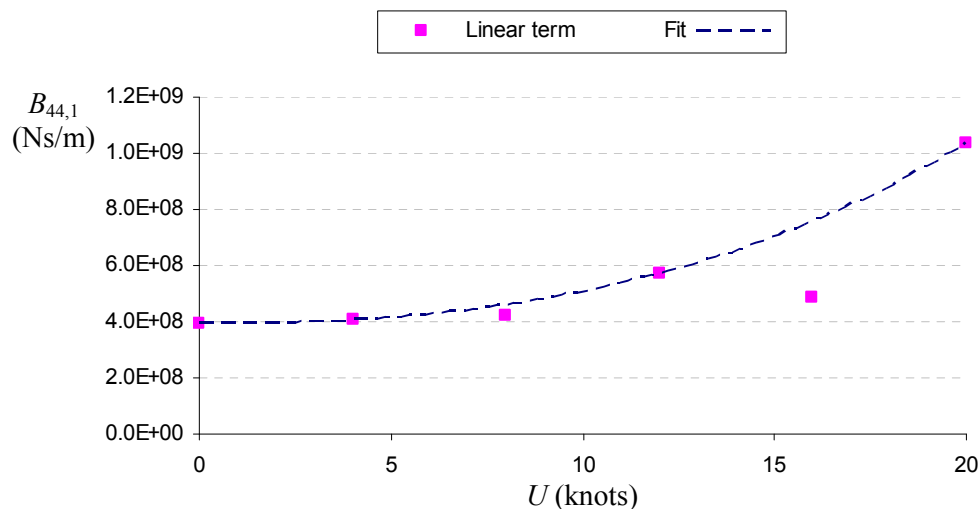


Figure 7-11. Evaluation of the linear component of damping for all speeds using decay tests 302 to 307

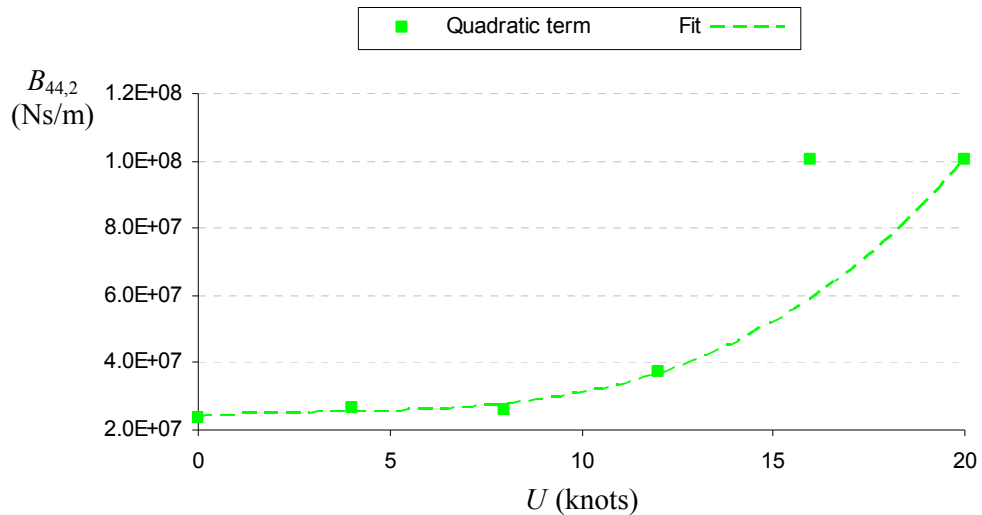


Figure 7-12. Evaluation of the quadratic component of damping for all speeds using decay tests 302 to 307

Note that term “linear” brings linear contribution to damping within the ship motion realizations (contribution) but not necessarily associated to the ship speed although a slight linearity (weakly nonlinearity would be more appropriate) is noticeable. Quadratic contribution is more assertive with the increase of the ship speed. As before, TEST 306 was discarded from the analysis.

To sum it up, it is believed that this may be the best solution based on the unorthodox readings from the decay data and at this point will serve the purpose.

7.3 Decay tests processing for the second group of decay tests with different loading condition

After performing calculations for all three models scattering of data is very evident as oppose to, for instance, TEST 302 (figure 6-10). This can be illustrated especially when using linear + quadratic + cubic model as seen in figure 7-13.

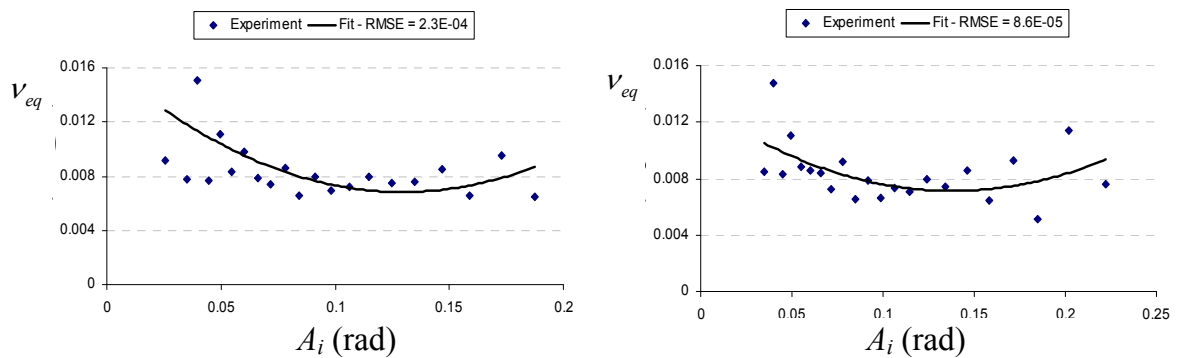


Figure 7-13. Linear + quadratic + cubic model for decay test “DECAY_TEST_GM1_U=0 knots” for both runs (Test 1 and Test2)

As previously mentioned, a chance of the test repetition is of extreme importance in such cases, and a possibility to aggregate as many data as possible for the roll decays performed for each model / condition actually should be considered almost obligatory. An example of the aggregated data analysis is shown on the next figure (7-14). The importance of having a second signal released at higher inclination is evident as it gives a better capability for the extrapolation prediction. Furthermore, a suspect data acquisition marked on the figure is practically repeated in the next test, making it very plausible.

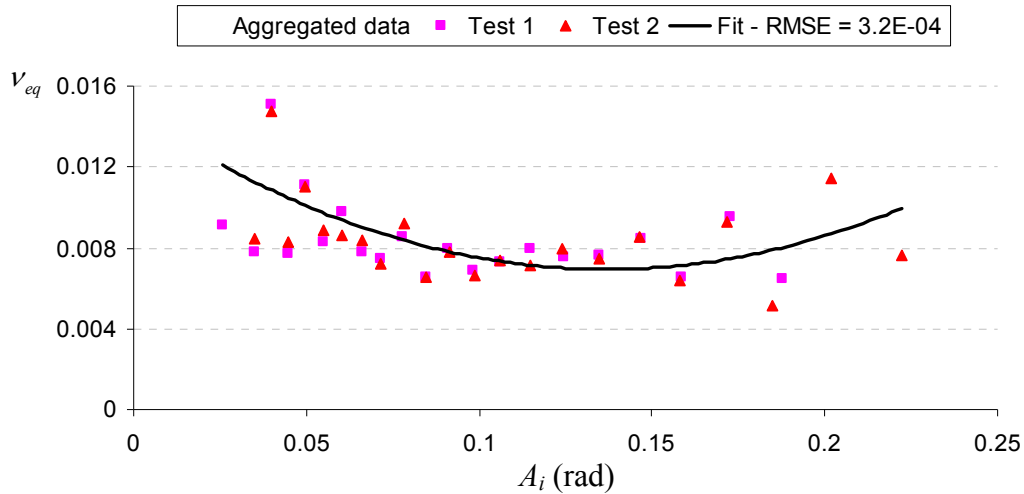


Figure 7-14. Linear + quadratic + cubic model for decay test “DECAY_TEST_GM1_ U=0 knots” by aggregating data from both runs

The next test was performed at a speed of 8 knots “DECAY_TEST_GM1_ U=8 knots” and 3 tests were repeated (technically 2 and a half since the last was aborted at the end). The figure 7-15 is giving a better indication on the stated.

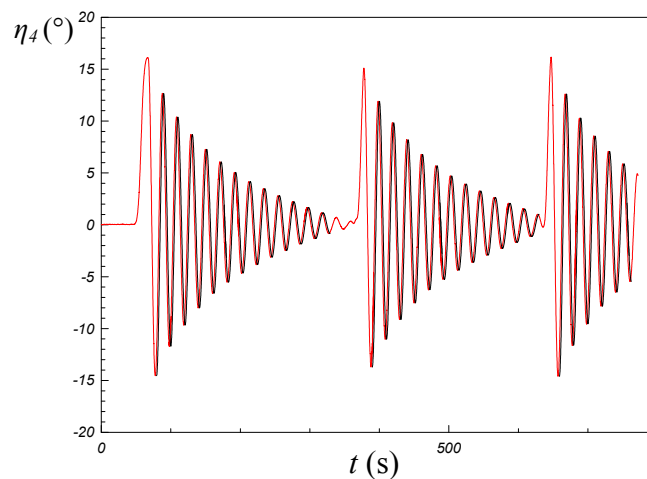


Figure 7-15. Time trace of decay test for 8 knots with filtering

Following figures (7-16 and 7-17) are showing a linear plus quadratic plus cubic model for the aggregated data for the first two tests and for the all three, respectively.

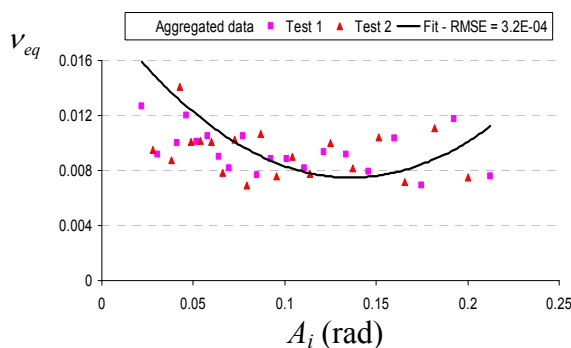


Figure 7-16. Linear + quadratic + cubic model for decay test by aggregating data (first 2 runs)

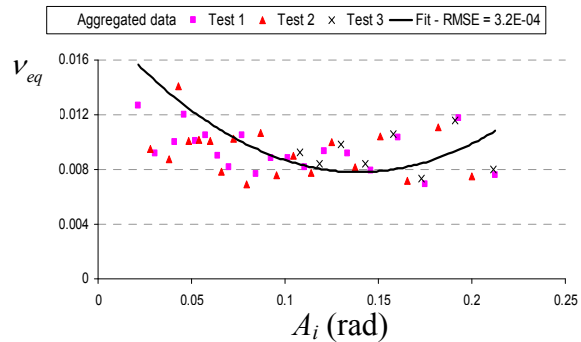


Figure 7-17. Linear + quadratic + cubic model for decay test by aggregating data (all 3 runs)

It is important to emphasize the importance of the data collection especially when investigating extrapolation capabilities of the models. It has been decided to use an analysis technique based on the determination of the roll amplitude dependence of the roll damping and oscillation

frequency by means of the so-called roll-decrement curve, namely because of the aggregation of different decays for each condition. The linear equivalent damping coefficient $\mu_{eq}(A)$ was calculated under the approximation that the undamped ($\omega_{0,eq}(A)$) and the damped ($\tilde{\omega}(A)$) amplitude dependent roll frequency were not significantly different. Strictly speaking a non-dimensionalization based on $\omega_{0,eq}(A)$ would be physically more consistent however, in the framework of the following analysis, the use of ω_0 was considered to be more effective for the presentation and the use of the results.

$$\begin{aligned} \nu_{eq} &= \nu + \frac{4}{3\pi} \cdot \alpha \cdot (\tilde{\omega}(A) \cdot A) + \frac{3}{8} \cdot \beta \cdot (\tilde{\omega}(A) \cdot A)^2 \approx \\ &\approx \nu + \frac{4}{3\pi} \cdot \alpha \cdot (\omega_{0,eq}(A) \cdot A) + \frac{3}{8} \cdot \beta \cdot (\omega_{0,eq}(A) \cdot A)^2 \end{aligned} \quad (7-28)$$

The 3rd test by itself doesn't "say" much but the influence of the linear equivalent damping coefficient $\nu_{eq}(A)$ assessment based on the shortened third signal (higher amplitudes) is evident when comparing the curves for the aggregated data of the first two tests as oppose to all three (figure 7-18).

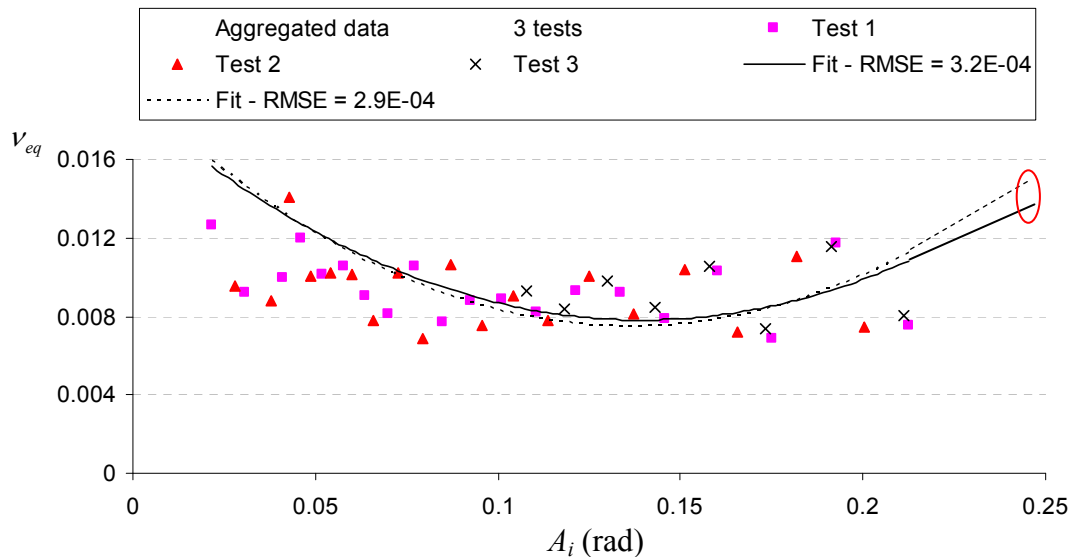


Figure 7-18. Linear + quadratic + cubic model for decay test by aggregating data (8 knots)

As visible from the figure a marker is showing a substantial difference in the expected values at the end tail of the linear equivalent damping coefficient $\nu_{eq}(A)$ outside the range of tested rolling amplitudes. It's possible to have an estimation of the prediction bounds for the fitting, i.e. a quantification of the residual dispersion of experimental data with respect to the assumed model, but once again better types of modeling should be sought in bare hull condition in order to avoid unreasonable increases of damping at large rolling angles with the consequent underestimation of roll amplitude at peaks.

Additional tests on the same line of those reported in this work should be carried out to reach a definite conclusion.

Finally a presentation of the results indicates the analogy to the tests elaborated before. An example of the two tests for DECAy_TEST_GM1_ U=0 knots is given in the following table 7-4 with linear plus quadratic model.

test1				test2			
Linear+Quadratic Model test1				Linear+Quadratic Model test2			
I44+A44 =	1.79E+10	I44 =	10952125920	I44+A44 =	1.79E+10	I44 =	10952125920
m =	76056430	77957400		m =	76056430	77957400	
GMt =	1.973			GMt =	1.973		
w =	0.286693748	0.2855993		w =	0.286693748	0.2855993	
T =	21.91601792	22	Assuming	T =	21.91601792	22	Assuming
		I44+A44 =	1.80E+10			I44+A44 =	1.80E+10
2miu =	1.35E-02	a1 =	7.41E-02	b44_1 =	2.41E+08	2miu =	1.36E-02
alpha =	9.18E-04	a2 =	1.22E-03	b44_2 =	1.64E+07	alpha =	9.12E-04
Check				Check			
B44_eq =	2.43E+08	Assuming	0.350408 = phi_m	B44_eq =	2.45E+08	Assuming	0.350408 = phi_m
B44_cr =	1.03E+10			B44_cr =	1.03E+10		
xsi =	2.35E-02			xsi =	2.38E-02		
U= 0.0 m/s				U= 0.0 m/s			
B44_eq =	2.43E+08			B44_eq =	2.45E+08		
b44_2 =	16435475.07			b44_2 =	16341161.01		
b44_1 =	2.43E+08			b44_1 =	2.45E+08		
Parameter	Uncertainty			Parameter	Uncertainty		
A(1) =	.000000	.000000		A(1) =	.000000	.000000	
A(2) =	.074476	.000000		A(2) =	.078477	.000000	
A(3) =	.001217	.000394		A(3) =	.000654	.000539	
A(4) =	.000000	.000000		A(4) =	.000000	.000000	
Chi-squared =	.351215E+02			Chi-squared =	.721604E+01		
Full covariance matrix				Full covariance matrix			
.00E+00	.00E+00	.00E+00	.00E+00	.00E+00	.00E+00	.00E+00	.00E+00
.00E+00	.00E+00	.00E+00	.00E+00	.00E+00	.00E+00	.00E+00	.00E+00
.00E+00	.00E+00	.16E-06	.00E+00	.00E+00	.00E+00	.29E-06	.00E+00
.00E+00	.00E+00	.00E+00	.00E+00	.00E+00	.00E+00	.00E+00	.00E+00
Damping coefficients				Damping coefficients			
Linear term =	1.359362E-02			Linear term =	1.432382E-02		
Quadratic term =	9.124043E-04			Quadratic term =	4.907430E-04		
Cubic term =	0.000000E+00			Cubic term =	0.000000E+00		
Kapa = B44/B44cr	2.370646E-02			Kapa = B44/B44cr	2.497988E-02		

Table 7-4. Linear + quadratic model for decay test (8 knots)

The results from test 2 are indicating slightly larger values of the equivalent damping, as expected from a decay test which is released less then couple of degrees higher then the first. The results for the test DECAy_TEST_GM1_U=8 knots are not given in detail here. A summary and comparison between all methods is present in table 7-5. While the results are already showing good correspondence with the implementation of the Roberts procedure one could expect even better agreement.

Test DECAy TEST GM1 U=0 knots			Test DECAy TEST GM1 U=8 knots		
Natural Period		21.915 s	Natural Period		21.76 s
Non dimensional Damping		0.0274	Non dimensional Damping		0.0301
$\omega =$		0.287 rad/s	$\omega =$		0.289 rad/s
$I_{44}+A_{44} =$		1.791E+10 kgm ²	$I_{44}+A_{44} =$		1.766E+10 kgm ²
Lin + Quad	B ₄₄ =	2.431E+08 Ns/m	Lin + Quad	B ₄₄ =	2.791E+08 Ns/m
Lin + Quad + Cub	B ₄₄ =	2.613E+08 Ns/m	Lin + Quad + Cub	B ₄₄ =	2.883E+08 Ns/m
Exponential	B ₄₄ =	2.814E+08 Ns/m	Exponential	B ₄₄ =	3.069E+08 Ns/m

Table 7-5. Comparison of equivalent linear damping using all three models

7.4 Decay tests processing for the third group of decay tests with different loading condition

An example of the impropriety of the usage of any of the “classical” means of decay processing techniques for the decay tests in waves is evident in the results for test 470 on the following figure 7-19.

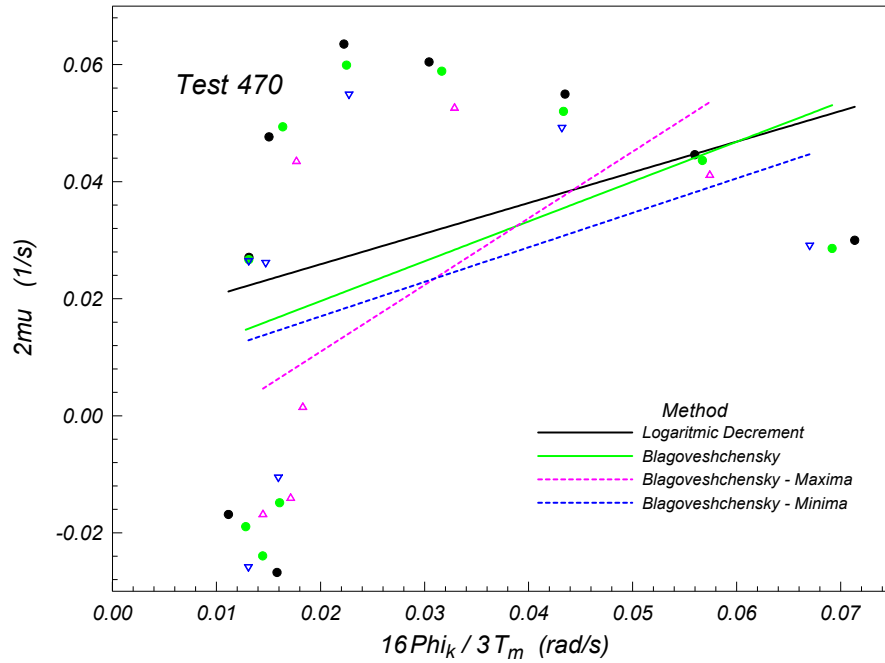


Figure 7-19. Linear + quadratic model for decay test 470

However, using an exponential fitting function considering full time series makes it possible to identify the rate of decay. In the following table 7-6, the results are presented for the four different tests. The results will be implanted in the seakeeping code based on the exact conditions for which decay tests in waves were conducted.

Test 468		Test 471	
Natural Period	19.487 s	Natural Period	21.748 s
Non dimensional Damping	0.0433	Non dimensional Damping	0.0339
$\omega =$	0.322 rad/s	$\omega =$	0.289 rad/s
$I_{44}+A_{44} =$	1.416E+10 kgm ²	$I_{44}+A_{44} =$	1.764E+10 kgm ²
$B_{44} =$	3.954E+08 Ns/m	$B_{44} =$	3.455E+08 Ns/m
Test 470		Test 472	
Natural Period	22.173 s	Natural Period	24.412 s
Non dimensional Damping	0.0956	Non dimensional Damping	0.0442
$\omega =$	0.283 rad/s	$\omega =$	0.257 rad/s
$I_{44}+A_{44} =$	1.833E+10 kgm ²	$I_{44}+A_{44} =$	2.222E+10 kgm ²
$B_{44} =$	9.933E+08 Ns/m	$B_{44} =$	5.056E+08 Ns/m

Table 7-6. Summary of all decay tests in waves with equivalent linear damping obtained by exponential fitting

7.5 Comparison between numerical model and experiments

The last part of the damping analysis concerns the validation of the numerical results versus experimental. So far there have been very few attempts to incorporate the effects of nonlinear damping into analytical model to predict roll motion amplitude. Many researchers have attempted to evaluate the effects of non-linear damping using complex time simulations which is very time consuming and does not help in understanding the behavior of the non-linearity throughout the entire domain. With hypothesis that using the seakeeping code developed and with its robustness and effectiveness one could tackle before mentioned shortcomings. On the other hand, due to the fact that strip theory calculation method utilized in these circumstances (usually limited to small angles) may be pushed far beyond its generally accepted limits of applicability, one could argue and raise the

global level of uncertainty involved in the complete procedure for the determination of roll damping, mainly due to:

- availability of an “adequate” motion calculation routine capable of predicting the time domain large amplitude responses under resonant conditions which has a strong dependence on roll damping characteristics of the vessel,
- quality of the obtained measurements which is also of major concern with the planned public dissemination of the measurements and the most effective use of them since it is quite easy to have a good measure of angular velocity, but it is not easy to have a good measure of the angle by means of non intrusive method.
- uncertainty associated to the methodology of analysis of the obtained data. This is probably one of the major sources of uncertainty. Here we should also include the fact that the analytical models used to represent the dissipation mechanism of roll damping have unavoidable limitations and cannot completely explain the behavior of the experimental results,
- proposition of the damping correction applied to the numerical code cross-referenced to the available experimental data. On the other hand some of the hypotheses on which such correction is based have been questioned but still logically explained and implemented. However, it is probably worth trying to develop a more sound and robust methodology for the roll damping assessment.

Based on the experimental data using the first group of tests in calm water (TESTS 302-307) the following can be presented (figure 7-20),

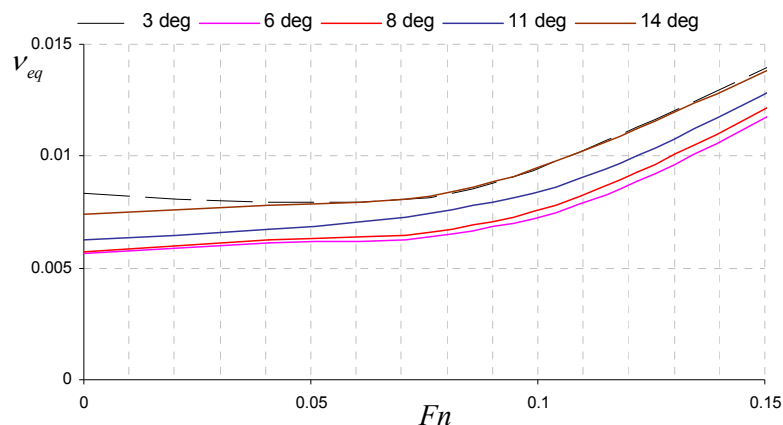


Figure 7-20 Equivalent linear damping $v_{eq}(A)$ using the linear + quadratic + cubic model

Note that the values of equivalent linear damping $v_{eq}(A)$ are extracted using the linear + quadratic + cubic model from each test corresponding to the forward speed increment. The reason being is an attempt to validate or even up to extent tune numerical model based on Ikeda’s method from the inner part of the tested range. As already stated chosen model enables better approximation and more precise fitting based on the known experimental data. Roll decrement tests were conducted with initial inclinations of less than 20° and since the first half cycle has been neglected for a series of reasons previously explained the only deterministic range of roll amplitudes is effectively less than 15° . Prediction of the fore tails of the curves at large rolling amplitudes is governed by the a-priori selection of the damping model (this time linear plus quadratic model was chosen) showing a linear asymptotic behavior for the equivalent linear damping coefficient. However, since this represents the domain associated with the extrapolation capabilities of a chosen model it is essentially uncertain. Thus, it may be advisable that the comparison between numerical model and experiment for the validation purposes should be restricted for the specified range of roll amplitudes ($<15^\circ$) where an additional cubic term is necessary to reproduce $v_{eq}(A)$ in bare hull condition.

As seen from figure 7-20 the values of equivalent linear damping corresponding to the roll amplitudes of each test associated with the forward speed (upon which are conducted) is given. What

is clearly visible is a significant overestimation of the damping for the small roll angles as already reported. Based on those readings the values of damping for the angles of 3° and 14° would practically be the same. An attempt to interpret the results was already made while discussing calm water tests stating the unorthodox behavior of the decay rate realization associated to the small roll amplitudes. However, as these statements were presented similar report was found by Hashimoto and Umeda, (2010). They conducted forced roll model test and compared it with those by a conventional roll decay model test and the Ikeda's semi-empirical prediction method using two post-panamax containers, one having almost the same principal dimensions albeit with the bilge keel installed. Similar from the reported here, roll damping estimated from the roll decay test is significantly overestimated for small roll angle and is slightly underestimated for large roll angle. However they failed to provide any explanation only expressing certain doubts with the results obtained. Bearing in mind that the bilge keel suppresses the nonlinearity of damping rate this behavior is even more evident in the case of bare hull condition. Still, a similar report as such, clearly eliminates any doubts as to validity of the tests conducted leaving one with the task of explaining such phenomenon.

Figure 7-21 represents the same but with the broader range of speeds with the inclusion of the additional curve with respect to damping associated to the roll amplitude of 17° . The chosen angle is deterministically available only for the TESTS 302 and 303 since they were conducted roughly from the same available inclinations while the other tests needed an extrapolation of the analytical model.

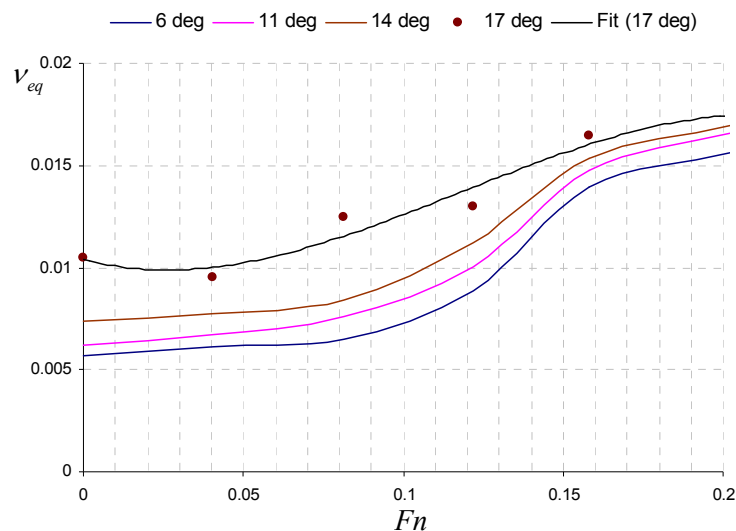


Figure 7-21. Equivalent linear damping $v_{eq}(A)$ using the linear + quadratic + cubic model up to 17°

It can be concluded that the fitted values of the equivalent linear damping for the roll amplitude of 17° obtained partly from the available experimental range and partly using extrapolation capabilities of a chosen linear plus quadratic model with respect to its linear asymptotic behavior agree quite nicely with the trend of other curves. From the reported graphs it can be said that the two methods applied are equivalent from an engineering point of view, and the differences for the linear damping coefficient and the natural frequency are negligible.

Better agreement is expected for smaller initial heeling angle cases, as one expects taking in mind the fact that approximate solutions usually work well for small nonlinearities and small amplitude of motion thus not extrapolating to far out of tested range of amplitudes. To be more assertive with the conclusions, tests with significantly larger roll angles are necessary. Anyway such large amplitudes are not common in free decay tests and the parameters obtained in these cases should also be treated with attention. Moreover, when large amplitudes motion is considered, a procedure based on a forced roll experiment is more suitable.

The experimental results are cross referenced to the numerical model based on the modified Ikeda's method. Keeping in mind the fact that those tests are conducted in calm water and since the developed model is intended as new module to the existing ship motions program the input data

differs from the originally Ikeda's procedure. More specifically, instead of natural roll frequencies the procedure takes into account frequency dependence between the ship and encountering waves. For that purpose calm water tests in numerical model are approximated with wave length over ship length ratio $\lambda/L_{pp} = 100$. As seen on figure 7-22 the code was validated by performing calculations for the headings 0° and 180° , respectively. Since there is no wave which makes the heading irrelevant, the intention was to check the values of the equivalent linear damping for both. Using the radiation damping, B_{w0} obtained from the strip theory it is evident that the curves are virtually overlapping. Comparison to the experimental results shows that the values for zero speed matches perfectly while with the speed increase the results from the Ikeda's method slightly overestimates damping especially in the higher range of speeds ($Fn > 0.15$). Furthermore, its accuracy becomes worse when the Froude number becomes large (reported also in Hamamoto, 2010.). This might be because the roll damping with the roll decay test is determined not only for a steady rolling but also for transiently decaying rolling. The encouraging results were solidified when the calculation is made for the more realistic conditions leading to the parametric rolling. A suspicion has been raised whether the decay tests and its implementation could suitably represent actual conditions. Thus, the remaining two curves are presented for the $\lambda/L_{pp} = 1$ and $\lambda/L_{pp} = 1.2$, respectively. As evident, the curves (figure 7-22) possess a characteristic "bump" in the range of 6 to 13 knots, associated with the radiation component which is to be expected due to encounter with the waves. Those realistic outcomes are highly favorable as a mean of damping characteristic of the roll motion while in parametric resonance. What was expected from the numerical model was in a way accomplished since the "resonant damping" has to be able to steady the transient motion in rational real time simulations.

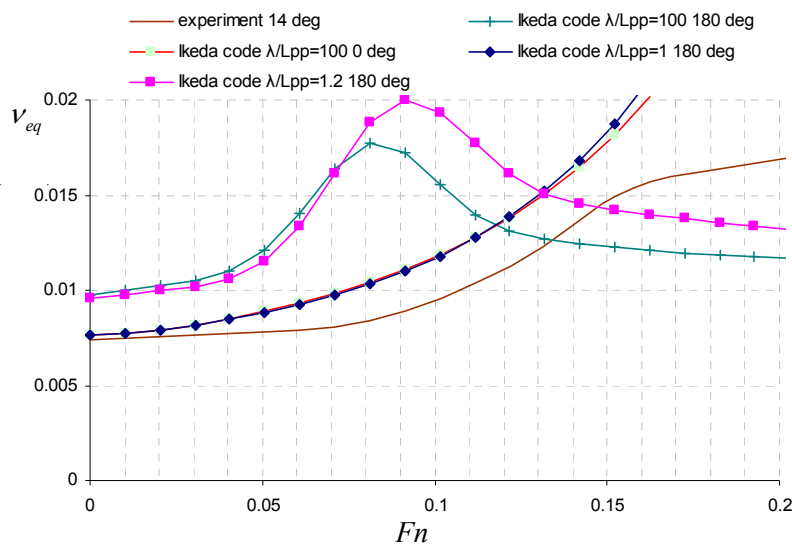


Figure 7-22. Equivalent linear damping $v_{eq}(A)$ for 14° compared to numerical model

If a hypothesis holds true that the numerical model is verified for the deterministic range of the roll amplitudes from the decay tests, the same has to be examined for the large angles typically occurring during the parametric rolling.

While in the former case the results from the decay tests are explicitly known (they still depend on the chosen model), the values of the equivalent linear damping for the large angles are highly sensitive to the extrapolation capabilities of the analytical model. Sometimes the best way to choose a model is from a preliminary visual observation of the experimentally obtained curves.

The results presented in the following figure 7-23 correspond to the same conditions but for the roll amplitude of 30° .

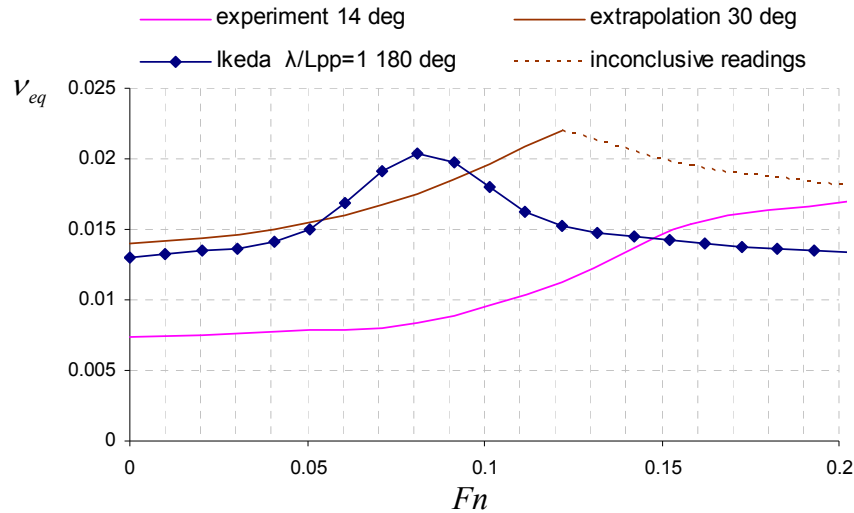


Figure 7-23. Equivalent linear damping $\nu_{eq}(A)$ for 30° compared to numerical model

Using the linear plus quadratic model and its applicability corresponding to the asymptotic linear behavior of the fore end of the decay curves a fairly good agreement is noticeable. However, since the TEST 306 corresponding to the 16 knots is discarded and the results from the TEST 307 (20 knots) are ambiguous, the dotted line emphasizes the inconclusive readings for that range as the values for the $\nu_{eq}(A)$ appear to be severely underestimated once compared to the 14° decay record. Yet, what can be affirmed as the most important finding is that the values obtained are in general quite concurring and thus applicable to the seakeeping model.

While in a way we can defend the absence of the decay tests for larger initial heeling angles the lack of tests with the bilge keel installed really “hurts” the validation of the numerical model. A systematic investigation and comparison of the damping results with bilge keel from the newly found Hamamoto et. al. 2010, is planned in the aftermath.

On the other hand, for the parametric rolling validation the decay tests should be considered with caution because they are to some extent governed by so called “resonant damping”. Therefore, the last group of tests conducted in waves will be collated to the existing numerical model. As indicated, the tests undergone in the pure parametric condition make it impossible to unveil the decay rate associated with the given condition. For that reason tests corresponding to similar conditions using exponential fitting function for the approximated decay curve full time series are considered as acceptable. One has to wonder about the results from the procedure because in order to capture the motion in waves 3DOF would have to be utilized.

As seen from the table 7-7, tests 470 and 471 although operated at similar conditions with the difference in the encounter period (marked on table 7-7) provided very distant expected values of B_{44} . This by itself indicates inconsistency in the procedure as stated by Bulian (2006), among others. Such tests are not conducted very often because of uncertainties involved. As reported from Lin et al. 2008, even if a damping coefficient could be measured from the amplitude variation in specified incident waves, the results are indefinite. The numerical model almost doubles the values of B_{44} . The trend for the test 472 is the same.

Test 470		Test 471	
Natural Period	22.173 s	Natural Period	21.748 s
Non dimensional Damping	0.0956	Non dimensional Damping	0.0339
$\omega =$	0.283 rad/s	$\omega =$	0.289 rad/s
$I_{44}+A_{44} =$	1.833E+10 kgm ²	$I_{44}+A_{44} =$	1.764E+10 kgm ²
$B_{44} =$	9.933E+08 Ns/m	$B_{44} =$	3.455E+08 Ns/m

Table 7-7. Equivalent linear damping for test 470 and 471

Results are quite fuzzy, and a definite conclusion on its suitability cannot be drawn but further investigation should provide more answers. Utilizing decay tests in calm water is still considered as a standard procedure although it comes with considerable limitations as well, but this approach is taken as a mean of treating nonlinear damping characteristic during parametric rolling simulations for the validation of the seakeeping code presented in the next chapter. With the quadratic assumption of the nonlinearity in the damping application, it will be interesting to see the effect it has in the resonant zone.

8 Analysis of parametric rolling experiments

8.1 Parametric rolling in regular waves with experimental validation

The analysis of the results obtained from the regular waves experiments and comparisons to the numerical are presented in scope of this section. A total of twelve tests were carried out for the above mentioned condition and the complete list of results is summarized in table 8-1.

Test N°	λ/Lpp	H_w (m)	T_w (s)	V (kts)	Roll Angle exp (°)	Roll Angle num (°)
5	0.8	6	11.59	8.0	31.0	/
6	1	6	12.95	8.0	23.2	17.58
7	1.2	6	14.19	8.0	2.0	/
8	1.4	6	15.33	8.0	0.5	/
9	0.8	8	11.59	8.0	32.8	/
10	1	8	12.95	8.0	25.0	45.04
11	1.2	8	14.19	8.0	1.7	/
12	1.4	8	15.33	8.0	0.8	/
13	0.8	10	11.59	8.0	35.7	11.57
14	1	10	12.95	8.0	27.3	/
15	1.2	10	14.19	8.0	1.3	/
16	1.4	10	15.33	8.0	0.6	/

Table 8-1. The results for regular waves at 180° heading

As noticeable, the figure 6-17 corresponds to the test number 6 which represents the condition where parametric rolling is likely to occur. A roll angle of 23.2° has been obtained. Figure 6-18 presents the same settings with a wave height of 8 meters which has resulted in a 1.8° increase in the maximum roll angle.

Moreover, when the wave length to ship length ratio was kept at unity (tests 6, 10 and 14), increasing the wave height has lead to larger roll angles. As confirmed by other experiments, this trend would continue until a certain threshold limit is reached.

The numerical results were compared with the experimental ones. It was found that the agreement between those results is not quite acceptable however the fact that parametric rolling is reproduced makes it more compelling. The problem with the code implementation notwithstanding the degree of nonlinearity selected is that the parametric rolling for wave heights of 10 m is effectuated at higher range of speed starting from 12 knots as seen on table 8-2. This is not quite in line with the experiment but is with the report from France, et al., 2003. The wave height has to be large enough to put parametric excitation above the threshold and still be realistic enough to be encountered during a severe storm. The wave height of 10 m seems to be the threshold value upon which the expected growth of roll amplitudes cannot be fully facilitated using this strip theory approach, in other words certain threshold limit is reached too soon.

Folder destination	speed (kts)	heading	λ/Lpp	height	roll amplitude	roll amp. rounded	B44 Ikeda	indication
..lc11ext\TDM\Speed_13_kts\Heading_180\LvoLpp_1.00\H_10	13.00	180.00	1.00	10.00	5.49	5.00	482000000.00	+
..lc11ext\TDM\Speed_14_kts\Heading_180\LvoLpp_1.00\H_10	14.00	180.00	1.00	10.00	21.35	20.00	652000000.00	+
..lc11ext\TDM\Speed_15_kts\Heading_180\LvoLpp_1.00\H_10	15.00	180.00	1.00	10.00	18.05	20.00	653000000.00	+
..lc11ext\TDM\Speed_16_kts\Heading_180\LvoLpp_1.00\H_10	16.00	180.00	1.00	10.00	14.35	10.00	554000000.00	+
..lc11ext\TDM\Speed_17_kts\Heading_180\LvoLpp_1.00\H_10	17.00	180.00	1.00	10.00	9.53	10.00	561000000.00	+

Table 8-2. The results of numerical simulations for regular waves at 180° heading for $H_w = 10m$

Since there was a relatively big difference of roll amplitude η_4 of about 20° observed for the “test No. 10” being case study scenario, the analysis was focused starting from it. This was accounted for by the inability to collect and process the free roll decay tests at that time, which would give accurate assessment of the roll damping values. Special attention was therefore given to the

usefulness of the rolling model experiments to validate numerical prediction of roll damping and the obtained results did confirm it which will be shown further down.

Later on, frequencies were altered corresponding to wavelengths from $\lambda/L_{pp} = 0.8$ to $\lambda/L_{pp} = 1.4$ and tested at different wave heights assuming same velocities.

While reviewing the results obtained it was found that for the equivalent speed and similar conditions i.e. $T_W = 11.59$ s (wave length to ship ratio of 0.8), parametric rolling manifested its most prolific effect (tests 5, 9 and 13) with the roll amplitude in excess of 31.0° , unfortunately not reproduced by a numerical model. The summary for this set of conditions is presented in the following table 8-3.

Folder destination	speed (kts)	heading	λ/L_{pp}	height	roll amplitude	roll amp. rounded	B44 Ikeda	indication
..\c11ext\TDM\Speed_2_kts\Heading_180LvoLpp_0.80H_8	2.00	180.00	0.80	8.00	39.41	40.00	929000000.00	+
..\c11ext\TDM\Speed_3_kts\Heading_180LvoLpp_0.80H_8	3.00	180.00	0.80	8.00	20.14	20.00	577000000.00	+
..\c11ext\TDM\Speed_4_kts\Heading_180LvoLpp_0.80H_8	4.00	180.00	0.80	8.00	17.14	20.00	597000000.00	+
..\c11ext\TDM\Speed_5_kts\Heading_180LvoLpp_0.80H_8	5.00	180.00	0.80	8.00	13.67	10.00	422000000.00	+
..\c11ext\TDM\Speed_6_kts\Heading_180LvoLpp_0.80H_8	6.00	180.00	0.80	8.00	5.20	5.00	352000000.00	+
..\c11ext\TDM\Speed_2_kts\Heading_180LvoLpp_0.80H_10	2.00	180.00	0.80	10.00	35.20	40.00	929000000.00	+
..\c11ext\TDM\Speed_3_kts\Heading_180LvoLpp_0.80H_10	3.00	180.00	0.80	10.00	45.74	40.00	962000000.00	+
..\c11ext\TDM\Speed_4_kts\Heading_180LvoLpp_0.80H_10	4.00	180.00	0.80	10.00	44.46	40.00	984000000.00	+
..\c11ext\TDM\Speed_5_kts\Heading_180LvoLpp_0.80H_10	5.00	180.00	0.80	10.00	43.24	40.00	1000000000.00	+
..\c11ext\TDM\Speed_6_kts\Heading_180LvoLpp_0.80H_10	6.00	180.00	0.80	10.00	18.83	20.00	637000000.00	+
..\c11ext\TDM\Speed_7_kts\Heading_180LvoLpp_0.80H_10	7.00	180.00	0.80	10.00	15.38	20.00	674000000.00	+
..\c11ext\TDM\Speed_6_kts\Heading_180LvoLpp_0.80H_10	8.00	180.00	0.80	10.00	11.57	10.00	543000000.00	+

Table 8-3. The results of numerical simulations for regular waves at 180° heading for $T_W = 11.59$ s

Although it does resemble the outcomes from the specific parametric condition for $\lambda/L_{pp} = 1$, especially in terms of the roll amplitudes and the distribution, whole realization is shifted toward lower velocities with the 8 knots actually being the first instance where the parametric excitation succumbs. Nevertheless, the simulations that were undertaken did approach the experimental results in a sense that it's usually only one immediate parameter, be it the velocity or the wave height, responsible for the extinction of this phenomena. In terms of realistic sailing condition whether it is 7 or 8 knots, wave height of 9 or 10 m, makes no big difference as oppose to the numerical model which is for now rather exclusive.

But overall, the numerical model dedicated to the assessment of the parametric rolling phenomena is very acceptable considering the assumptions and simplifications taken. This might appear very surprising because the Froude-Krylov approximation which is the base of the proposed numerical model is quite crude in terms of the fully nonlinear problem treatment. However, one should keep in mind that operating conditions leading to the parametric rolling are special (wave length approximately equal to ship length), heading is close to longitudinal seas, meaning that the contribution of diffraction and radiation forces is not very strong. Given those facts, the best performance is evident exactly for the $\lambda/L_{pp} = 1$.

This implies that the main wave effects are included in the incident wave field, rather correctly covered by the Froude-Krylov approximation. For that reason precisely, it is quite unrealistic to expect same kind of comparisons for different conditions associated with nonlinear contributions in which the Froude-Krylov force is not that dominant while other phenomena like diffraction or free surface nonlinearities (especially at quartering waves) are of more importance.

The numerical simulation systemized in table 8-4, shows that the parametric rolling is expected starting from 13 knots meaning the ship has to encounter incident (longer) waves at higher rate for the phenomena to begin.

Folder destination	speed (kts)	heading	λ/L_{pp}	height	roll amplitude	roll amp. rounded	B44 Ikeda	indication
..\c11ext\TDM\Speed_12_kts\Heading_180LvoLpp_1.20H_8	12.00	180.00	1.20	8.00	0.00	0.00	0.00	-
..\c11ext\TDM\Speed_13_kts\Heading_180LvoLpp_1.20H_8	13.00	180.00	1.20	8.00	0.03	0.00	0.00	-
..\c11ext\TDM\Speed_14_kts\Heading_180LvoLpp_1.20H_8	14.00	180.00	1.20	8.00	1.30	0.00	0.00	-
..\c11ext\TDM\Speed_15_kts\Heading_180LvoLpp_1.20H_8	15.00	180.00	1.20	8.00	42.92	40.00	830000000.00	+
..\c11ext\TDM\Speed_16_kts\Heading_180LvoLpp_1.20H_8	16.00	180.00	1.20	8.00	38.85	40.00	823000000.00	+
..\c11ext\TDM\Speed_17_kts\Heading_180LvoLpp_1.20H_8	17.00	180.00	1.20	8.00	19.19	20.00	667000000.00	+
..\c11ext\TDM\Speed_18_kts\Heading_180LvoLpp_1.20H_8	18.00	180.00	1.20	8.00	13.78	10.00	596000000.00	+
..\c11ext\TDM\Speed_19_kts\Heading_180LvoLpp_1.20H_8	19.00	180.00	1.20	8.00	8.31	10.00	603000000.00	+
..\c11ext\TDM\Speed_20_kts\Heading_180LvoLpp_1.20H_8	20.00	180.00	1.20	8.00	0.02	0.00	0.00	-

Table 8-4. Results of numerical simulations for regular waves at 180° heading for $T_W = 14.19$ s and $H_W = 8$ m

The importance of the results is such that it showed that the occurrence of parametric rolling depends on the wave period, the natural roll period, ship's forward speed and a threshold wave height

and thus ship operators should be aware of this risk and take precaution measures to reduce it. It is a complex recipe of factors, brewed in a cauldron of intangibles, and boosting the performance of the code is feasible within the better evaluation of the instantaneous hydrodynamic coefficients and with the damping refinement.

Following waves

A total of 8 tests for $GM_2 = 0.990$ m were carried out for the above mentioned condition and the complete list of results is summarized in table 8-5. Investigation of the conditions in which the parametric rolling occurs in regular following waves ($\beta = 0^\circ$, varying the ships speed and wave frequency (corresponding to a variable wavelength: first equal to 0.8 L_{pp} of the model and then increasing up to 1.4 L_{pp} , passing by the condition where the wavelength is exactly equal the L_{pp}) and different wave amplitudes as well. In the example below (table) the lowest GM value is indeed more inclined to yield parametric roll then the others do. A change in the GM value affects the natural roll period, which is one of the main parameters that will influence the risk of parametric roll (together with the encounter wave period, wave length, speed and roll damping).

Test N°	λ/L_{pp}	H_w (m)	T_w (s)	V (kts)	Roll Angle exp (°)	Roll Angle Num GM1 (°)	Roll Angle Num GM2 (°)
309	0.8	6	11.59	0.00	35.79	/	32.82
310	1	6	12.95	0.00	35.79	/	11.28
311	1.2	6	14.19	0.00	31.53	/	/
312	1.4	6	15.33	0.00	25.96	/	/
313	0.8	8	11.59	0.00	35.74	21.81	21.56
314	1	8	12.95	0.00	38.20	/	45.35
315	1.2	8	14.19	0.00	34.07	/	11.58
316	1.4	8	15.33	0.00	26.35	/	23.23
317	0.8	10	11.59	0.00	/	/	/
318	1	10	12.95	0.00	/	/	/
319	1.2	10	14.19	0.00	/	/	/
320	1.4	10	15.33	0.00	/	/	/

Table 8-5. Comparison between experimental and numerical calculations for following waves

The shaded selection corresponding to the test No. 314 is also presented on figures 6-20 and 8-1, from the experimental and numerical standpoint. More on this topic is investigated and reported in Turk et al. 2011.

The increase of GM value reduces the natural roll period and as the significant wave height is also one of the ruling parameters that will unleash parametric roll, adopting a GM value that will yield lower natural roll period is certainly a rather efficient way to reduce the risk of encountering unfavourable wave conditions. Therefore, the dynamic criteria proposed could be to ensure that the initial minimum still water GM has to be attained for a specific hull form sufficient to compensate the crest trough alteration in a given reference wave. This means, as seen in chapter 3 that the still water area should be proportional to the crest/trough alteration which is practically a constant value for a specific hull form. Although the results did improve in a sense that the parametric rolling was achieved for almost all the cases, the roll amplitude distribution was quite anomalous. Therefore, the implementation of the corresponding second group of experiments associated with decay tests will be addressed in the following section to evaluate the eligibility of the results.

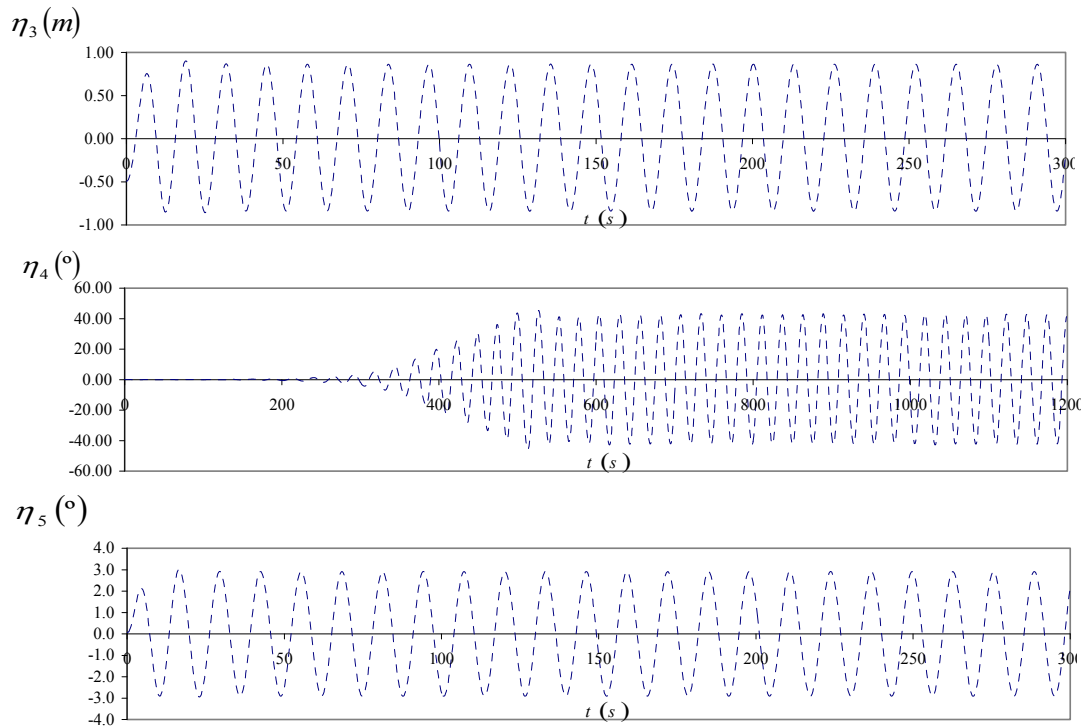


Figure 8-1. Numerical development of parametric rolling with regular following waves ($H_W = 8$ m, $T_W = 12.95$ s, speed 0 knots)

8.2 Direct damping calculation and decay test implementation on parametric rolling simulations

Going back to the procedure timeline however, and since the procedural requirement is the computational efficiency, for this methodology to function a certain number of iterative simulations are required. Therefore, direct calculation is implemented with full coupling of the *SHIPATSEA* and *IKEDADAMP* programs. With this rather difficult computational implementation it is enabled to intervene directly in the time domain seakeeping execution. For that reason the damping coefficients are being recalculated for the steady state realization and precise damping evaluation is possible with respect to actual roll angles. Since the two routines are executed within one simulation they are also quite inefficient in terms of CPU time consuming.

A better approach might be convergence method, ran by limited number of iterations. Then, a specific set of conditions can be retrieved and processed taking rather individual approach. This is especially convenient for irregular wave’s survey which was a motivation for this concept. An example is presented for the case study scenario of the “test No. 10” for the regular head waves with the specific parametric condition ($T_W = 12.95$ s, speed 8 knots, $H_W = 8$ m) which corresponds to $\lambda/L_{pp} = 1$. The plotted time histories (figure 8-2) correspond to the 3 realizations with respect to the concept implemented. The first one is obtained facilitating the original albeit optimized procedure. The second is a result of convergence method while the third shows the outcome of the direct calculations. Note that a direct calculation is performed while completely omitting convergence method. The results are as always summarized in table 8-6, within the parametric rolling report with the notation corresponding to the method implemented.

Folder destination	speed (kts)	heading	λ/L_{pp}	height	roll amplitude	roll amp. rounded	B44 Ikeda	delta
..\c11ext\TDM\Speed_8_kts\Heading_180\LvoLpp_1.00\H_8	8.00	180.00	1.00	8.00	45.04	40.00	1040000000.00	
..\c11ext\TDM\Speed_8_kts\Heading_180\LvoLpp_1.00\H_8	8.00	180.00	1.00	8.00	34.67	45.00	1100000000.00	10.37
..\c11ext\TDM\Speed_8_kts\Heading_180\LvoLpp_1.00\H_8	8.00	180.00	1.00	8.00	32.81	none	time domain	12.22

Table 8-6. Comparison of roll responses between the original methodology, convergence method and direct coupling for test No. 10

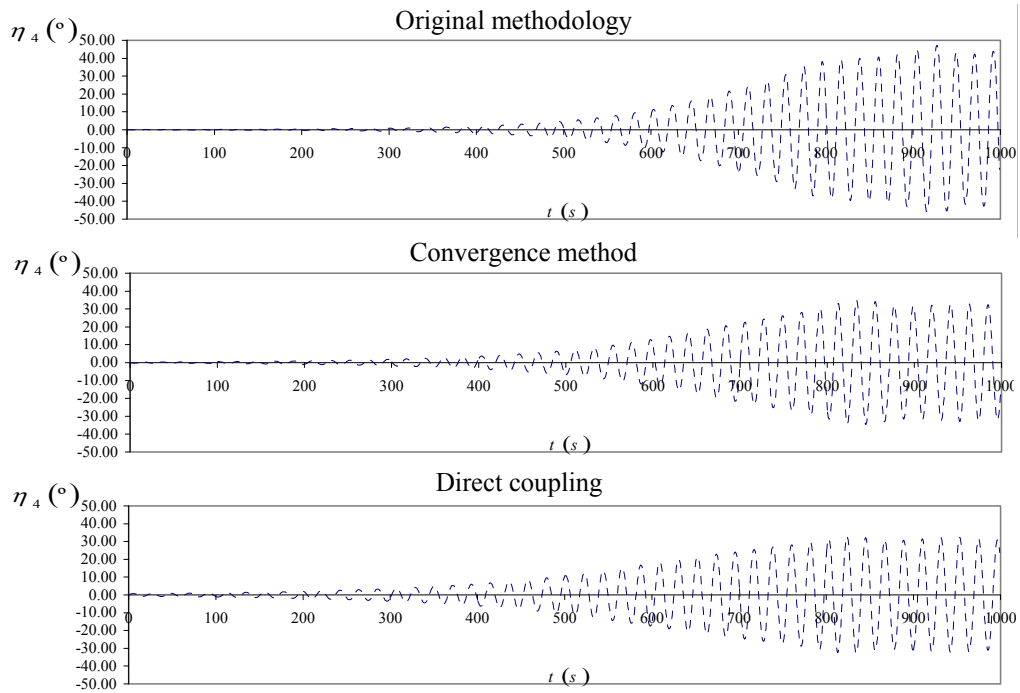


Figure 8-2. Time traces comparison of roll responses between the original methodology, convergence method and direct coupling for test No. 10

The enhancement of the result through all the stages is obvious as the final roll amplitude reached is around 32.8° . This is as close as one could get using this numerical procedure although it is still some 8° removed from the experimental results. Also the results from the convergence method and the direct calculation are relative vicinity with the roll angle difference of less than 2° .

Stated as highly important in this parametric rolling investigation, is the availability of an adequate motion calculation routine capable of predicting the time domain large amplitude responses under resonant conditions which has a strong dependence on roll damping characteristics of the vessel. Hence, an extensive group of roll decay tests to calibrate the existing prediction methods was performed. These results and its operative limitations suggest that at this point the decay results (TEST 304) can be implemented in particular modified SHIPATSEA program for the use of the linear plus quadratic (plus cubic) model sought as the most appropriate for this specific case (figure 8-3).

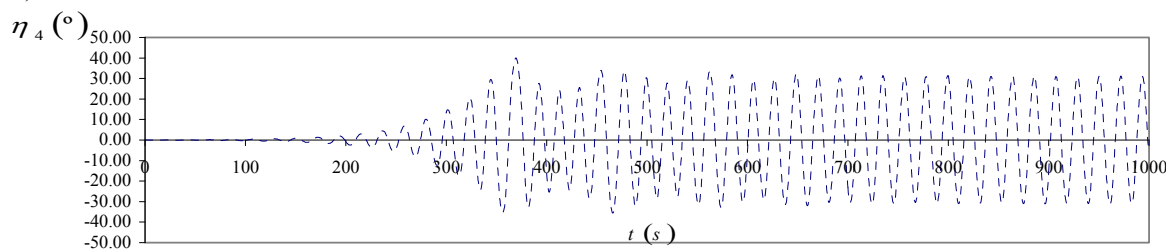


Figure 8-3. Time traces of roll responses with linear + quadratic damping model from decay test No. 304

The amplitude of $\eta_4 \approx 31.9^\circ$ was reached. As for damping influence, it is interesting to note that the final amplitude of roll motion is not that sensitive to the variation of the roll damping values expressed in equivalent linear terms. The figure 8-4 exemplifies above stated as the difference of $\eta_4 \approx 1^\circ$ when steady state reached suggests.

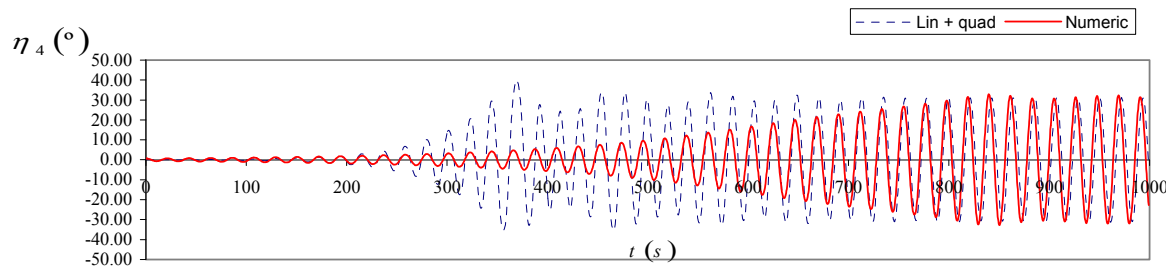


Figure 8-4. Time traces comparison of roll responses between equivalent linear damping by direct calculations and linear + quadratic model for test No. 304.

However, the duration and the characteristic transient state is affected, which indeed makes the parametric roll to happen earlier due to its adopted nonlinear nature within the linear plus quadratic model. It looks as though the nonlinear term affects the roll response in a sense that the transition between two states is not only faster but also more irregular. The influence on the roll angle could be more significant for the “normal” seakeeping motions but with resonant damping at hand, final amplitude of roll motion is not that susceptible. The difference in roll amplitude by comparison with experimental result is still appreciable and it has to be attributed to the limitations of the time domain strip theory derivative.

An example regarding following waves (figure 8-5) associated with low speeds is also taken with the “test No. 313” for the specific parametric condition ($T_W = 11.59$ s, speed 0 knots, $H_W = 8$ m). The decay results (Test DECA_Y_TEST_GM1_U=0 knots) can likewise be implemented. The plotted time histories correspond to the three realizations with respect to the concept implemented. On the upper figure using the original procedure the roll amplitude of $\eta_4 \approx 21.81^\circ$ was obtained. What strikes out here is the parametric resonance outlook. It takes unrealistically too much time for the phenomenon to occur and the steady state forms non-uniform envelope. This usually suggests that the damping values are overestimated as the dissipated energy is too stiff for the steady state to stabilize. Note that for irregular waves it is completely different as this type of time histories are to be expected. The plot on figure 8-5b is a result of convergence method using the modified Ikeda’s method. The result visibly differs from the first run of the convergence method with the roll amplitude of $\eta_4 \approx 49.73^\circ$ obtained. However, the convergence was unfeasible. In such individual analysis, a simple bisection method was used which repeatedly bisects an interval then selects a subinterval in which a root must lie for further processing. It is a very simple and robust method, but it is also relatively slow. With this procedure it was possible to “push” the convergence in between two mutually excluding boundary solution. A practical implementation of this method must guard against the uncommon occurrence that the midpoint is indeed a solution (not in this case as the convergence shifts toward higher values).

The ultimate way to test the performance of both is to implement decay results and utilize SHIPATSEA_D program. It has to be stated that this is acceptable only in the longitudinal seas since the tests were restrained to this conditions. The 3rd figure 8-5c corresponds to the decay results (Test DECA_Y_TEST_GM1_U=0 knots) implemented simulation with recorded roll angle of $\eta_4 \approx 45.71^\circ$. The experimental readings detected the roll amplitude of $\eta_4 \approx 35.74^\circ$. It is the difference of exactly 10° . It has to be said that the first run of the convergence method is the closest in comparison with the decay tests implemented as is the result of the bisection method needed for this PR development. Based on this, one can conclude that the new Ikeda’s method works better but the overall simplifications of the seakeeping routine prevent the possibility of acquiring the results measured by the experiments. But the overall tendency as evidenced from all decay nonlinear implementations is such that the difference in roll amplitudes is in range of plus 7-10°. This is very positive since it exhibits steady trend which adds to the method credibility.

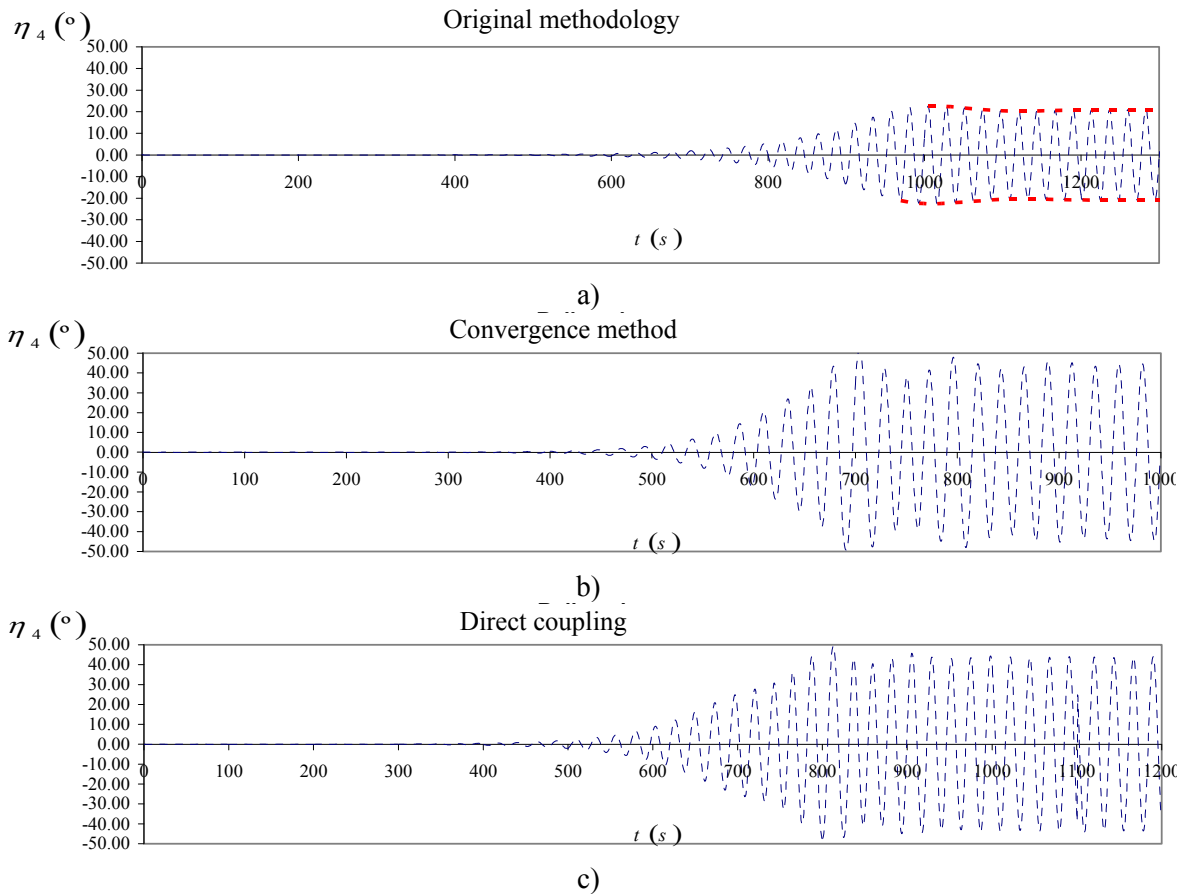


Figure 8-5. Time traces comparison of roll responses between the original methodology, convergence method and direct coupling for test No. 313.

If one recalls the evaluation of the second group of decay tests associated with different metacentric height a damping reduction of close to 50% was calculated. This itself implies the necessity of such tests as the original numerical procedure was unable to yield parametric rolling in most following waves cases. Whereas, looking at the whole set of simulations, these particular conditions can be addressed as the numerically most problematic, what remains is essentially the fallback to the decay tests implementation.

The results obtained from the decay tests in the previous chapter facilitated within the nonlinear damping model in SHIPATSEA_D program allow a better physical resemblance while describing the phenomena especially in the cases where the standard numerical model fails short. The last analysis is therefore concentrated on the test No. 310 and test No. 312 (table 8-7), with former taken because of the largest amplitude discrepancies and the later because the numerical model was unable to reproduce the roll resonance amplification.

Test N°	λ/L_{pp}	H_w (m)	T_w (s)	V (kts)	Roll Angle exp (°)	Roll Angle Num GM1 (°)	Roll Angle Num GM2 (°)
310	1	6	12.95	0.00	35.79	11.28	46.52
312	1.4	6	15.33	0.00	25.96	/	25.27

Table 8-7. Comparison between experimental and numerical calculations for test No. 310 and test No. 312

The figure 8-6 shows very differing roll response between the standard numerical implementation and from the decay acquisition both in terms of roll amplitudes and the roll response distribution.

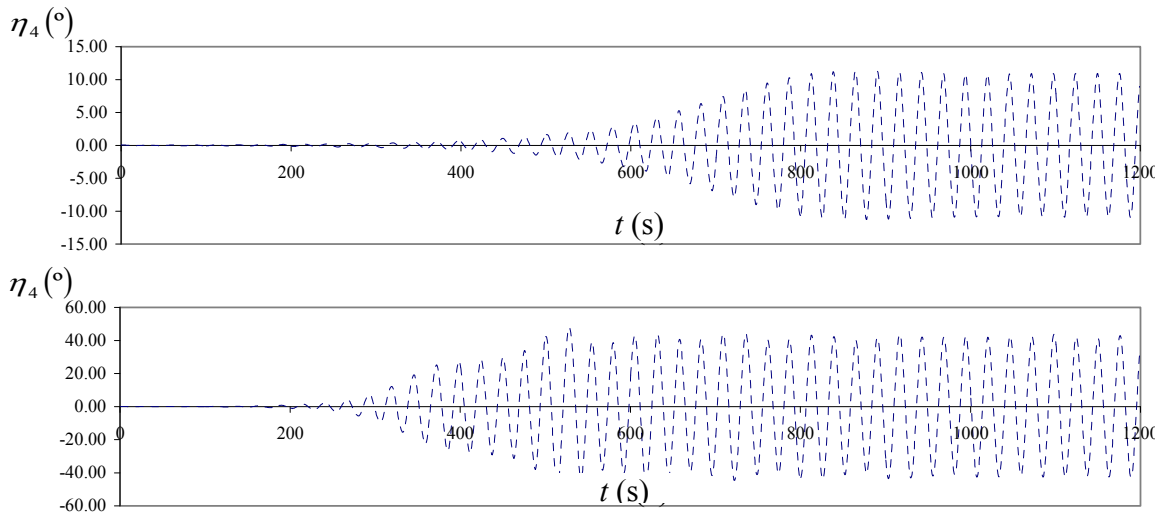


Figure 8-6. Time traces comparison of roll responses between numerical implementation and from the decay acquisition for test No. 310.

However, when comparing directly the time histories of the parametric rolling development from the experiment (on the test No. 310) and the decay tests implementation ((Test DECA_Y_TEST_GM1_U=0 knots)) using nonlinear damping in ship motions program a very good concurring is noticeable as seen on figure 8-7. Standard roll amplitude deviation of around 10° still exists, but again as a general trend actually works in favor of the method predictability.

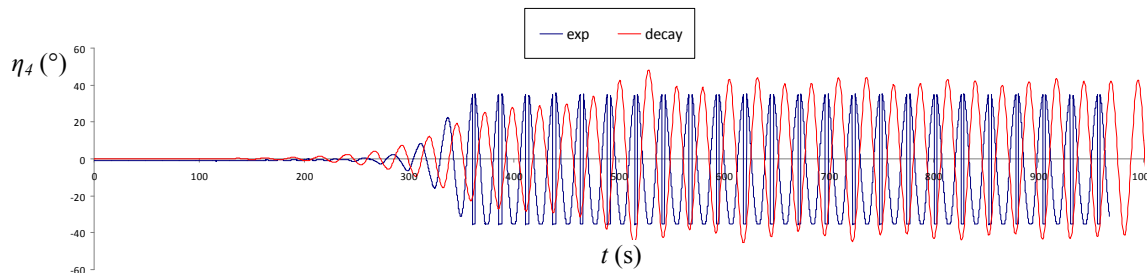


Figure 8-7. Time traces comparison of roll responses between the decay acquisition and experiment for test No. 310.

The development of parametric rolling begins at almost the same time instant (cca 200 s) albeit with the phase shift. The next example (test No. 312) was the crucial one since the inability to predict parametric rolling has to be considered as the major obstacle. The results however, were almost in complete compliance. To further illustrate this equivalence an extended selection of motions is presented. It is easy to deduce that both the heave and pitch motions from the decay model insertion (figure 8-8) and experiment (figure 8-9) are essentially the same with heave amplitudes of $\eta_3 \approx 1.75$ m and pitch angles of $\eta_5 \approx 2.3^\circ$.

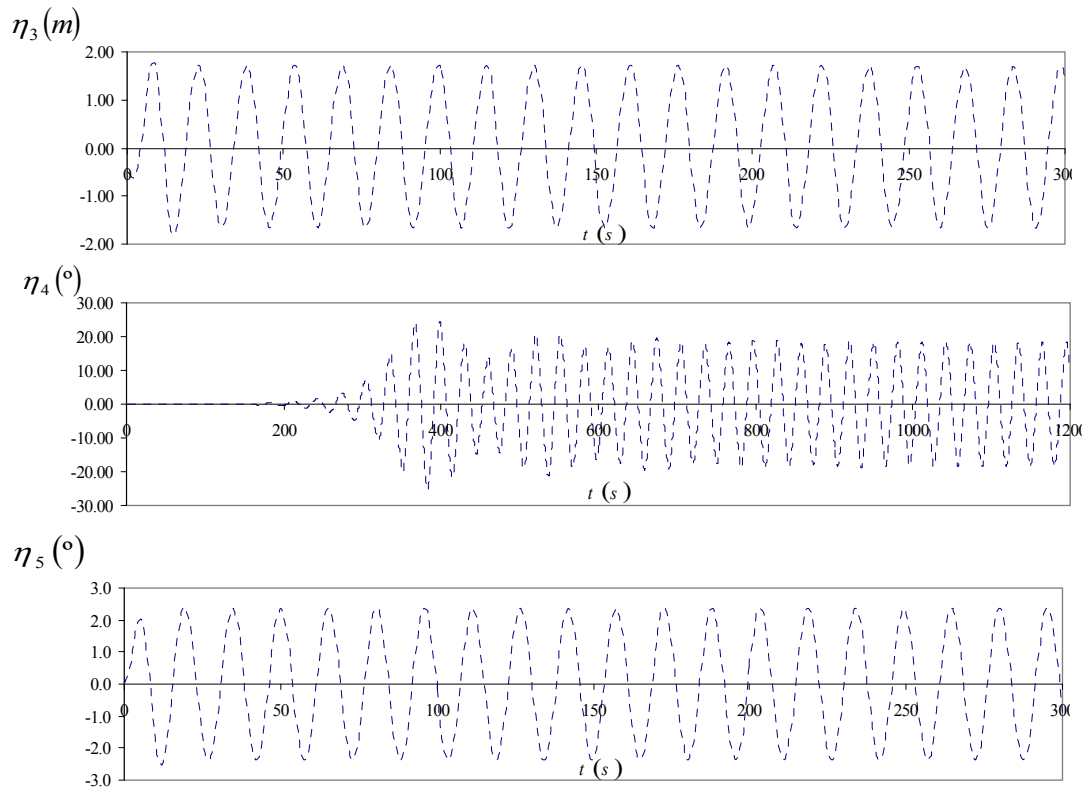


Figure 8-8. Time traces of motions for linear + quadratic model implementation (test No. 312)

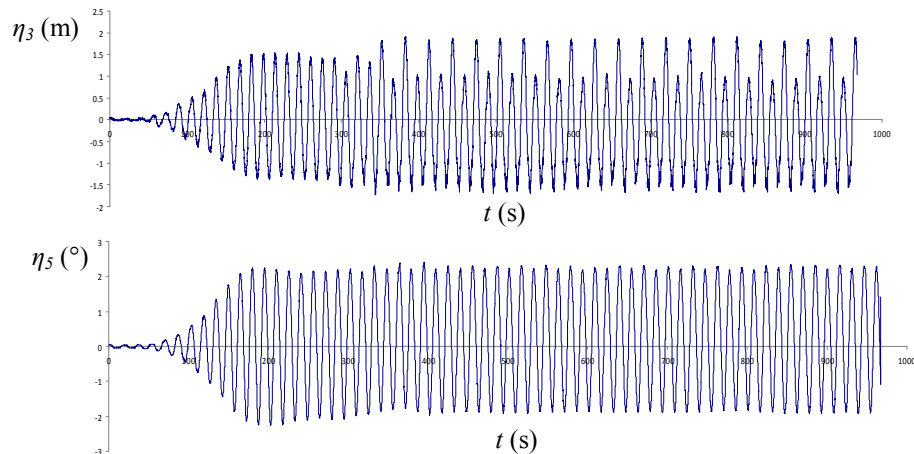


Figure 8-9. Heave and pitch motions in experiment (test No. 312)

It is argued here, that although the roll response matches remarkably as seen on figure 8-10, it is the opposite of the observed pattern from the other comparisons, some of which were above presented. The possible explanation could be raised from the fact the proposed methodology had difficulties in establishing parametric rolling in the first place. Once the nonlinear damping model was implemented which enabled parametric rolling to take place the amplitudes obtained are as a consequence much closer to the experimental ones. Still, this result should be treated as the exception, more so than the rule.

On the other hand, and to sum it up, when the numerical simulation is able to reproduce PR from the start it usually overestimates the amplitudes ($\sim 10^\circ$), with the best performance still evident from decay tests implementation but also from the new damping treatment. This is simply attributed to characteristics of the proposed methodology. That said, the emphasis should be more of the ability to predict parametric rolling rather than pinpointing the roll amplitudes.

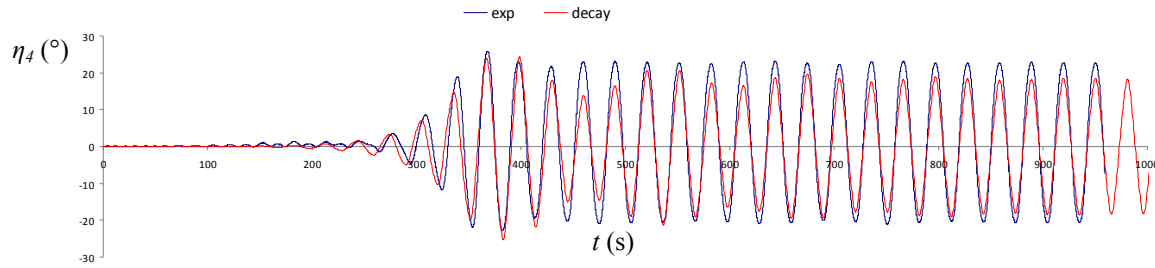


Figure 8-10. Time traces comparison of roll responses between the decay acquisition and experiment for test No. 312.

Keeping in mind that the head and following seas parametric rolling experiments were performed with the different metacentric height ($GM1$ and $GM2$, respectively), condition then led to PR in following waves ($GM2$) is going to be exerted (figure 8-11) for the head waves to evaluate the vessels loading condition impact on the phenomena.

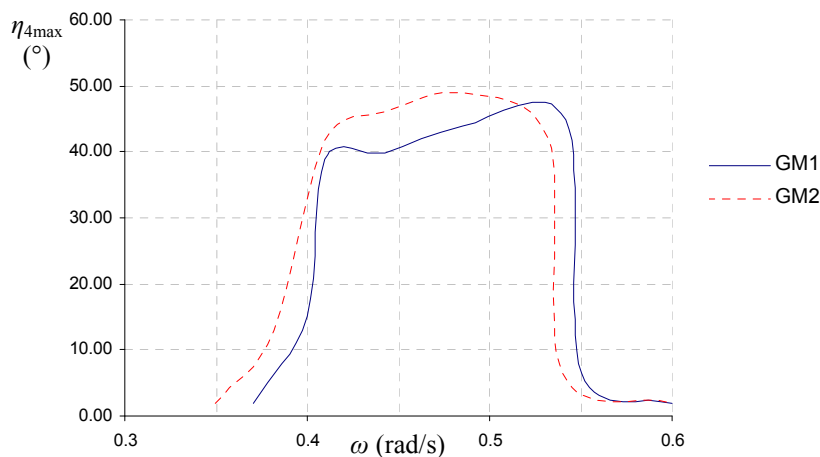


Figure 8-11. The loading condition influence on the parametric rolling relization

Figure 6-68 describes the effect of the changing metacentric height, for a displacement kept constant. Decreasing metacentric height ($GM2$) not only increases the peak amplitudes (although not significantly) but also shifts resonant frequencies to lower values. The effect of changing displacement was not sufficiently studied although preliminary it looks as though the increased displacement narrows the frequency range where the parametric rolling is possible. A popular trend is also to study the wave steepness effect (Ribeiro e Silva et al. 2009).

Comparisons of roll amplitude of parametric roll in regular head seas between the model experiment (Ribeiro e Silva et al, 2009, and Sogawa et al., 2010) and the numerical simulations with the roll damping estimated by the roll decay test and the Ikeda's prediction method (both original and modified) are shown in Fig.8-12. The experimental results although conducted on the same vessel and even though Sogawa's were performed with bilge keel installed are not in accordance (Sogawa's measured roll amplitudes were higher which is much closer to the numerical model and for the decay tests implemented) which is quite peculiar. If necessary, similar graphs can be drawn for the fixed λ/L_{pp} ratio by varying wave height. Sogawa et al., 2010 measured roll amplitudes for three cases of roll frequencies namely $\lambda/L_{pp} = 0.8, 1.0$ and 1.2 seen as triangles on the following chart.

Numerical result with the roll damping by the roll decay test comes closest with the model experiment for all wave steepness and Froude numbers although as already stated it wasn't the amplitude that was affected the most but the fact that parametric rolling embarks much sooner. Not only is the time history more realistic but the decay tests implemented have successfully enlarged the grouped parametric rolling range which is most evident for $\lambda/L_{pp} = 1.0$ and thus approximated Sogawa's measurement. The parametric rolling is extended in range from 5 to 14 knots as oppose to 7 to 13 knots before. The results from the decay test implementation and the Sogawa's experimental

values for the condition ($T_w = 12.95$ s, speed 8 knots, $H_w = 8$ m) are in full agreement and the modified Ikeda's approach differs only slightly.

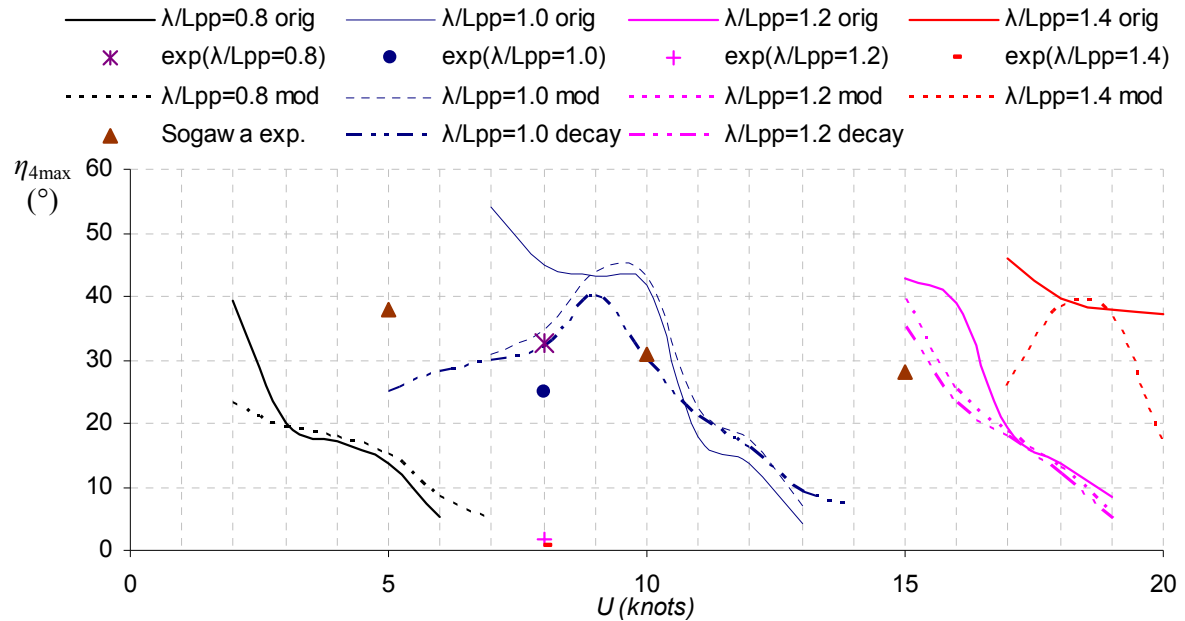


Figure 8-12. Numerical results of parametric roll with the roll damping estimated from a roll decay tests, Ikeda's method and modified damping feature with $H_w = 8$ m

This implies that at a given frequency, above a certain level of wave amplitude, the increase in rigidity defuses the unstable increase of the amplitude of parametric excitation. Comparing the limits it is possible to conclude that the main influence of damping is to raise the set of limits of stability.

The numerical result with the roll damping by the Ikeda's semi-empirical prediction method overestimates the model experiment (Cehipar) although it's uncertain whether it is because of its underestimation of roll damping (usually an overestimation is reported but it can be attributed to the bilge keels largely) or the procedure ineptitude to capture full nonlinear behavior or the uncertainties of measurements. Further investigation, such as a forced roll motion test for the C11 containership and the similar examination for other types of ships, is required for further discussion.

To quote, "since the amplitude of roll restoring variation increases its nonlinearity with a roll angle as does the damping, the difference of estimation methods of roll damping could significantly affect on parametric roll prediction and could result in different amplitude" (Hashimoto et al. 2010.), all of which was proved by this novel damping feature implementation. Therefore, attention to the estimation methods of roll damping paid for quantitative validation of numerical simulation of parametric roll is essential and the next course of action would be to test it within a simulation tool equipped with time convolution effect to more accurately simulate the nonlinearities involved regardless of the CPU time spent.

8.3 Final observations on regular waves parametric rolling

After the experimental and numerical results were cross-referenced and debriefed one has to provide possible explanation for those outcomes. While it was clearly evident that a blending method utilized in damping estimation efficiently reduces roll amplitudes it is also rather obvious that the experimental values were not quite achieved. Nevertheless, a comparison of the results did show a good agreement with experimental data and the hybrid approach appears to be actually independent of the technique used in the frequency domain, even if the reliability of the results is strongly related with the accuracy of the evaluation of the hydrodynamic terms. However, an optimization study on hydrodynamic terms is not the aim of this work rather the optimization of the damping procedure

again using a hybrid approach. As shown, this methodology is capable to be applied employing different techniques starting from the frequency domain analysis.

Some of the parametric rolling realizations in the experiment were not reproduced by the numerical calculations. It was also explained that while that is true the simulations performed did exhibit the resonance effects in the vicinity of those set of conditions leading to the parametric rolling. This can be attributed to limitations of to the strip theory method itself. Moreover, nonlinear simulations are strongly conditioned by the evaluation in the frequency domain of linear radiation and diffraction forces and errors in these calculations could affect the correct assessment of nonlinear effects.

While the common stance of the scientific community regarding the development of the parametric rolling is that what causes it, is the time varying righting arm stability as the wave crests pass along the ship hull, while the damping merely affects the roll amplitude. However, it was argued in the last chapter that based on the evidence from the decay tests vessels of this type possess a damping deficiency at relatively small roll angles that may push the ship in the parametric resonance mode. The problem of roll damping which is highly influenced by the viscous effect and thus not applicable to be solved with potential theory is that it has to be represented by the equivalent linear term. The equivalent linear term unfortunately cannot capture the nonlinear behavior especially the extreme one as reported from the previous chapter. While the linear plus quadratic plus cubic model can effectively reproduce this highly nonlinear attitude in the range up to 15° , it ultimately fails for the higher roll amplitudes with its lack of extrapolation capabilities due to the observed linear asymptotic behavior (severe overestimation). Therefore, in order to reproduce parametric rolling one has to rely on the correct assessment of nonlinear effects other than damping, especially with the exact determination of the hydrodynamic terms. In the absence of any means of decay damping approximations the equivalent linear term indeed only influences the roll amplitude quantity but not in the manner that could be anticipated. Still, as seen from the results whether a convergence method or direct calculations is utilized, better agreement is enabled.

The biggest benefits of the proposed methods are that it can be applicable to any seakeeping code with various degree on nonlinearities employed. The biggest drawback is the overall impediment on the capabilities of those seakeeping programs. The new damping implementation can only affect simulation that registered parametric rolling in the first place. If the program is unable to achieve resonance realization due to the simplifications or hypothesis implemented then damping treatment becomes redundant. The very essence of damping, being hydrodynamically unsolved, is to adequately simulate its contribution, in this case referred to as quasi-nonlinearly. The time varying roll amplitude dependence on damping is one way. The equivalent linear damping, although a suitable and adequate mean of quantitative assessment of any damping model proposition is only a measure of the dissipated energy. If the “loss” of energy per cycle caused by damping is more than the energy “gain” caused by the changing stability in longitudinal seas the parametric resonance will not develop. We can establish an analogy with the spectral representation of the irregular seas. While for instance a JONSWAP spectrum represents energy of certain wave system each spatial and temporal realization is always different. The realization of the equal equivalent linear damping can also take many shapes and forms represented by a suitable model.

With the coupling of the SHIPATSEA and IKEDADAMP programs the following was observed. Ikeda method although from theoretical aspects very comprehensive sometimes may not predict a correct values especially for a large vessels like C11. This was precisely the motivation to upgrade the existing and commonly used platform for the damping assessment. However, it was not an intention to tune up damping values to a certain seakeeping code, rather to get as adequate values as possible. This derivative of a strip theory method though, would favor higher damping values in order to approach the experimental values. Whereas the user inputted values (both lower and higher) would certainly suit the simulation better it can only be used as the orienteer to check the overall propensity, rather the damping demeanor.

While there are undeniable uncertainties in both calculations one has to question the following:

- a) the repercussions on the seakeeping simulation with respect to the uncertainty in the damping modeling,
- b) the repercussions on the reliable damping assessment using the strip theory method while attempting to “duplicate” results from experiments.

The answer is usually somewhere in between. Therefore, the goal doesn't have to be achieving full correspondence with the parametric rolling experiments but rather to better identify an “appropriate” share of the provisions against parametric roll between design, loading and ship mastering with respect to damping threshold and amplitude. A fully nonlinear approach with time convolution integral would be more appropriate especially in terms of damping evaluation. But such numerical model are very CPU time consuming and its extension to irregular waves is even more expensive, which is why more approximate models such as this might be preferable.

Since this is an ongoing process in the development of the optimal code the biggest link is seen to be the fact it allows a better understanding of the instantaneous hydrodynamic problem for asymmetric (inclined) cross-sections together with the established damping deficiency in the same range. The theoretical assumption is that under the uncharacteristic roll decrement “appearance” some discrepancies can be traced and explained within the forced oscillation tests for the ship inclined (0° , 5° and 10°) even though it mainly addresses heave and pitch motion. But the hull form specifics with streamlined underwater tapering can be accounted for that presumption while being manifested in all degrees of freedom, though not necessarily with the same impact. This is to be investigated further.

8.4 Parametric rolling in polychromatic waves with experimental validation

Investigation of the conditions in which parametric rolling occurs in N harmonic wave components in head and oblique waves ($\beta = 180^\circ$, 170° , 160°) and (3, 5, ..., 11 harmonic wave components), were undertaken considering the equivalent wave heights and mean wave encounter frequencies recorded during the most critical test of parametric rolling in regular head waves (1 harmonic wave component). Note that all the subsequent analysis is preformed using the modified methodology which was thoroughly explained in the regular waves section, consequently the details of the implemented damping procedure will be left out. The first analysis addresses the Test No. 17 for the wave generation No. 29. Since there were 3 harmonic components utilized the wave surface elevation appears almost regular. The measured peak amplitude of $\eta_4 = 28.1^\circ$ agree quite well with the $\eta_4 = 34.52^\circ$ obtained from the numerical simulation. In the figures 8-13 and 8-14 below time traces are given for the heave, roll and pitch motion and wave height during a run in polychromatic wave No. 29.

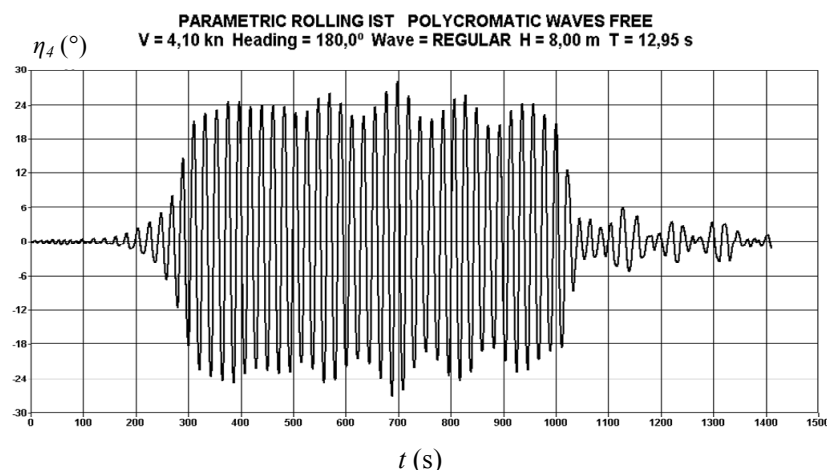


Figure 8-13. Experimental time trace of rolling motion for Test No. 17 provided by Cehipar

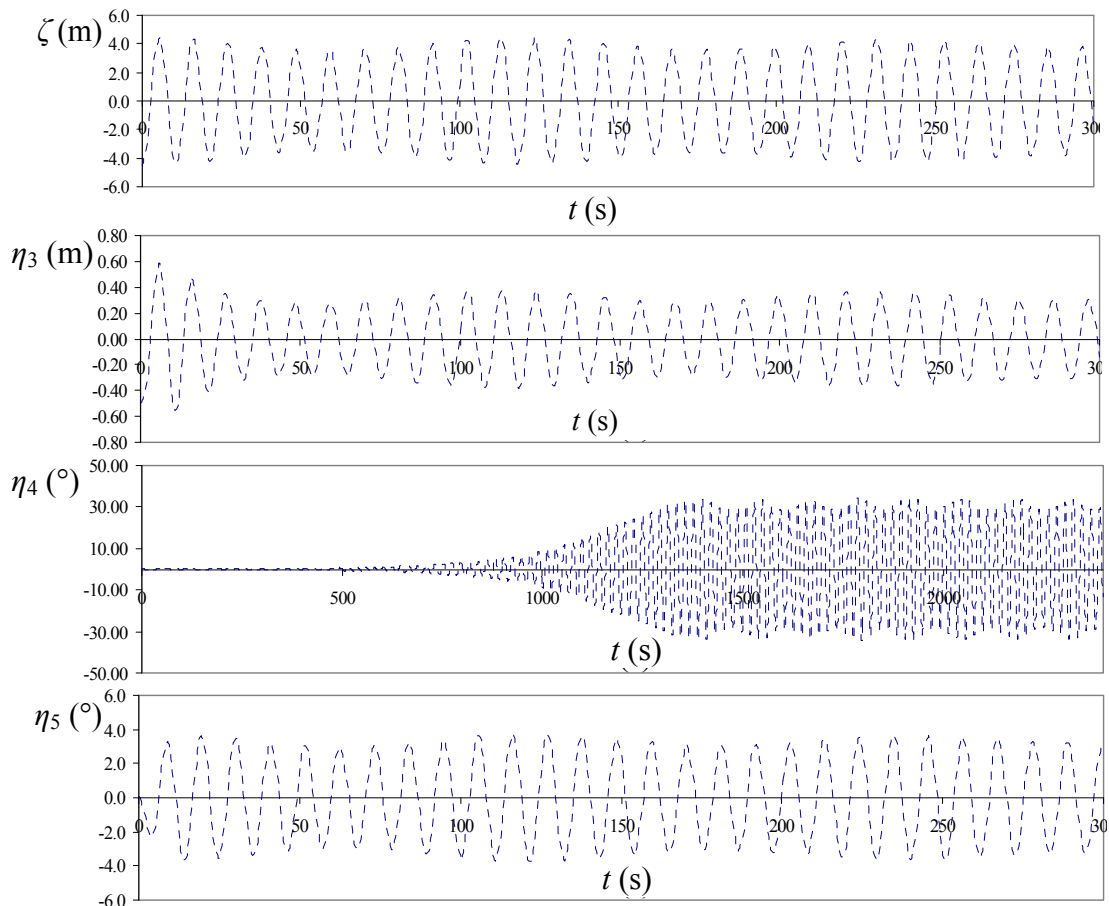


Figure 8-14. Numerical simulation associated with Test No. 17

When the vessel encounters a sequence of wave components of a certain period and height, parametric rolling is initiated if the conditions are right. As compared to heave and pitch motions, which are reaching stabilised solutions for a small number of oscillations, the induced roll motion has firstly a transitory phase and then the rolling amplitude slowly increases until the steady state is reached. However, unlike the regular wave excitation, time trace of all steady states reveals light fluctuations both on experiment and numerical.

The following figures 8-15 and 8-16 present the simulations for Tests No. 18 and No. 19 with particular details given in tables 6-5 and 6-6.

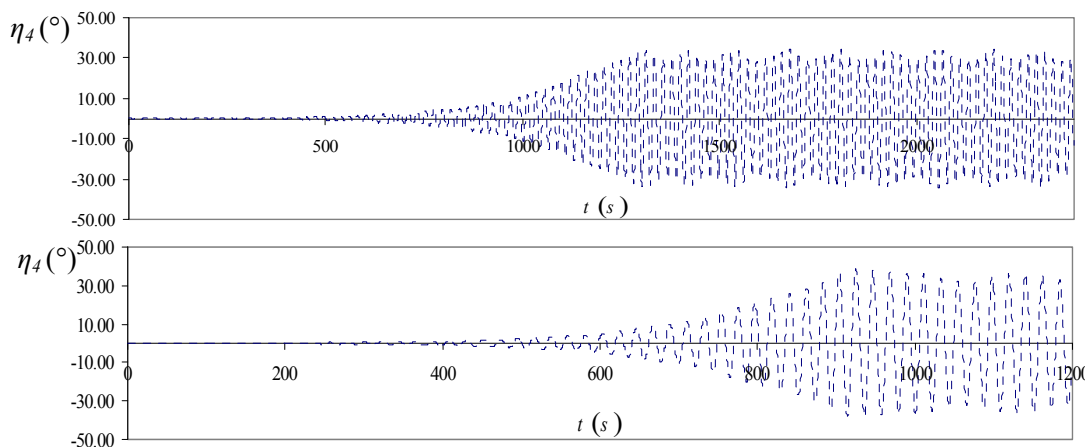


Figure 8-15. Numerical simulation associated with Test No. 18 and Test No. 19.

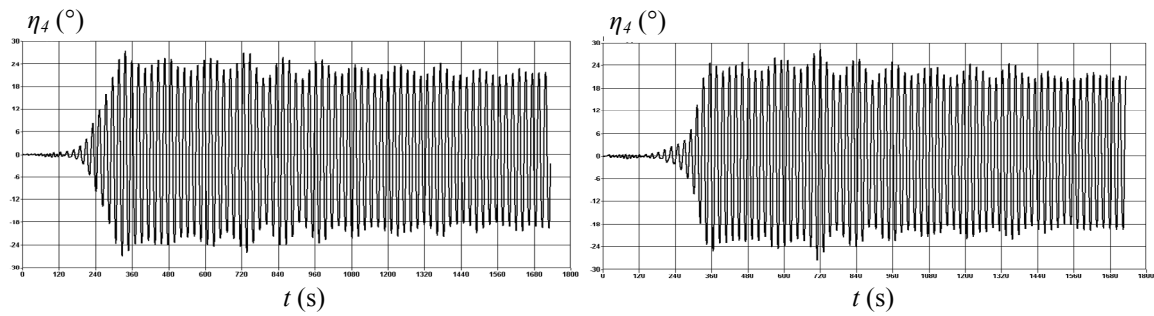


Figure 8-16. Experimental time trace of rolling motion for Test No. 18 and Test No. 19. provided by Cehipar

Looking at the wave profile one can deduce that increased number of harmonic components induces more irregularities in the wave profile, although in terms of roll response simulation, with $\eta_4 = 34.52^\circ$ and $\eta_4 = 34.69^\circ$ for both tests, the difference is barely discernible. Once again the experimental readings for both experimental investigations are around $\eta_4 \approx 28^\circ$. It has to be stated that full correspondence of the roll responses is unfeasible since the basin generated wave profile cannot achieve theoretical distribution and vice versa. Therefore the roll responses will not be overlapped since in fact they do not represent exactly the same conditions. This will be much more evident in irregular wave's survey. However, general trend is evident with characteristic fluctuations of all steady states regimes. The first component of all calibrated waves is of $H_W = 8$ m and $T_W = 12.95$ s and its contribution is such that all the other harmonics have in general suppressed effect on overall profile. Meaning, although the chosen polychromatic wave structure was intended to provide variations in the roll response, those wave groups are in essence very similar as are the roll responses seen on figure 8-15 and confirmed by the experiments.

The next group of tests was performed for different heading (170°), namely Tests No. 23 and No. 25 were selected among others. Looking at the results obtained from the regular wave survey the vessel speed has to be increased while navigating in slightly oblique seas in order for parametric rolling to initiate as seen with the spread distribution on figure 8-17.

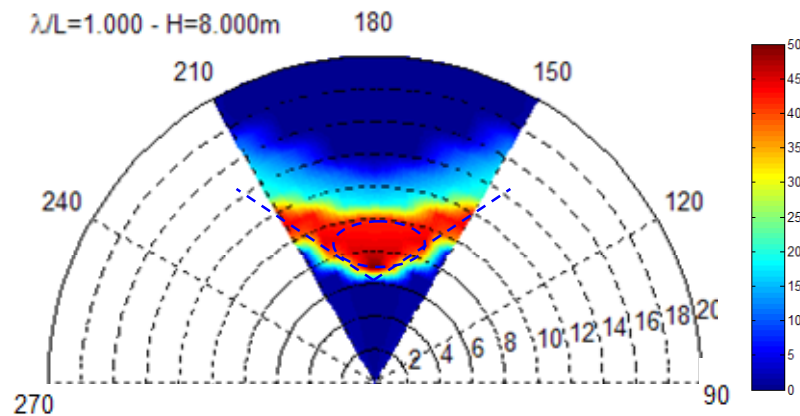


Figure 8-17. Speed increase for slightly oblique waves due to the established occurrence groupiness.

Therefore the input ship speed was modified to 4.2 m/s. The main difference between the two is of course different wave excitation. The latter as the more irregular one produces slightly lower amplitudes which are to be expected. The trend evidenced in the head waves is evidenced in this group of tests as well (figures 8-18 and 8-19). The amplitudes for the test No. 25 for instance, of $\eta_4 = 33.97^\circ$ are in correspondence with the experimental results of $\eta_4 \approx 27^\circ$, a statement that can be applied for all tests but one presented further below.

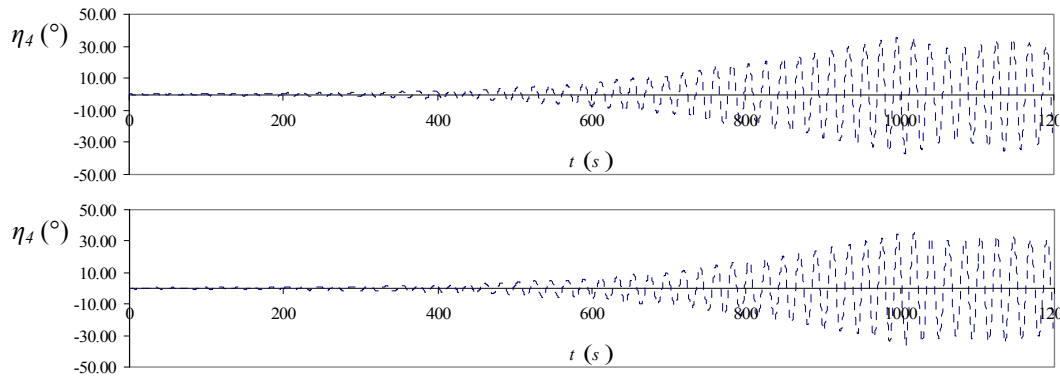


Figure 8-18. Numerical simulation associated with Test No. 23 and Test No. 25.

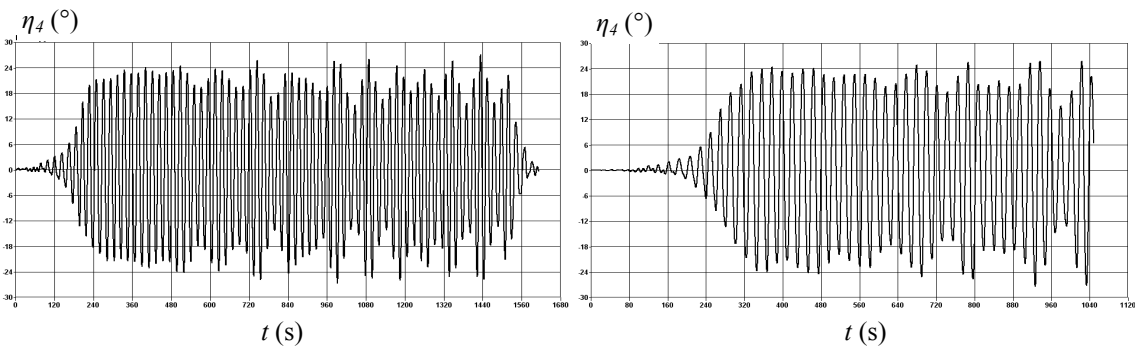


Figure 8-19. Experimental time trace of rolling motion for Test No. 23 and Test No. 25. provided by Cehipar

The last group of tests for bow waves is for the 160° heading with ship speed modified to 4.3 m/s. The experiment chosen for the presentation is Test No. 31 for the wave generation No. 31 (figure 8-20). Recall that this wave profile forms out of 7 harmonic components, which implies the strongest irregularity of all (although not necessary).

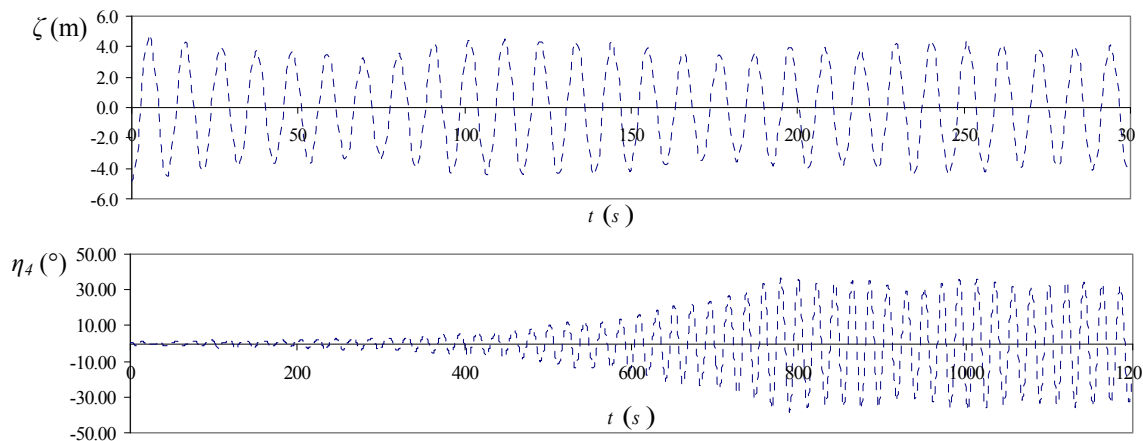


Figure 8-20. Numerical simulation associated with Test No. 31.

Based on those readings, one physical consequence on the parametric rolling response stands out. It is very interesting to observe the roll amplitude dependence on the slightly irregular wave excitation. For the purpose of better visualization the wave elevation is multiplied 8 times tuning up to the roll amplitude values. The intention is to demonstrate the wave excitation influence to the roll response outlook in terms of level identification. Looking at the steady state regime on the right of the figure 8-21, it's almost as though the roll amplitudes and the wave elevation are equal. The matching of those lightly fluctuating envelopes suggests that the higher roll amplitudes are the result of the higher wave excitation and vice versa, something that wasn't explicitly seen in the regular wave's survey. This fact can be transcended to the irregular wave's survey as one of the parameter

that constitutes for setting-up the parametric rolling. It has to be stated that this figure does not represent true physical state of the parameters involved but rather the exaggerated one.

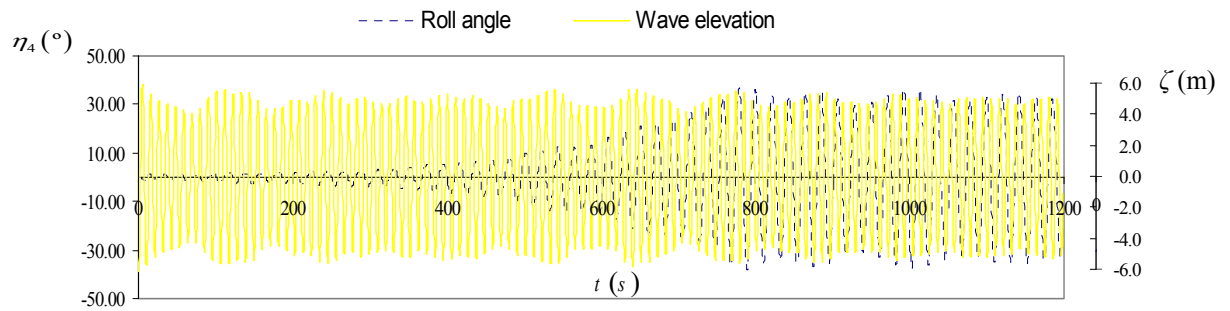


Figure 8-21. Excitation level identification

The obtained roll angles of $\eta_4 = 33.17^\circ$ are slightly more distant from the experimental ($\eta_4 \approx 24.1^\circ$) on figure 8-22 then for the previous cases.

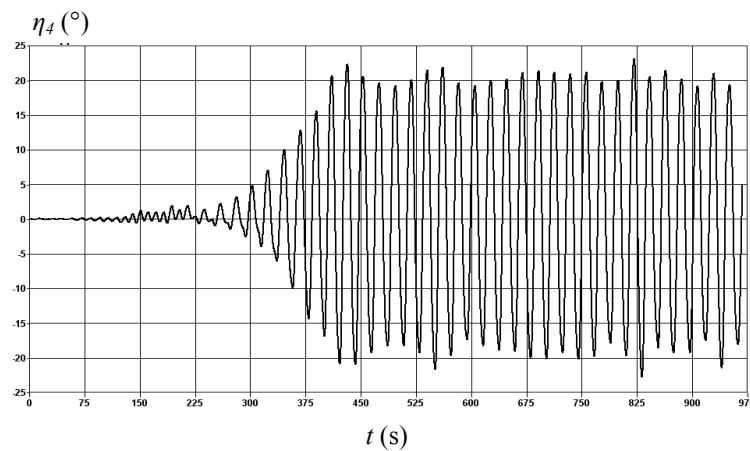


Figure 8-22. Experimental time trace of rolling motion for Test No. 31

The trend of decreasing amplitude as the heading alters from the longitudinal waves is already well established (France at al. 2003.) and even confirmed from the modified numerical analysis from regular waves. It has to said that experimental decrease of roll amplitudes is steeper compared to the numerical.

The general tendency for this group of tests is in good compliance, both looking at the physical behavior and quantitative measurements, and as such very similar to the reported from the regular waves. For that reason two experiments are going to be compared for this heading, namely, Test No. 34 on a polychromatic wave and Test No. 34a on the regular wave, as seen table 6-6 and on figure 8-23.

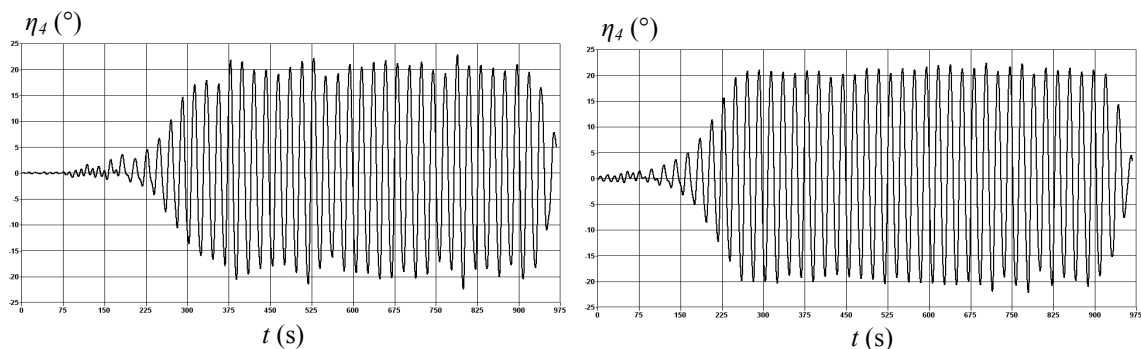


Figure 8-23. Comparison between the polychromatic and regular wave excitation for Test No. 34 and Test No. 34a

What was already established during the previous analysis is here confirmed with this direct comparison. The roll response matches the wave excitation which in regular waves produces uniform steady state, whereas the maximum roll angles are nearly identical.

These results however would nullify the purpose for which above presented tests were designed if not for one polychromatic wave that didn't initiate parametric rolling. Those 3 tests for the respective headings were performed on the Wave No. 32. The harmonic components of this wave are given in table 6-6. Contrary to the other waves this one has a significant amplitude contribution on the broader range of frequencies. Looking at the wave profile on figure 8-24, a sudden drop of amplification is clearly visible (dominant influence of the secondary wave contributions). The wave height threshold value is not sustained long enough to initiate parametric resonance. The effect of wave groupiness is self-explanatory.

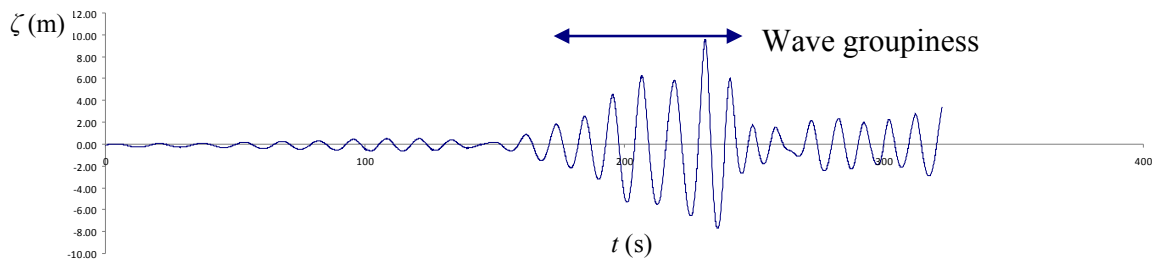


Figure 8-24. Wave elevation profile of Wave No. 32

The question however is the number of cycles necessary for the parametric rolling to develop. This feature is of great importance when studying irregular wave's excitation especially in terms of ergodicity concepts. As seen from the figure 8-25, numerical simulation of test No. 20 did not exhibit parametric rolling concurred by the experiment as well (figure 8-26).

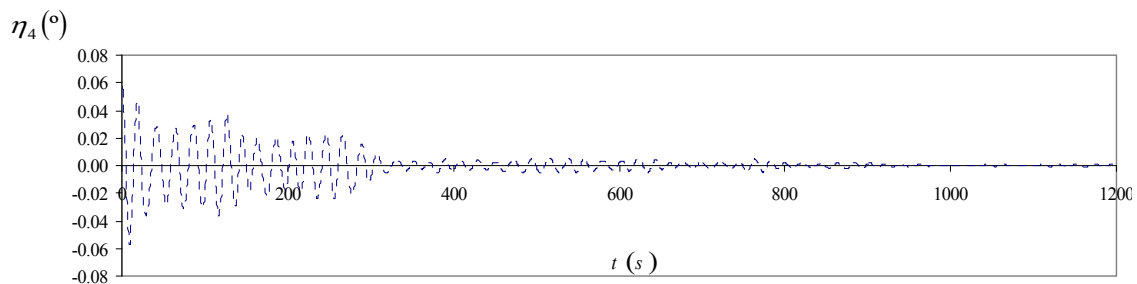


Figure 8-25. Numerical simulation associated with Test No. 20.

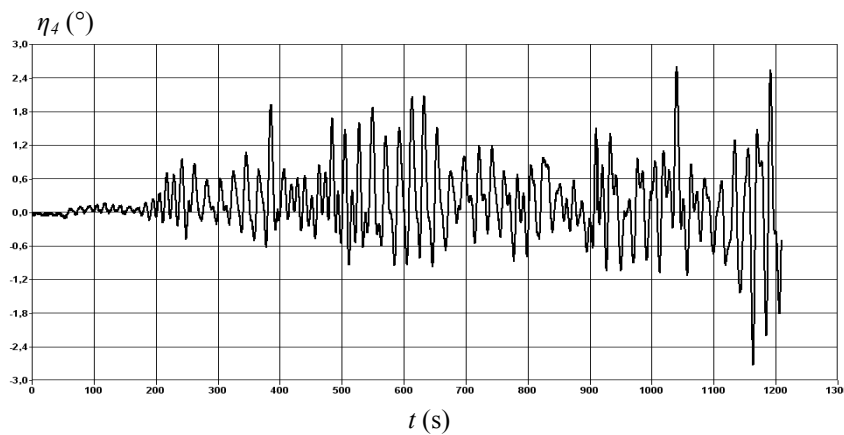


Figure 8-26. Experimental time trace of rolling motion for Test No. 20.

The only instant where the simulation was unable to match experimental results is for the test No. 26 for 170° heading. Comparing the roll responses on figures 8-27 and 8-28 particularly in the

range of first 200 seconds of time trace shows almost identical amplifications of around 3° marked on both figures.

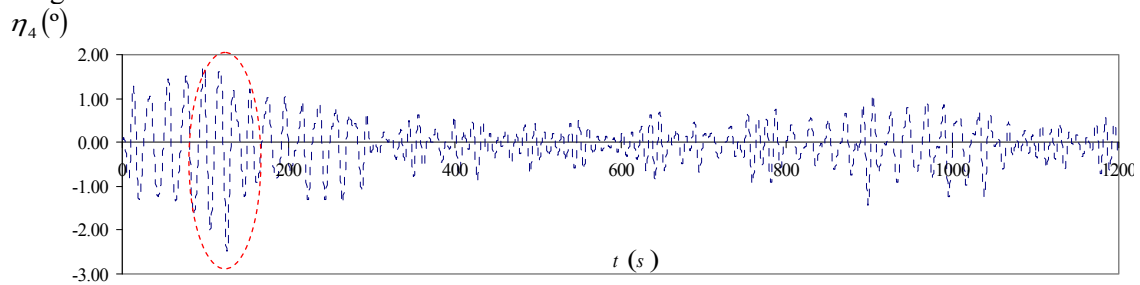


Figure 8-27. Numerical simulation associated with Test No. 26.

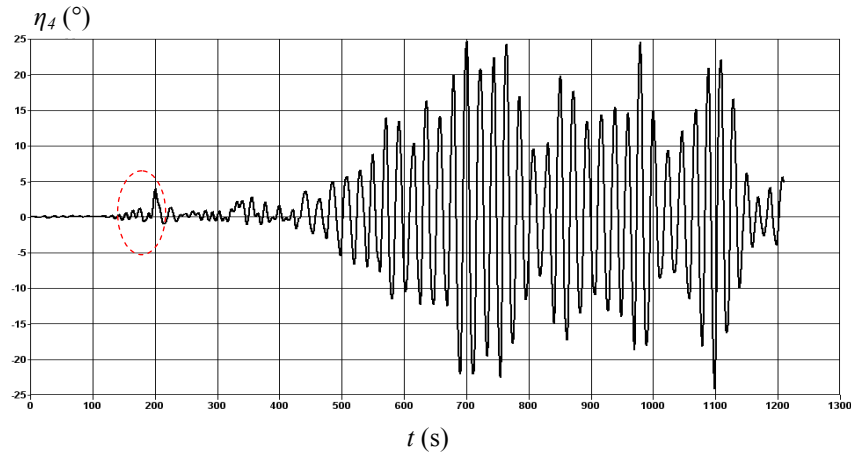


Figure 8-28. Experimental time trace of rolling motion for Test No. 26.

However, as wave excitation succumbs, the numerical simulation is unable to gain another momentum to establish the parametric resonance whereas the experiment shows parametric amplification starting at around 400 seconds.

To explain that, effective wave profile is presented with the segment extracted (marked in red) from the whole time history. As seen from the figure 8-29 the required threshold wave height of 4 m is sustained for 8 cycles, therefore the prolonged excitation makes it possible to effectuate the extreme roll amplification.

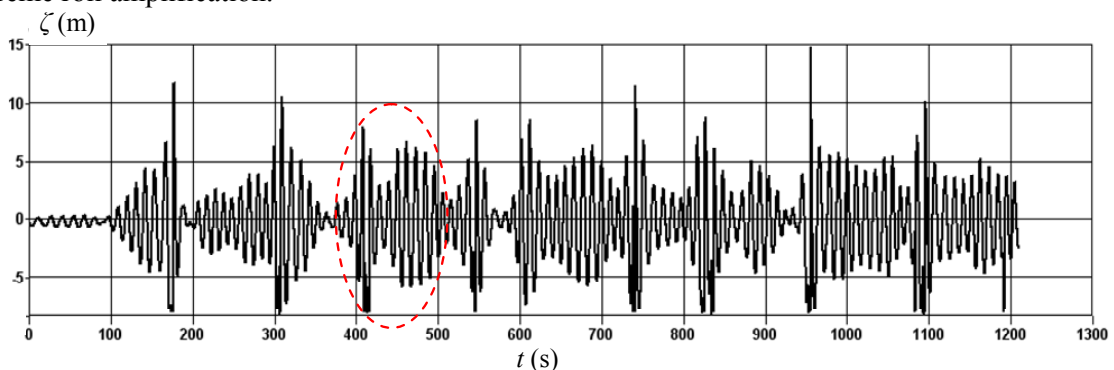


Figure 8-29. Wave elevation segment that enable parametric rolling.

Test No. 32 for the 160° heading is almost the same as for test No. 20.

A string that can be traced from all the experimental and numerical comparisons is the fact that numerical simulations are in retardation in terms of initiating parametric rolling except when the linear plus quadratic (plus cubic) damping model is utilized. Due to the fact that parametric rolling happens later the restoring impulse associated with alternate crest-trough variations is not kept long enough, and by that time the wave excitation falls under the threshold wave height. Such findings

suggest that a possible parametric rolling in irregular waves may not be reproduced by the numerical calculations if the number of relatively regular wave cycles of sufficient wave heights is not enabled.

The same procedure can adequately be applied for the following polychromatic wave's tests. However, the obtained results are in correspondence to the reported previously and due the extensive nature of this work are deliberately omitted from the presentation but the consequent public dissemination is planned in the aftermath.

Summarizing the section, for majority of the tests conducted the wave elevation profile has overly regular characteristics which can only explain the wave excitation influence on the roll response curve. Limited wave generation enabled reasonable hindsight especially in terms of wave "groupiness" range (figure 8-29) necessary to establish resonance phenomena. However, based on such restricted experimental occurrences, it is impossible to draw any definite conclusion especially towards gaining certain understanding of the kick up mechanism for the parametric rolling in irregular waves.

8.5 Parametric rolling in irregular waves with experimental validation

Although parametric roll in longitudinal regular waves is, nowadays, a quite well understood phenomenon, difficulties still exist (also from a conceptual point of view) concerning the case of irregular waves. While generally less severe, the parametric roll phenomenon is also present in irregular waves. The literature available is of far lesser degree for studying parametric rolling in irregular waves. In particular, by making reference to the available scientific literature (see, e.g., Roberts, 1982 ; Dunwoody, 1989 ; Bulian et al., 2004 ; Levadou and van't Veer, 2006 ; Bulian, 2006), it seems that the determination of instability boundaries in irregular waves is complicated by the fact that:

- the definition of "unstable condition" in irregular waves is, from the theoretical point of view, not unique,
- the instability boundaries in irregular waves are strongly dependent on the nondimensional linear damping.

Thus, in case of irregular waves, however, the theory seems to be not yet ready to give reliable values for threshold and amplitude. This could be explained in view of poor experimental data for irregular waves available in the literature as well as due to the complicated nature of the ship behaviour in such conditions which raises difficulties in comparative studies. The simulations in irregular waves, with both randomly distributed amplitude and phase components, are utilised to generate an incident wave realization and are highly dependant whether irregular wave's generation based on a selected spectrum with certain number of user pre-defined harmonic wave components can be implemented in the basin. As already seen the difficulties had arisen even for the polychromatic wave of limited number of harmonic components. Since the irregular numerical simulation using the superposition principle deals with one spatial and temporal wave realization it is difficult to achieve a correspondence of such complex mechanism within the laboratory created. Thus, the phenomenon of parametric resonance is governed by the synchronization between the irregular free surface elevation and lateral stability characteristics of the vessel.

Because a (container) vessel will sail with different loading conditions and encounter different wave conditions at different speeds the amount of information which is needed for a reliable operational guidance is rather large and possibly infeasible. However, with actual knowledge of the different physical phenomena that yields large roll motions and possibilities to use reliable numerical models and/or model tests databases, the identification of cases when large roll motions will occur can be made by employing the results from regular wave's excitation.

Once again the results are compared with the modified simulation procedure only. The first analysis addresses the Test No. 35 for the wave generation No. 27a. The particulars of the wave 27a

are the significant wave height of $H_S = 8$ m and $T_W = 12.95$ s with the JONSWAP spectra of $\gamma = 3.3$ utilised as seen on figure 8-30, together with calculated statistics on table 8-10.

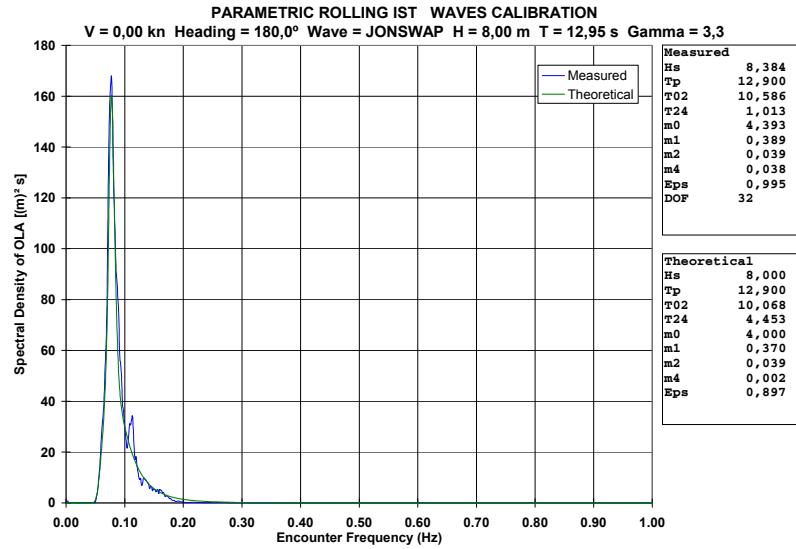


Figure 8-30. Wave 27a with significant wave height of $H_S = 8$ m, $T_W = 12.95$ s, JONSWAP spectra $\gamma = 3.3$

The measured peak amplitude is $\eta_4 = 6.39^\circ$ seen on figure 8-31. The results reveal the parametric rolling begins to emerge at around 1100 seconds from the start of the test (figure 8-31). Some cases of numerical calculations were also performed for 3 hours simulation to identify number of groups with parametric roll (short term statistics).

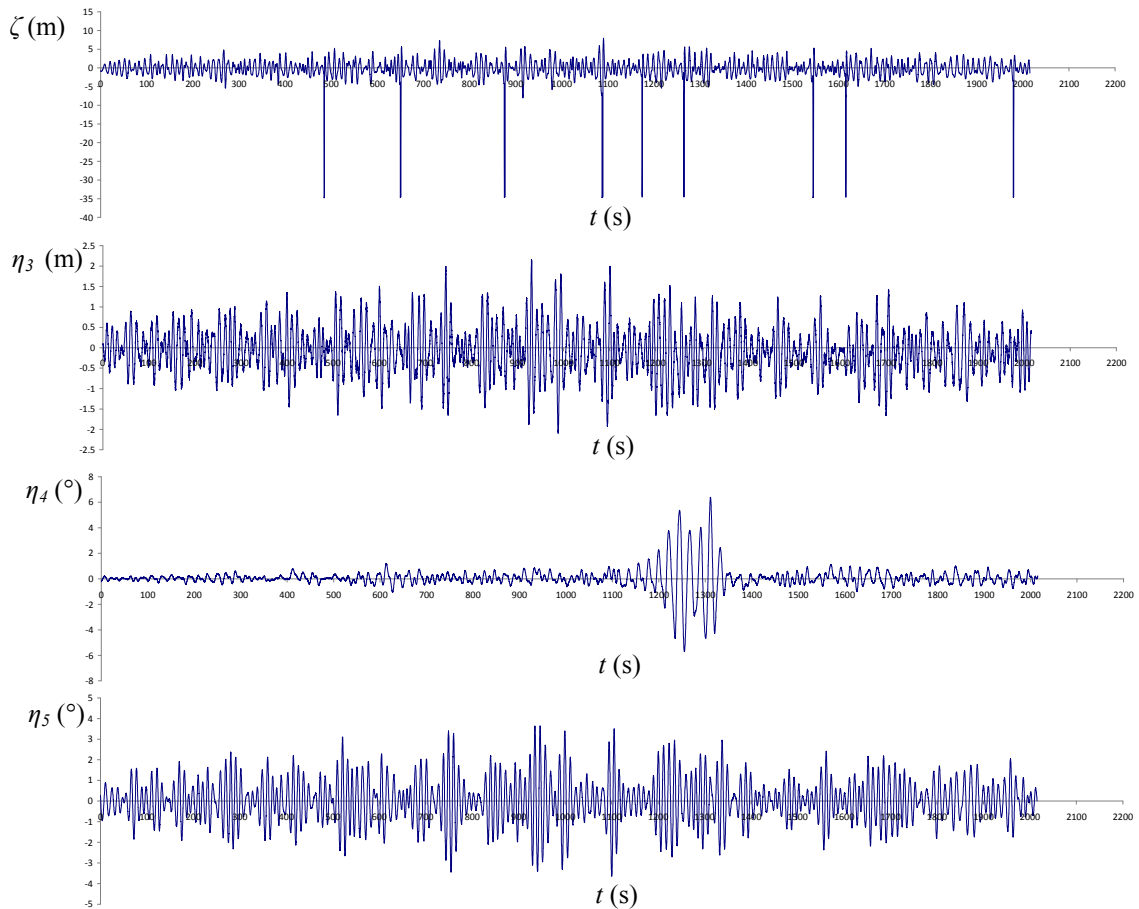


Figure 8-31. Time history of Test No. 35

It is interesting to see that when parametric rolling starts the heave and pitch motions became more regular. That pattern is significant since it reiterates the regular wave behavior observed from the correlation between the wave excitation and the heave or pitch motions. Therefore, more regular excitation yields more regular motions which in turn possibly lead to parametric rolling. The following figure 8-32 over plots the wave and roll time history. Sudden roll amplification, however, lags behind the wave excitation. In other words, in order to “see” the parametric resonance a certain number of quasi-regular wave cycles are needed. Also, roll period shifting is evidenced in the prediction of the parametric roll phenomenon.

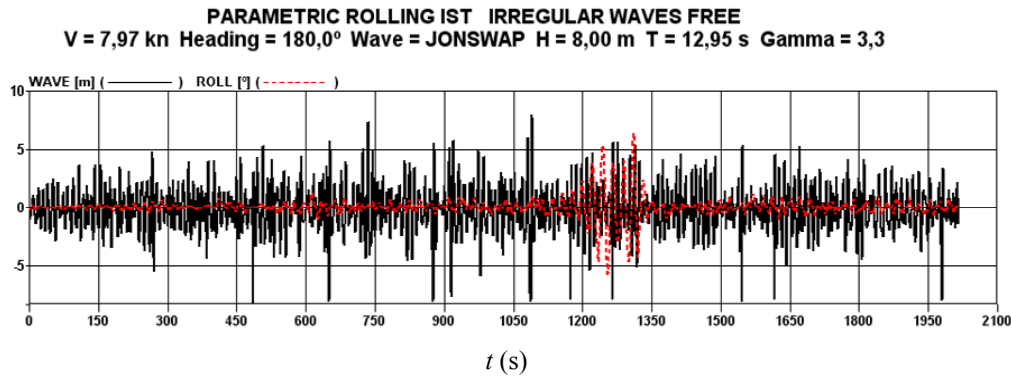


Figure 8-32. Wave elevation and roll time history of Test No. 35

The wave groups for which the parametric rolling is possible are presented on the figure 8-33. Irregular wave’s structure, with a group of relative high waves is followed by several relatively small waves. The parametric rolling as seen on the right, losses momentum in between two wave groups only to increase again after which completely disappears as the wave height falls under the threshold value.

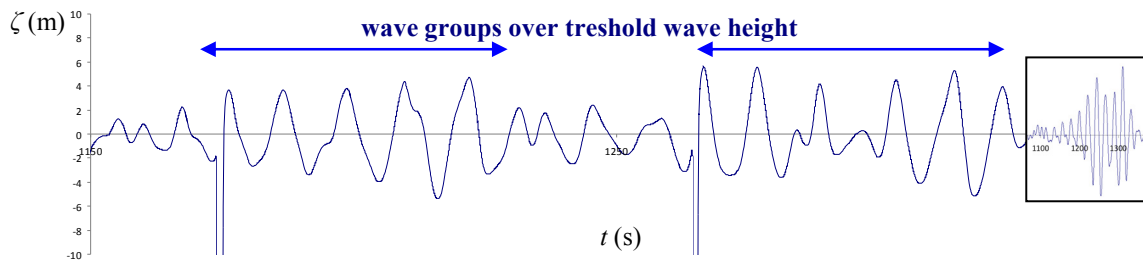


Figure 8-33. Segment of wave profile for which the parametric rolling initiates

Better visualisation of the above stated is possible when looking at the Test No. 36 for 170° heading outcome. The speed increment is analogous to the polychromatic tests. The first figure 8-34 represents the numerical simulation with the calculated peak amplitude of $\eta_4 = 16.83^\circ$

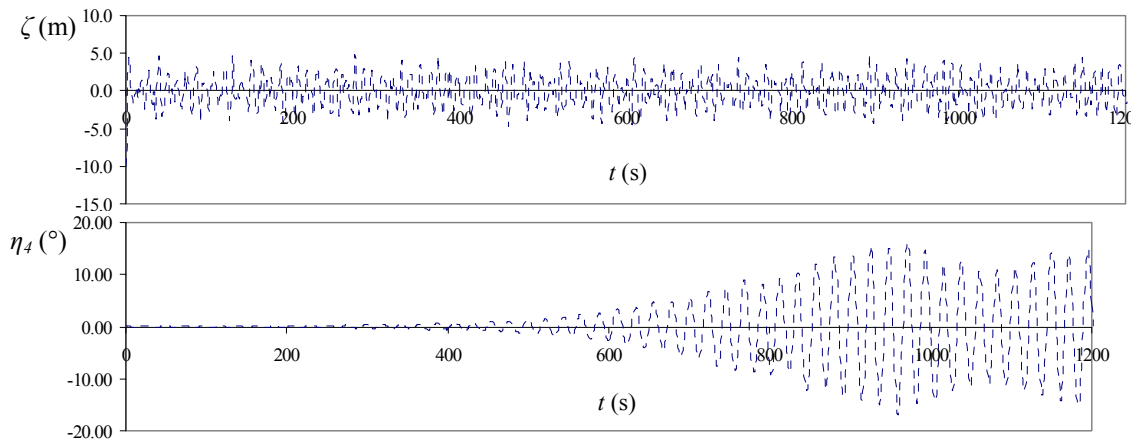


Figure 8-34. Numerical simulation associated with Test No. 36.

Using the same JONSWAP spectra of $\gamma = 3.3$ the measured peak amplitude of $\eta_4 = 17.06^\circ$ are observed on the figure 8-35. Although the obtained amplitudes are matched perfectly it is evident that for the numerical simulation parametric rolling persists while for the experiment stops. Also as stated before, resonance can develop quicker in the experiments than in numerical simulations. Nonlinearity of the dynamic system makes description of its response to random excitation more complicated and the greatest concern is ergodicity and distribution. Then, there is also a damping issue. The irregular excitation makes it harder to assess it. In particular, for the case of zero linear damping (a conservative approximation proposed for examination purposes), theoretical results predict the potential inception of parametric roll in irregular waves in whatever environmental and loading condition.

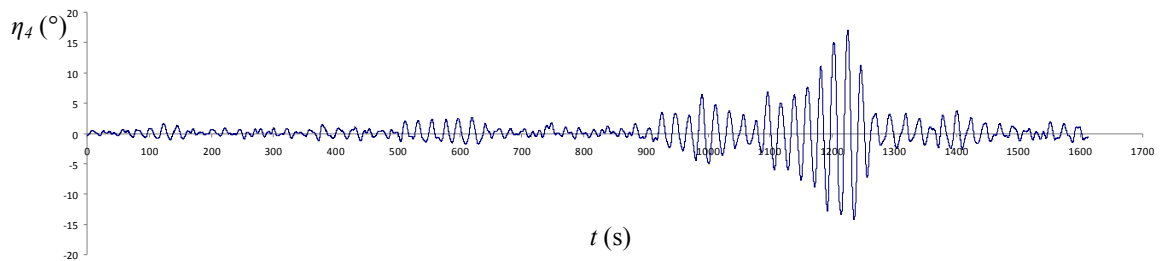


Figure 8-35. Experimental time trace of rolling motion for Test No. 36.

In order to illustrate the dynamic effect that triggers parametric rolling the wave and roll time history are presented on the figure 8-36. Pointed by the blue arrow is the time instant upon which the sustained wave regularity ceases which consequently terminates parametric resonance as indicated by the red arrow. Looking at that particular time instant the biggest amplification is observed precisely when the wave height “diminishes” which reaffirms the lag explanation from above.

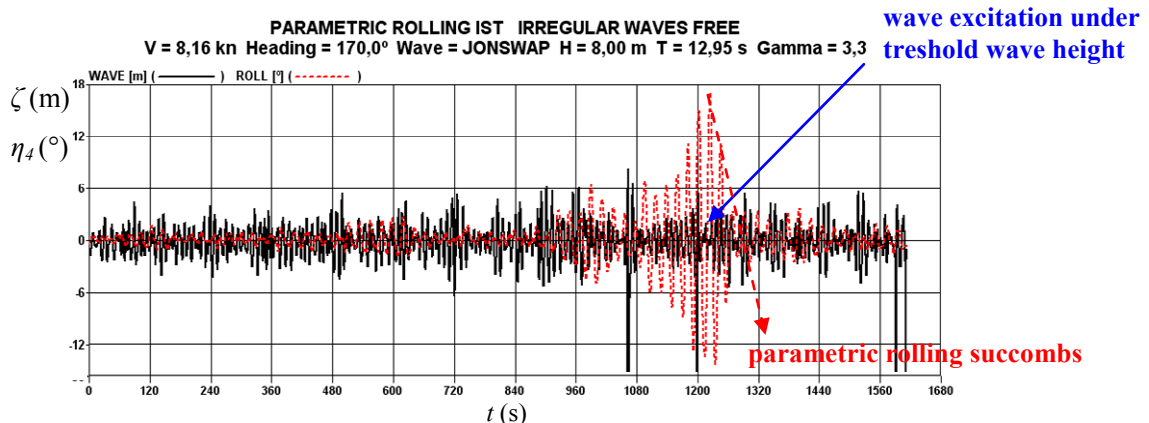


Figure 8-36. Wave elevation and roll time history of Test No. 36 with physical explanation

Test No. 32 for the 160° heading is almost the same as for test No. 20.

The same procedure is now implemented on the following wave cases. The remaining 3 tests are subsequently presented starting from Test No. 339 corresponding to the 0° heading. The peak amplitude of $\eta_4 = 25.25^\circ$ are measured. Time traces of wave elevation and roll motion are seen on figure 8-37. As oppose to the head waves set up these tests were performed for the significant wave height of $H_S = 4$ m and period of $T_W = 14.19$ s. The smaller wave height determined as the design wave threshold value is of significant importance in terms of establishing the start up of parametric rolling mechanism.

The wave group necessary for build up of parametric roll is best exemplified on figure 8-37 and thus corresponding the head wave samples.

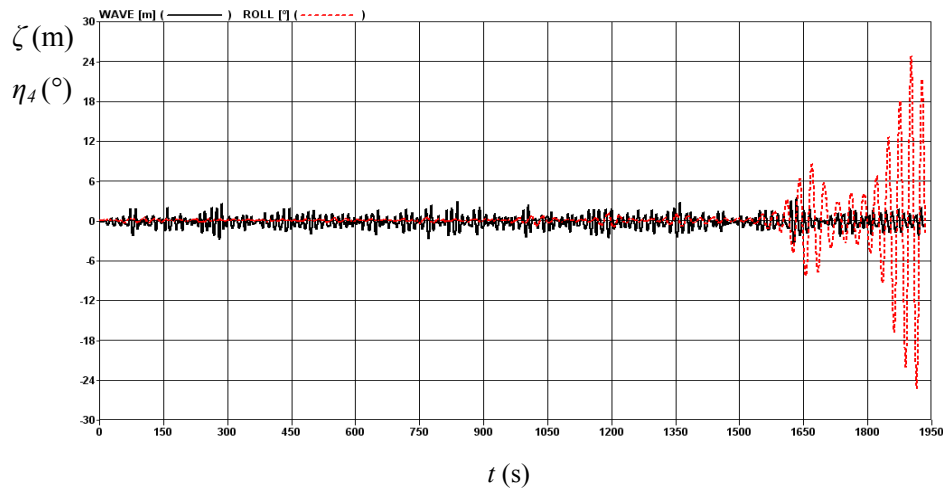


Figure 8-37. Wave elevation and roll time history of Test No. 339

Numerical simulation performed for the same set of conditions revealed following outcome as seen on figure 8-38.

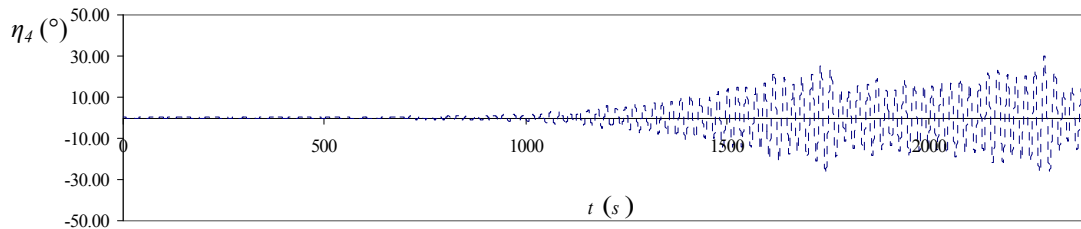


Figure 8-38. Numerical simulation associated with Test No. 339.

However, looking at Test No. 340 with the peak amplitude of $\eta_4 = 28.29^\circ$ measured, the characteristic wave groupiness isn't deterministically identifiable. While in the deterministic case the choice of initial conditions determines whether the system exhibits large amplitude motions or settles down to the trivial solution, large amplitude motions in irregular waves occur in stochastic patterns. Figure 8-39 shows the time history of a roll realization, where the occurrence of large amplitude motions was observed two times within a period of 20 minutes.

One thing that is indeed in common with the previous tests is the fact that the roll amplitude matches the wave excitation. However, as one would expect that once the wave height is under the certain threshold, parametric rolling will cease, while in fact it persists. Although parametric roll is more likely to occur when ships encounters a longer group of higher waves, the periods of waves in the group proved to be of equal importance.

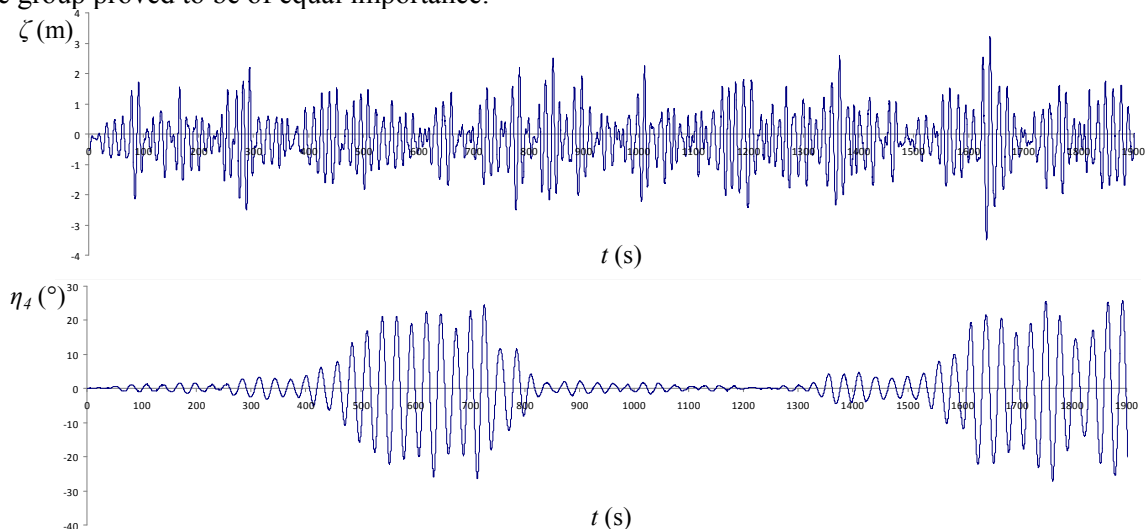


Figure 8-39. Time history of Test No. 339

This is even more illustrative as given by the figure 8-40.

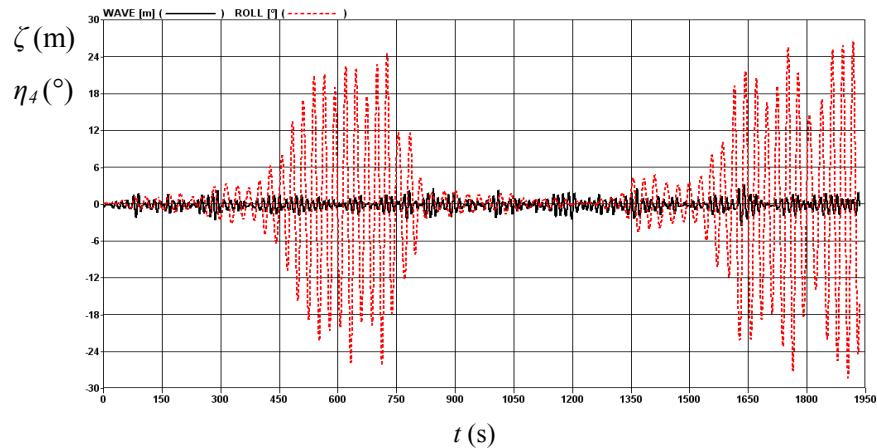


Figure 8-40. Wave elevation and roll time history of Test No. 340

The numerical simulation yielded following outcome (figure 8-41) which resembles the experiment in terms of amplitude achieved however as evidenced from the majority of the simulations it turned out that above a certain wave height the number of groups decreases because the vessel is continually subject to parametric roll.

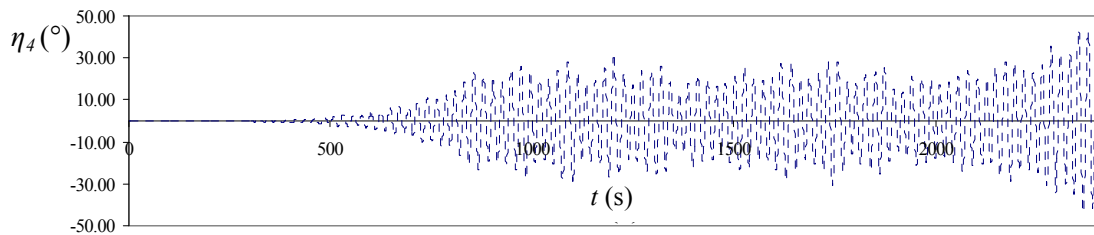


Figure 8-41. Numerical simulation associated with Test No. 340.

Test No. 341 with the peak amplitude of $\eta_4 = 27.48^\circ$ provides very similar trend. Once again during the run, parametric roll developed not only once (figure 8-42).

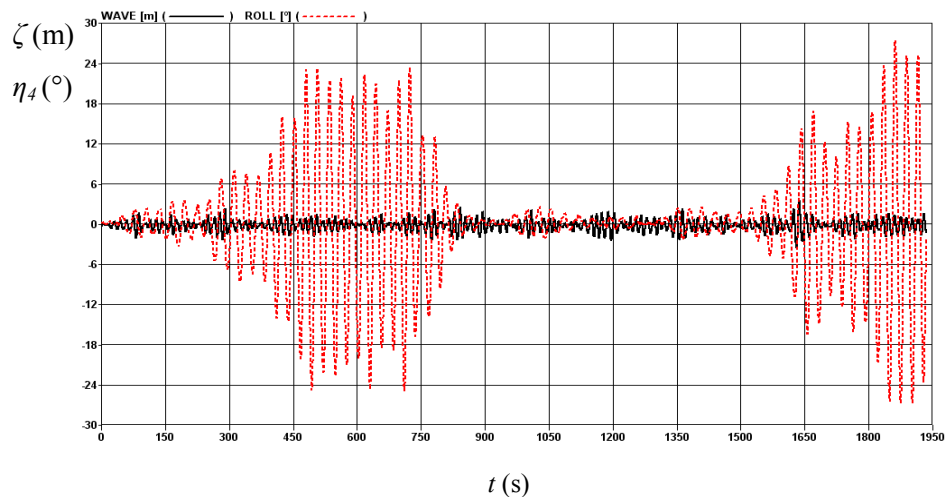


Figure 8-42. Wave elevation and roll time history of Test No. 341.

In fact it faded away and then developed for a second time, while in both occurrences reaching large angles. As seen, a sequence of short groups with similar periods, although below wave height threshold proved to be very dangerous (important experiment since the significant wave height of $H_S = 4$ m produces quite a number of even smaller wave groups and still enables parametric rolling).

The statistical results of measurements in irregular waves are given as the probability of exceedance of roll angles of the model test results (figure 8-43). As by nature irregular waves are random, thus the two created wave profiles will not be the same. In order to facilitate the numerical simulations, 20 randomized profiles using certain predefined settings were enforced in trying to establish parametric rolling. They consisted of 20 realizations generated from the same JONSWAP spectrum, but with a different set of random phases for each realization. Usually around 10% of all random wave profiles were able to reproduce parametric rolling, even though the damping ratio was deliberately tuned over with the critical one, to check the inception to parametric rolling. Although the differences in the extreme values are small the distribution throughout all the simulations is very different. The statistical results of the numerical simulation are thus not implemented, because the probability of the exceedance once the parametric rolling is established would be unrealistically too high. Also, statistical results cannot be used to determine if the vessel suffered from parametric roll in that particular condition, because the vessel could indeed be in parametric roll conditions only for a small period of time, which wouldn't influence the statistical results.

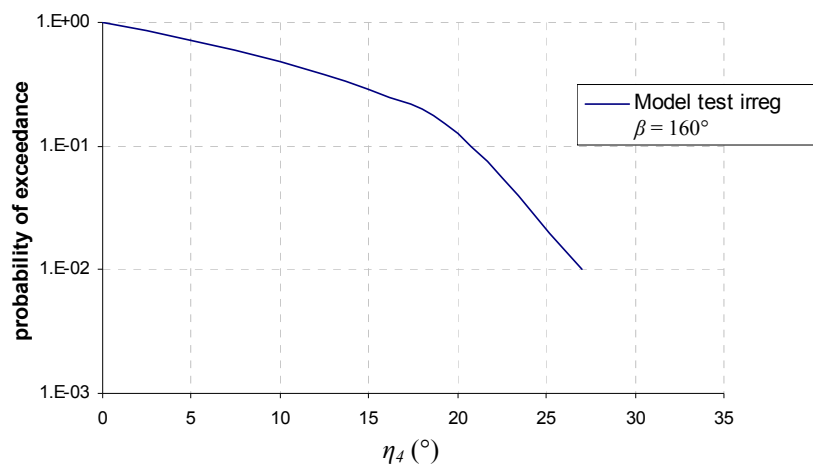


Figure 8-43. Comparison of the distribution of maxima

From the presented one thing also stands out. Throughout the experiment a pattern where the highest amplitudes are measured for the purely longitudinal seas is not obtained here. That is also contrary to the other reports. Based on this, it is possible to deduce that there is alternate mechanism that supports large roll angles even though the wave excitation is not sufficient by itself.

The effect is identified as a pure loss of stability in oblique following seas. The problem with the broadside of a C11 hull is that it's inclined towards inner direction, so the roll restoring moment does not sufficiently increase even when it rolls. A pure loss of stability failure is modelled as the persistence of the metacentric height below a critical level for a too long time. Different approaches, not necessarily leading to the same outcomes, can be employed for the determination of the spectrum of the fluctuation of the metacentric height although precisely because of this it is difficult to aggregate irregular waves parametric rolling in comparative studies.

The captive model experiment that were conducted to measure roll restoring variation in following seas which is a major cause of pure loss of stability, need to be compared with numerical result estimated for the righting lever based on the determination of static righting levers. It reflects the most important dynamic effects with a sufficient accuracy without making the calculation procedure too complicated. It is valid for the given position of the wave crest, but if this position is varied, then the correct pitching amplitude and phase must be used for the calculations to obtain the correct results. This certainly is an aspect that will be worked on in the future especially in distinguishing between such important stability phenomena.

Although the pure loss of stability isn't the part of the current investigation a finding like this suggest that sufficient safety against parametric rolling or pure loss can only be achieved by the combination of these criteria.

8.6 Proposition of probabilistic methodology for irregular waves parametric rolling survey

After the individual analysis the survey of parametric rolling in irregular waves is in order. An equivalent design wave from the regular wave's survey can be used in order to assess parametric roll. One can assume that the design wave length defines the average zero-crossing period and design wave height is set equal to significant wave height. Each combination of averaged zero-crossing wave period T_z and significant wave height H_s is mapped to statistical frequency or probability estimate of the observation. To analyze the probability of parametric roll in each condition the individual time traces can be used.

Using the same resolution with the regular wave's simulations the irregular waves simulations were designed to be carried out for randomized wave profile using certain settings. Irregular waves in the open sea are known to be ergodic processes within the period of quasi-stationarity. One of the possible ways is to use a wave scatter table, where each combination of averaged zero-crossing wave period T_z and significant wave height H_s is mapped to statistical frequency or probability estimate of observation. However, the response of a nonlinear system such as this might be non-ergodic and repeated realizations for the same conditions are necessary to obtain reliable statistical estimates.

That was a major obstacle since one full analysis is very computationally extensive (over a month). Fully nonlinear codes with time convolution integral would take much longer. With the limited number of analysis it is impossible to get sufficient data for any definite conclusion to be drawn. For that reason the results are not fully processed yet. The same simulation of a given set of environmental conditions needs to be repeated many times as seen on individual examples due to the absence of ergodicity which requires substantial adding to computational effort.

The distribution of parametric roll was found to be quite different from normal as may be seen in Belenky, et al., (2003), with the peak of the distribution significantly sharper. Parametric roll distribution's deviation from Gaussian curve is caused by the non-existence of ergodic properties but using this computational tool it can be avoided here, as it is always possible to generate as many realizations as are needed to achieve the required statistical accuracy of the parametric roll response (note that the tool is fully functional and the only thing preventing immediate results is time restriction).

Therefore, the gap realised between those outcomes on the sketch, is seen to be the assessment of roll extremes with small probability called risk parameter (figure 8-45) by extrapolating the results fitted with the suitable theoretical distribution (Rayleigh or Weibull) to the generated statistics to achieve a correlation between the distribution of peak values of η_{4a} on one sea state (short term) and the distribution of extremes η_{4max} on a certain number of equal sea states (long term). It is even possible to evaluate joint probabilities of a certain sea state with the probability of pre-defined parametric rolling amplitude exceedence.

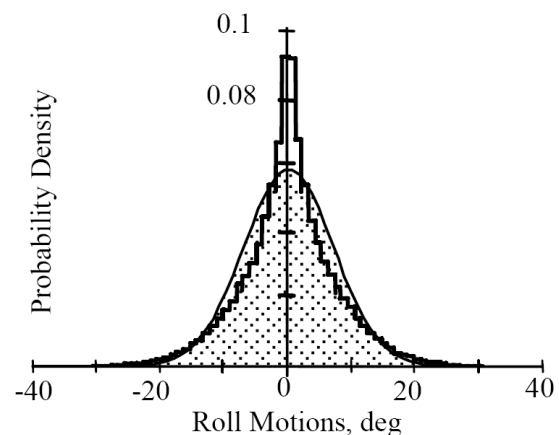


Figure 8-44. Distribution of parametric roll

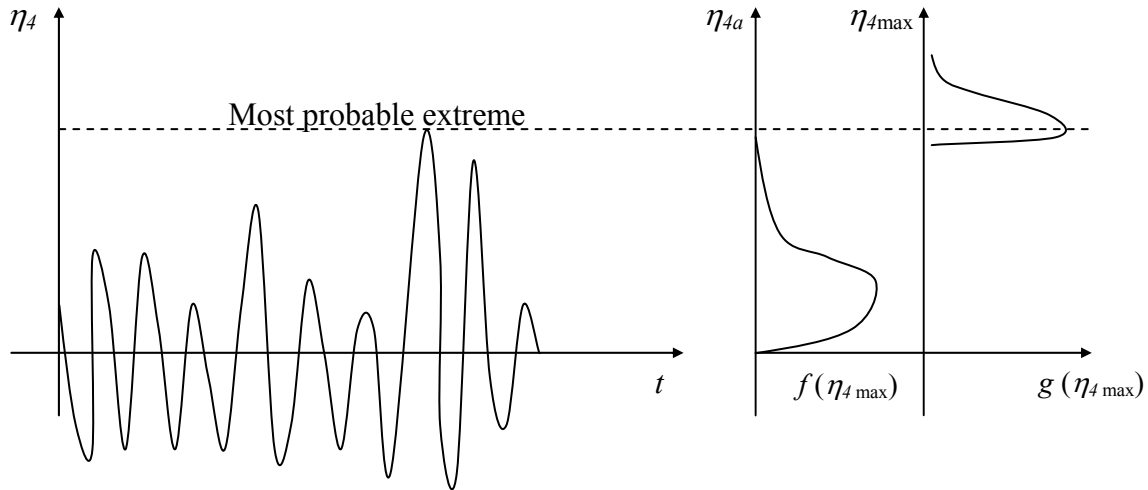


Figure 8-45. Assessment of roll extremes with small probability methodology

Table 8-8 will be representing the distribution of collected simulations of the parametric rolling amplitudes in excess of for instance $\eta_4 > 20^\circ$, for a significant wave height and the mean zero crossing periods representing a sea state. These approaches have also been utilised by the author as a part of previous studies in particular with the application to the wave height extremes (Prpić-Oršić et al. 2007.) and extreme wind load assessment (Turk and Prpić-Oršić, 2009). Only a small modification of the existing program is required to facilitate the implementation for the roll response extremes. The aim as said is to generate a database containing the probability of parametric roll for a range of speeds, wave heading, wave conditions and loading conditions by running the systematic series of simulations. The shaded portions of the table represent the conditions which are already established by the undertaken calculations as the one prone to the parametric rolling. As the waves created are irregular (i.e. randomized using certain settings) the two created wave profiles will not be the same. Therefore each irregular waves simulation has to be repeated for a single speed and heading.

Parametric rolling scatter diagram ($\eta_4 > 10^\circ$, or 20° , or 30°)											
Total											
14.5											
13.5											
12.5											
11.5											
10.5											
9.5											
8.5											
7.5											
6.5											
5.5											
4.5											
3.5											
2.5											
1.5											
0.5											
$H_{s,m} / T_{z,s}$	7.5	8.5	9.5	10.5	11.5	12.5	13.5	14.5	15.5	16.5	17.5
											Total

Table 8-8. Parametric rolling scatter diagram

Considering that is possible to have multiple parametric rolling realizations in each simulation time traces has to be analysed for these groups to be determined with the total duration of

all groups in one simulation. A few large roll angles in limited number of cycles are sufficient to cause large damage to the vessel which however won't influence individual statistical results. Also noticed from the simulations, the accuracy of such an approach is highly dependent on the reliability of the roll damping terms.

The proposed probabilistic methodology is the most accurate but also most demanding both in terms of execution and time effort which is the reason why it wasn't implemented in any of the studies cross-referenced. Even though it may be impractical such thorough investigation can be compared for the validation purposes of the simplified methods debriefed below and sketched on the right. Although there is no well established standard method to evaluate the probability of parametric roll, there are available alternatives that were pursued in order to develop such a capability (figure 8-46.). Since most of the analytical tools to treat parametric roll, e.g., the Mathieu equation, are available for regular waves, the wave envelope approach is also a logical choice used for parametric roll and validated against model test; see (Bulian, et al., 2003). Also the use of the "effective wave concept" or so called "Grimm wave" was applied to the problem of parametric roll by Umeda, et al., (2004) (see the application in Ch. 2). The concept in which the irregular wave is replaced by a regular one with the length equal to the length of a ship and its crest or trough situated at the center of gravity was very efficient.

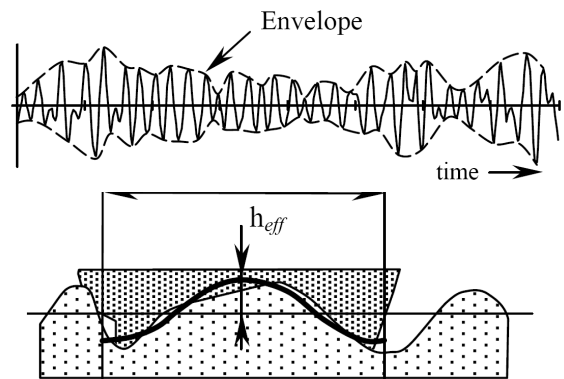


Figure 8-46. Alternative probabilistic methodology

However, within the recent framework for the development of IMO New Generation Intact Stability Criteria mentioned in the chapter 1, a significant role is played for the development of a "vulnerability assessment methodology" to be applied in the early design stage with the aim of identifying ships prone to the inception of parametrically excited rolling motion. The term susceptibility is omitted on purpose and the new term vulnerability is introduced to distinguish the basic difference since it accounts for the case of irregular waves based on a "regular wave environment" by considering the following "practical equivalence":

- wave length is equal to the wave length associated to the modal spectral frequency,
- wave height is equal to the significant wave height.

Following the above proposed methodology, a plot (figure 8-47) is presented for irregular waves. The irregular waves are developed on a Jonswap spectrum using 41 wave frequencies ranging from 0.2 rad/s to 2 rad/s. Consider that this outcome was available after 20 repeated simulations for the same conditions of speed and heading. Only the maximum amplitude obtained from those simulations is considered to be plotted. Loading condition GM1 is applied for the head waves while loading condition GM2 is enforced for the following waves. The reason is that for the following waves loading condition GM1 is not susceptible to parametric rolling. It is assumed that the design wave length defines the average zero-crossing period and design wave height is equal to significant wave height. Then, it is possible to determine the height using equal statistical frequency. The conditions upon which the irregular survey was concentrated to affirm the numerical predictions is for the zero up-crossing period of 12.95 seconds and significant wave height same as with the regular waves at $H_s = 8.0$ meters. Whilst comparing both the regular and irregular outcomes it is evident that the spread is very much in agreement. Due to the non-ergodicity of inception of parametric rolling with respect to the nonlinear irregular waves response, the spread is somewhat fractionalised. Even so, the results seem to be complying as the number of iterations is progressed. The occurrence is randomized although with more repetitions a spread would achieve a smoother layout. The definite conclusion that can be drawn is that the irregular wave excitation yields less severe roll angles although under a real world scenario, the vessel may encounter unexpected large roll motions in a relatively short time and quicker than numerically. This was identified as the condition of principal

resonance and the figure illustrates that parametric rolling is possible under the maximum sustained speed. The maximum sustainable speed is evaluated with LAMP program given in (Levadou et al. 2003)

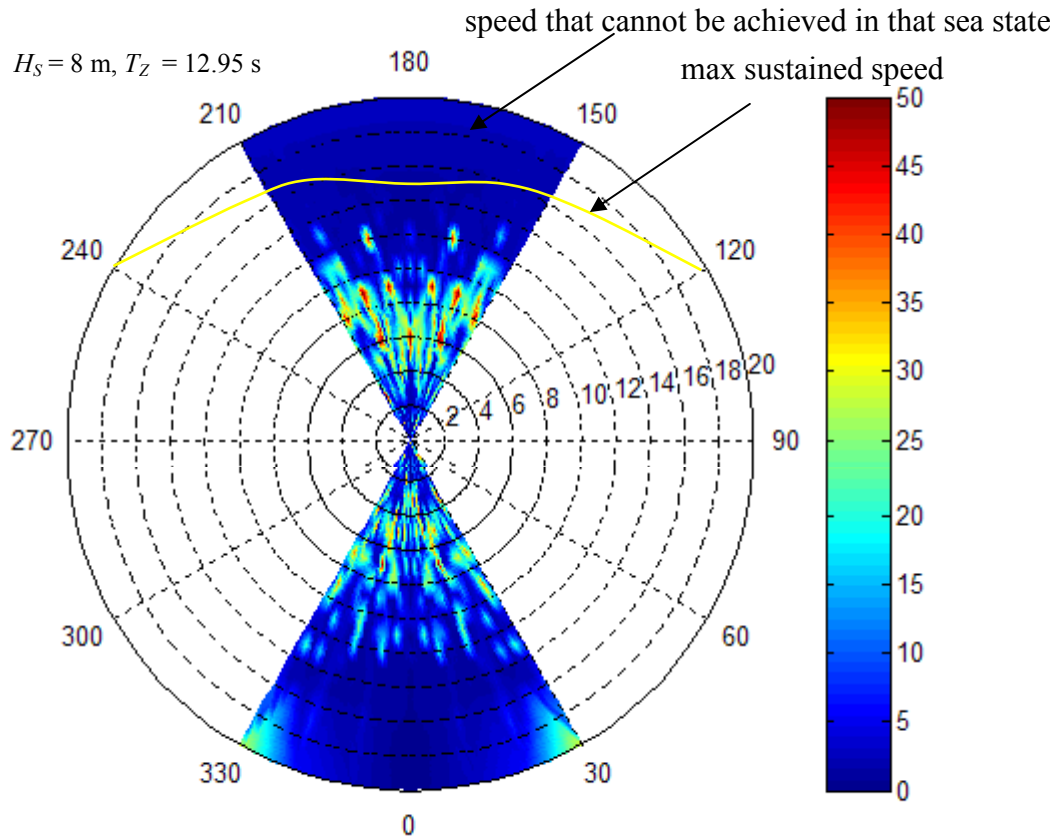


Figure 8-47. Numerical evidence with polar plots of parametric rolling for ($H_S = 8$ m, $T_Z = 12.95$ s).

The results, in addition, have demonstrated that the increasing of speed, in certain conditions, can be an effective means for the reduction of the parametrically excited rolling motion but an increase in speed is likely to increase undesired effects, such as slamming or water on deck. On the other hand, more severe sea states would lower the sustainable speed curve and together with the presented in which parametric rolling becomes possible at higher speeds actually excludes the possibility that the vessel will be encountered to this phenomenon.

The reason that envelope and effective wave probabilistic approach are suitable is coming from the essential information on the roll behavior in irregular seas that is contained within the analysis in regular waves. Numerical simulations of the roll equation also show that for an average wave frequency of 0.5 rad/s, large amplitude motions do not occur for significant wave heights smaller than 4.0 m. For greater wave heights, large amplitude motions are observed, and the maximum roll angles correspond to the limiting values found in the analysis of the deterministic case.

8.7 Proposition of blending methodology for irregular waves parametric rolling survey contained within the regular waves analysis

Although the visual inspection confirms the above stated a generalized weighted formula is applied where data points contribute with its weighted coefficients, in this case roll angles, determining the relative importance of each quantity on the average. The example on the following figure 8-48 for irregular wave excitation with significant wave heights of 6 and 10 meters exemplifies it. Note that the plot represents only the head case scenario while mirrored around 90-270°.

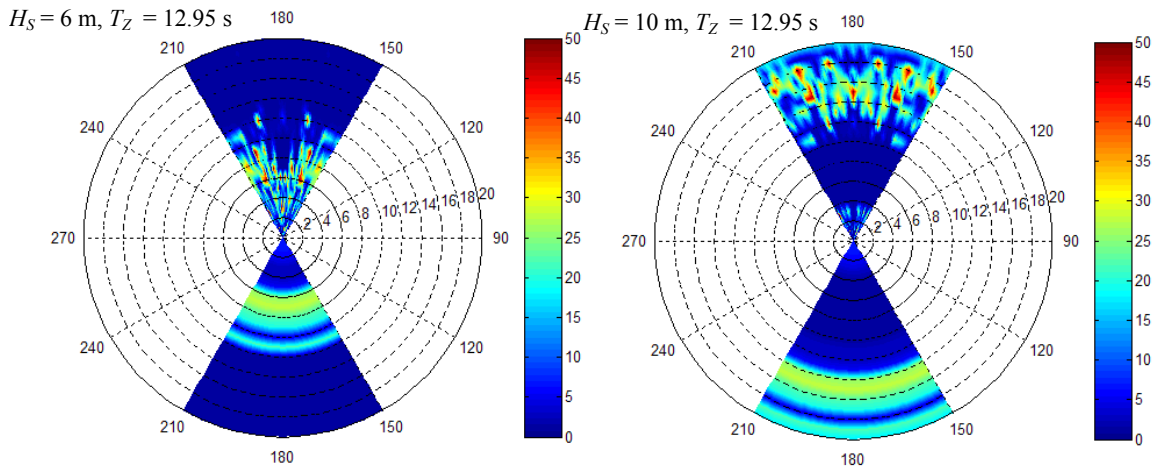


Figure 8-48. Weighted generalization of the irregular parametric excitation for ($H_S = 6$ and 10 m, $T_Z = 12.95$ s).

If we were to compare such a generalized distribution with the regular wave excitation of $H_S = 6$ m, it is possible to see the essence of the roll behavior in irregular seas which is contained within the regular waves analysis. The irregular spread is rather generalized but the trend is obvious with the ability to minimize the inherent uncertainties related to the simulation in irregular waves.

The reason that the amplitudes in irregular generalized plot are smaller lies in the fact that both the irregular wave excitation yields less severe amplitudes while also being decreased because of the weighted averaging performed. The intention was to stress out the link in between the deterministic and stochastic excitation for the parametric rolling rather than dealing with the roll angle quantity.

The non ergodic properties of the parametric rolling effectuations in irregular seaway are manifested within the possibility that parametric rolling indeed happens outside of the region as designated by the regular analysis. It can be easily explained since one generation of wave can contain groups that are either quite bigger or smaller than the significant wave height. For instance parametric rolling is not possible for speeds below 3 knots in the deterministic case of $H_W = 6$ m, but it can be within the stochastic pattern as seen on figure 8-49, also for the $H_S = 6$ m.

Recall that smaller wave heights shift the realization toward lower velocities, therefore it is entirely possible that a single generation of $H_S = 6$ m produced a group of waves with the smaller effective wave height. Consequently, the parametric rolling was initiated even for the lower speed. On the other hand, again, experiments and numerical computations have shown that change of heading could not be an efficient way of escaping from parametric resonance, especially in short-crested irregular waves, where the pure parametric autoparametric excitation combines with a “beam-sea-type” excitation of the ideal source of energy type. The usual way of keeping bow/head sea at reduced speed in rough weather has been shown by facts to be sometimes not only ineffective, but even dangerous.

The reasons that led to the consideration of regular waves with respect to irregular waves are briefly discussed in the description of the methodology. Basing the method on the analysis of the “range of dangerous speeds” allows to significantly reduce the effect of the unavoidable uncertainty associated to the estimation of the ship's linear roll damping concerning irregular excitation. Although the methodology contains a certain level of presumptions, it seems it could fulfill the target of a relative rational comparison between different operational design condition alternatives. Finally, a 3D plot for the significant wave height of 6, 8, and 10 m is presented for the irregular excitation (figure 8-50). Due to the extensive computational effort other crossing periods T_Z are still not fully processed.

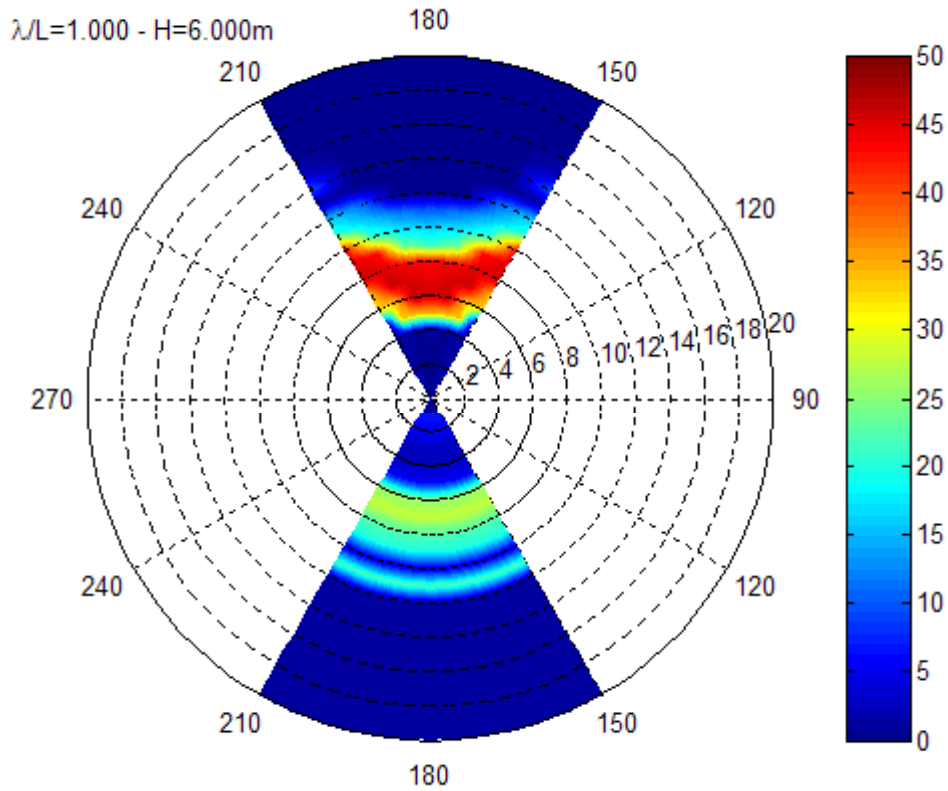


Figure 8-49. Weighted generalization of the irregular parametric excitation compared to regular for ($H_S = 6$ m and $H_W = 6$ m, $T_Z = 12.95$ s and $T_W = 12.95$ s).

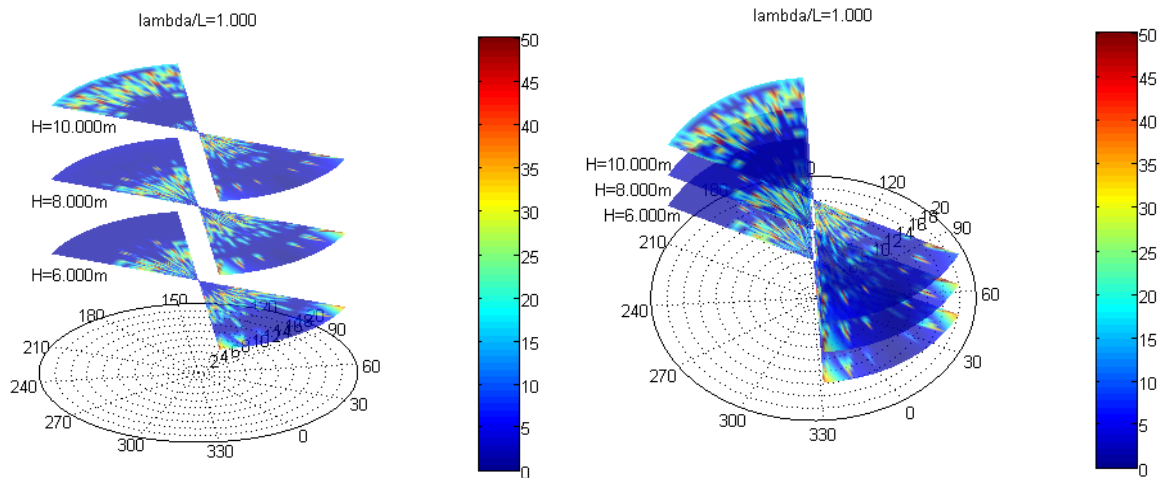


Figure 8-50. Numerical evidence with 3D polar plots of parametric rolling with irregular following waves ($T_Z = 12.95$ s).

It has to be noted that following seas outcome due to the adopted loading condition 2 is somewhat unrealistic, meaning that normally it is manifested around 0 knots and around 20 knots but not in between, which was proved when analyzing regular following waves (figure 8-51).

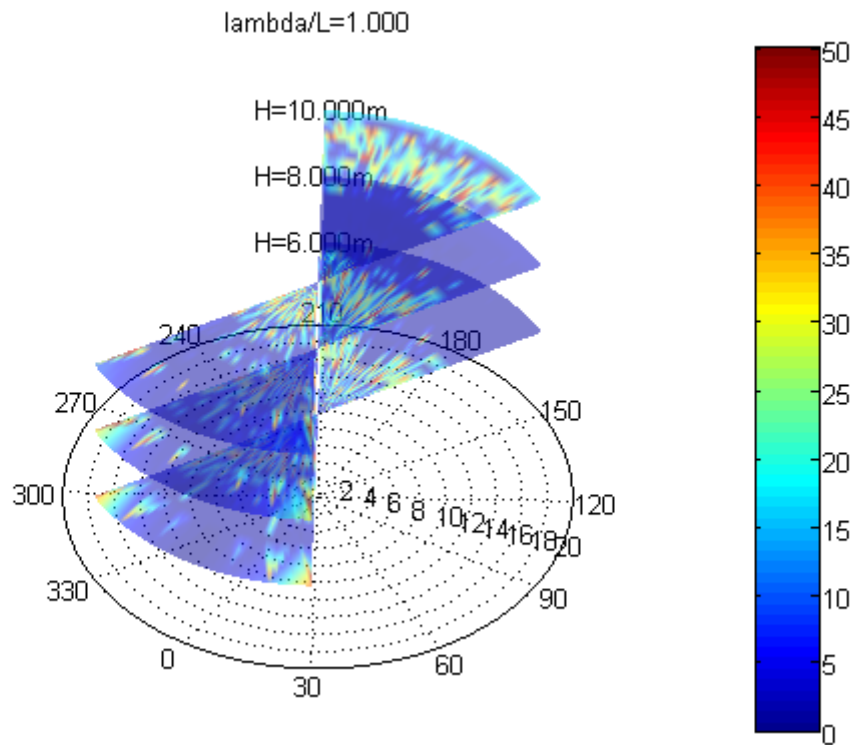


Figure 8-51. Numerical evidence with 3D polar plots of parametric rolling with irregular following waves ($T_z = 12.95$ s).

It was important to get insight into the parametric roll phenomenon in realistic environmental conditions, i.e., mainly irregular sea, and for this reason this model seems very effective especially in a preliminary phase of the research. Although they are not fully reliable for accurate predictions, they can give important information on the underlying physics of the phenomenon under analysis. Despite the theoretical, numerical and experimental evidence of the potential danger associated to this phenomenon, the real encountering at sea is up to now, according to ship operators, quite limited in comparison to what scientific literature would lead to imagine.

This last observation probably contains the key of the matter: ships as we saw are very often “susceptible” to parametric roll, however skilled ship handling together with the usual irregularity of the sea can avoid it in a vast majority of cases.

9 Conclusion

Parametric rolling is an unstable phenomenon, which can quickly generate large roll angles that are coupled with significant pitch motions. The phenomenon of parametric roll has been known over the last decades, but it only recently garnered attention from a regulatory and prevention standpoint because of the practical implications related to the induced large amplitude roll motions and due to its complicated highly non-linear character that makes its prediction quite difficult in actual seaways.

9.1 Physical insights

Although the contribution to the existing method of Riberio e Silva and Guedes Soares (2005) is described in detail in chapters 3 and 5, what stand about the work involved in developing the present theory and code with the experimental model data is new physical insights that led to better understanding of this resonance phenomena. The coupling between the induced roll and pitch motions along with the nonlinear character of the restoring moment associated with large amplitude wave induced motions have been found to be the determinant factors of the observed roll resonance phenomenon. Furthermore, along with the variation in GM from trough to crest conditions associated with bow flare immersion and emergence in head sea conditions, also damping values with pitch resonance in the longitudinal waves are here said to be the prime reason for parametric rolling.

While the nonlinear change to the hydrostatic and Froude-Krylov force can be significant, it may not be enough to over-power ships to parametric rolling mode if not for the damping deficiency found in relatively low roll angles. Because of the specific hull form at inclined position, these particular vessels seem unable to “trap” the water resulting in the “sweep down” mechanism leading to larger roll angles. This leads to the hypothesis that the inclusion of nonlinear damping procedure is necessary to capture this effect. The validation cases seem to support such a modeling decision.

The presented work also revealed several aspects of the time domain simulation method, which are quite valuable for the validation of the method prior to its application for the assessment of the probability of the parametric roll in actual sea waves. For that reason designed polychromatic waves provided reasonable hindsight especially in terms of wave “groupiness” range necessary to establish resonance phenomena. In the event of parametric roll, it should be realised that the transient stage, which is influenced by initial conditions, might be of considerable duration. This fact is important, since it sets requirements to the discretisation of the applied interval of wave frequencies used for the description of the stochastic sea.

Although parametric roll in longitudinal regular waves is, nowadays, a quite well understood phenomenon, difficulties still exist (also from a conceptual point of view) concerning the case of irregular waves. However, with actual knowledge of the different physical phenomena that yields large roll motions and possibilities to use reliable numerical models and/or model tests databases, the identification of cases when large roll motions will occur can be made by employing the results from regular wave’s excitation which is of immense importance.

Still, the results presented support the non-ergodicity concept due to the nonlinear responses, even though a clear physical connection to the regular wave inducement was proved with a weighted averaging method useful to identify sub-critical range directly on the onset of parametric rolling in longitudinal seas. With the original quasy-modular approach kept, the optimisation of the calculation procedures led to the methodology for predicting the likelihood and magnitude of large roll events for everyday engineering analysis given that a not insignificant risk of parametric roll in head seas cannot be avoided, especially for large container carriers. The influences of some important factors with respect to parametric rolling of ships have been thoroughly analyzed by means of the simulation tool. The factors include wavelength, wave height, encounter angle of seaway, ship speed, surging motion, GM value, etc...

9.2 Overview

The complete methodology and its respective findings with conclusions were given at the end of each chapter and therefore it will be presented here only in brief. This work constituted of the introductory section with the state-of-the art overview, after which the theoretical background for parametric rolling of ships was presented. The prediction of the occurrence of parametric rolling in regular waves (susceptibility criteria) and the prediction of amplitude of parametric rolling (severity criteria) was also examined. The third chapter concentrated on strip theory which is based upon the potential flow theory. The linear and non-linear seakeeping theories were examined as the theoretical background upon which the numerical code is constructed.

Linear strip theory can provide quick answers for preliminary design, but is often unable to predict behaviour for extreme events which are often of interest. The goal of this dissertation was to formulate an approach that can predict nonlinear events while being computationally efficient and robust. This approach can then be used in the design stage or for real-time simulations to predict vessel responses. Fortunately, nature has its way of taking care of things. Therefore, the main nonlinear contributions such as Froude-Krylov forcing and damping, to this resonance effect can be quite effectively implemented while other nonlinear contributions that do not account much in terms of parametric rolling build up can be treated linearly without sacrificing accuracy. The computation speed is very fast, executing near real-time (few seconds per simulation) on a desktop PC. The robust capabilities of this method make it a good candidate for large motion simulations of any hull form that meets the slender-body requirements. Loading the hull offsets is straightforward, and maybe a wide range of analyses is available.

The numerical code is based on the transfer of frequency domain data to time domain and the inclusion of so called Froude-Krylov nonlinear part of the loading in time domain. Use of simplified 2½D method showed only slight improvement over classical 2D method with the disadvantage of being more computationally intense than standard strip theory, but certainly less so than 3D codes. Given modern computer capabilities and the development of 3D seakeeping codes, using a higher fidelity 3D panel code would seem to be the preferred choice but then all the benefits from this method would seem in vain.

Therefore, the model proposed by Riberio e Silva et al. (2005) applied to describe the dynamics of a container vessel subject to parametric roll resonance conditions was further developed, modified and upgraded to be cross referenced and validated against experimental data on parametric rolling hydrodynamic characteristics. One of the primary aims of the present theory was to develop a code that would be extremely computationally efficient. Therefore, assessment of the present theory's computation speed should be considered a part of the theory's validation. The aspect of the present theory that provides an advantage in computational effort over any other theories is that the hydrodynamic forces can be developed solely from 2D potentials that are independent of ship speed and relative wave heading. That is, the 2D independent hull radiation potentials at a given frequency of encounter are used in the determination of 3D total radiation (including interaction forces) and diffraction forces. The 2D radiation potentials on each section can be computed and stored for a set of "basis" encounter frequencies that cover an appropriate range with an appropriate resolution. For a "run" in the frequency domain at a particular ship speed, relative wave heading, and wave frequency, the radiation potentials on each 2D panel at the resulting encounter frequency can be used from the stored potentials at the basis frequencies. This avoids significant computational expense given that experience has shown that maximum 10 basis frequencies to be adequate in parametric rolling prediction, providing seakeeping predictions at multiple ship speeds and wave headings will almost certainly benefit from this approach.

Because the numerical tool will automatically generate and analyze hundreds or thousands of parametric rolling scenarios, it is imperative that the analysis tools are computationally efficient. Yet at the same time, in order to incorporate meaningful optimization logic, the tools must be accurate up

to the operational requirement levels. The interface that was programmed for the purpose of carrying out the time domain simulations is not limited to the scope of this work and may be used for any other vessel under any other settings.

The extensive experimental programme which consist as a large part of this work has been divided in four main groups of tests with the particular interest in,

1. free heave, roll and pitch tests in both regular and irregular waves;
2. roll decay tests in both calm water and waves.

which was utilised to investigate and explain these two consisting inseparable treatments of the damping and seakeeping simulations, respectively. The experiments were conducted under the project title “Experimental Assessment of the Parametric Rolling on a C11 Class Containership”, with the vessel chosen because of its established propensity towards parametric rolling.

Special attention as said was given to damping evaluation. The Miller method that was used from the start was abandoned (considered too crude and unable to efficiently reconstruct damping presence) and all the simulations were performed using the modified Ikeda’s method. For that reason a completely new module was introduced based on this very comprehensive strip theory approach with a state of the art application designed especially for a large vessels like C11, upgrading the existing commonly used platform for the damping assessment. The proposed methodology very much enables scrutinizing the damping components that contribute it. The reliability of the implemented model in simulating damping behaviour is validated against experimental data. Based on the evidence from the decay tests vessels of this type possess a damping deficiency at relatively small roll angles that may push the ship in the parametric resonance mode. Therefore, it is argued that damping not only affects the roll amplitude but is also equivalent to the time varying righting arm stability in terms of importance, with respect to the development of the parametric rolling. The problem of roll damping prediction probably will not be fully solved in the near future. In the present code, a nominal value is proposed not as an absolute design value but as a starting point for predicting susceptibility especially in irregular wave’s survey.

Since the computer program works with the quasi-modular approach with different parts of the code that work in conjunction this new module was also implemented in the simulations with the blending method that utilizes the roll amplitude as a nonlinear variable (both as a converging iterative process or in-time direct calculations) which efficiently reduces roll amplitudes resembling the experimental results. The hybrid approach appears to be actually independent of the technique used in the frequency domain, even if the reliability of the results is strongly related with the accuracy of the evaluation of the hydrodynamic terms. The simulation method in the work is a well functioning program code and appears to give very plausible and coherent results. The nonlinear model from decay test was also implemented as a modification of the existing program again validating the results obtained by using two coupled nonlinear models (needed to simulate “parasitic” effect at smaller roll angles) tuned with the exponential fitting procedure.

While there are undeniable uncertainties in both calculations a question regarding repercussions on the seakeeping simulation with respect to the uncertainty in the damping modeling, and the repercussions on the reliable damping assessment using the strip theory method while attempting to “duplicate” results from experiments, was raised and successfully answered. The validation has shown good agreement with the experimental results for roll both in the experiments where parametric roll resonance occurred and in the experiments where it did not occur. Aside from severe rolling in head seas, other significant results of the investigations were decreased roll response with greater vessel speed and also with increased GM and significantly dampened roll response due to free surface effects. The simulated results and subsequent analysis provided insight and improved understanding of the parametric roll resonance mechanism.

Because a (container) vessel will sail with different loading conditions and encounter different wave conditions at different speeds the amount of information which is needed for a reliable operational guidance is rather large. To be more visually plausible, all the results, be it from regular, polychromatic or irregular waves were presented in 3D polar plots, quite intuitive and applicative to

the vessel crew. Specifically, simulations can be used to study the mean out-crossing rate relative to a fixed critical level. The mean out-crossing rate might then be used in decision support systems as the basic number, again to predict about the probability of exceeding certain response levels.

9.3 Further work

This work actually opened up a wealth of opportunities to study in future. Some of these features are already started up while some will need more attention. During the work there were two main problems addressed and it is the cohesion between the damping and the effect it has on the onset of the parametric rolling. The new damping program is designed as a separated entity; however it was the blending method with the seakeeping code which allowed the biggest benefits. Still, as constituted the state of the art Ikeda's method is by no means an absolute reference and a further consideration of its applicability is in order. Continuing, this research can be used in evaluating certain roll stabilizing devices and antiroll tanks in order to improve their response to roll motion. Wave motions initiate this roll and, if in close synchronization with the hull's natural roll period, roll may build to uncomfortable or even dangerous proportions. The idea is to counteract the tendency of a vessel to roll with an equivalent and opposite righting moment applied in exactly the proper phase and proportion.

The asymmetric cross-section experiments with the ship inclined processed by the other group in the project have revealed the change in added masses and damping coefficients of heave and pitch due to the heeling of the vessel. Since the decay experiments revealed distinct possibility that the ship loses "damping ability" in the same range of inclinations due to its uncharacteristic and novel form triggering the excessive roll motion even stronger a suggestion would be to perform comparative analysis of the heave-roll coupling added mass and damping effects for asymmetric cross-sections.

The theoretical assumption is that under the uncharacteristic roll decrement "appearance" some discrepancies can be traced and explained within the forced oscillation tests for the ship inclined (0° , 5° and 10°) understanding the rate of change in all hydrodynamic coefficients due to heeling expected through heeled angle experiments. The calculation of these coefficients may be incorporated on the time domain code to take the differences into account and to develop the code further. The procedure of calculating the damping coefficients in time domain instead of calculating them in frequency domain and keeping them constant was already utilized and the same can be adapted to the hydrodynamic coefficients.

While analyzing the experimental results during the irregular following waves survey a combination of various dangerous phenomena constituting of reduction of intact stability, synchronous rolling motion, parametric rolling or even surf-riding and broaching-to was found to be possible. The dynamic behavior of a ship in following and quartering seas is very complex. Ship motion is three-dimensional and various detrimental factors or dangerous phenomena may occur in combination with the above-mentioned simultaneously or in a sequence. This could create extremely dangerous combination which may cause ship capsize. Each of these phenomena requires separate studying.

The parametric rolling in irregular waves is rather unpredictable in real seas when multiple seas and swells coming from different directions. As already confirmed parametric roll is not ergodic and not (necessarily) a Gaussian stochastic process which raises the question of the risk involved associated with the assessment of roll extremes with the small probability. While the methodology for evaluating probability of extremes for parametric rolling inception is already in works establishing the risk of encountering critical conditions based on scenario simulations on given routes of operations process is only possible with large sample of repeated simulations. The generated realizations as are needed to achieve the required statistical accuracy of the parametric roll response fitted to the suitable theoretical distribution to achieve a good statistical correlation. These

requirements are expensive and tough to meet in every stage of design but will give a reference to the approximate methods that are being implemented instead. Another advantage of this probabilistic viewpoint is contained within the risk assessment methodology. The probability of parametric rolling can also be seen as joint to the current theoretical probability distributions of wave parameters, with for instance, probability of encountering critical wave groups.

The most efficient way to present this roll database information contained within the 3D plots is an onboard application which would be put for the ship specific motions choosing both loading condition and wave condition. It can act as an automatic tool efficiently signaling the danger or taking precautionary measures to avoid it. In this way it would have to be interfaced with the weather forecast or from onboard radar for example, informing the master on potential risk by showing which headings and speeds to avoid, or acting automatically.

REFERENCES

- ABS, 2004. ABS Guide for the Assessment of Parametric Roll Resonance in the Design of Container Carriers. American Bureau of Shipping. Sweden, "Recordings of head sea parametric rolling on a PCTC." IMO Document SLF47/INF.5, June 10, 2004.
- Bass, D., Haddara, M. R., 1988. *Nonlinear Models of Ship Roll Damping*, Int. Shipbuilding Prg., Vol. 35, 5–24.
- Belenky, V. L., Weems, K. M., Lin, W. M., Paulling, J. R., 2003. *Probabilistic Analysis of Roll Parametric Resonance in Head Seas*. Proc. 8th Int. Conf. on Stability of Ships and Ocean Vehicles STAB, 325–340.
- Bertaglia, G., Serra, A., Francescutto, A., 2003. *The Intact Stability Rules Are Changing: Impact on the Design of Large Cruise Ships*. Proc. RINA International Conference on Passenger Ship Safety, March 2003, London, 45–54.
- Bertaglia, G., Serra, A., Francescutto, A., Bulian, G., 2003. *Experimental Evaluation of the Parameters for the Weather Criterion*. Proc. 8th Intl. Conference on Stability of Ships and Ocean Vehicles STAB2003, Madrid, September 2003., 253–263.
- Blendermann, W., 1996. *Wind loading on ships-collected data from wind tunnel tests in uniform wind*, Institut für Schiffbauder Universität Hamburg, Report 574.
- Blocki, W., 1980. *Ship safety in connection with parametric resonance of the roll*. International Shipbuilding Progress 27 (306), 36–53.
- Blume, P., Hattendorf, H. G., 1982. *An Investigation on Intact Stability of Fast Cargo Liners*. Proceedings of the 2nd International Conference on Stability of Ships and Ocean Vehicles (STAB'82), Tokyo, Japan.
- Bulian, G., Francescutto, A., 2003. *On the non-linear modeling of parametric rolling in regular and irregular waves*. Proc. 8th International Conference on the Stability of Ship and Ocean Vehicles, Madrid, 305–323.
- Bulian, G., Francescutto, A., Lugni, C., 2006. *Theoretical, numerical and experimental study on the problem of ergodicity and 'practical ergodicity' with an application to parametric roll in longitudinal long crested irregular sea*. Ocean Engineering, Vol. 33, 1007–1043.
- Bulian, G., Lugni, C. and Francescutto, A., 2004. *A contribution on the problem of practical ergodicity of parametric roll in longitudinal long crested irregular sea*. Proc. 7th International Ship Stability Workshop, Shanghai, 101–117.
- Bureau Veritas, 2005. Parametric roll - Bureau Veritas approach, Technical note.
- Cardo, A., Francescutto, A., Nabergoj R., 1982. *On Damping Models in Free and Forced Rolling Motion*. Ocean Engineering, Vol. 9, No. 2, 171–179.
- Carmel, S. M. 2006. *Study of parametric rolling event on a panamax container vessel*. Journal of the Transportation Research Board, 1963:56–63.
- Chakrabarti, S., 2001. *A technical note on empirical calculation of roll damping for ships and barges*. Ocean Engineering, 28, 915–932.
- Chang B. C., 2008. *On the parametric rolling of ships using a numerical simulation method*. Ocean Engineering, 35, 447–457.
- Clauss, G. F., Hennig, J., 2003. *Deterministic Analysis of Extreme Roll Motions Using Tailored Wave Sequences*. Proc. 8th Int. Conf. on Stability of Ships and Ocean Vehicles STAB, 441–455.
- Contento, G., Francescutto, A., Coppola, C., Penna, R., 1994. *A Methodology for the Analysis of the Roll Decay Curves*. Tecnica Italiana, Vol. 59, 1–14.
- Cramer, H., Krüger, S., 2001. *Numerical Capsizing Simulations and Consequences for Ship Design*. Proc. German Society of Naval Architects, 95, 72–78.
- Cummins, W. E., 1962. *The impulse response function and ship motions*. Schiffstechnik, 101–109.
- Dallinga, R. P., Blok, J. J., Luth, H. R., 1998. *Excessive rolling of cruise ships in head and following waves..* In: RINA International Conference on Ship Motions and Manoeuvrability, Royal Institute of Naval Architects, London, UK.
- Dalzell, J. F. 1978. *A note on the form of ship roll damping*. Journal of Ship Research, 22, 178–185.
- DeKat JO, Paulling JR., 1989. *The simulation of ship motions and capsizing in severe seas*. Transactions. The Soc of Nav Archit and Mar Eng V 97 France WN.
- DNV. (2005). Distribution of Mean wave Directions for H>6. *Det Norske Veritas*, Internal Report.
- Dreossi, M., 2004-2005. *Analisi critica di un metodo semi-empirico per la previsione dello smorzamento del moto di rollio*. Università degli Studi di Trieste.

- Dunwoody, A. B. , 1989. *Roll of a ship in astern seas—metacentric height spectra*. J. Ship Res., 33, 221–228.
- Fan, Y. T., Wilson, P. A., 2004. *Time Domain Non-linear Strip Theory for Ship Motions*. Transactions of the Royal Institution of Naval Architects, Vol. 146, 33–47.
- Fonseca, N., Guedes Soares, C., 1998, *Time-Domain Analysis of Large-Amplitude Vertical Motions and Wave Loads*. Journal of Ship Research 42.2: 100–113.
- France, W. N., Levadou, M., Treacle, T. W., Paulling, J. R., Michel, R. K., and Moore, C. 2001. *An investigation of head-sea parametric rolling and its influence on container lashing systems*. In SNAME Annual Meeting.
- France, W. N., Levadou, U. M., Treacle, T. W., Paulling, J. R., Michel, R. K., Moore, E. C., 2003. *An Investigation of Head-Sea Parametric Rolling and its Influence on Container Lashing Systems*. Marine Technology vol 40.
- Francescutto, A. 2001. *An experimental investigation of parametric rolling in head waves*. Journal of Offshore Mechanics and Arctic Engineering, 123:65–69.
- Francescutto, A., Bulian, G., 2002. *Nonlinear and stochastic aspects of parametric rolling modelling*. In Proc. of the 6th International Ship Stability Workshop.
- Francescutto, A., 2002. *Roll-Sway-Heave Coupling in Beam Waves*. Proc. (CD) of 12th International Symposium on Offshore and Polar Engineering - ISOPE'2002, Kita-Kyushu, Vol. 3, 281–287.
- Francescutto, A., Contento, G., 1998. *The Modeling of the Excitation of Large Amplitude Rolling in Beam Waves*, Proc. 4th International Ship Stability Workshop, St.Johns, Newfoundland.
- Frank, W., 1967. *Oscillation of Cylinders in or Below the Free-Surface of Deep Fluids*. Report 2375, Naval Ship Research and Development Center, Washington D.C.
- Froude, W., 1863., *Remarks on Mr. Scott Russell's paper on rolling transactions*. INA 4, 232–275.
- Grim, O., 1952. *Rollschwingungen, Stabilität und Sicherheit im Seegang*. Schiffstechnik, vol. 1., 10–21.
- Grim, O., 1961. *Beitrag zu dem Problem der Sicherheit des Schiffes im Seegang*. Schiff und Hafen, 6(6), 490–497.
- Haddara, M. R., Cumming, D., 1990. *Experimental investigation into roll damping characteristics of a warship hullform*. Institute for Marine Dynamics (Canada).
- Haddara, M. R., 1980. *On the Parametric Excitation of Nonlinear Rolling Motion in Random Seas*. International Shipbuilding Progress, Vol. 27, No. 315.
- Haddara, M. R., Leung, S. K., 1994. *Experimental Investigation of the Lift Component of Roll Damping*. Ocean Engineering, Vol. 21, No 2, 115–127.
- Hamamoto, M , Panjaitan, J. P., 1996. *A Critical Situation Leading to Capsize of Ships in Astern Seas*. Journal of the Society of Naval Architects of Japan , Vol.180, 215–221.
- Hashimoto, H., Umeda, N. , 2010. *A study on Quantitative Prediction of Parametric Roll in Regular Waves*. 11th International Ship Stability Workshop Dunwoody, 1989 A.B. Dunwoody, Roll of a ship in astern seas—metacentric height spectra. J. Ship Res., 33 (1989), 221–228.
- Hasselmann, K. et al. 1973, 1976 *Measurements of wind-wave growth and swell decay during the joint North Sea wave project (JONSWAP)*. Dtsch. Hydrogr. Z., 8A (Suppl.), 1–95.
- Hayashi, C., 1953. *Forced Oscillations in Nonlinear Systems*, Nippon Printing and Publishing Co., Osaka, 14+164 pp, ASIN B00071VW4I.
- Helas, G., 1982. *Intact stability of ships in following waves*. Proceedings of the Second International Conference on Stability of Ships and Ocean Vehicles, Tokyo, 689–700.
- Hennig, J., 2005. *Generation and Analysis of Harsh Wave Environments*. Proc. German Society of Naval Architects, 99 .
- Hennig, J., Brink, K. E., Kuehnlein, W. L., 2003. *Innovative Deterministic Seakeeping Test procedures*. Proc. 8th Int. Conf. on Stability of Ships and Ocean Vehicles STAB, 457–465.
- Himeno, Y., 1981. *Prediction of ship roll damping—state of the art*. Dept. Naval Arch.& Mar. Engrg., University of Michigan, Rep. no 239.
- Holloway, D. S., Davis, M.R., 2001. *Computation of ship motions by a high Froude number time domain strip theory*. University of Tasmania School of Engineering Research Report SERR 08/01.
- Hsiu, T. C., Zhou, C. G., 1990. *Identification of Nonlinear Rolling Damping Model, Report*. The Naval Academy of Engineering, China.
- Hua, J., Wang, W. H., Chang , J.R., 1999. *A representation of GM-variation in waves by the volterra system*. Journal of Marine Science and Technology, Vol. 7, No.2, 94–100.

- Hua, J.; 1992. *A study of the parametrically excited roll motion of a RO-RO ship in following and heading waves*. International Shipbuilding Progress 39 (420), 345–366.
- Hutchison, B. L., 1991. *The Transverse Plane Motions of Ships*. Marine Technology. Vol. 28, No. 2, 55–72.
- Hutchison, B. L., Bringle, J. T., 1978. *Application of seakeeping analysis*. Society of Naval Architects and Marine Engineers, 48.
- Ikeda, Y., Himeno, Y., Tanaka, N., 1976. *On Roll Damping Force of Ship – Effects of Friction of Hull and Normal Force of Bilge Keels*. Journal of Kansai Society of Naval Architecture, Japan, Vol.161, 41–49.
- Ikeda, Y., Himeno, Y., Tanaka, N., 1977. *On Roll Damping Force of Ship – Effects of Hull Surface Pressure Created by Bilge-keels*. Journal of Kansai Society of Naval Architecture, Japan, Vol.165, 31–40.
- Ikeda, Y., Himeno, Y., Tanaka, N. 1977. *On Eddy Making Component of Roll Damping Force on Naked Hull*. Journal of the Society of Naval Architects of Japan, No.142, 59–69.
- Ikeda, Y., Himeno, Y., Tanaka, N. 1978. *Component of Roll Damping of Ship at Forward Speed*. Journal of the Society of Naval Architects of Japan, No.143, 121–133.
- Ikeda, Y., 2004. *Prediction methods of roll damping of ships and their application to determine optimum stabilization devices[J]*. Marine Technology, 41(2): 89–93.
- IMO 2005. Document SLF48/4/12, "On the development of performance-based criteria for ship stability in longitudinal waves", Submitted by Italy, 11 July.
- IMO, 2006. Revision of the Intact Stability Code, Sub-committee on Stability and Load Lines and on Fishing Vessels Safety, 49th session, May.
- IMO, 2007. Revised Guidance to the Master for Avoiding Dangerous Situations in Adverse Weather and Sea Conditions, Resolution MSC.1/Circ.1228. International Shipbuilding Progress 27, 139–142.
- IMO 2008a. Document SLF51/4/1, "Report of the Intersessional Correspondence Group on Intact Stability", Submitted by Germany, 10 April 2008, London, UK.
- IMO 2008b. Resolution MSC.267(85), "Adoption of the International Code on Intact Stability, 2008 (2008 IS CODE)" in MSC85/26/Add.1, Adopted on 4 December 2008, London, UK.
- ITTC, 2005. Proceedings 24th International Towing Tank Conference, Report of the Stability in Waves Committee, 40pp.
- ITTC 2006. Recommended Procedures and Guidelines; Predicting the Occurrence and Magnitude of Parametric Rolling.
- Journée, J. M. J., 2000. *Theoretical Manual of SEAWAY (Release 4.18)*. Technical Report 1216, Delft University of Technology, Netherlands.
- Kawahara, Y., Maekawa, K., Ikeda, Y., 2008. *Characteristics of Roll Damping of Various Ship Types and A Simple Prediction Formula of Roll Damping on the Basis of Ikeda's Method*. Proceedings of the 4th Asia-Pacific Workshop on Marine Hydrodynamics, Taipei, 79–86.
- Kempf, G., 1938. *Die Stabilitätsbeanspruchung der Schiffe durch Wellen und Schwinungen*. Werftreederei-Hafen, 19, 202.
- Kerwin, J.E., 1955. *Notes on rolling in longitudinal waves*. International Shipbuilding Progress 02, 597–614.
- Kreuzer, E. J., Sichertmann, W. M., 2004. *Investigation of Large Amplitude Roll Motions and Capsizing*. Proc. 9th Int. Symp. on Practical Design of Ships and other Floating Structures PRADS, 2, 689–696.
- Krüger, S., 2006. *Evaluation of Cargo Loss of a large Container Carrier due to Parametric Roll*. Int. Marine Design Conf. IMDC, Michigan.
- Krüger, S., Hinrichs, R., Cramer, H., 2004. *Performance Based Approaches for the evaluation of Intact Stability Problems*. Proc. 9th Int. Symp. on Practical Design of Ships and other Floating Structures PRADS, 2, 697–703.
- Krylov, A. 1856. *A new theory of the pitching motion of ships on waves, and of the stresses produced by this motion*. Transactions of the Institute of Naval Architects, vol. 65, 590–632.
- Kühnlein, W. K., Brink, K. E. 2002. *Model Tests for the Validation of Extreme Roll Motion predictions*. Proc. 21st Int. Conf. on Offshore Mechanics and Arctic Engineering OMAE, 28269.
- Levadou, M., Gaillarde, G., 2003. *Operational guidance to avoid parametric roll*. Proc. RINA Int. Conf. on Design and Operation of Container Ships, 75–86.
- Levadou, M., Van Walree, F., 2004. *The occurrence and avoidance of parametric roll*. 1st MARIN_NMRI workshop, October, National Maritime Research Institute, Tokyo, Japan.
- Levadou, M; van't Veer, R., 2006. *Parametric Roll and Ship Design*. Proc. 9th Int. Conf. on Stability of Ships and Ocean Vehicles STAB.

- Lin W. M., Yue D.K.P., 1990. *Numerical solution for large amplitude ship motions in the time-domain*. Proceeding of the 18th Symposium on Naval Hydrodynamics, University of Michigan, Ann Arbor. National Academy of Sciences.
- Lloyd's Register, 2003. Head-sea parametric rolling of container ships, Marine Services Information Sheet.
- Lövstadt, M., Bloch Helmers, J., 2004. *Decision Support for the Ship's Crew by DNV Active Operator Guidance System based on WASIM*. Proc. German Society of Naval Architects, 98, 33–39.
- Malenica, Š., Chen, X. B., Orozco J. M., Xia J. 2006. *Parametric roll - Validation of a numerical model*, 7th International Conference on Hydrodynamics.
- Maritime Reporter Magazine, 2008, Page 55.
- Mathisen, J. B., Price, W. G. 1984. *Estimation of Ship Roll Damping Coefficients*. Trans. RINA, 295–307.
- Matusiak, J., 2003. *On the effects of wave amplitude, damping and initial conditions on the parametric roll resonance*. Proc. 8th International Conference on the Stability of Ship and Ocean Vehicles, Madrid, 341–348.
- McCue, L. S., Belknap, W., Campbell, B., 2007. *On the Parametric Resonance of Tumblehome Hullforms in a Longitudinal Seaway*. American Society of Naval Engineers, Technical paper.
- McCue, L. S., Bulian, G., 2007. *A Numerical Feasibility Study of a Parametric Roll Advance Warning System*. Journal of Offshore Mechanics and Arctic Engineering, Vol. 129, 165–175.
- Meyers, W.G., Applebee, T. R, Baitis, A.E., 1981. *User's manual for the standard ship motion program, SMP*. David Taylor internal report DTNSRDC/SPD-0936-01.
- Miller, E. R., 1974. *Unknown Title of a Report on Roll Damping*. Technical Report 6136-74-280, NAVSPEC.
- Moideen, H., Falzarano, J., 2010. *A Critical Assessment of Ship Parametric Roll Analysis*. 11th International Ship Stability Workshop. Wageningen, Netherlands.
- Muhuri, P. K., 1980. *A study of the stability of the rolling motion of a ship in an irregular seaway*.
- Munif, A., Umeda, N., 2000. *Modelling extreme roll motions and capsizing of a moderate-speed ship in astern seas*. J Soc Nav Archit Jpn 187:51–58
- Munif, A, Umeda, N., 2006. *Numerical prediction on parametric roll resonance for a ship having no significant wave-induced change in hydrostatically-obtained metacentric height*, International Shipbuilding Progress 53, 183–203.
- Nabergoj, R., Tondl, A., Virag, Z., 1994. *Autoparametric Resonance in an Externally Excited System*. Chaos, Solitons & Fractals, Vol. 4, No. 2, 263–273.
- Nayfeh, A. H., Mook, D.T., 1979. *Nonlinear Oscillations*. John Wiley & Sons, Inc.
- Nayfeh, A.H., 1973. *Perturbation methods*. John Wiley & Sons Inc.
- Neves, M. A. S. Rodríguez, C. A., 2005. *A coupled third order model of roll parametric resonance*. Maritime Transportation and Exploitation of Ocean and Coastal Resources.
- Neves, M. A. S., 2002. *On the excitation of combination modes associated with parametric resonance in waves*. In Proc. of the 6th International Ship Stability Workshop.
- Neves, M. A. S., Rodríguez, C. A. 2006. *An investigation on roll parametric resonance in regular waves*. In Proc. of the 9th International Conference on Stability of Ships and Ocean Vehicles.
- Neves, M. A. S.; Perez, N. A.; Valerio, L., 1999. *Stability of small fishing vessels in longitudinal waves*. Ocean Engineering, 26(12), 1389–1419.
- Neves, M.A.S., Valerio, L., 1994. *Parametric stability of fishing vessels*. Proceedings of the Fifth International conference on Stability of Ships and Ocean Vehicles, Florida.
- Newman, J. N., 1978. *The Theory of Ships*. Advances in Applied Mechanics, Vol. 18, 221–283.
- Nielsen, U. Jensen, J. 2009. *Numerical simulations of the rolling of a ship in a stochastic sea - evaluations by use of mcs and form*. Proceedings of OMAE 2009, 28th International Conference on Ocean, Offshore and Arctic Engineering.
- Odabasi A.Y., Vince J., 1982. *Roll response of a ship under the action of sudden excitation*,. Int. Shipbuilding Prog. 29, 327–333.
- Ogilvie, T. F., 1964. *Recent progress toward the understanding and prediction of ship motions*. The Fifth Symposium on Naval Hydrodynamics, 3–128.
- Oh, I.G., Nayfeh, A.H., Mook, D. T., 2000. *A Theoretical and Experimental Investigation of Indirectly Excited Roll Motion in Ships*, Phil. Trans. R. Soc. Lond. A., 358, 1731–1881.
- Palmquist, M. and Nygren, C., 2004. *Recording of head-sea parametric rolling on a PCTC*. Technical report, International Maritime Organization.

- Paulling, J.R., 1961. *The transverse stability of a ship in a longitudinal seaway*. Journal of Ship Research 4, 37–49.
- Paulling, J.R., Rosenberg, R.M., 1959. *On unstable ship motions resulting from nonlinear coupling*. Journal of Ship Research 2, 36–46.
- Perez, N., Sanguinetti, C., 1995. *Experimental results of parametric resonance phenomenon of roll motion in longitudinal waves for small fishing vessels*. International Shipbuilding Progress 42 (431), 221–234.
- Peşman, E., Bayraktar, D., Metin Taylan, M., 2007. *Influence of Damping on the Roll Motion of Ships*. 2nd International Conference on Marine Research and Transportation, Napoli (Ischia), İtalya.
- Prpić-Oršić, J. 1998. *Modifikacija STF metode proračuna njihanja vitkih tijela na harmoničnom valu za područje nelinearnih značajki odziva* (doktorska disertacija, Tehnički fakultet Sveučilišta u Rijeci, 9.10. 1998., 106 str.)
- Prpić-Oršić, J., Čorić, V., Turk, A., 2007. *The influence of large amplitudes on the accuracy of parametric rolling estimation*. International Journal Advanced Engineering. 2, 1; 87–97.
- Ribeiro e Silva, S., Uzunoglu, E., Guedes Soares, C., Maron, A., Gutierrez, C., 2011. *Investigation of the hydrodynamic characteristics of asymmetric cross-sections advancing in regular wave*. Proceedings of the 30th International Conference on Offshore Mechanics and Arctic Engineering (OMAE'2011), (Rotterdam). Paper OMAE2011-50322.
- Ribeiro e Silva, S.; Guedes Soares, C., 2000. *Time Domain Simulation of Parametrically Excited Roll in Head Seas*. Proceedings of the 7th International Conference on Stability of Ships and Ocean Vehicles (STAB'2000); Renilson, M. (ed) Launceston, Tasmania, Australia, 652–664.
- Ribeiro e Silva, S.; Santos, T.A.; Guedes Soares, C., 2005. *Parametrically excited roll in regular and irregular head seas*. Int. Shipbuild. Progr., 52, 29–56.
- Ribeiro e Silva, S. 2008. *Instabilities in the nonlinear dynamic behaviour of ships at sea* (in Portuguese). PhD thesis, Universidade Tecnica de Lisboa, Instituto Superior Tecnico.
- Ribeiro e Silva, S., Guedes Soares, C., 2009. *Parametric Rolling of a Container Vessel in Longitudinal Waves*. Stability of Marine Structures and Ocean Vehicles - STAB 2009 Conference St. Petersburg (Russia).
- Ribeiro e Silva, S., Guedes Soares, C., Turk, A., J. Prpić-Oršić, J., Uzunoglu, E., 2010. *Experimental assessment of parametric rolling on a C11 class containership*. Proceedings of the HYDRALAB III Joint User Meeting, (Hannover), 267–270.
- Ribeiro e Silva, S., Turk, A., Guedes Soares, C., Prpić-Oršić, J. 2010. *On the parametric rolling of container vessels*. Časopis Brodogradnja, 61. 4; 347–359.
- Roberts, J. B., 1982. *Effect of Parametric Excitation on Ship Rolling Motion in Random Waves*. Journal of Ship Research, Vol. 26, 246–253.
- Roberts, J. B., Spanos, P. D., 1990. *Random Vibration and Statistical Linearization*. John Wiley & Sons, Chichester.
- Roenbeck, R. G., 2003. *Containership Losses Due to Head-Sea Parametric Rolling: Implications for Cargo Insurers*. International Union of Marine Insurance Conference.
- Salvesen, N., Tuck, O. E., Faltinsen, O., 1970. *Ship motions and sea loads*. Transactions of SNAME, 78, 250–287.
- Sanchez, N. E., Nayfeh, A. H., 1990. *Nonlinear Rolling Motions of Ships in Longitudinal Waves*. Int. Shipbuilding Progress, 37(411), 247–272.
- Schalck, S., Baatrup, J., 1990. *Hydrostatic Stability Calculations by Pressure Integration (March 1989)*. Ocean Engineering, Vol. 17, No. 1.
- Schmitke, R. T., 1978. *Ship Sway, Roll, and Yaw Motions in Oblique Seas*. Sname Transaction, vol. 86, 19/8, 26–46.
- Shin, Y. S., Belenky, V.L., Paulling, J. R., Weems, K. M. Lin, W. M., 2004. *Criteria for Parametric Roll of Large Containerships in Longitudinal Seas*. Trans. Soc. of Naval Architects and Marine Engineers SNAME, 112, 117–147.
- Skomedal, N. G., 1982. *Parametric excitation of roll motions and its influence on stability*. Proceedings of the 2nd International Conference on Stability of Ships and Ocean Vehicles, Tokyo, 113–125.
- Soliman, M., Thompson, J. M. T., 1992. *Indeterminate Sub-Critical Bifurcations in Parametric Resonance*, Proc. R. Soc. Lond. A, 438, 511–518.

- Sogawa, Y, Umeda N, Hashimoto, H., 2010. *Parametric roll of a post panamax containership in regular waves: experiment, analytical method and simulation*. Proceedings of the 5th Asia-Pacific Workshop on Marine Hydrodynamics, Sakai, Japan, 99–102.
- Spouge, J. R., 1990. *Non-Linear Roll Damping Measurements*. Trans. RINA, 1–12.
- Spyrou, K. J. 2000. *Designing against parametric instability in following seas*. Ocean Engineering 27, 625–653.
- Spyrou, K. J., 2004. *Design criteria for parametric rolling*. Oceanic Engineering International, Vol.9, 11–27.
- Spyrou, K. J., Tigkas, I., Scanferla, G., Pallikaropoulos, N., Themelis, N., 2008. *Prediction potential of the parametric rolling behaviour of a post-panamax containership*. Ocean Engineering 35, 1235–1244.
- St Denis, M., Pierson W. J., 1953. *On the motion of ships in confused seas*. SNAME Transactions 61, 280–332.
- Surendrana, S., Leeb, S. K., Sohn K. H., 2007. *Simplified model for predicting the onset of parametric rolling*. Ocean Engineering 34, 630–637.
- Sverdrup, H. U., Munk, W. H. 1947. *Wind, sea, and swell: Theory of relations for forecasting*. Hydrographic Office, U.S. Navy, Publ. No. 601.
- Taguchi, H., Ishida, S., Sawada, H., Minami, M., 2004. *A model experiment on parametric rolling of a post-panamax container ship in head waves*. 1st MARIN_NMRI workshop, October, National Maritime Research Institute, Tokyo, Japan.
- Takaki, M., Tasai, F., 1973. *On the Hydrodynamic Derivative Coefficients of the Equations for Lateral Motions of Ships*. T West-Japan SNA, Vol. 46.
- Tanaka, N. 1957. *A study on the bilge keel*, Part 1. JSNA Japan 101, 99–105.
- Taylan, M. 2000. *The effect of nonlinear damping and restoring in ship rolling*. Ocean Engineering, 27, 921–932.
- Taylan, M., 2007. *On the parametric resonance of container ships*. Ocean Engineering 34, 1021–1027.
- Themelis, N., Spyrou, K. J., 2003. *Lashing of Trailers on Board Ro/Ro Ships under Intensive Rolling*. Proc. 8th Int. Conf. on Stability of Ships and Ocean Vehicles STAB, 111–127.
- Turk, A., Ribeiro e Silva, S. Guedes Soares, C., Prpić-Oršić, J. 2009. *An investigation of dynamic instabilities caused by parametric rolling of C11 class containership*. The 13th Congress IMAM, Gore, O., Okan, B. Karakas, S. (ed.). Istanbul : Graphis Matbaa, 167–175.
- Turk, A., Prpić-Oršić, J., Riberio e Silva, S., Guedes Soares, C. 2011. *Dynamic instabilities in following seas caused by parametric rolling of C11 class containership*. Proceedings of the 14th International Congress of the International Maritime Association of the Mediterranean (IMAM)- Sustainable Maritime Transportation and Exploitation of Sea Resources / Rizzuto, E. & Guedes Soares, C. (ed.). London : Taylor & Francis Group, 25–135.
- Umeda, N., Renilson, M.R., 2001. *Benchmark Testing of Numerical Prediction on Capsizing of Intact Ships in Following and Quartering Seas*. Proc. 5th Int. Workshop Ship Stability Operational Safety, Uni Trieste, 6.1.1–6.1.10.
- Umeda, N.; Hashimoto, H.; Vassalos, D.; Urano, S.; Okou, K., 2004. *Nonlinear Dynamics on Parametric Roll Resonance with Realistic Numerical Modelling*. International Shipbuilding Progress 51:2/3, 205-220.
- Umeda, N.; Takaishi, Y.; Matsuda, A.; Suzuki, S.; Watanabe, K.; Hamamoto, M.; Chiba, Y.; Sera, W., Spyrou, K., 1999. *Model Experiments of Ship Capsize in Astern Seas*. Journal of the Society of naval Architects of Japan, Vol. 177.
- Ursell, F., 1949. *On the Heaving Motion of a Circular Cylinder on the Surface of a Fluid*. Quarterly Journal of Mechanics and Applied Mathematics, Vol. II.
- Vinje, T., 1976. *On stability of ships in irregular following sea*. Norwegian Maritime Research 4 (2), 15–19.
- Watanabe, Y., 1934. *On the Dynamic Properties of the Transverse Instability of a Ship Due to Pitching (in Japanese)*, J. Soc. Naval Architects Japan, 53, 51–70.
- Wehausen, J. V., Laitone, E. V., 1960. *Surface waves*. Flügge, S. (Ed.), Handbuch der Physik, Vol. 9. Springer, 445–814.
- Witz, J. A., Patel, M. H., 1984. *A Pressure Integration Technique for Hydrostatic Analysis*. Transactions of the Royal Institution of Naval Architects, 285–294.
- Yaminouchi, Y., 1961. *Analysis of Ship Responses in Waves*. Part 1, JSNA Japan, Vol. 109.
- Yeung, R. W., Liao, S. W., Roddier, D., 1998. *On Roll Hydrodynamics of Rectangular Cylinders*. Proceedings of the Eighth. International Offshore and Polar Engineering Conference, Montreal, Canada, 24–29.
- Yumuro, A., 1970. *Research on Anti-Rolling Fin*. Part 2, I.H.I. Tech. Rep., Vol. 10, No. 2.

NOMENCLATURE

a_{kj}	2D added mass coefficients in the k -direction due to motions in the j -mode
b_{kj}	2D damping coefficients in the k -direction due to motions in the j -mode
a_n, b_n	Fourier expansion series coefficients determining characteristics of GZ curve
c_3, c_5	nonlinear restoring stiffness coefficients
c_x	wetted contour of cross sections
c_0	mean contour of cross sections
$f(\eta_{4max})$	short term or long term distribution
f_k^I	sectional Froude-Krylov force for the incident waves of unit amplitude
f_k^D	sectional diffraction force for the incident waves of unit amplitude
f_{kj}^R	three dimensional radiation forces in the k direction due to an oscillatory motion of unit amplitude in the j direction
g	gravitational acceleration, $m\ s^{-2}$
$g(\eta_{4max})$	probability density function of extreme values
h	scaled amplitude of variation of metacentric height
k, j	subscripts associated with forces in the k -direction due to motions in the j -mode ($k = 1, 2, 3$ represent the surge, sway and heave directions, and 4, 5, 6 represent roll, pitch and yaw directions)
k	wave number, m^{-1}
k_1, k_2, k_3	damping criterion coefficients
k_n	lift gradient
$k\zeta$	slope of the wave
\vec{n}	unitary vector normal
p	fluid pressure, Pa
p	function of the ratio of forcing and natural frequency
q	parameter that dictates the amplitude of parametric excitation
r	mean distance from the roll axis to the bilge keel, m
r_f	equivalent radius, m
t	time variable, s
u	component of the velocity of fluid particles in the direction of the axis x , $m\ s^{-1}$
v	component of the velocity of fluid particles in the direction of the axis y , $m\ s^{-1}$
w	component of the velocity of fluid particles in the direction of the axis z , $m\ s^{-1}$
x_0, y_0, z_0	coordinate system fixed in space
x, y, z	translational coordinate system advancing with the ship forward speed U
x', y', z'	coordinate system fixed on the vessel
A_{kj}	added mass coefficients in the k direction due to an oscillatory motion in the j direction
$A_{n_{4v}}$	area under the GZ curve
A_{wl}	static waterplane area
B	ship breath, m
B_{kj}	damping coefficients in the k direction due to an oscillatory motion in the j direction
B_e	equivalent linear damping coefficient
B_F	hull skin friction damping
B_E	hull eddy shedding damping
B_W	free surface wave damping
B_{W0}	free surface wave damping for zero speed

B_L	lift force damping
B_{BK}	bilge keel damping
C_{kj}	restoring coefficients in the k direction due to an oscillatory motion in the j direction
C_b	block coefficient
C_D	equivalent drag coefficient
C_e	drag coefficient
C_M	mid-ship cross-section coefficient
C_f	equivalent flat plate frictional coefficient
C_P	pressure coefficient
C_x	cross section contour
F^R	radiation force
F_k^I	Froude – Krylov forces in the k direction ($k = 1, 2, 3$), N, ($k = 4, 5, 6$), Nm
F_k^D	diffraction forces in the k direction ($k = 1, 2, 3$), N, ($k = 4, 5, 6$), Nm
F_k^H	restoring forces in the k direction ($k = 1, 2, 3$), N, ($k = 4, 5, 6$), Nm
F^M	inertial force ($k = 1, 2, 3$), N
F_k^P	force exerted by the propeller in the k direction ($k = 1, 2, 3$), N, ($k = 4, 5, 6$), Nm
F_k^R	force exerted by the rudder in the k direction ($k = 1, 2, 3$), N, ($k = 4, 5, 6$), Nm
F_k^W	wind induced force in the k direction ($k = 1, 2, 3$), N, ($k = 4, 5, 6$), Nm
F_k^{DW}	green water on deck force in the k direction ($k = 1, 2, 3$), N, ($k = 4, 5, 6$), Nm
F_n	Froude number
$\overline{GM}_T = GM$	transversal metacentric height, m
\overline{GM}_L	longitudinal metacentric height, m
GM_m	mean value of the metacentric height, m
GM_a	amplitude of the metacentric height changes in waves, m
$\overline{GZ}_{(cond)}$	righting arm variation for wave crest, trough and still water condition, m
H_S	significant wave height, m
H_W	wave height, m
H_0	half breadth / draft ratio
I_{kj}	mass moment of inertia coefficients in the k -direction due to motions in the j -mode
K_C	Keulegan-Carpenter number
L_{PP}	length between perpendiculars, m
M_{kj}	components of the mass matrix for the ship
$M = \Delta$	mass (displacement) of the ship, kg
M^M	moment of inertia ($k = 4, 5, 6$), Nm
M_L	damping moment due to lift effect, Nm
N_{data}	total number of data
\overline{OG}	distance from the water surface to the center of gravity, m
R_b	bilge circle radius, m
S_ζ	wave spectrum, $m^2 s^{-1}$
S_{JS}	JONSWAP spectra, $m^2 s^{-1}$
S_{PM}	Pierson-Moskowitz spectra, $m^2 s^{-1}$
S_f	surface frictional area, m^2
T	draft, m
T_W	wave period, s
T_Z	zero up-crossing period, s

T_0	natural rolling period of ship, s
T_e	period of metacentric height variation, s
U	ship forward speed, m s^{-1}
V	velocity vector
V_B	volume of the whole ship, m^3
∇	gradient operator
∇_0	volume of the immersed hull, m^3
ν, α, β	roll decay coefficients
β	heading, deg
γ	JONSWAP peakedness factor
ε	phase difference
ϕ^R	2D radiation potential for harmonic motions of unit amplitude
ϕ_j^R	radiation potential for an oscillatory motion of unit amplitude in the mode j
ϕ^0	3D potential independent of the speed
$\phi = \eta_4$	angular roll motion
ζ	wave elevation, m
ζ_a	wave amplitude, m
η_k	$k = 1, 2, 3$ surge, sway and heave (m); $k = 4, 5, 6$ roll, pitch, yaw (deg) amplitudes
η_{4v}	angle of vanishing stability, deg
λ	wavelength, m
μ	linearised damping coefficient
ω_0	wave frequency, rad s^{-1}
ω_e	encounter frequency, rad s^{-1}
ω_m	mean rolling frequency, rad s^{-1}
ω_a	rolling variation frequency, rad s^{-1}
$\omega_{0,eq}$	equivalent natural frequency, rad s^{-1}
ρ_B	specific mass of the body, kg m^{-3}
ρ	specific mass of the fluid, kg m^{-3}
σ	area coefficient at a cross section along the hull
ν	coefficient of kinematic viscosity, $\text{m}^2 \text{s}^{-1}$
ν_{eq}	equivalent extinction damping coefficient
τ	nondimensional time
ξ	integrative variable in x direction
Φ	velocity potential function
Φ_U	potential of the steady motion in still water, $\text{m}^2 \text{s}^{-1}$
Φ_I	incident wave potential, $\text{m}^2 \text{s}^{-1}$
Φ_D	diffraction potential $\text{m}^2 \text{s}^{-1}$
Φ_R	forced motion potential, $\text{m}^2 \text{s}^{-1}$

LIST OF FIGURES

- Figure 1-1. Casualties due to the parametric rolling on APL China.
- Figure 2-1. Profile of waterline in wave crest.
- Figure 2-2. Profile of waterline in wave trough.
- Figure 2-3. Schematic representation of a hull contact with the sea, with respect to beam changes as a cause of parametric roll resonance.
- Figure 2-4. Schematics of the restoring moment as a function of wave position and heel angle, ABS (2004)
- Figure 2-5. The righting arm (GZ) curves
- Figure 2-6. Equivalent righting arm curves up to 45° on a wave trough GZ (trough), in still water GZ (still) conditions, and on a wave crest GZ (crest) condition.
- Figure 2-7. Wave-induced variation of the metacentric height $GM_{(wave)}$.
- Figure 2-8. Stability charts using ABS procedure
- Figure 2-9. Stability diagram for the Mathieu equation
- Figure 2-10. Linear (solid) and high-order (dashed) approximations for the boundary of the first instability zone (Turk et al. 2009).
- Figure 2-11. Ince-Strutt diagram for Mathieu's equation with constant damping.
- Figure 3-1. Boundary conditions surrounding the fluid domain
- Figure 3-2. Mathematical relationships between the three coordinate systems
- Figure 3-3. Coordinate system of incident harmonic wave
- Figure 3-4. Rigid body motions of the vessel
- Figure 3-5. Radiation condition on a two dimensional strip
- Figure 3-6. Displacement caused by coupling of the heave, roll and pitch motions
- Figure 3-7. Transfer functions for C11 containership in heave and pitch in head seas at zero speed
- Figure 3-8. Transfer functions for C11 containership in heave and pitch in head seas for 8 knots
- Figure 3-9. Transfer functions for C11 containership in sway and yaw in beam seas at zero speed
- Figure 3-10. Transfer functions for C11 containership in roll motion in beam seas at zero speed
- Figure 3-11. Variations of the hydrodynamic added mass and damping coefficients in heave and pitch depending on the various encounter frequencies
- Figure 3-12. Variations of the hydrodynamic added mass and damping coefficients in sway and yaw depending on the various encounter frequencies
- Figure 3-13. Added mass and damping coefficients of roll motion (Ribeiro e Silva et al. 2005.)
- Figure 3-14. Typical variations (for vessels with conventional forms) of the hydrodynamic added mass and damping coefficients in roll depending on the various encounter frequencies
- Figure 3-15. Linear and nonlinear simulation of Froude-Krylov force in roll
- Figure 3-16. Linear and nonlinear simulation of Froude-Krylov force in heave
- Figure 3-17. Linear and nonlinear simulation of Froude-Krylov force in pitch
- Figure 3-18. Nonlinear outlook of roll displacement with 2D and $2\frac{1}{2}$ D methods adopted
- Figure 3-19. Discretization of the segments and the normal vectors along a hull for the purpose of hydrostatic calculations (Ribeiro e Silva et al. 2010.)
- Figure 3-20. Righting arm realization for parametric rolling condition
- Figure 3-21. Nonlinear effects of restoring.
- Figure 3-22. Time race of irregular wave elevation
- Figure 3-23. The principle of temporal and frequency analysis of wave disturbance
- Figure 4-1. Skin friction coefficient as a function of the Reynolds number.
- Figure 4-2. Roll damping distribution of wave component.
- Figure 4-3. Simulated 3D roll damping distribution of wave component.
- Figure 4-4. Characteristics of roll wave damping coefficient for a two dimensional section.
- Figure 4-5. Distribution of pressures along the contour of the sections according to the Ikeda method
- Figure 4-6. Cancellation of damping moment for 2D sections due to the effect of a gradual increase in B_x/T_x ratio with high damping ratio at a point of separation (Dreossi, 2004).
- Figure 4-7. Roll damping distribution of coefficient C_R for original and modified methodology.
- Figure 4-8. Roll damping distribution of eddy making component for original and modified methodology

- Figure 4-9. General scheme of subdivision of the linear components of damping.
- Figure 4-10. Curve of the new function $f\left(\frac{OG}{T}\right)$ given for calculating the lift damping coefficient
- Figure 4-11. Geometry for calculating sectional damping coefficient due to normal force of the anti-roll fins.
- Figure 4-12abc. Comparison of the bare hull damping components for the 3 cases of wave radiation damping, B_{w0} with respect to velocity
- Figure 4-13abc. Comparison of the damping components for the 3 cases of wave radiation damping B_{w0} with the bilge keel with respect to velocity
- Figure 4-14. Schematic view of roll damping components with advance speed
- Figure 4-15. Schematic view of roll damping components with respect to roll amplitude
- Figure 4-16. Nonlinear effect of roll damping components for speed of 8 kts
- Figure 4-17. Effect of roll frequency on roll damping components for 0 kts
- Figure 4-18. Effect of roll frequency on roll damping components for a ship with advance speed of 8 kts
- Figure 5-1. Numerical model code flowchart
- Figure 5-2. Development of parametric rolling in regular waves ($H_W = 6$ m, $T_W = 12.95$ s, speed 7 knots)
- Figure 5-3. Phase diagram of the roll motion ($H_W = 6$ m, $T_W = 12.95$ s, speed 7 knots)
- Figure 5-4. Expanded view of roll and pitch motions at largest roll
- Figure 5-5. Regular wave parametric roll response for C11-class ship (original methodology)
- Figure 5-6. Regular wave parametric roll response for C11-class ship (updated methodology)
- Figure 5-7. Risk of parametric as a function of significant wave height and sustained speed
- Figure 5-8. Stable and unstable realizations of roll responses
- Figure 5-9. Maximum roll responses for bow waves for $T_W = 12.95$ with updated methodology
- Figure 5-10. Quantitative validation of regression fit for the occurrence regions of parametric rolling
- Figure 5-11. Linear fitting for varying speeds with roll responses as a function of wave heights
- Figure 5-12. Maximum roll responses for stern waves for $T_W = 12.95$ with updated methodology
- Figure 5-13. Comparison of roll response from both original and modified methodology for different headings
- Figure 5-14. Comparison of number of occurrences from both original and modified methodology for all simulations
- Figure 5-15. Numerical evidence with polar plots (GM1) of parametric rolling for ($H_W = 4$ m, $T_W = 12.95$ s).
- Figure 5-16. Numerical evidence with polar plots (GM1) of parametric rolling for ($H_W = 5 / 6$ m, $T_W = 12.95$ s).
- Figure 5-17. Numerical evidence with polar plots (GM1) of parametric rolling for ($H_W = 7 / 8$ m, $T_W = 12.95$ s).
- Figure 5-18. Numerical evidence with polar plots (GM1) of parametric rolling for ($H_W = 9/10$ m, $T_W = 12.95$ s).
- Figure 5-19. Numerical evidence with 3D polar plots (GM1) of parametric rolling with $T_W = 12.95$ s.
- Figure 5-20. Numerical evidence with 2D and 3D polar plots (GM1) of parametric rolling with $T_W = 11.59$ s.
- Figure 5-21. Numerical evidence with 2D and 3D polar plots (GM1) of parametric rolling with $T_W = 14.19$ s.
- Figure 5-22. Numerical evidence with 2D and 3D polar plots (GM1) of parametric rolling with $T_W = 15.33$ s.
- Figure 6-1. Basin with wave maker and CPMC (Computerized Planar Motion Carriage)
- Figure 6-2. The graphical representation of the model, distances are in millimetres
- Figure 6-3. Experimental setup for the parametric rolling tests
- Figure 6-4. Spectrum of the original and filtered signals
- Figure 6-5. Roll amplitude response with both the original and filtered signals
- Figure 6-6. Filtering of TEST 302
- Figure 6-7. Close-up of TEST 302 filtering
- Figure 6-8. Drift removal a) polynomial fitting to positive and negative peaks b) corrected peak values
- Figure 6-9. Application of drift removal procedure for TEST302
- Figure 6-10. Results of the drift removal procedure for TEST302

- Figure 6-11. Time trace of decay test for 0 knots with filtering
- Figure 6-12. Checking of drift removal procedure for 0 knots (1 run)
- Figure 6-13. Checking of drift removal procedure for 0 knots (2 run)
- Figure 6-14. Decay test 470 with filtering
- Figure 6-15. No damping for decay test 469
- Figure 6-16. Development of parametric rolling in experiments with regular waves ($H_W = 6$ m, $T_W = 12.95$ s, speed 8 knots)
- Figure 6-17. Development of parametric rolling in experiments with regular waves ($H_W = 8$ m, $T_W = 12.95$ s, speed 8 knots)
- Figure 6-18. No parametric rolling in experiments with regular waves ($H_W = 8$ m, $T_W = 14.19$ s, speed 8 knots)
- Figure 6-19. Experimental development of parametric rolling in experiments with regular following waves ($H_W = 8$ m, $T_W = 12.95$ s, speed 0 knots)
- Figure 6-20. Comparison of the measured and adjusted wave signal
- Figure 7-1. Example of roll decay curve
- Figure 7-2. Influence of the first half roll cycle
- Figure 7-3. Linear + quadratic + cubic model for decay test 302
- Figure 7-4. Dimensional roll damping evaluation by means of different methods (lin+quad)
- Figure 7-5. Non-dimensional roll damping evaluation by means of different methods
- Figure 7-6. Dimensional roll damping evaluation by means of different methods (lin+quad)
- Figure 7-7. Non-dimensional roll damping evaluation by means of different methods
- Figure 7-8. Comparison between time series from experiment and time series obtained by Runge Kutta method
- Figure 7-9. Decay test 302 processed by the exponential fitting method
- Figure 7-10. Comparison of results by utilizing different models for decay tests 302 to 307
- Figure 7-11. Evaluation of the linear component of damping for all speeds using decay tests 302 to 307
- Figure 7-12. Evaluation of the quadratic component of damping for all speeds using decay tests 302 to 307
- Figure 7-13. Linear + quadratic + cubic model for decay test “DECAY_TEST_GM1_U=0 knots” for both runs (Test 1 and Test2)
- Figure 7-14. Linear + quadratic + cubic model for decay test “DECAY_TEST_GM1_U=0 knots” by aggregating data from both runs
- Figure 7-15. Time trace of decay test for 8 knots with filtering
- Figure 7-16. Linear + quadratic + cubic model for decay test by aggregating data (first 2 runs)
- Figure 7-17. Linear + quadratic + cubic model for decay test by aggregating data (all 3 runs)
- Figure 7-18. Linear + quadratic + cubic model for decay test by aggregating data (8 knots)
- Figure 7-19. Linear + quadratic model for decay test 470
- Figure 7-20. Equivalent linear damping $v_{eq}(A)$ using the linear + quadratic + cubic model
- Figure 7-21. Equivalent linear damping $v_{eq}(A)$ using the linear + quadratic + cubic model up to 17°
- Figure 7-22. Equivalent linear damping $v_{eq}(A)$ for 14° compared to numerical model
- Figure 7-23. Equivalent linear damping $v_{eq}(A)$ for 30° compared to numerical model
- Figure 8-1. Numerical development of parametric rolling with regular following waves ($H_W = 8$ m, $T_W = 12.95$ s, speed 0 knots)
- Figure 8-2. Time traces comparison of roll responses between the original methodology, convergence method and direct coupling for test No. 10
- Figure 8-3. Time traces of roll responses with linear + quadratic damping model from decay test No. 304
- Figure 8-4. Time traces comparison of roll responses between equivalent linear damping by direct calculations and linear + quadratic model for test No. 304.
- Figure 8-5. Time traces comparison of roll responses between the original methodology, convergence method and direct coupling for test No. 313.
- Figure 8-6. Time traces comparison of roll responses between numerical implementation and from the decay acquisition for test No. 310.
- Figure 8-7. Time traces comparison of roll responses between the decay acquisition and experiment for test No. 310.

- Figure 8-8. Time traces of motions for linear + quadratic model implementation (test No. 312)
- Figure 8-9. Heave and pitch motions in experiment (test No. 312)
- Figure 8-10. Time traces comparison of roll responses between the decay acquisition and experiment for test No. 312.
- Figure 8-11. The loading condition influence on the parametric rolling relization
- Figure 8-12. Numerical results of parametric roll with the roll damping estimated from a roll decay tests, Ikeda's method and modified damping feature with $H_W = 8$ m
- Figure 8-13. Experimental time trace of rolling motion for Test No. 17 provided by Cehipar
- Figure 8-14. Numerical simulation associated with Test No. 17
- Figure 8-15. Numerical simulation associated with Test No. 18 and Test No. 19.
- Figure 8-16. Experimental time trace of rolling motion for Test No. 18 and Test No. 19. provided by Cehipar
- Figure 8-17. Speed increase for slightly oblique waves due to the established occurrence groupiness.
- Figure 8-18. Numerical simulation associated with Test No. 23 and Test No. 25.
- Figure 8-19. Experimental time trace of rolling motion for Test No. 23 and Test No. 25. provided by Cehipar
- Figure 8-20. Numerical simulation associated with Test No. 31.
- Figure 8-21. Excitation level identification
- Figure 8-22. Experimental time trace of rolling motion for Test No. 31
- Figure 8-23. Comparison between the polychromatic and regular wave excitation for Test No. 34 and Test No. 34a
- Figure 8-24. Wave elevation profile of Wave No. 32
- Figure 8-25. Numerical simulation associated with Test No. 20.
- Figure 8-26. Experimental time trace of rolling motion for Test No. 20.
- Figure 8-27. Numerical simulation associated with Test No. 26.
- Figure 8-28. Experimental time trace of rolling motion for Test No. 26.
- Figure 8-29. Wave elevation segment that enable parametric rolling.
- Figure 8-30. Wave 27a with significant wave height of $H_S = 8$ m, $T_W = 12.95$ s, JONSWAP spectra $\gamma = 3.3$
- Figure 8-31. Time history of Test No. 35
- Figure 8-32. Wave elevation and roll time history of Test No. 35
- Figure 8-33. Segment of wave profile for which the parametric rolling initiates
- Figure 8-34. Numerical simulation associated with Test No. 36.
- Figure 8-35. Experimental time trace of rolling motion for Test No. 36.
- Figure 8-36. Wave elevation and roll time history of Test No. 36 with physical explanation
- Figure 8-37. Wave elevation and roll time history of Test No. 339
- Figure 8-38. Numerical simulation associated with Test No. 339.
- Figure 8-39. Time history of Test No. 339
- Figure 8-40. Wave elevation and roll time history of Test No. 340
- Figure 8-41. Numerical simulation associated with Test No. 340.
- Figure 8-42. Wave elevation and roll time history of Test No. 341.
- Figure 8-43. Comparison of the distribution of maxima
- Figure 8-44. Distribution of parametric roll
- Figure 8-45. Assessment of roll extremes with small probability methodology
- Table 8-8. Parametric rolling scatter diagram
- Figure 8-46. Alternative probabilistic methodology
- Figure 8-47. Numerical evidence with polar plots of parametric rolling for ($H_S = 8$ m, $T_Z = 12.95$ s).
- Figure 8-48. Weighted generalization of the irregular parametric excitation for ($H_S = 6$ and 10 m, $T_Z = 12.95$ s).
- Figure 8-49. Weighted generalization of the irregular parametric excitation compared to regular for ($H_S = 6$ m and $H_W = 6$ m, $T_Z = 12.95$ s and $T_W = 12.95$ s).
- Figure 8-50. Numerical evidence with 3D polar plots of parametric rolling with irregular following waves ($T_Z = 12.95$ s).
- Figure 8-51. Numerical evidence with 3D polar plots of parametric rolling with irregular following waves ($T_Z = 12.95$ s).

LIST OF TABLES

Table 4-1.	Summary table for lift component $f\left(\frac{OG}{T}\right)$ calculation.
Table 5-1.	Summary table for parametric rolling realizations in following waves.
Table 5-2.	Scatter diagram of the parametric rolling in regular waves (one specific condition)
Table 5-3.	Summary of parametric rolling survey for regular head waves ($H_W = 8$ m, $T_W = 12.95$ s)
Table 5-4.	Summary of parametric rolling survey for regular head waves ($H_W = 8$ m, $T_W = 12.95$ s) with damping blending method
Table 5-5.	Summary of parametric rolling survey for regular head waves ($H_W = 8$ m, $T_W = 11.59$ s) with damping blending method
Table 6-1.	Summary of the decay tests conducted (provided by Cehipar)
Table 6-2.	Summary of the decay tests conducted
Table 6-3.	Particulars of decay test 469
Table 6-4.	Summary of parametric rolling experiments with emphasis on different loading condition (provided by Cehipar)
Table 6-5.	List of all experimental polychromatic waves tests (provided by Cehipar)
Table 6-6.	List of all theoretical polychromatic waves (provided by Cehipar)
Table 6-7.	List of actual measured polychromatic waves generated in the basin (provided by Cehipar)
Table 6-8.	Polychromatic head waves tests (provided by Cehipar)
Table 6-9.	Lists of the complete free irregular wave's tests
Table 7-1.	Linear + quadratic + cubic model for decay test 302
Table 7-2.	Linear + quadratic model for decay test 302
Table 7-3.	Decay tests processed by the exponential fitting method
Table 7-4.	Linear + quadratic model for decay test (8 knots)
Table 7-5.	Comparison of equivalent linear damping using all three models
Table 7-6.	Summary of all decay tests in waves with equivalent linear damping obtained by exponential fitting
Table 7-7.	Equivalent linear damping for test 470 and 471
Table 8-1.	The results for regular waves at 180° heading
Table 8-2.	The results of numerical simulations for regular waves at 180° heading for $H_W = 10$ m
Table 8-3.	The results of numerical simulations for regular waves at 180° heading for $T_W = 11.59$ s
Table 8-4.	Results of numerical simulations for regular waves at 180° heading for $T_W = 14.19$ s and $H_W = 8$ m
Table 8-5.	Comparison between experimental and numerical calculations for following waves
Table 8-6.	Comparison of roll responses between the original methodology, convergence method and direct coupling for test No. 10
Table 8-7.	Comparison between experimental and numerical calculations for test No. 310 and test No. 312

Curriculum vitae

Anton Turk was born in Rijeka, 12th March 1974. He attended primary school in Rijeka up until 1988 and high school, "Andrija Mohorovicic," until 1992. He earned the degree in Naval Architecture from the Faculty of Engineering, University of Rijeka in 1999 with the thesis "Numerical optimisation of stiffened plate structures" under the supervision Prof. Josip Brnić, Ph.D. evaluated with an excellent grade.

He was employed in the shipyard "Viktor Lenac" as an intern and spent four months in the manufacturing sector. After that he went to the military service. After the military obligations he continued to work as a design engineer in the project office of the shipyard. He has worked on design and hydro-mechanical modelling calculations using the software package TRIBON - M1.

Since June 2001 he has been employed at the Faculty of Engineering as a research assistant under the mentorship of Prof. Jasna Prpic-Oršić, Ph.D. In October 2004 he enrolled the postgraduate study in order to get the doctoral degree at the Faculty of Engineering University of Rijeka, in the field of design and building of floating objects. He has been participating as assistant with the following courses in the faculties undergraduate and graduate university study program of Naval Architecture: Ship geometry, Ship hydrostatics, Ship stability, Ship structural elements, Ship construction, Ship vibrations, Ship strength, Dynamics of vessels, Modelling of environment and environmental loads, Stability of the ship in exploitation.

Since 2002 he has been participating in the scientific research projects supported by the Ministry of Science, Education and Sports: Numerical modelling in ship hydrodynamics (No. 0069007) and Numerical modelling of hydrodynamic loads and responses of marine structures (No. 069-0691736-1667) under the head researcher Prof. Jasna Prpic-Oršić, Ph.D. He has participated in international TEMPUS Joint European Project (2006-2010) named "Advanced Ship Design for Pollution Prevention" with the participated course title "Modelling of the environment and environmental loads", as an assistant. Since 2008, as part of a doctoral dissertation work he participated in the international scientific research project FP6 HydraLab III - Experimental Assessment of Parametric Rolling on a C11 class containership in cooperation with the Technical University of Lisbon (Instituto Superior Tecnico) and El Pardo Ship Model Basin (Canal de Experiencias Hidrodinámicas de El Pardo CEHIPAR), Madrid, funded by the European Committee. He is a co-author of 19 scientific papers.

In 2002, he attended an international seminar on Dynamic Load on Ships & Marine Structure in Genoa, CETENA Centro per gli studi tecnica navale - Italian research centre. In July 2003, he attended and successfully completed the course in modules TRIBON Tribon Hull, TRIBON Drafting, TRIBON Planar Hull Modelling, Curved Hull Modelling TRIBON, TRIBON Nesting, TRIBON Production. In 2005, he participated in the workshop "Intelligent underwater systems and technologies - a vision of development in the Republic of Croatia - Zagreb IPSIT05". In September 2006, in Udine, CISM, International Centre for Mechanical Sciences, he attended the course "Wind Effects on Buildings and Design of Wind-Sensitive Structures". In the framework of the international exchange students (Erasmus) program (September - December 2009), he received a scholarship for a scientific training leading to a doctoral dissertation at the Università degli Studi di Trieste; Dipartimento Navale di Ingegneria, with Prof. Alberto Francescutto, Ph.D. and Gabriele Bulian, Ph.D. He also participated in the development of several expert projects and studies.

He took part in the organisation of two scientific conferences, Symposium on Marine Technology - In Memoriam of the Academician Zlatko Winkler (2005, 2007). As representative of the postgraduate students he was member of the faculty council (2004/2005). He is a member of the Association of Alumni and Alumnae of the Faculty of Engineering, University of Rijeka (AKDMI). He is fluent in English and has substantial knowledge of Italian and German languages. He is married and has two children.

5. CONCLUSION AND RECOMMENDATION

With the detailed insight into the content of the proposed doctoral dissertation, and by the previously reported in the above, the professional Committee assessed a doctorate as the original scientific work that meets all the criteria of original scientific achievement and therefore submits to the Faculty Council of the Faculty of Engineering following

RECOMMENDATION

that the dissertation of Anton Turk, titled,

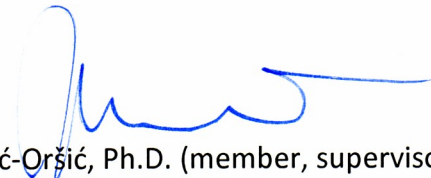
COUPLED NONLINEAR PARAMETRIC RESONANCE MODEL FOR CONTAINER SHIPS

is accepted as a doctoral dissertation in the scientific area of Technical sciences in the scientific field of Naval architecture, the scientific branch of Hydromechanics of floating and offshore objects, and may set a the Defence Committee and the date of the public verbal defence.

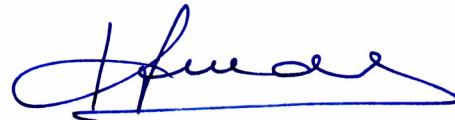
Evaluation Committee members:



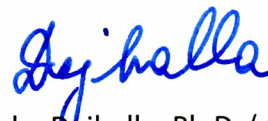
Prof. Bruno Čalić, Ph.D. (president)




Prof. Jasna Prpić-Oršić, Ph.D. (member, supervisor)



Prof. Carlos Guedes Soares, Ph.D. (member, supervisor, IST, Lisbon, Portugal)



Prof. Roko Dejhalla, Ph.D. (member)



Prof. Većeslav Čorić Ph.D. (member, FAMENA, Zagreb)